



HAL
open science

Mathematical and numerical modelling of fluids at nanometric scales

Rémi Joubaud

► **To cite this version:**

Rémi Joubaud. Mathematical and numerical modelling of fluids at nanometric scales. General Mathematics [math.GM]. Université Paris-Est, 2012. English. NNT : 2012PEST1088 . tel-00771757v2

HAL Id: tel-00771757

<https://pastel.hal.science/tel-00771757v2>

Submitted on 25 Mar 2013

HAL is a multi-disciplinary open access archive for the deposit and dissemination of scientific research documents, whether they are published or not. The documents may come from teaching and research institutions in France or abroad, or from public or private research centers.

L'archive ouverte pluridisciplinaire **HAL**, est destinée au dépôt et à la diffusion de documents scientifiques de niveau recherche, publiés ou non, émanant des établissements d'enseignement et de recherche français ou étrangers, des laboratoires publics ou privés.



THÈSE

présentée pour l'obtention du titre de
Docteur de l'Université Paris-Est
Spécialité : Mathématiques Appliquées

par **Rémi Joubaud**

Thèse préparée au CERMICS, École des Ponts Paristech, Université Paris-Est
Doctorant bénéficiaire d'une allocation de thèse de l'Andra

Sujet : Modélisation mathématique et numérique
des fluides à l'échelle nanométrique

Soutenue le 20 Novembre 2012
devant le jury composé de :

Rapporteurs :	Grégoire Allaire Erwan Faou
Examineurs :	Jean-François Dufrêche Vincent Giovangigli Grigorios Pavliotis Frédéric Plas
Directeurs de thèse :	Alexandre Ern Tony Lelièvre
Invité :	Gabriel Stoltz

Modélisation mathématique et numérique des fluides à l'échelle nanométrique

Résumé :

Ce travail présente quelques contributions mathématiques et numériques à la modélisation des fluides à l'échelle nanométrique. On considère deux niveaux de modélisation. Au premier niveau, une description atomique est adoptée. On s'intéresse aux méthodes permettant de calculer la viscosité de cisaillement d'un fluide à partir de cette description microscopique. On étudie en particulier les propriétés mathématiques de la dynamique de Langevin hors d'équilibre permettant de calculer la viscosité. Le deuxième niveau de description se situe à l'échelle du continu et l'on considère une classe de modèles pour les électrolytes à l'équilibre incorporant d'une part la présence d'un confinement avec des parois chargées et d'autre part des effets de non-idéalité dus aux corrélations électrostatiques entre les ions et au phénomène d'exclusion stérique. Dans un premier temps, on étudie mathématiquement le problème de minimisation de l'énergie libre dans le cas où celle-ci reste convexe (non-idéalité modérée). Puis, on considère le cas non convexe (forte non-idéalité) conduisant à une séparation de phase.

Mots-clés : Physique statistique computationnelle - Dynamique moléculaire hors d'équilibre - Électrolytes - Équations aux dérivées partielles non linéaires - Méthodes variationnelles - Éléments finis

Mathematical and numerical modelling of fluids at nanometric scales

Abstract :

This work presents some contributions to the mathematical and numerical modelling of fluids at nanometric scales. We are interested in two levels of modelling. The first level consists in an atomic description. We consider the problem of computing the shear viscosity of a fluid from a microscopic description. More precisely, we study the mathematical properties of the nonequilibrium Langevin dynamics allowing to compute the shear viscosity. The second level of description is a continuous description, and we consider a class of continuous models for equilibrium electrolytes, which incorporate on the one hand a confinement by charged solid objects and on the other hand non-ideality effects stemming from electrostatic correlations and steric exclusion phenomena due to the excluded volume effects. First, we perform the mathematical analysis of the case where the free energy is a convex function (mild non-ideality). Second, we consider numerically the case where the free energy is a non convex function (strong non-ideality) leading in particular to phase separation.

Keywords : Computational statistical physics - Nonequilibrium molecular dynamics - Electrolytes - Nonlinear partial differential equations - Variational methods - Finite elements

À mes grands parents.

Remerciements

Je tiens en premier lieu à remercier mes deux directeurs de thèse, Alexandre Ern et Tony Lelièvre, ainsi que mon troisième directeur “officieux”, Gabriel Stoltz. Merci à vous trois, ce fut un réel plaisir de travailler ensemble. J’ai eu beaucoup de chance d’être aussi bien encadré pendant ces trois années de thèse, ainsi que pendant mon stage de Master que j’ai effectué avec vous à l’École des Ponts. Merci pour tout vos conseils et votre très grande disponibilité.

Ce travail est le fruit d’une collaboration avec les collègues physico-chimiste de l’équipe PECSA de l’Université Pierre et Marie Curie. Je souhaite très chaleureusement remercier Olivier Bernard, Marie Jardat, Virginie Marry, Benjamin Rotenberg et Pierre Turq. Merci à vous pour tout ce que vous m’avez appris concernant la modélisation en physico-chimie et pour l’accueil toujours chaleureux au laboratoire. J’en profite pour remercier Alexandru Botan avec qui il a été très agréable de discuter des problèmes liés aux calculs de viscosité dans les argiles.

Je tiens aussi à remercier l’Agence nationale pour la gestion des déchets radioactifs pour avoir financé et suivi cette thèse avec beaucoup d’intérêt. Je souhaite en particulier remercier Frédéric Plas et Scott Altmann qui m’ont fait confiance et qui m’ont permis de démarrer ma carrière de jeune thésard sur une thématique extrêmement intéressante, en lien avec des problèmes industriels et environnementaux.

Je remercie vivement Grégoire Allaire et Erwan Faou pour avoir accepté d’examiner ce travail en qualité de rapporteur. Je tiens aussi à remercier Jean-François Dufrêche, Vincent Giovangigli et Greg Pavliotis de m’avoir fait l’honneur de participer à mon jury de thèse.

Une pensée pour les collègues du groupement MoMas et aux participants des journées modélisation en électrocinétique, tout particulièrement merci à Andro Mikelić et Pierre Turq pour avoir organisé ces journées.

Je souhaite aussi remercier toutes les personnes qui m’ont permis d’enseigner à l’École des Ponts et l’Université Pierre et Marie Curie, en particulier Éric Cancès, Jean-Philippe Chancelier et Michel De Lara.

Je tiens à exprimer toute ma gratitude à ceux qui ont pu apprécier ma présence (intermittente ou permanente !) dans leurs bureaux en commençant par Kimiya, Arnaud Anantharaman, Ronan, Pablo, Laurent, Olivier, David Doyen, Julie, David Benoit, Marie, Fabien, Virginie, Adela, Christelle, Patrick, Abdel, Maxence, José, Julien. Une dédicace spéciale pour Fabien en

hommage à notre “fruitful collaboration” du CEMRACS 2011, j’en profite pour remercier Michel Fouquembergh et Fabien Mangeant (EADS IW) pour avoir proposé le projet.

Pour finir, merci à tout(e)s les collègues du CERMICS à l’École des Ponts. Merci à la Perla et aux Pères populaires d’avoir été là pour terminer les semaines. Quelques mots pour les participants de la SEME 2011 à l’IHP ainsi que pour les participants du CEMRACS 2011 avec qui ce fut un plaisir de partager ces 6 semaines de recherche. Merci pour toutes ces coïncidences endiablées et merci aux calanques de Luminy. Merci aux amis qui ont eu à endurer mes plaintes de thésard. Merci à Pink Floyd et G.R.R Martin.

Un dernier mot pour mes parents, ma tante Marcelle, ma grand-mère Andrée, ma soeur Julia et mon frère Nicolas pour leur soutien bienveillant.

Table des matières

1	Introduction générale	1
1.1	Contexte industriel : le stockage des déchets radioactifs	1
1.1.1	Le stockage en couche géologique profonde	1
1.1.2	L'argile : un matériau multi-échelles comme barrière de confinement naturelle	2
1.1.3	Modélisation et simulation des petites échelles	2
1.2	Contributions de la thèse	3
1.2.1	Calcul de coefficients de transport à partir d'une description microscopique	3
1.2.2	Modèles continus pour les électrolytes	6
1.3	Liste de publications	12
1.3.1	Liste des articles parus dans des revues à comité de lecture	12
1.3.2	Article en préparation	12
1.3.3	Autres travaux	12

Part I Computing transport coefficients from microscopic models

2	Some elements of statistical mechanics and molecular dynamics	15
2.1	Computational statistical mechanics	16
2.1.1	Microscopic description of the system	16
2.1.2	Potential energy	16
2.1.3	Thermodynamic ensembles	18
2.1.4	The equilibrium Langevin dynamics	20
2.1.5	Numerical aspects	24

2.2	Nonequilibrium dynamics and Green-Kubo formula	27
2.2.1	Nonequilibrium dynamics	28
2.2.2	Invariant measure of the nonequilibrium dynamics	28
2.2.3	Linear response and correlation functions	29
2.2.4	Discussion on the choice of the underlying dynamics	30
2.3	Computation of transport coefficients: the example of the shear viscosity	31
2.3.1	Some elements of continuous fluid mechanics	31
2.3.2	Equilibrium methods	32
2.3.3	Steady state nonequilibrium	35
2.3.4	Transient nonequilibrium dynamics	39
3	Nonequilibrium shear viscosity computations with Langevin dynamics	41
3.1	Aim of the study	41
3.2	The nonequilibrium Langevin dynamics	42
3.2.1	Existence and uniqueness of an invariant measure	42
3.3	Mathematical analysis of the viscosity	43
3.3.1	Linear response	43
3.3.2	Local conservation of the longitudinal velocity	44
3.3.3	Definition and closure relation for shear viscosity computations	46
3.3.4	Asymptotic behaviour of the viscosity for large frictions	46
3.4	Numerical results for the Lennard–Jones fluid	49
3.4.1	Numerical implementation	49
3.4.2	Numerical results	52
3.5	Proof of the results	60
3.5.1	Proof of Theorem 4	60
3.5.2	Proof of Proposition 1	62
3.5.3	Proof of Theorem 5	64
3.5.4	Proof of Theorem 6	68

Part II Continuous models for equilibrium electrolytes

4	Modelling of non-ideal equilibrium electrolytes	73
4.1	Bibliography overview on ideal and non-ideal electrolytes	74

4.2	Mathematical statement of the electrochemical model	75
4.2.1	Geometry and equilibrium equations	75
4.2.2	First variational formulation	79
4.2.3	Second variational formulation	82
4.2.4	Modelling of non-ideality	83
4.2.5	Mild and strong non-ideality	85
4.2.6	Application: mechanical equilibrium and evaluation of the pressure	86
4.2.7	Previous mathematical results	87
4.3	The primitive model for homogeneous electrolytes	89
4.3.1	Hamiltonian of the isolated system	89
4.3.2	The ideal gas bulk free energy density	90
4.3.3	The non-ideal bulk free energy density	92
4.4	Derivation of the free energy functional \mathcal{F} for confined electrolytes	98
4.4.1	A microscopic model for confined electrolytes	98
4.4.2	Inhomogeneous Ornstein–Zernike equation	100
4.4.3	Ansatz for the free energy functional	102
4.4.4	Derivation of \mathcal{F}_{mf}	103
4.4.5	Approximations of $\mathcal{F}_{\text{corr}}$	104
5	Mild non-ideality: convex bulk free energy	107
5.1	Introduction	107
5.2	Mathematical analysis	108
5.2.1	Non-dimensionalization	108
5.2.2	Assumptions	110
5.2.3	Main result and main steps of its proof	111
5.2.4	Technical results	113
5.3	Numerical aspects	118
5.3.1	Physical input	118
5.3.2	Verification of assumptions for MSA	119
5.3.3	Numerical methods	120
5.3.4	Validation of the approach: flat nanochannel	121
5.3.5	Periodic medium with charged inclusions	122

6	Strong non-ideality: non convex bulk free-energy and phase separation	127
6.1	Bulk thermodynamics of the one-species setting	127
6.1.1	Chemical potential	128
6.1.2	Free energy density	129
6.1.3	Osmotic pressure	129
6.1.4	Phase separation	130
6.1.5	The Maxwell equal area rule	130
6.1.6	Convex hull: numerical illustrations	131
6.2	Confined electrolytes: Theory and method	132
6.2.1	Canonical constraints and thermodynamic equilibrium	133
6.2.2	Mechanical equilibrium	133
6.2.3	Regularizations	134
6.2.4	Discretization and nonlinear solver	135
6.2.5	Validation test cases	137
6.3	Confined electrolytes: Numerical results	139
6.3.1	Flat nanochannel	140
6.3.2	Periodic network of charged inclusions and wavy channel	142
6.4	An approach for symmetric salts	144
6.5	Some mathematical aspects	146
6.5.1	Minimizing properties of \mathcal{F}^{**}	147
6.5.2	Minimizing properties of $\mathcal{F}_{\kappa}^{**}$	148
6.5.3	Existing Γ -convergence results	148
7	Summary and perspective of future work (Part II)	151

Part III Annexes

8	Other work in fluid mechanics and thermal modelling	155
8.1	Numerical study of a thin liquid film flowing down an inclined wavy plane	155
8.2	A multiscale problem in thermal science	155

Introduction générale

1.1	Contexte industriel : le stockage des déchets radioactifs	1
1.1.1	Le stockage en couche géologique profonde	1
1.1.2	L'argile : un matériau multi-échelles comme barrière de confinement naturelle	2
1.1.3	Modélisation et simulation des petites échelles	2
1.2	Contributions de la thèse	3
1.2.1	Calcul de coefficients de transport à partir d'une description microscopique	3
1.2.2	Modèles continus pour les électrolytes	6
1.3	Liste de publications	12
1.3.1	Liste des articles parus dans des revues à comité de lecture	12
1.3.2	Article en préparation	12
1.3.3	Autres travaux	12

1.1 Contexte industriel : le stockage des déchets radioactifs

1.1.1 Le stockage en couche géologique profonde

La gestion des déchets nucléaires en France est assurée par l'Agence nationale pour la gestion des déchets radioactifs (ANDRA) depuis la loi *du 30 décembre 1991* puis celle du *28 juin 2006*. Il existe plusieurs types de déchets radioactifs, classifiés selon leur degré de radioactivité (haute activité (HA), moyenne activité (MA), faible activité (FA) et très faible activité (TFA)) ainsi que leur durée d'activité (vie longue (VL), vie courte (VC)) ; on pourra consulter [82] pour un inventaire de ces déchets et les différents secteurs d'activité à l'origine de ceux-ci. Les déchets de haute activité à vie longue, qui sont les plus radioactifs, proviennent en grande partie de la production d'électricité. Ces déchets représentent moins de 1% du volume total de déchets mais totalisent à eux seuls environ 96% de la radioactivité. Depuis la loi du *28 juin 2006*, le mode de référence pour la gestion des déchets de haute et moyenne activité à vie longue (HA/MAVL) est le stockage réversible en couche géologique profonde (environ à 500 mètres de profondeur).

1.1.2 L'argile : un matériau multi-échelles comme barrière de confinement naturelle

La principale barrière de confinement envisagée dans le cadre du projet de stockage en couche géologique profonde est d'origine naturelle, à savoir une argile de type Callovo-Oxfordien, localisée en Meuse/Haute-Marne. Il s'agit d'une roche sédimentaire formée il y a environ 165 millions d'années. Les argiles sont des matériaux multi-échelles. La plus petite échelle, inférieure au nanomètre, fait intervenir des feuillets. L'empilement de ceux-ci forme des particules de taille nanométrique. Entre ces particules peuvent se mouvoir un solvant (eau) et des ions. L'interaction entre ces particules, lorsque la roche est soumise à des efforts extérieurs, détermine la réponse mécanique observée à plus grande échelle.

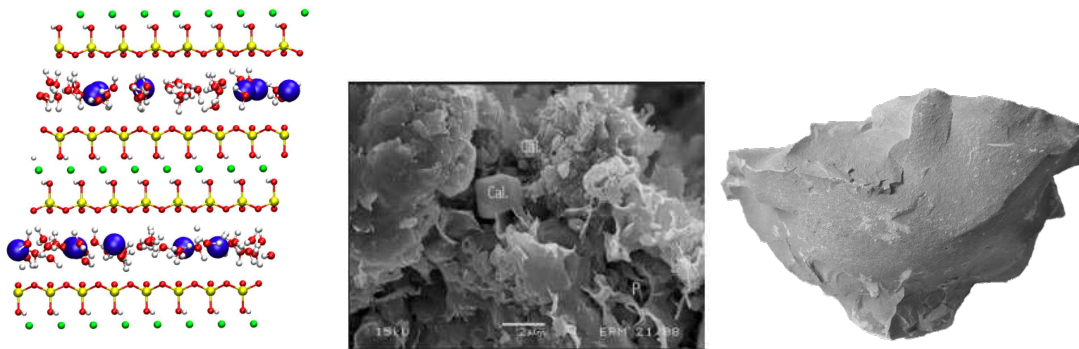


Figure 1.1. Gauche : description microscopique du système argile, eau et ions (image de B. Rotenberg) ; Centre : Argile à l'échelle du micromètre (ANDRA, 2005) ; Droite : échantillon d'argilite du Callovo-Oxfordien à l'échelle du centimètre.

1.1.3 Modélisation et simulation des petites échelles

De nombreuses propriétés aux petites échelles ne sont pas accessibles expérimentalement. On peut alors avoir recours à une approche numérique en les déterminant à partir de simulations microscopiques de type *ab initio*, en résolvant le problème de structure électronique ou l'équation de Schrödinger, ou classiques (dynamique moléculaire, méthode de Monte Carlo) ou à partir de modèles de milieux continus pour les plus grandes échelles. Dans tous les cas, on s'appuie sur les outils de la physique statistique [8] (équations intégrales, théorie de la fonctionnelle de la densité). Pour les plus petites porosités, il s'agit de prédire les propriétés d'un système à partir d'une description à l'échelle atomique et des interactions moléculaires. Ces approches reposent sur une description simplifiée du système (structure, composition) et des interactions et doivent donc être validées par la comparaison avec les données expérimentales disponibles (spectroscopies, diffraction, micromécanique, *etc*). Deux niveaux peuvent être considérés dans une description discrète du matériau, du plus fin au plus grossier, l'étape suivante étant le passage au continu. Le premier niveau correspond à une description complète des feuillets d'argile et du système composé des molécules d'eau et des espèces ioniques. On peut avoir alors recours aux techniques de la dynamique moléculaire à l'équilibre (propriétés statiques, coefficients de transport) ou hors

d'équilibre [28] (transport). Mentionnons par exemple une étude récente en dynamique moléculaire hors d'équilibre portant sur la validité des équations de l'hydrodynamique dans les feuillets d'argile [14] (validité de la loi de Newton, condition aux limites pour le champ de vitesse en bordure de feuillet). Une deuxième échelle se situe à un niveau mésoscopique où l'eau est considérée comme un solvant continu en conservant une description discrète de l'argile et des ions ou des ions seulement. Cette approche se justifie dès lors que l'on considère que les ions sont beaucoup plus gros que les molécules d'eau. Pour traiter les questions d'équilibre, on peut faire appel aux méthodes de Monte Carlo. Concernant les problèmes de transport, les techniques de dynamique Brownienne permettent de calculer numériquement les coefficients de diffusion ou la conductivité électrique dans ce cadre simplifié [55]. Par ailleurs, les simulations en temps long de dynamique Brownienne permettent aussi de déterminer l'équilibre thermodynamique par le calcul de moyennes ergodiques. Les méthodes d'équation intégrales pour les fluides inhomogènes se situent à un niveau intermédiaire car les corrélations spatiales sont décrites explicitement. C'est le cas par exemple pour des méthodes d'Ornstein–Zernike inhomogène [1, 58, 59]. Enfin les modèles continus, tels que Poisson–Boltzmann et théorie de la fonctionnelle de la densité (équilibre) ou Navier–Stokes couplé à Poisson–Nernst–Planck (transport), constituent une alternative aux modèles microscopiques, efficace numériquement dès lors que l'on a pu valider ces modèles grâce aux simulations des modèles les plus fins. On pourra consulter [54] pour une comparaison entre simulation moléculaire directe, dynamique brownienne et théorie de la fonctionnelle de la densité.

1.2 Contributions de la thèse

L'objectif de cette thèse est l'étude mathématique et numérique de modèles microscopiques et mésoscopiques pour les fluides chargés confinés, en vue d'une meilleure compréhension des phénomènes physico-chimiques dans les argiles aux échelles où ils se posent. Une perspective de ces travaux est l'intégration de ces phénomènes aux plus grandes échelles afin de décrire notamment le comportement mécanique de la roche. La contribution de cette thèse relevant des mathématiques appliquées, on s'est attaché en particulier aux aspects méthodologiques des techniques mathématiques et numériques permettant de simuler les modèles physiques aux différentes échelles. Les contributions de cette thèse s'articulent en deux volets correspondant à deux échelles de description du système physique.

1.2.1 Calcul de coefficients de transport à partir d'une description microscopique

Le premier volet concerne le problème du calcul de coefficients de transport, partant d'une description microscopique (atomique) du système. Le formalisme adopté est celui de la physique statistique computationnelle. Le système est modélisé à l'échelle atomique selon une description classique de la matière par N atomes (N étant en général très grand, même pour des systèmes de quelques nanomètres d'épaisseur où N est de l'ordre du millier). Les variables du problème sont les positions des atomes q , évoluant dans un espace d'état $\mathcal{M} \subset \mathbb{R}^{dN}$ ($d = 2, 3$) et leurs impulsions p évoluant dans \mathbb{R}^{dN} . Les atomes interagissent via des potentiels empiriques V . La comparaison des propriétés physiques du système avec des données expérimentales vient confirmer l'utilisation de ces potentiels.

Une observable A est une fonction du couple position/impulsion et représente une grandeur physique (énergie, température, pression). Par exemple, l'énergie totale du système est donnée par le Hamiltonien classique

$$H(q, p) = \frac{1}{2} p^T M^{-1} p + V(q),$$

où $M \in \mathbb{R}^{dN \times dN}$ désigne la matrice de masse du système. Les variables (q, p) déterminent le micro-état du système physique, mais apportent trop d'information. Il est donc souhaitable de passer à une description plus grossière. Pour ce faire, il s'agit de faire le lien avec un état macroscopique du système. Ce macro-état est décrit par une mesure de probabilité ν , "la moins biaisée" vis à vis des conditions d'observation. À l'équilibre thermodynamique, les quantités telles que la température ou la pression d'un système peuvent être déterminées par la seule connaissance de cette mesure de probabilité. Ainsi, le lien avec le système microscopique est fait par le biais d'une moyenne d'ensemble de la forme

$$\langle A \rangle := \int_{\mathcal{M} \times \mathbb{R}^{dN}} A(q, p) \nu(dq, dp). \quad (1.1)$$

Un exemple de mesure de probabilité ν est la mesure canonique NVT (correspondant à fixer le nombre N de particules, le volume accessible V et la température T) donnée par la formule

$$\nu_{\text{NVT}}(dp, dq) = Z^{-1} e^{-\beta H(q, p)} dq dp, \quad Z = \int_{\mathcal{M} \times \mathbb{R}^{dN}} e^{-\beta H(q, p)} dq dp, \quad (1.2)$$

où $\beta = (k_B T)^{-1}$ est proportionnel à l'inverse de la température, k_B étant la constante de Boltzmann. Le plus souvent, le calcul de quantités macroscopiques selon la formule (1.1) est une tâche numérique impraticable par les méthodes de quadratures usuelles en raison de la très grande dimensionalité du problème (fléau de la dimension). On aura le plus souvent recours à des techniques d'échantillonnage de mesures de probabilité, déterministes ou stochastiques. Par exemple, le calcul de (1.1) est très souvent remplacé par le calcul d'une moyenne en temps long :

$$\lim_{s \rightarrow \infty} \frac{1}{s} \int_0^s A(q_t, p_t) dt = \langle A \rangle, \quad (1.3)$$

sous le postulat que la dynamique régissant les (q_t, p_t) est ergodique pour la mesure ν .

La situation est différente lorsque l'on souhaite déterminer les coefficients de transport d'un système (conductivité thermique, diffusion, viscosité) partant d'une description microscopique. Les coefficients de transport mesurent la réponse du système par rapport à une petite perturbation. Il existe plusieurs approches pour calculer les coefficients de transport notamment :

- (a) des méthodes d'équilibre, reposant sur la formule de Green–Kubo [34, 62], qui permettent de relier une propriété de transport (typiquement la viscosité de cisaillement) à une intégrale en temps infini de l'autocorrélation d'une propriété dérivée ;
- (b) des méthodes transientes, pour lesquelles on perturbe un système initialement à l'équilibre, et on étudie le retour à l'équilibre en simulant explicitement la dynamique du système [52, 100] ;
- (c) des méthodes hors d'équilibre en régime stationnaire (*Steady-state Non-Equilibrium Molecular Dynamic*). Dans ce cas, on impose un flux dans le système (flux d'énergie, flux de quantité de mouvement, etc), et on mesure les transferts au sein du système une fois qu'un état stationnaire est établi. Enfin, on en déduit les coefficients de transport en postulant une loi macroscopique qui relie le flux au gradient de la quantité qui pilote ce flux [28, 104].

Dans ce cadre, afin de pouvoir quantifier la réponse d'un système, il est nécessaire de pouvoir quantifier les flux thermodynamiques (flux de chaleur, flux de quantité de mouvement). Contrairement à un système à l'équilibre, la connaissance de la dynamique sous-jacente est alors primordiale. Dans cette thèse, on a en grande partie considéré les méthodes hors d'équilibre en régime stationnaire et fait le lien avec les méthodes d'équilibre (*via* les résultats de réponse linéaire). Une méthode standard en dynamique hors d'équilibre consiste à perturber un système suivant une dynamique de référence (\mathcal{D}_{ref}) par un forçage extérieur $\xi \mathcal{F}_{\text{ext}}$ non gradient et indépendant du temps. On peut alors calculer la réponse à cette perturbation en mesurant le flux thermodynamique actif à l'état stationnaire (du moins s'il existe), dans le régime où ξ est petit. Par analogie avec un système macroscopique, on peut alors définir un coefficient de transport α par

$$\alpha = \lim_{\xi \rightarrow 0} \frac{\langle R \rangle_{\xi}}{\xi}, \quad (1.4)$$

où R est le flux thermodynamique activé par la perturbation et $\langle R \rangle_{\xi}$ est la moyenne de R dans l'état stationnaire. D'un point de vue physique, la dynamique de référence (\mathcal{D}_{ref}) la plus pertinente semble être la dynamique Hamiltonienne :

$$\begin{cases} dq_t = M^{-1} p_t dt, \\ dp_t = -\nabla V(q_t) dt. \end{cases} \quad (1.5)$$

Cependant, comme le forçage agit sur toutes les particules et que la dynamique (1.5) n'est pas dissipative, l'énergie du système avec un forçage extérieur ne peut que croître et l'état stationnaire ne peut être atteint. Il s'agit alors de modifier la dynamique (\mathcal{D}_{ref}) pour permettre au système d'atteindre un état stationnaire sans toutefois trop perturber la physique intrinsèque du problème. En particulier, si l'on souhaite calculer un coefficient de transport à une certaine température, il est souhaitable que la dynamique sous-jacente préserve la température. Il existe plusieurs dynamiques de thermostatage : chaînes de Nosé–Hoover [49, 85], thermostat Gaussien [28, Chapitre 3], dynamique de particules dissipative (DPD) [56, 99], équation de Langevin. D'un point de vue mathématique, l'existence et l'unicité d'une mesure invariante et *a fortiori* l'ergodicité des dynamiques thermostatées peut être une question difficile (et pour laquelle on sait parfois apporter une réponse négative [65, 66]). Une dynamique simple pour laquelle on a de bons résultats mathématiques concernant l'existence et l'unicité d'un état stationnaire et l'ergodicité est la dynamique de Langevin [93]. La dynamique de Langevin (sans forçage extérieur) s'écrit

$$\begin{cases} dq_t = M^{-1} p_t dt, \\ dp_t = -\nabla V(q_t) dt - \gamma(q_t) M^{-1} p_t dt + \sigma(q_t) dW_t, \end{cases} \quad (1.6)$$

où W_t est un mouvement Brownien standard dans \mathbb{R}^{dN} et $\gamma, \sigma \in \mathbb{R}^{dN \times dN}$ sont des matrices de frottement et de diffusion satisfaisant la relation de fluctuation-dissipation

$$\sigma(q) \sigma(q)^T = \frac{2}{\beta} \gamma(q). \quad (1.7)$$

De façon générale, l'ajout d'un mécanisme de dissipation dans la dynamique Hamiltonienne engendre *a priori* une dépendance des coefficients de transport, α , en les paramètres opératoires, γ , régissant l'intensité de cette dissipation. D'un point de vue théorique et numérique, il est alors important de comprendre comment le coefficient de transport calculé peut dépendre de ces paramètres opératoires.

Cette partie de la thèse fait l’objet de deux chapitres dans lesquels on s’intéresse au calcul numérique de la viscosité de cisaillement d’un fluide simple. Dans le chapitre 2, on présente le formalisme et les méthodes mathématiques et numériques couramment utilisées en physique statistique computationnelle. Puis, après avoir présenté les méthodes hors d’équilibre dans un cadre abstrait, on présente les grandes classes de méthodes utilisées pour calculer numériquement la viscosité (technique de Green–Kubo, méthode hors d’équilibre). Le chapitre 3 est tiré d’un article publié [P1]. Il porte sur l’analyse mathématique d’une dynamique de Langevin hors d’équilibre en régime permanent où toutes les particules ressentent la même perturbation (“bulk driven” steady state nonequilibrium dynamics) et qui prend la forme (en dimension 2)

$$\begin{cases} dq_{i,t} = \frac{p_{i,t}}{m} dt, \\ dp_{xi,t} = -\nabla_{q_{xi}} V(q_t) dt + \xi F(q_{yi,t}) dt - \gamma_x \frac{p_{xi,t}}{m} dt + \sqrt{\frac{2\gamma_x}{\beta}} dW_t^{xi}, \\ dp_{yi,t} = -\nabla_{q_{yi}} V(q_t) dt - \gamma_y \frac{p_{yi,t}}{m} dt + \sqrt{\frac{2\gamma_y}{\beta}} dW_t^{yi}, \end{cases} \quad (1.8)$$

où ξ mesure l’amplitude du forçage et F est une fonction d’une variable réelle périodique sur $L_y\mathbb{T}$ (où $\mathbb{T} = \mathbb{R}/\mathbb{Z}$ est le tore unité). On montre l’existence et l’unicité de la probabilité invariante de la dynamique. On obtient ensuite un résultat de réponse linéaire permettant de dériver une équation de conservation macroscopique satisfaite par le profil de vitesse longitudinal u_x et le terme extra-diagonal du tenseur des contraintes macroscopiques σ_{xy} sous la forme

$$(\sigma_{xy})'(Y) + \frac{\gamma_x \rho}{m} u_x(Y) = \frac{\rho}{m} F(Y), \quad Y \in L_y\mathbb{T}, \quad (1.9)$$

ρ étant la densité (constante) du système. La viscosité peut être déduite en postulant une relation de fermeture pour l’équation (1.9). La relation la plus simple est la loi de Newton

$$-\frac{\sigma_{xy}(Y)}{u'_x(Y)} = \eta(Y) \equiv \eta > 0 \text{ constant}, \quad (1.10)$$

exprimant que pour un fluide Newtonien, le tenseur des contraintes est proportionnel au taux de cisaillement. L’équation fermée pour le profil de vitesse est alors

$$-\eta u''_x(Y) + \gamma_x \frac{\rho}{m} u_x(Y) = \frac{\rho}{m} F(Y), \quad Y \in L_y\mathbb{T}. \quad (1.11)$$

La viscosité du système peut être déduite de l’équation (1.11) en analysant, par exemple, les modes de Fourier des profils de vitesse $u_x(Y)$ calculés à partir de la dynamique (1.8). En outre, on établit que les coefficients de transport calculés par cette méthode peuvent être obtenus par une formule de Green–Kubo. Ensuite, on étudie théoriquement la dépendance de la viscosité vis à vis des paramètres de dissipation de la dynamique de Langevin en adaptant et étendant des résultats obtenus dans l’étude des coefficients d’auto-diffusion [38, 39, 88]. Enfin, ces résultats sont illustrés numériquement pour différents régimes de paramètres dans le cas d’un système de Lennard–Jones 2D.

1.2.2 Modèles continus pour les électrolytes

Dans la seconde partie de cette thèse, on s’intéresse à la modélisation et à l’étude mathématique et numérique d’une classe de modèles continus pour les électrolytes confinés par un

solide négativement chargé. Selon l'échelle d'espace considérée, ces modèles permettent de décrire la porosité interfoliaire (de l'ordre du nanomètre) ou inter-particulaire (quelques dizaines de nanomètres). Les propriétés d'équilibre de ces électrolytes confinés permettent de comprendre la distribution spatiale des espèces ioniques présentes dans la porosité et d'étudier les propriétés de gonflement ou de rétractation de la roche à plus grande échelle. Les modèles que l'on considère entrent dans la classe des théories de la fonctionnelle de la densité "classique" (par opposition à la théorie quantique). La théorie de la fonctionnelle de la densité consiste à introduire un potentiel thermodynamique, l'énergie libre du système (souvent dérivé de considérations microscopiques) qui est fonction des concentrations des espèces ioniques (ou densités ioniques). Le paradigme de la théorie de la fonctionnelle de la densité est alors d'imposer des contraintes (température, volume accessible, pression, potentiel chimique) et de déterminer l'équilibre du système en minimisant l'énergie libre sous ces contraintes. En outre, de nombreux autres champs d'application peuvent être abordés à l'aide de ces modèles, par exemple en biologie, génie chimique, énergétique, *etc.*

Les variables d'intérêt des modèles de fonctionnelle de la densité sont les concentrations des espèces ioniques $(c_i)_{1 \leq i \leq M}$ (exprimées en m^{-3} et pour M espèces), ainsi que le potentiel électrostatique ψ (exprimé en V). À ce niveau de description d'un électrolyte, le solvant, de l'eau en général, est considéré comme un milieu continu et à l'équilibre, ce milieu étant uniquement caractérisé par sa constante di-électrique ε (exprimée en $\text{CV}^{-1}\text{m}^{-1}$). En général, on considère un cadre périodique dans une cellule $[0, L_*]^d$, $d \in \{2, 3\}$, et une échelle de longueur L_* (exprimée en m). La cellule élémentaire contient des inclusions Ω_S dont la frontière $\partial\Omega_S$ porte une charge négative de densité de charge surfacique $-\Sigma_S$ (exprimé en Cm^{-2} avec la convention $\Sigma_S > 0$, voir Figure 1.2, à gauche). Un deuxième cas d'intérêt est le cas des nano-canaux avec conditions périodiques en entrée et sortie (voir Figure 1.2 à droite). Dans les deux cas, les espèces ioniques

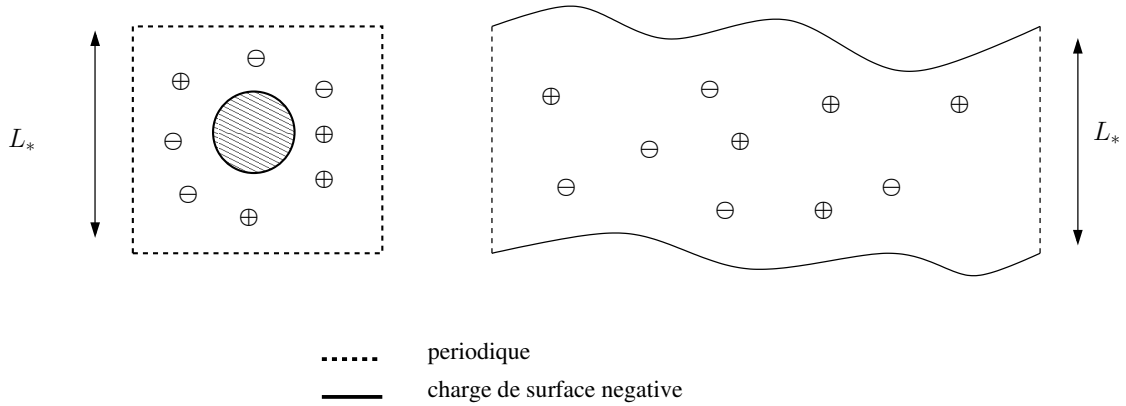


Figure 1.2. Géométrie type pour Ω : milieu périodique avec inclusion chargée (gauche) ; canal nanométrique avec murs chargés (droite)

occupent donc le volume $\Omega := [0, L_*]^d \setminus \Omega_S$. La théorie classique de la fonctionnelle de la densité des liquides ioniques est la théorie de Poisson–Boltzmann. L'état d'équilibre du système est déterminé en résolvant l'équation de Poisson non-linéaire suivante :

$$-\varepsilon \Delta \psi = \sum_{i=1}^M Z_i e \Lambda_i^{-3} e^{\beta \mu_i^{\text{bulk}}} e^{-\beta Z_i e \psi}, \quad (1.12)$$

où $e = 1.6 \times 10^{-19}$ C désigne la charge élémentaire (en Coulomb), $\{Z_i\}_{1 \leq i \leq M}$ la valence des espèces et $\{\mu_i^{\text{bulk}}\}_{1 \leq i \leq M}$ sont des potentiels chimiques (en J) donnés ou bien des multiplicateurs de Lagrange déterminés par des contraintes à préciser. Le paramètre Λ_i (exprimé en m) est la longueur de de Broglie et sera défini ultérieurement. Selon les conditions d'observation, des conditions de Dirichlet (potentiel imposé au bord) ou de Neumann (dérivée normale du potentiel égale à la charge de surface au bord) sont imposées. L'équation (1.12) signifie que le potentiel électrostatique est calculé de façon auto-consistante en supposant que les concentrations des espèces sont distribuées spatialement selon la statistique de Boltzmann :

$$\Lambda_i^3 c_i = e^{\beta \mu_i^{\text{bulk}}} e^{-\beta Z_i e \psi}. \quad (1.13)$$

Ce niveau de modélisation est une vision idéalisée de la physique, où, au niveau continu, les ions sont des charges ponctuelles interagissant au travers du potentiel de champ moyen ψ . Afin d'explicitier la dérivation de l'équation de Poisson–Boltzmann, précisons les conditions aux limites et les contraintes que nous imposons dans cette thèse. On a considéré le cas de conditions de Neumann non-homogènes/périodiques sous la forme

$$\psi \text{ est périodique sur } \partial\Omega \setminus \partial\Omega_S, \quad (1.14a)$$

$$\nabla\psi \cdot \mathbf{n} = -\frac{1}{\varepsilon} \Sigma_S \quad \text{sur } \partial\Omega_S, \quad (1.14b)$$

où \mathbf{n} est le vecteur normal extérieur à $\partial\Omega_S$. Le potentiel électrostatique étant défini à une constante additive près, on choisit de fixer $\langle \psi \rangle_\Omega = 0$ où $\langle \cdot \rangle_\Omega$ désigne la moyenne sur Ω .

Il est commode de définir l'opérateur non-local Ψ_{Σ_S} (explicitant ainsi la dépendance du potentiel électrostatique en la donnée au bord) comme étant un opérateur affine agissant sur $L^2(\Omega)$ tel que pour toute fonction $g \in L^2(\Omega)$,

$$-\varepsilon \Delta \Psi_{\Sigma_S}(g) = g - \langle g \rangle_\Omega + |\Omega|^{-1} \int_{\partial\Omega_S} \Sigma_S, \quad \text{dans } \Omega, \quad (1.15a)$$

$$\Psi_{\Sigma_S}(g) \text{ est périodique sur } \partial\Omega \setminus \partial\Omega_S, \quad (1.15b)$$

$$\nabla \Psi_{\Sigma_S}(g) \cdot \mathbf{n} = -\frac{1}{\varepsilon} \Sigma_S \quad \text{sur } \partial\Omega_S, \quad (1.15c)$$

$$\langle \Psi_{\Sigma_S}(g) \rangle_\Omega = 0. \quad (1.15d)$$

Par ailleurs, on a considéré le cas de contraintes canoniques sur les concentrations, consistant à fixer la moyenne dans Ω des concentrations sous la forme

$$\langle c_i \rangle_\Omega = c_i^{\text{bulk}}, \quad i = 1, \dots, M. \quad (1.16)$$

Les concentrations c_i^{bulk} sont données de sorte que la relation d'électro-neutralité globale suivante soit satisfaite

$$\sum_{i=\pm} Z_i e c_i^{\text{bulk}} = \frac{1}{|\Omega|} \int_{\partial\Omega_S} \Sigma_S, \quad (1.17)$$

exprimant le fait que les cations et les anions compensent la charge de surface négative portée par le solide Ω_S . On observe alors qu'en minimisant l'énergie libre suivante

$$\mathcal{F}_{\text{PB}}(c) := \sum_{i=1}^M \left\{ \int_{\Omega} \beta^{-1} c_i \left(\log(\Lambda_i^3 c_i) - 1 \right) \right\} + \frac{1}{2} \left(\int_{\Omega} \rho(c) \Psi_{\Sigma_S}(\rho(c)) - \int_{\partial\Omega_S} \Sigma_S \Psi_{\Sigma_S}(\rho(c)) \right). \quad (1.18)$$

on peut obtenir la solution de l'équation de Poisson–Boltzmann [71, 72]. Dans l'équation (1.18), $\rho(c)$ est la densité de charge

$$\rho(c) = \sum_{i=1}^M Z_i e c_i. \quad (1.19)$$

En effet, sous la condition (1.17), on montre formellement qu'un point critique de (1.18) est tel que le potentiel électro-chimique défini par

$$\mu_i^{\text{el}}(\psi, c) := \beta^{-1} \log(\Lambda_i^3 c_i) + Z_i e \psi, \quad (1.20)$$

satisfait l'équation

$$\mu_i^{\text{el}}(\Psi_{\Sigma_S}(\rho(c)), c) = \mu_i^{\text{bulk}}, \mu_i^{\text{bulk}} \in \mathbb{R}, i = 1, \dots, M, \quad (1.21)$$

les constantes μ_i^{bulk} étant les multiplicateurs de Lagrange associés à la contrainte (1.16). On vérifie alors formellement que résoudre l'équation de Poisson–Boltzmann (1.12) revient à minimiser sous contrainte la fonctionnelle (1.18), puis à inverser l'équation d'Euler–Lagrange (1.21) associée à ce problème de minimisation pour obtenir l'équation (1.13).

L'énergie libre (1.18) est la somme de termes idéaux décrivant, au niveau macroscopique, l'énergie libre d'un gaz parfait multi-espèces et le terme d'interaction électrostatique de champ moyen. Cette description est dite idéale dans le sens où elle néglige les corrélations entre les ions et en particulier les corrélations électrostatiques dues à la taille des ions et les effets d'exclusion stérique aux hautes concentrations. En particulier, cette description idéalisée s'avère efficace dans le régime dilué des basses concentrations, où les effets de taille peuvent être négligés, mais peut s'avérer insuffisante pour décrire les phénomènes physiques lorsque le confinement est nanométrique pour des solutions concentrées, en particulier lorsque la charge de surface extérieure est relativement importante (ce qui est le cas pour l'argile où $\Sigma_S = 0.13 \text{ Cm}^{-2}$).

Une approche qui est souvent considérée afin d'enrichir la théorie de Poisson–Boltzmann consiste à incorporer des corrections modélisant l'écart à l'idéalité dans la fonctionnelle de Poisson–Boltzmann [13, 31, 40, 78, 84]. Ce programme peut être accompli en partant d'une description microscopique enrichie. Une approche consiste à considérer le modèle primitif des liquides ioniques dans lequel les ions sont des sphères dures chargées de diamètre σ . Ces corrections sont calculées au coeur du milieu, le “bulk”, (*i.e* loin de toute interface et lorsque les effets de bord sont négligeables) par le biais de la théorie des fonctions de distribution radiale $(g_{i,j})_{1 \leq i, j \leq M}$ décrivant la statistique configurationnelle des ions selon les différents types présents dans le système. Les fonctions de distribution radiale sont calculées par le biais de la théorie d'Ornstein–Zernike reliant les fonctions de corrélation directe et indirecte [41]. Ces équations ne sont pas fermées et requièrent une approximation pour pouvoir être résolues soit analytiquement (fermeture Percus–Yevick, ou Mean spherical approximation de Waisman et Lebowitz [63], [64] et son extension par Blum [10]), soit numériquement (théorie hyper netted chain (HNC)). Dans certains cas, la résolution analytique de ces équations a pu être effectuée donnant lieu à des expressions approchées des corrections f_{corr} (dues aux corrélations) à la densité d'énergie libre.

L'idée est ensuite d'incorporer ces corrections du bulk dans l'énergie libre totale du système confiné et inhomogène, de sorte que pour une densité d'énergie libre bulk f , l'énergie libre s'écrit

$$\mathcal{F}(c) := \int_{\Omega} f(c) + \frac{1}{2} \left(\int_{\Omega} \rho(c) \Psi_{\Sigma_S}(\rho(c)) - \int_{\partial\Omega_S} \Sigma_S \Psi(\rho(c)) \right), \quad (1.22)$$

où

$$f(c) = \left\{ \sum_{i=1}^M \beta^{-1} c_i \left(\log(\Lambda_i^3 c_i) - 1 \right) \right\} + f_{\text{corr}}(c). \quad (1.23)$$

Ce traitement des termes d'excès de l'énergie libre est local dans le sens où la fonctionnelle d'énergie libre est la somme de l'intégrale d'une densité d'énergie libre et du terme de champ moyen [35]. On montre alors formellement qu'un minimiseur de \mathcal{F} est tel que le potentiel électrochimique non-idéal de l'espèce i défini par

$$\mu_i^{\text{el}}(\psi, c) := \beta^{-1} \log(\Lambda_i^3 c_i) + \beta^{-1} \log(\gamma_i(c)) + Z_i e \psi, \quad (1.24)$$

vérifie l'équation

$$\mu_i^{\text{el}}(\Psi_{\Sigma_S}(\rho(c)), c) = \mu_i^{\text{bulk}}, \mu_i^{\text{bulk}} \in \mathbb{R}, i = 1, \dots, M. \quad (1.25)$$

Le nombre sans dimension $\gamma_i(c)$ est le coefficient d'activité de l'espèce i et est donné par la formule

$$\log(\gamma_i(c)) = \beta \frac{\partial f_{\text{corr}}}{\partial c_i}(c), \quad i = 1, \dots, M. \quad (1.26)$$

D'un point de vue physique, la densité d'énergie libre bulk f_{corr} est la somme de deux contributions et s'écrit

$$f_{\text{corr}}(c) := f_{\text{Coul}}(c) + f_{\text{HS}}(c). \quad (1.27)$$

Le premier terme provient des corrélations électrostatiques et est, en général, une fonction concave des concentrations $c = \{c_i\}_{1 \leq i \leq M}$ se comportant comme $-c_i^{\frac{3}{2}}$ quand $c_i \rightarrow 0$. Le second terme, dit de sphères dures, rend compte du phénomène d'exclusion stérique et est, en général, une fonction convexe des concentrations qui tend vers l'infini quand $c_i \rightarrow +\infty$ (où même pour des valeurs finies de c_i). Enfin, on remarque que le terme idéal

$$\left\{ \sum_{i=1}^M \beta^{-1} c_i \left(\log(\Lambda_i^3 c_i) - 1 \right) \right\} \quad (1.28)$$

est une fonction convexe des concentrations. La densité d'énergie libre bulk f est donc, en général, la somme de trois contributions : deux contributions convexes et une concave. La fonction f_{corr} dépend des paramètres physiques du système, en particulier le diamètre des ions σ ainsi que la température T . On peut distinguer deux cadres dans l'étude des fonctionnelles du type (1.22). Un premier cadre est celui dans lequel la convexité du terme idéal et du terme de sphères dures compense la concavité des corrélations électrostatiques ("grand" diamètre des ions à température fixée). On parlera dans cette thèse de non-idéalité modérée. Le second cadre est celui où les corrélations électrostatiques dominent les deux termes convexes à basse concentration (en particulier pour les petits diamètres d'ions à température fixée). Cette situation conduit à une rupture de convexité si bien que la densité d'énergie libre bulk f a l'allure générale d'un potentiel double puits. On parlera dans cette thèse de non-idéalité forte. La conséquence physique de ce phénomène est la coexistence de deux phases par analogie au problème de transition liquide-vapeur du gaz de Van der Waals. Ici, chacune des deux phases correspond à un intervalle de valeurs disjoint que peuvent prendre les concentrations.

Cette partie de la thèse fait l'objet de trois chapitres. Le chapitre 4 est un chapitre introductif de modélisation. On y détaille le cadre mathématique dans lequel les études théoriques et numériques sont menées puis on y présente une dérivation formelle des fonctionnelles

du type (1.22). Le chapitre 5 est tiré d'un article publié [P2]. Il traite de l'analyse du cas modérément non-idéal. On y démontre l'existence et l'unicité des concentrations et du potentiel électrostatique satisfaisant l'équation de conservation du potentiel électro-chimique

$$\left\{ \mu_i^{\text{el}}(\psi, c) \right\}_{i=\pm} \text{ est constant sur } \Omega, \quad (1.29)$$

dans le cas de deux espèces (des cations et des anions). La preuve repose sur l'existence d'un point selle d'une fonctionnelle \mathcal{E} concave-convexe des concentrations et du potentiel électrostatique ainsi que sur l'obtention de bornes positives inférieures et supérieures uniformes en espace pour les concentrations. Des simulations numériques basées sur la résolution des équations d'Euler-Lagrange associées au point-selle de \mathcal{E} sont présentées. Les hypothèses assurant la convexité en c de la densité d'énergie libre bulk sont testées numériquement dans le cas où l'énergie libre résultant des corrélations électrostatiques est évaluée grâce à l'approximation sphérique moyenne (MSA). Enfin, le chapitre 6 traite du cas fortement non-idéal et est l'objet d'une publication en cours d'achèvement [Pr1]. On s'intéresse à l'étude numérique du cas où la densité d'énergie libre n'est plus une fonction convexe des concentrations, ce qui conduit à la coexistence de deux phases (l'une appelée phase diluée et l'autre phase condensée). Il s'agit alors de déterminer l'équilibre thermodynamique. On présente un problème régularisé consistant à chercher un minimiseur de l'enveloppe convexe de \mathcal{F} en utilisant une méthode de viscosité évanescence. Les concentrations présentent alors une discontinuité au niveau d'une interface séparant la phase diluée de la phase condensée. La méthode numérique permettant de calculer une solution approchée est détaillée. Enfin, par le biais de simulations numériques du cas à une espèce (contre-ions multivalents), on a étudié la sensibilité des propriétés d'équilibre (concentration, pression osmotique) aux paramètres géométriques du système (simulations 1D et 2D) pour des charges de surface relativement élevées. Enfin, une approche numérique est proposée dans le cas d'un électrolyte binaire et symétrique ($Z_+ = -Z_-$).

1.3 Liste de publications

1.3.1 Liste des articles parus dans des revues à comité de lecture

- [P1] R. Joubaud and G. Stoltz. Nonequilibrium shear viscosity computations with langevin dynamics. *Multiscale Model. Simul.*, 10 :191–216, 2012.
- [P2] A. Ern, R. Joubaud, and T. Lelièvre. Mathematical study of non-ideal electrostatic correlations in equilibrium electrolytes. *Nonlinearity*, 25 :1635–1652, 2012.

1.3.2 Article en préparation

- [Pr1] R. Joubaud, O. Bernard, A. Ern, B. Rotenberg, and P. Turq. Phase separation in highly charged confined ionic systems. *In preparation*.

1.3.3 Autres travaux

- [A1] A. Ern, R. Joubaud, and T. Lelièvre. Numerical study of a thin liquid film flowing down an inclined wavy plane. *Physica D*, 240 :1714–1723, 2011.
- [A2] F. Casenave, M. Ghatassi, and R. Joubaud. A multiscale problem in thermal science. *ESAIM Proc.*, 2012. in press.

Computing transport coefficients from microscopic models

Some elements of statistical mechanics and molecular dynamics

2.1	Computational statistical mechanics	16
2.1.1	Microscopic description of the system	16
2.1.2	Potential energy	16
2.1.3	Thermodynamic ensembles	18
2.1.4	The equilibrium Langevin dynamics	20
2.1.5	Numerical aspects	24
2.2	Nonequilibrium dynamics and Green-Kubo formula	27
2.2.1	Nonequilibrium dynamics	28
2.2.2	Invariant measure of the nonequilibrium dynamics	28
2.2.3	Linear response and correlation functions	29
2.2.4	Discussion on the choice of the underlying dynamics	30
2.3	Computation of transport coefficients: the example of the shear viscosity	31
2.3.1	Some elements of continuous fluid mechanics	31
2.3.2	Equilibrium methods	32
2.3.3	Steady state nonequilibrium	35
2.3.4	Transient nonequilibrium dynamics	39

It is nowadays common to characterize the properties of materials by relying to a description at the atomistic level, using the theory of statistical mechanics. In the study of fluids at nanometric scales, it is useful to resort to the statistical mechanics approach since experiments are often costly and difficult to perform, particularly in extremely confined situations. The determination of the macroscopic properties of a material given its microscopic description is the fundamental goal of statistical mechanics [8]. Macroscopic properties can be classified into two categories: (i) equilibrium properties, such as the heat capacity or the equation of state of the system (relating the pressure, the density and the temperature); and (ii) transport properties, such as the thermal conductivity or the shear viscosity. The determination of transport properties is conceptually and numerically more challenging than the determination of equilibrium properties since transport phenomena depend both on the chosen thermodynamic ensemble and on the prescribed microscopic dynamics (which has to leave the thermodynamic state of the system invariant).

The purpose of this part is the mathematical and numerical study of the methods of molecular dynamics allowing to compute transport coefficients, in particular the calculation of the shear viscosity of a fluid. This introducing chapter is organized as follows: in Section 2.1, we present the basic ideas behind computational statistical mechanics and make precise the rigorous

mathematical tools and the available results we need in the sequel. In Section 2.2, we present the methodology adopted in this thesis concerning the computation of transport coefficient. We cast in an abstract setting the method relying on nonequilibrium dynamics and relate it to the Green-Kubo formalism. Finally, in Section 2.3, we review alternative standard methods used to compute transport coefficients with an emphasis on the shear viscosity of fluids.

2.1 Computational statistical mechanics

2.1.1 Microscopic description of the system

We start by considering N atoms of different type $i = 1, \dots, \mathcal{M}$ ($N = \sum_{i=1}^{\mathcal{M}} N_i$) occupying a domain \mathcal{D} of volume $|\mathcal{D}|$ at temperature T (expressed in K). We denote by m_i the masses of the particles of type i (expressed in kg). A scale length of importance for atomic systems is the de Broglie thermal wavelength defined by:

$$A_i = \left(\frac{2\pi\beta\hbar^2}{m_i} \right)^{\frac{1}{2}}, \quad (2.1)$$

where $\hbar = 1.054 \times 10^{-34}$ J s is the reduced Planck constant, $\beta^{-1} = k_B T$ where T is the temperature (expressed in K), and $k_B = 1.381 \times 10^{-23}$ J K⁻¹ is the Boltzmann constant. If the following inequality is satisfied

$$\frac{A_i}{a_i} \ll 1, \quad (2.2)$$

where $a_i = (N_i |\mathcal{D}|^{-1})^{\frac{1}{3}}$ is the typical distance between atoms of type i , then a classical description of the matter is assumed to be sufficient [41] and quantum effect can be neglected.

The micro-state of the system is described by the positions of all atoms and their momenta $(q, p) \in \mathcal{M} \times \mathbb{R}^{dN}$ (with $d = 2, 3$) where $\mathcal{M} = \mathcal{D}^N$ is the space of positions. For periodic system, such as the ones we consider, $\mathcal{D} = L_x \mathbb{T} \times L_y \mathbb{T} \times L_z \mathbb{T}$ (for $d = 3$) where $\mathbb{T} = \mathbb{R}/\mathbb{Z}$ is the one-dimensional torus. The energy of the microstate is given by the Hamiltonian function of the system, which can be decomposed as a sum of kinetic and potential energies:

$$H(q, p) = \frac{1}{2} p^T M^{-1} p + V(q), \quad (2.3)$$

where $M = \text{Diag}(m_1 I_d, \dots, m_N I_d) \in \mathbb{R}^{dN \times dN}$ is the mass matrix.

2.1.2 Potential energy

The potential energy contains all the physics of the system and can be decomposed as:

$$V(q) = \mathcal{V}_{\text{inter}}(q) + \mathcal{V}_{\text{ext}}(q),$$

where $\mathcal{V}_{\text{inter}}$ accounts for the interactions between the particles and \mathcal{V}_{ext} is an external potential applied to the system. In our context, the potential \mathcal{V}_{ext} induces a confinement so that the

system is inhomogeneous. We assume for simplicity that the potential $\mathcal{V}_{\text{inter}}$ is the sum of pair interactions,

$$\mathcal{V}_{\text{inter}}(q_1, \dots, q_N) = \sum_{1 \leq i < j \leq N} v(|q_i - q_j|), \quad (2.4)$$

for a smooth function v . For the applications we consider, when describing condensed matter, the most widely used interaction potentials are Lennard–Jones (LJ), hard-sphere, and the Coulomb potential. For molecular fluids, the interactions between the atoms in a molecule, have to be modelled as well. For example the Lennard–Jones potential is given by the formula

$$v_{\text{LJ}}(r) = 4\varepsilon_{\text{LJ}} \left(\left(\frac{d_{\text{LJ}}}{r} \right)^{12} - \left(\frac{d_{\text{LJ}}}{r} \right)^6 \right). \quad (2.5)$$

In general, modifications of an empirical potential have to be performed. When periodic bound-

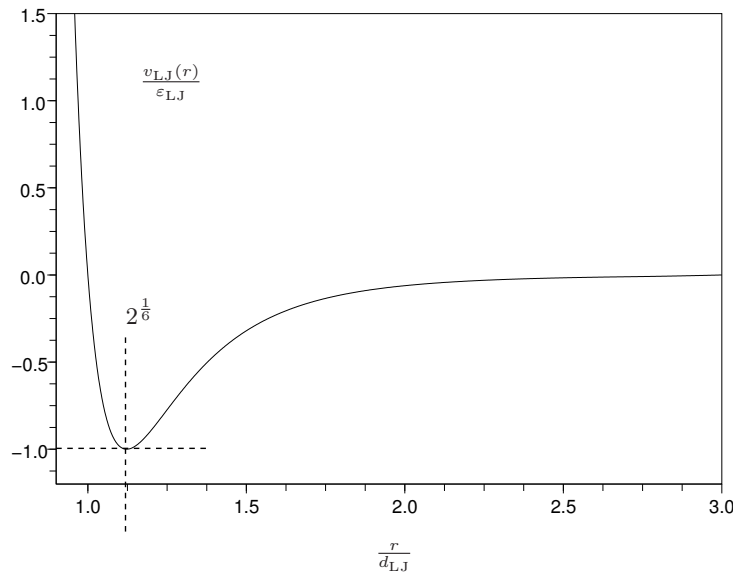


Fig. 2.1. Lennard–Jones interaction energy as a function of the nondimensional distance $\frac{r}{d_{\text{LJ}}}$.

ary conditions are enforced, a truncation at finite distance r_{cut} is needed (see discussion in § 2.1.5). The second modification accounts for the singularity at the origin of the potential. In practice, we may determine a level of potential energy for which we can make a truncation of the empirical potential v .

The Lennard–Jones potential depends on two parameters, namely ε_{LJ} and d_{LJ} , respectively a unit of energy (J) and a length (the diameter of the atom in m). To characterize the system, we also need a reference mass m^* (expressed in kg). For instance, in the case of argon fluid, we have $\varepsilon_{\text{LJ}}/k_{\text{B}} = 120\text{K}$, so that the energy per atom is $\varepsilon_{\text{LJ}} = 1.66 \times 10^{-21}$ J, the diameter of an atom is $d_{\text{LJ}} = 3.405 \text{ \AA}$, and the mass of an argon atom is $m_{\text{LJ}} = 6.64 \times 10^{-26}$ kg. For convenience, we will work with the nondimensional form of the potential energy

$$\overline{v}_{\text{LJ}}(r) = 4 \left(\left(\frac{1}{r} \right)^{12} - \left(\frac{1}{r} \right)^6 \right). \quad (2.6)$$

We will express every quantity in Lennard–Jones units, and rescale every quantity with these characteristic values. For example, a time unit (expressed in s) is given by

$$t^* = \sqrt{\frac{m_{\text{LJ}}}{\varepsilon_{\text{LJ}}}} d_{\text{LJ}} = 2.154 \times 10^{-12} \text{ s}. \quad (2.7)$$

Table 2.1 gives the correspondence from Lennard–Jones units to real units for common physical quantities.

Physical quantity	Reference value
Temperature	120 K
Energy	1.66×10^{-21} J
Pressure	42 MPa
Density	1681 kg m^{-3}
Viscosity	$9.06 \times 10^{-5} \text{ Pa s}^{-1}$

Table 2.1. Various physical quantities evaluated with the reference LJ units.

2.1.3 Thermodynamic ensembles

In this part of the thesis, we only consider bulk, homogeneous, monatomic fluids so that there is only one type of particle ($\mathcal{M} = 1$) and that no external potential confines the system ($\mathcal{V}_{\text{ext}} = 0$). Moreover, we express all the physical quantities in reduced Lennard–Jones units.

The macro-state of the system is described by some probability measure ν depending on the thermodynamic conditions of observation (energy, number of particles volume, fixed exactly or in average, *etc*). A macroscopic quantity \mathcal{A} of interest (*e.g.* energy, pressure, temperature) can be computed by averaging an observable A (*i.e.* a function defined on $\mathcal{M} \times \mathbb{R}^{dN}$) with respect to the probability measure ν :

$$\mathcal{A} = \int_{\mathcal{M} \times \mathbb{R}^{dN}} A(q, p) \nu(dq, dp). \quad (2.8)$$

For example, we might be interested in computing the pressure of a system in which case the observable is

$$P(q, p) = \frac{1}{d|\mathcal{D}|} \sum_{j=1}^N \frac{p_j^2}{m_j} - q_j \cdot \nabla_{q_j} V(q), \quad (2.9)$$

or the kinetic temperature of a system, associated to the observable

$$T_{\text{kin}}(q, p) = \frac{1}{dN} \sum_{j=1}^N \frac{p_j^2}{m_j}. \quad (2.10)$$

One standard probability measure that appears in molecular dynamics is the micro-canonical measure ν_{NVE} corresponding to the NVE ensemble (fixed number of particles N , accessible volume and energy). This measure naturally appears as the least biased probability measure with fixed energy and is an invariant measure of the classic Hamiltonian dynamics:

$$\begin{cases} dq_t = M^{-1}p_t dt, \\ dp_t = -\nabla V(q_t) dt. \end{cases} \quad (2.11)$$

A rigorous definition of the micro-canonical measure can be found in [67].

Another standard choice for the probability measure ν is to consider the canonical measure NVT (fixed number of particles N , accessible volume V and temperature T) given by the formula

$$\nu_{\text{NVT}}(dq, dp) = Z^{-1} e^{-\beta H(q,p)} dq dp, \quad Z = \int_{\mathcal{M} \times \mathbb{R}^{dN}} e^{-\beta H(q,p)} dq dp. \quad (2.12)$$

This measure is the “least biased” under the constraint that the energy is fixed in average. Let us give a mathematical argument about the derivation of the canonical measure. Such derivation is performed in [8, 67] using a variational principle, by maximizing the statistical entropy

$$S(\rho) = - \int_{\mathcal{M} \times \mathbb{R}^{3N}} \rho(q, p) \log(\rho(q, p)) dq dp, \quad (2.13)$$

under the constraints

$$\rho \geq 0, \quad \int_{\mathcal{M} \times \mathbb{R}^{3N}} \rho(q, p) = 1, \quad \int_{\mathcal{M} \times \mathbb{R}^{3N}} H(q, p) \rho(q, p) = E, \quad (2.14)$$

for some energy level E . The interpretation of S is that it measures the disorder of the system. Other thermodynamic ensembles can be considered. In the context of the modelling of fluids, the grand canonical ensemble μVT is relevant (fixed chemical potential μ and fluctuating number of particles) or also isobaric ensembles μVT or NPT (more details can be found for example in [4], [41], [67]).

Remark 1 (*Thermodynamic limit*) *To end up the passage from the microstate to the macrostate, one has to consider the thermodynamic limit of an observable, that is $|\mathcal{D}| \rightarrow +\infty$ with fixed thermodynamic constraints (ρ, T) in the case of the canonical ensemble. The definition of a macroscopic quantity such as energy density, temperature or pressure of a system has to be understood in this sense. The interest of the thermodynamic limit is that in this regime, it is common to consider, in molecular dynamics, that all the thermodynamic ensembles are equivalent [94]. In practice, in the simulations, we choose a number N of particles sufficiently large so that the thermodynamic limits is numerically achieved.*

Let us now turn to the difficulties encountered in the evaluation of the integral (2.8). First, the set of integration is high-dimensional so that standard quadrature rules cannot be used. One has to resort to numerical methods that circumvent the curse of dimensionality, namely methods relying on ergodic averages:

$$\lim_{s \rightarrow \infty} \frac{1}{s} \int_0^s A(q_t, p_t) dt = \mathcal{A}, \quad (2.15)$$

where the trajectory $(q_t, p_t)_{t \geq 0}$ is generated by some dynamics ergodic with respect to the probability measure ν . Second, the ergodic limit in (2.15) may be difficult to obtain (s should be very large) in particular for metastable dynamics. We refer to [67] for an overview of the sampling method used in molecular simulation. In the sequel, we focus on the Langevin dynamics which allows to sample the canonical measure (2.12).

2.1.4 The equilibrium Langevin dynamics

As we have seen previously, the Hamiltonian dynamics (2.11) allows to sample the micro-canonical measure but since this dynamics preserves energy, the Hamiltonian dynamics is not ergodic with respect to the canonical measure since to obtain the correct temperature, several levels of energy have to be visited.

A dynamics which is ergodic with respect to the canonical measure is the Langevin dynamics:

$$\begin{cases} dq_t = M^{-1}p_t dt, \\ dp_t = -\nabla V(q_t)dt - \gamma(q_t)M^{-1}p_t dt + \sigma(q_t)dW_t, \end{cases} \quad (2.16)$$

where W_t is a standard \mathbb{R}^{dN} Brownian-motion and γ and σ are, in general, position dependant $\mathbb{R}^{dN \times dN}$ matrices. The Langevin dynamics (2.16) preserves the canonical measure ν_{NVT} if the following fluctuation dissipation relationship holds

$$\sigma(q)\sigma(q)^T = \frac{2}{\beta}\gamma(q), \quad \gamma(q) > 0. \quad (2.17)$$

Basically the term $-\gamma M^{-1}p_t dt$ dissipates energy while the fluctuation term σdW_t brings enough energy for the system to stabilize at the desired kinetic temperature T . In order to avoid irrelevant technical issues, in this thesis, we make the following assumption:

Assumption 1 *The potential V belongs to $C^\infty(\mathcal{D}^N)$ and unless explicitly specified, we consider $\gamma := \text{diag}(\gamma_x \mathbf{I}_N, \gamma_y \mathbf{I}_N, \gamma_z \mathbf{I}_N)$ (for $d = 3$).*

Also, to simplify the notations, we consider that all the masses are identical ($m_i = m, \forall i \in \{1, \dots, N\}$). To make precise the fact that the Langevin dynamics is ergodic with respect to the canonical measure, we introduce the infinitesimal generator of the equilibrium Langevin process $(q_t, p_t)_{t \geq 0}$ satisfying (2.16):

$$\mathcal{A}_0 = \mathcal{A}_{\text{ham}} + \mathcal{A}_{\text{thm}},$$

where

$$\mathcal{A}_{\text{ham}} = \frac{p}{m} \cdot \nabla_q - \nabla V(q) \cdot \nabla_p,$$

is the infinitesimal generator of the Hamiltonian dynamics (2.11) and

$$\mathcal{A}_{\text{thm}} = \sum_{\alpha=x,y} \gamma_\alpha \left(-\frac{p_\alpha}{m} \cdot \nabla_{p_\alpha} + \frac{1}{\beta} \Delta_{p_\alpha} \right) = \frac{e^{\beta H}}{\beta} \sum_{\alpha=x,y} \gamma_\alpha \text{div}_{p_\alpha} \left(e^{-\beta H} \nabla_{p_\alpha} \cdot \right),$$

is the generator of the Ornstein–Uhlenbeck process for momenta

$$dp_t = -\gamma M^{-1}p_t dt + \sigma dW_t. \quad (2.18)$$

In the following, we denote by

$$\psi_0 = Z^{-1} e^{-\beta H(q,p)}, \quad (2.19)$$

the density of the canonical measure where Z is the canonical partition function given by (2.12). For further purposes, it is convenient to consider the reference space $L^2(\psi_0)$ (where the measure ψ_0 is defined (2.19)), endowed with the scalar product

$$\langle f, g \rangle_{L^2(\psi_0)} := \int_{\mathcal{D}^N \times \mathbb{R}^{dN}} f(q, p) g(q, p) \psi_0(q, p) dq dp.$$

We also introduce the Hilbert space

$$\mathcal{H} = \left\{ f \in L^2(\psi_0) \mid \int_{\mathcal{D}^N \times \mathbb{R}^{dN}} f \psi_0 = 0 \right\} = L^2(\psi_0) \cap \{1\}^\perp,$$

where the orthogonality is with respect to the $L^2(\psi_0)$ scalar product. Define also the adjoint operator on $L^2(\psi_0)$ of the generator:

$$\mathcal{A}_0^* = -\mathcal{A}_{\text{ham}} + \mathcal{A}_{\text{thm}}.$$

Let $\psi(q, t)$, being the law of the Langevin process $(q_t, p_t)_{t \geq 0}$ at time $t \geq 0$ with

$$\psi(t, \cdot) := \psi_0 f(t, \cdot). \quad (2.20)$$

Then, we can check that f is the unique solution of the Fokker-Planck equation

$$\partial_t f = \mathcal{A}_0^* f, \quad (2.21)$$

Hypoellipticity of the infinitesimal generator and stochastic analysis allow to show the existence and the uniqueness of the invariant measure of (2.16), see the work of Rey-Bellet [93]. Thus, it can be verified that ψ_0 solves the stationary Fokker-Planck equation (see for instance [93]). The uniqueness of the reference invariant measure ψ_0 means that $\text{Ker}(\mathcal{A}_0^*) = \text{Span}(\mathbf{1})$.

Remark 2 *These results are available for smooth potential since hypoellipticity requires this regularity. The singular potentials discussed in § 2.1.2 do not enter in this class since they present a singularity at the origin. The rigorous mathematical analysis of such difficult problem has been recently addressed in [19].*

We will also make use of nice properties of the operator \mathcal{A}_0 on the weighted space \mathcal{H} . Let us point out that \mathcal{A}_0 is not an elliptic operator since the diffusion acts only in the velocity variables, but still enjoys nice properties since it enters in the abstract setting of hypoellipticity and hypocoercivity [109]. For convenience of the reader, let us recall some useful results.

To state these results, we need to introduce the notion of Lie algebra. This is the vector space $L(X_0, \dots, X_m)$ associated to a family of vector fields (X_0, \dots, X_m) which is the vectorial space of operator containing $\text{Span}(X_0, \dots, X_m)$ and satisfying the stability property:

$$B \in (X_0, \dots, X_m) \implies [B, X_i] \in L(X_0, \dots, X_m), \quad i = 0, \dots, m, \quad (2.22)$$

where the Lie bracket between two operators U and V is

$$[U, V] = UV - VU. \quad (2.23)$$

Consider the stochastic differential equation

$$dx_t = b(x_t)dt + \sigma(x_t)dW_t, \quad x_t \in \mathcal{S} \subset \mathbb{R}^d \quad (2.24)$$

where $b \in \mathbb{R}^d$ is a vector valued function, $\sigma \in \mathbb{R}^d \times \mathbb{R}^n$ is matrix valued, and W_t is a standard d -dimensional Brownian motion (so that the noise does not act in all the directions), and assume that b and σ are smooth. We write the generator of (2.24) under the “sum of square” form

$$\mathcal{A}_0 := \frac{1}{2} \sum_{k=1}^d X_k^2 + X_0, \quad (2.25)$$

where

$$X_k := \sum_{i=1}^d \sigma^{i,k}, \quad k = 1, \dots, n, \quad (2.26)$$

and

$$X_0 := \sum_{i=1}^d b^i \partial_i - \sum_{i,j}^d \sum_{k=1}^n \sigma^{i,k} \partial_i (\sigma^{j,k}) \partial_j. \quad (2.27)$$

We have the following results

Theorem 1 (*Hörmander condition* [51]). *If*

$$L(X_0, \dots, X_n) = \text{Span}(\partial_1, \dots, \partial_d), \quad (2.28)$$

then \mathcal{A}_0 is hypoelliptic.

A consequence of this result is

Theorem 2 (*Sufficient conditions for ergodicity* [60]). *Assume there exists a strong solution of (2.24) for all times $t \geq 0$ and that condition (2.28) holds true. Then if a stationary probability distribution π exists, then pathwise ergodicity holds for any initial condition x_0 :*

$$\lim_{s \rightarrow +\infty} \frac{1}{s} \int_0^s \varphi(x_t) dt = \int_{\mathcal{S}} \varphi d\pi, \quad \text{almost surely.} \quad (2.29)$$

The application we consider is $x_t = (q_t, p_t) \in \mathcal{D}^N \times \mathbb{R}^{3N}$, the Langevin process, with generator \mathcal{A}_0 for which we can verify Hörmander condition ([67, Section 2.2.3.1]).

Another useful tool in the study of the Langevin dynamics is the theory of hypocoercivity [109]. This theory concerns evolution equations of the form

$$\partial_t f + Lf = 0, \quad (2.30)$$

in the case when

$$L = A^*A + B, \quad (2.31)$$

in a Hilbert H space where A^* is the adjoint of the operator A with respect to the H scalar product denoted (\cdot, \cdot) here. In Chapter 3, we mainly use the result [109, Theorem 18], and we refer to this work. The operator A and B are, in general, first order differential operator with smooth coefficients. The operator B is assumed to be antisymmetric ($B^* = -B$, the adjoint being computed with respect to the H scalar product) whereas the operator A^*A is symmetric. The situation is well illustrated with the infinitesimal generator of the Langevin processing for which $H = H^1(\psi_0) \cap \mathcal{H}$, $A^*A = \mathcal{A}_{\text{thm}}$, and $B = \mathcal{A}_{\text{ham}}$. Let us mention the following important result providing hypocoercivity for the infinitesimal generator of the Langevin process:

Theorem 3 (*Sufficient condition for hypocoercivity* [109, Section I.4, Theorem 18]). Consider a linear operator $L = A^*A + B$, B antisymmetric, and define $C := [A, B]$. Assume the existence of constants a_1, a_2 such that

- (i) A and A^* commute with C , A commutes with A (i.e. each A_i commutes with each A_j);
- (ii) $[A, A^*]$ is a_1 -bounded relatively to I and A ;
- (iii) $[B, C]$ is a_2 -bounded relatively to A, A^2, C and AC ;

Then there is a scalar product $((\cdot, \cdot))$ on H , which defines a norm equivalent to the H norm, such that

$$\forall h \in H, ((h, Lh)) \geq K \left(\|Ah\|^2 + \|Ch\|^2 \right), \quad (2.32)$$

for some constant $K > 0$, only depending on a_1, a_2 . If, in addition, $A^*A + C^*C$ is κ -coercive i.e

$$\forall h \in H, (h, (A^*A + C^*C)h) \geq \kappa \|h\|^2, \quad (2.33)$$

for some $\kappa > 0$, then there is a constant $\lambda > 0$, only depending on a_1, a_2 and κ , such that

$$\forall h \in H, ((h, Lh)) \geq \lambda((h, h)). \quad (2.34)$$

In particular, L is hypocoercive in H :

$$\|e^{-tL}\|_{H \rightarrow H} \leq ce^{-\lambda t}, \quad (c < \infty), \quad (2.35)$$

where both λ and c can be estimated explicitly in terms of upper bounds on a_1, a_2 , and a lower bound on κ .

This theorem in particular gives a nice coercivity estimate of the operator L under a suitable modification of the scalar product on H (2.34) together with the exponential decay of the semi group e^{-tL} in the norm associated to this modified scalar product (2.35). Note that the difference between coercivity and hypocoercivity lies in the presence of a constant $0 < c < \infty$ in the estimate (2.35). In the case where the operator L is coercive, we would obtain the estimate (2.35) with constant $c = 1$. The issue with estimate (2.35) for the hypocoercive operator L is that the constant c might be very large.

In the case of the infinitesimal generator of the Langevin process, we have

$$\mathcal{A}_{\alpha, \text{thm}} = -\frac{1}{\beta} \sum_{i=1}^N (\partial_{p_{\alpha i}})^* \partial_{p_{\alpha i}} = A^*A. \quad (2.36)$$

A simple calculation shows that

$$C = [\partial_{p_{\alpha i}}, \mathcal{A}_{\text{ham}}] = \frac{1}{m} \partial_{q_{\alpha i}}, \quad (2.37)$$

so that conditions (i-iii) in Theorem 3 are easily verified (see [109, Section I.7] for a detailed study of this case).

Others technical results that we need are boundedness and compactness properties of the operator \mathcal{A}_0^{-1} on weighted Sobolev spaces $H^k(\psi_0) \cap \mathcal{H}$, $k \in \mathbb{N}$. Under the assumption that the potential V is smooth on the compact position space \mathcal{D}^N , we have the following results

- (i) The operator \mathcal{A}_0^{-1} is a compact operator from \mathcal{H} to \mathcal{H} ([46], [25]);
- (ii) For any integer $m \geq 0$, \mathcal{A}_0^{-1} is a bounded operator from $H^k(\psi_0) \cap \mathcal{H}$ to $H^k(\psi_0) \cap \mathcal{H}$ ([103]).

These properties are very useful in the proofs performed in Chapter 3 and are inherent to the Langevin dynamics.

2.1.5 Numerical aspects

Let us now turn to the numerical methods used to discretize the Langevin dynamics, and more generally methods relying on using a dynamics to compute static and transport properties. Traditionally, steady equilibrium properties in the canonical ensemble can be computed owing to Monte Carlo methods ([43, 77]) and require generally only a statistical information on the configurational space since velocities are independent Gaussian random variables, and are therefore straightforward to sample. The Langevin dynamics provides an efficient numerical method to compute equilibrium properties owing to discretized version of formula (2.15) but is not especially necessary.

There are roughly three steps to follow when running a molecular simulation:

- (i) Definition and approximations used to compute the forces $\nabla V(q)$, since in general V is a complex function of all the positions $q \in \mathbb{T}^{3N}$ with N large and the choice of the physical conditions of observation (density of the system, temperature *etc*);
- (ii) Time integration of the dynamics with dedicated algorithms preserving (approximatively) the invariants of the dynamics in view of computing reliable approximations of the integral (2.15);
- (iii) Careful post-processing of the obtained results (that can be long time trajectory, self-correlations functions, localized observables). This step requires also an analysis of the statistical and numerical errors induced by the noise in the dynamics (2.16).

On the computational side, the most computationally intensive part is the evaluation of the forces at each time step which requires a special care in the implementation. When dealing with periodic boundary conditions, one can resort to truncated potential energy when the long range tail is not dominant. This procedure is systematically performed for the Lennard–Jones system (see Figure 2.1). Practitioners resort to long range corrections for standard observables (such as pressure or energy) by analytical computations of the tail integral, assuming that the particles decorrelate for large distances [4, Chapter II, Section 8]. For long range potentials such as Coulomb interaction potentials, encountered in the study of water models or charged system, the decay of the energy versus the distance is slow (r^{-1}) and computations of the force including the periodic replicas of the particles have to be considered. Ewald type summations methods are generally used to this end and allow to obtain results in good agreement with experiments. Note that the implementation of such algorithms requires quite some work and are generally performed by specialists of the domain of application so that there is a wide variety of computational code available (LAMMPS, NAMD *etc*). Most of the numerical results presented in this thesis have been obtained for a Lennard–Jones system implemented in a home-

made C++ computational code. We verified a posteriori that the methods we used are easily implementable in more sophisticated computational code (LAMMPS).

In the case of the Langevin dynamics, we take care of step (ii) owing to a standard splitting strategy. Observe that when $\gamma = 0$, the Langevin dynamics (2.16) reduces to the Hamiltonian dynamics which can be discretized using the following symplectic scheme, that is Störmer-Verlet:

$$\begin{cases} p^{n+1/2} = p^n - \frac{\delta t}{2} \nabla V(q^n), \\ q^{n+1} = q^n + \delta t p^{n+1/2}, \\ p^{n+1} = p^{n+1/2} - \frac{\delta t}{2} \nabla V(q^{n+1}). \end{cases} \quad (2.38)$$

We can see that an iteration $(q^n, p^n) \mapsto (q^{n+1}, p^{n+1})$ requires only one evaluation of the forces. The basic properties of this integrator can be found in [37].

Note now that in the case $V = 0$ and $dq_t = 0$, the Langevin dynamics reduces to the dynamics of an Ornstein–Uhlenbeck process, and thus can be integrated explicitly, so that we use the scheme

$$p^{n+1} = \alpha p^n + \sqrt{\frac{1}{\beta}(1 - \alpha)} G^n \quad (2.39)$$

where $\alpha = \exp(-\gamma\delta t)$, and G^n are independent and identically distributed standard Gaussian random variables. The numerical scheme can then be written

$$\begin{cases} p^{n+1/2} = p^n - \frac{\Delta t}{2} \nabla V(q^n), \\ q^{n+1} = q^n + \Delta t p^{n+1/2}, \\ \tilde{p}^{n+1} = p^{n+1/2} - \frac{\Delta t}{2} \nabla V(q^{n+1}), \\ p^{n+1} = \alpha \tilde{p}^{n+1} + \sqrt{\frac{1}{\beta}(1 - \alpha^2)} G^n, \end{cases} \quad (2.40)$$

Step (iii) might be considered as the crucial step in view of the application, since all the physical information will be deduced from the post-processing. A single molecular dynamics simulation provide a lot of information about the physical system of interest. It can provide long time trajectory of an observable, allowing to deduce the equilibrium properties and also self-correlation function, allowing sometime to evaluate transport coefficients. In this way, it is important to check that the system is in steady state at the end of the simulation. For example, one can check that the kinetic temperature of the system coincides with the temperature imposed by the Langevin bath. For simple systems such as Lennard–Jones system, there is an extensive bibliography about the equilibrium or transport properties and the comparison with these data is a way to validate a newly proposed computational code.

Eventually, an important issue with molecular dynamics simulation is to quantify the statistical uncertainty coming from the use of stochastic methods or from randomness in the choice of the initial conditions when deterministic dynamics are used. Assume we have run a simulation for a number of iterations N_{iter} of the scheme (2.40). Denote by $\langle A \rangle$ the average of

an observable A with respect to a thermodynamic ensemble. Assuming we estimated $\langle A \rangle$ by an ergodic average:

$$\langle A \rangle := \lim_{N_{\text{iter}} \rightarrow +\infty} \bar{A}_{N_{\text{iter}}} = \lim_{N_{\text{iter}} \rightarrow +\infty} \frac{1}{N_{\text{iter}}} \sum_{n=0}^{N_{\text{iter}}-1} A(q^n, p^n), \quad (2.41)$$

and that a Law of large number holds true, we define the asymptotic variance σ^2 as

$$\sigma^2(A) := \left(\langle A^2 \rangle - \langle A \rangle^2 \right) + 2 \sum_{n=1}^{+\infty} \mathbb{E}_{\tilde{\nu}} \left((A(q^0, p^0) - \langle A \rangle) (A(q^n, p^n) - \langle A \rangle) \right). \quad (2.42)$$

The asymptotic variance decomposes as the sum of the intrinsic variance $\langle A^2 \rangle - \langle A \rangle^2$ (that we would obtain if the $A(q^n, p^n)$ were independent and identically distributed) and the correlation between the sampled configuration (the infinite series). The notation $\mathbb{E}_{\tilde{\nu}}$ corresponds to the average of a random variable distributed according to the numerical approximation $\tilde{\nu}$ of the invariant probability measure ν (note that in general there is non-zero bias between $\tilde{\nu}$ and ν due to the time-step error, nevertheless we do not discuss these issues here). In order to quantify the statistical uncertainty in the simulations, there are several strategies to compute an approximation of the correlation. In this thesis we considered two techniques to estimate the variance:

- Multiple replica strategy, where M independent trajectories are run and the variance is estimated by an empirical average over the realizations:

$$\Sigma_{N_{\text{iter}}, M}^{\text{replica}} := \frac{N_{\text{iter}}}{M} \sum_{k=0}^{M-1} \left(\bar{A}_{N_{\text{iter}}}^k - \frac{1}{M} \sum_{p=1}^{M-1} \bar{A}_{N_{\text{iter}}}^p \right)^2. \quad (2.43)$$

This estimation being more accurate for a large number M of replicas (owing to the Central limit theorem). The corresponding estimator for the asymptotic variance is then

$$\sigma_{\text{est},1}^2(A) := \lim_{N_{\text{iter}} \rightarrow +\infty} \lim_{M \rightarrow +\infty} \Sigma_{N_{\text{iter}}, M}^{\text{replica}}. \quad (2.44)$$

- Block averaging, where only one trajectory of size $N_{\text{iter}} := NM$ is integrated, where M is the number of block and N the number of points within a block. The variance is computed as follow: Defining the average of A within the k -th block,

$$\bar{A}_N^k := \frac{1}{N} \sum_{j=(k-1)N+1}^{kN} A(q^j, p^j), \quad k = 1, \dots, M, \quad (2.45)$$

the variance is estimated by

$$\Sigma_{N_{\text{iter}}, M}^{\text{BA}} := \frac{N}{M} \sum_{k=1}^M \left(\bar{A}_N^k - \bar{A}_{N_{\text{iter}}} \right)^2. \quad (2.46)$$

This definition assumes that the averages over one block $(\langle A \rangle_N^k)_{k=1, \dots, M}$ are independent and identically distributed and that a Central limit Theorem holds within each block (see [67])

and the cited references therein). The corresponding estimator for the asymptotic variance is then

$$\sigma_{\text{est},2}^2(A) := \lim_{N_{\text{iter}} \rightarrow +\infty} \lim_{M \rightarrow +\infty} \Sigma_{N_{\text{iter}},M}^{\text{BA}}. \quad (2.47)$$

In practice, we may consider several trajectories of size $N_{\text{iter}} = 2^p = NM$ and monitor the quantity $\Sigma_{N_{\text{iter}},M}^{\text{BA}}$ for each trajectory as a function of p , so that the variance is extracted when a plateau value is reached (see Figure 2.2). Nevertheless, in most of the simulations, we extract the variance with only one trajectory.

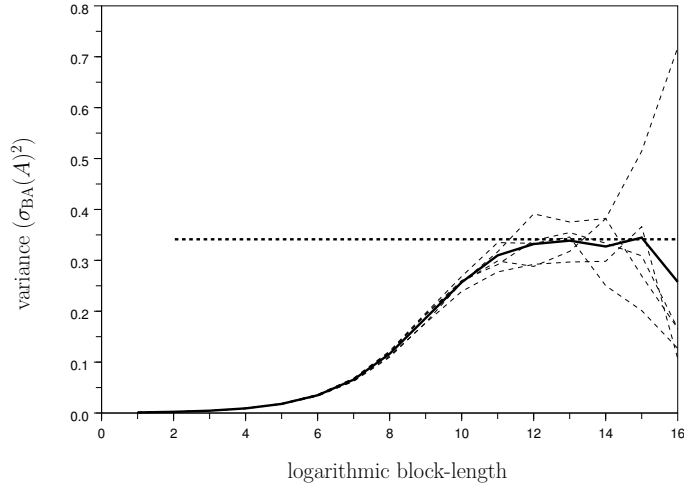


Fig. 2.2. Illustration of the block-averaging procedure for an observable of the simulations of Chapter 3. The dashed line represent several replica of the procedure. The bold line indicates the average of these replicas, and the bold dashed line exhibits the plateau value of σ_{BA}^2 .

Once an estimator of the variance is computed, a 95% confidence interval can be deduced in the form

$$I_{\text{conf}} := \left[\langle A \rangle_{N_{\text{iter}}} - 1.96 \left(\frac{\sigma_{\text{est},i}(A)}{\sqrt{N_{\text{iter}}}} \right), \langle A \rangle_{N_{\text{iter}}} + 1.96 \left(\frac{\sigma_{\text{est},i}(A)}{\sqrt{N_{\text{iter}}}} \right) \right], \quad (2.48)$$

with $\sigma_{\text{est},i}(A)$, $i = 1, 2$ estimated with either formula (2.43) or (2.46) (which are respectively approximations of (2.44) or (2.47)) thus providing an error bar (the standard deviation), which will be presented in most the numerical results.

2.2 Nonequilibrium dynamics and Green-Kubo formula

In this section, we present nonequilibrium dynamics in an abstract setting and how it can be related to the Green-Kubo formalism. This formalism will be motivated by examples allowing to compute the shear viscosity of a fluid, but the study of the other transport coefficients (thermal conductivity, diffusion) is similar, see for instance [101].

2.2.1 Nonequilibrium dynamics

We consider a reference equilibrium dynamics with infinitesimal generator \mathcal{A}_0 and consider a perturbation of this dynamics. We denote by $\xi\mathcal{A}_1$ the generator of the perturbation, where ξ is a small parameter measuring the amplitude of the perturbation. When the equilibrium process is the Langevin process, the expression of \mathcal{A}_0 is $\mathcal{A}_{\text{ham}} + \mathcal{A}_{\text{thm}}$. We restrict ourselves to perturbations of the form

$$\begin{cases} dq_t = M^{-1}p_t dt + \xi C(q_t, p_t) dt, \\ dp_t = -\nabla V(q_t) dt - \gamma(q_t)M^{-1}p_t dt + \xi D(q_t, p_t) dt + \sigma(q_t) dW_t, \end{cases} \quad (2.49)$$

where C and D are smooth functions so that

$$\mathcal{A}_1 = C(q, p) \cdot \nabla_q \cdot + D(q, p) \cdot \nabla_p \cdot . \quad (2.50)$$

We give below examples of admissible perturbation in the case of shear flows. In general D is a nongradient perturbation and in that case, an analytical expression of the invariant measure of the system is unknown.

2.2.2 Invariant measure of the nonequilibrium dynamics

The invariant measure of the nonequilibrium dynamics (if it exists, see [93] for a condition relying on the existence of a Lyapunov function for the system) satisfies the following Fokker-Planck equation (written here in the weak sense)

$$\int_{\mathcal{M} \times \mathbb{R}^{dN}} (\mathcal{A}_0 + \xi\mathcal{A}_1) \varphi \psi_\xi = 0, \quad (2.51)$$

for all test functions φ . It is convenient to write ψ_ξ as a perturbation of the reference measure:

$$\psi_\xi = f_\xi \psi_0,$$

and to work in the Hilbert space $L^2(\psi_0)$.

The function f_ξ is then the unique solution of the Fokker-Planck equation

$$(\mathcal{A}_0^* + \xi\mathcal{A}_1^*) f_\xi = 0, \quad \int_{\mathcal{M} \times \mathbb{R}^{dN}} f_\xi \psi_0 = 1, \quad (2.52)$$

where adjoints are considered on $L^2(\psi_0)$. Note that the invariance of the reference measure ψ_0 is expressed in this framework as

$$\mathcal{A}_0^* \mathbf{1} = 0.$$

In Chapter 3 we prove the following result concerning the invariant measure of the nonequilibrium dynamics, and for convenience we recast it on the abstract setting. The result gives the expression of the function f_ξ as a power series in ξ when ξ is sufficiently small, under appropriate assumptions on the perturbation \mathcal{A}_1 .

Theorem 2.1. *Assume that (2.52) has a unique solution, and that*

- (a) (properties of the equilibrium dynamics) $\text{Ker}(\mathcal{A}_0^*) = \mathbf{1}$ and \mathcal{A}_0^* is invertible on \mathcal{H} ;
 (b) (properties of the perturbation) $\text{Ran}(\mathcal{A}_1^*) \subset \mathcal{H}$ and $(\mathcal{A}_0^*)^{-1} \mathcal{A}_1^*$ is bounded on \mathcal{H} .

Denote by r the spectral radius of the bounded operator $(\mathcal{A}_0^*)^{-1} \mathcal{A}_1^* \in \mathcal{B}(\mathcal{H})$:

$$r = \lim_{n \rightarrow +\infty} \left\| \left((\mathcal{A}_0^*)^{-1} \mathcal{A}_1^* \right)^n \right\|^{1/n}.$$

Then, for $|\xi| < r^{-1}$, the unique solution of (2.52) can be written as

$$f_\xi = \left(1 + \xi (\mathcal{A}_0^*)^{-1} \mathcal{A}_1^* \right)^{-1} \mathbf{1} = \left(1 + \sum_{n=1}^{+\infty} (-\xi)^n \left[(\mathcal{A}_0^*)^{-1} \mathcal{A}_1^* \right]^n \right)^{-1} \mathbf{1}. \quad (2.53)$$

The linear term in ξ in the expression of f_ξ is denoted by

$$f_1 = - (\mathcal{A}_0^*)^{-1} \mathcal{A}_1^* \mathbf{1}.$$

Note that the measure (2.53) is a probability measure: the normalization constant for ψ_ξ does not depend on ξ . This owes to the fact that $\text{Ran}((\mathcal{A}_0^*)^{-1} \mathcal{A}_1^*) \subset \mathcal{H}$, and

$$\int_{\mathcal{M} \times \mathbb{R}^{dN}} h \psi_0 = 0$$

for any $h \in \mathcal{H}$, so that

$$\int_{\mathcal{M} \times \mathbb{R}^{dN}} \psi_\xi = \int_{\mathcal{M} \times \mathbb{R}^{dN}} \psi_0 = 1.$$

The first assumption in the above theorem means that the equilibrium dynamics has good ergodic properties, while the second one ensures that the perturbation is not too strong. A typical way of proving that $(\mathcal{A}_0^*)^{-1} \mathcal{A}_1^*$ is bounded on \mathcal{H} is to show that \mathcal{A}_1 is \mathcal{A}_0 -bounded: $D(\mathcal{A}_0) \subset D(\mathcal{A}_1)$ and there exists $a, b > 0$ such that $\|\mathcal{A}_1 \varphi\| \leq a \|\mathcal{A}_0 \varphi\| + b \|\varphi\|$ for $\varphi \in D(\mathcal{A}_0)$.

Average properties under the nonequilibrium steady state are obtained by integration of a microscopic observable h with respect to the nonequilibrium measure:

$$\langle h \rangle_\xi = \int_{\mathcal{M} \times \mathbb{R}^{dN}} h(q, p) \psi_\xi(q, p) dq dp = \langle h, f_\xi \rangle_{L^2(\psi_0)} \quad (2.54)$$

while equilibrium averages, denoted by $\langle h \rangle_0$, correspond to an integration with respect to ψ_0 .

2.2.3 Linear response and correlation functions

The appropriate response functions to be averaged, denoted by R in the sequel, are determined by the macroscopic property we are interested in, *e.g.* the stress tensor for the shear viscosity or the heat flux for the thermal conductivity. Susceptibilities or transport coefficients are then defined as follows (recall that $R \in \mathcal{H}$):

$$\alpha = \lim_{\xi \rightarrow 0} \frac{\langle R \rangle_\xi}{\xi}. \quad (2.55)$$

In practice, an estimate of α can be obtained by choosing a value of ξ sufficiently small, approximating $\langle R \rangle_\xi$ by a longtime average over one realization of the dynamics similar to (2.15), and dividing this quantity by ξ . In order to check that the value of ξ is indeed small enough to neglect higher order contributions, it is possible for instance to check the linearity of the response by computing approximations of $\langle R \rangle_\xi$ with ξ replaced by, say, $\xi/2$ or 2ξ , see Chapter 3.

The choice of the reference dynamics is crucial. Theoretically, results are available in the case where $\mathcal{A}_0 = \mathcal{A}_{\text{thm}} + \mathcal{A}_{\text{ham}}$ but less physical than the standard Hamiltonian dynamics for which $\mathcal{A}_0 = \mathcal{A}_{\text{ham}}$. Using the expression (2.53) of the invariant measure in terms of the perturbation parameter ξ , and the equality

$$-\mathcal{A}_0^{-1} = \int_0^{+\infty} e^{t\mathcal{A}_0} dt$$

as operators on \mathcal{H} (which, requires some decay properties of the semi-group), linear response properties can be rephrased using correlation functions. Introducing the function $S = \mathcal{A}_1^* \mathbf{1}$, also called the dissipative flux (see [107]), it holds

$$\alpha = \int_{\mathcal{M} \times \mathbb{R}^{dN}} R f_1 \psi_0 = - \int_{\mathcal{M} \times \mathbb{R}^{dN}} [\mathcal{A}_0^{-1} R] [\mathcal{A}_1^* \mathbf{1}] \psi_0 = \int_0^{+\infty} \langle R(q_t, p_t) S(q_0, p_0) \rangle_{\text{eq}} dt, \quad (2.56)$$

where the expectation $\langle \cdot \rangle_{\text{eq}}$ is taken over all initial conditions distributed according to $\psi_0(q, p) dq dp$, and over all realizations of the reference equilibrium dynamics (with generator \mathcal{A}_0). Note that its expression is determined by the applied perturbation \mathcal{A}_1 , and not by the response function R . The self-correlation of R is recovered for perturbations such that $S \propto R$. In the case of a perturbation given by (2.50) the general formula for the dissipative flux is

$$S = \mathcal{A}_1^* \mathbf{1} = -\beta C \cdot \nabla_q V - \beta D \cdot M^{-1} p. \quad (2.57)$$

Examples of application of the abstract setting will be given in a formal way in Section 2.3.2 and in a rigorous framework in Chapter 3.

2.2.4 Discussion on the choice of the underlying dynamics

We now discuss some issues concerning the choice of the underlying dynamics. Often, the Hamiltonian dynamics is considered as the reference dynamical evolution of the microscopic system. However, this dynamics exactly preserves the energy of the system, while energy exchanges with the environment are expected to happen. The choice of the underlying dynamics of the system is a modelling choice. In any case, a careful study of the dependence of the computed transport properties as a function of the parameters of the dynamics should be performed.

Since the system is driven out-of-equilibrium by a nongradient force, some thermostating mechanism is required to prevent the uncontrolled increase of the energy and to ensure that a steady-state can indeed be reached. In many works focusing on the computation of shear viscosity, the thermostating is performed with deterministic dynamics, such as Nosé-Hoover like thermostats [49, 85] or isokinetic dynamics (see [28, Chapter 3]). The ergodicity of these dynamics is at most unclear (and non-ergodicity can even be proved rigorously in some limiting cases [65, 66]). The mathematical analysis of these methods is therefore untractable. Only *formal*

results of linear response can be written down. In some studies, the thermostating is performed using dissipative particle dynamics [56, 99], which includes stochastic terms. The ergodicity of these dynamics is however a very difficult issue, and the only existing results we are aware of concern one-dimensional systems [98].

2.3 Computation of transport coefficients: the example of the shear viscosity

In this section, we present a short overview of the different approaches to computing the shear viscosity of a fluid using molecular simulations. There is a huge number of references reporting shear viscosity computations since the beginning of molecular simulations in the middle of the 20th century. Nowadays, the computation of the shear viscosity of a system is still an important and active topic of research in the chemical and physical communities and still require a substantial computational effort. A review of the most standard approaches to computing the shear viscosity can be read in [28]. See also [104] for a focus on nonequilibrium methods and [48] for a comparison between various numerical approaches. Let us first, recall basic concepts of continuous fluid mechanics. The end of the chapter is devoted to the comparison of several methodologies to compute numerically the shear viscosity of a fluid.

2.3.1 Some elements of continuous fluid mechanics

We recall here some basic concepts of fluid mechanics. Let us consider a fluid described at the continuous level. We assume the fluid to be isothermal, and incompressible. Its motion is governed by the Navier–Stokes equations which express the conservation of momentum and mass in the form

$$\begin{cases} \partial_t(\rho \mathbf{u}) + \operatorname{div}(\rho \mathbf{u} \otimes \mathbf{u}) - \operatorname{div} \Pi = F, \\ \operatorname{div}(\mathbf{u}) = 0. \end{cases} \quad (2.58)$$

Here, \mathbf{u} is the fluid velocity with Cartesian components (u_x, u_y, u_z) , ρ the density of the fluid, Π the stress tensor, and F some volume force. We assume that the fluid occupies a volume Ω . The stress tensor Π is defined by

$$\Pi = -pI_d + \sigma, \quad (2.59)$$

where I_d is the identity tensor on \mathbb{R}^3 and σ is the viscous strain tensor. In order to deal with a closed system of equations, a constitutive relationship between the viscous strain σ and the velocity field needs to be specified. Assuming the fluid is Newtonian, we define the shear viscosity of the fluid by the coefficient η such that

$$\sigma := 2\eta D(u), \quad D(u) = \frac{1}{2}(\nabla \mathbf{u} + \nabla \mathbf{u}^T). \quad (2.60)$$

Let us examine some special flow. To this end, we need to specify some boundary conditions. A first simple situation is to consider a flow between two flat plates so that the domain $\Omega := L_x \mathbb{T} \times [0, L_y] \times L_z \mathbb{T}$ (in 3D). Assuming a stationary velocity profile of the form

$$\mathbf{u} = u_x(x, y, z)\mathbf{e}_x, \quad (2.61)$$

we observe that owing to the divergence free constraint, we necessarily have

$$\mathbf{u} = \varphi(y)\mathbf{e}_x, \quad (2.62)$$

for some function φ . We impose that the fluid's velocity field $u_x = \mathcal{U}$ at the boundary $y = L_y$ and is equal to $u_x = 0$ at $y = 0$. Neglecting pressure gradients, which amounts to consider a Couette flow, we find that

$$\varphi(y) = \frac{\mathcal{U}y}{L_y}, \quad y \in [0, L_y], \quad (2.63)$$

is solution of the Navier–Stokes equation (2.58). We can define the strain rate $\dot{\gamma}$ by taking the derivative of φ so that

$$\dot{\gamma} := \frac{\mathcal{U}}{L_y}, \quad (2.64)$$

so that in this case, the shear viscosity satisfy the relation

$$-\eta\dot{\gamma} = \sigma_{xy}. \quad (2.65)$$

In the context of molecular simulations, in particular in nonequilibrium method and linear response theory, the aim is to compute the shear viscosity η through the knowledge of (nonzero) microscopic version of σ_{xy} by imposing a velocity field in a microscopic system, so that the strain rate is $\dot{\gamma}$. At the microscopic level, an equation such as (2.65) is in fact a definition for the shear viscosity, and this definition needs to be numerically validated, its validity depending on the physical system under consideration. In the case where (2.65) is not satisfied numerically (as often observed for complex fluids [86, Chapter 4]), we need to improve the constitutive law linking the shear stress to the velocity field. We will see in the sections below some analogies with the macroscopic theory in the study of equilibrium method in the next paragraph and nonequilibrium methods, for the Couette flow in § 2.3.3.

2.3.2 Equilibrium methods

We now turn to the first class of method we consider, being equilibrium methods. Equilibrium methods are based on time integrals of correlation functions, the so-called Green-Kubo formulas [34, 62] or the Einstein relations ([41], [48] for systems with periodic boundary conditions). These correlation functions are obtained by sampling initial conditions according to the thermodynamic ensemble at hand, and averaging over all possible evolutions from these initial conditions. The standard formula for the shear viscosity is

$$\eta = \beta|\mathcal{D}| \int_0^{+\infty} \langle \Sigma_{xy}^0 \Sigma_{xy}^t \rangle_{\text{eq}} dt, \quad (2.66)$$

In practice, the computation of η by formula (2.66) is an expansive computational task and requires a careful treatment. To explain this formula, we define the microscopic version of an off-diagonal term of the Cauchy stress-tensor:

$$\Sigma_{xy}(q, p) = \frac{1}{|\mathcal{D}|} \left(\sum_{i=1}^N \frac{p_{xi}p_{yi}}{m} - \sum_{1 \leq i < j \leq N} v'(|q_i - q_j|) \frac{(q_{xi} - q_{xj})(q_{yi} - q_{yj})}{|q_i - q_j|} \right) \quad (2.67)$$

The time-dependent version of the stress tensor for a time $t \geq 0$ as to be understood as:

$$\Sigma_{xy}^t := \Sigma_{xy}(\Phi_t(q_0, p_0)), \quad (2.68)$$

where Φ_t is often the Hamiltonian flow starting from initial condition $(q_0, p_0) \in \mathcal{M} \times \mathbb{R}^{dN}$. The integrand, given by

$$\langle \Sigma_{xy}^0 \Sigma_{xy}^t \rangle_{\text{eq}}, \quad (2.69)$$

is the canonical average of the self-correlation function of the off-diagonal stress tensor component.

The Green–Kubo formula could cast in the previous abstract setting. Indeed, it is shown formally in [107, Chapter 13 §3.3.1], that the Green-Kubo formula for the shear viscosity is recovered when the perturbation is of the form (2.50) with

$$\begin{aligned} C_i(q, p) &= q_{yi} e_x, \\ D_i(q, p) &= -p_{yi} e_x. \end{aligned} \quad (2.70)$$

In that case we have:

$$S = \mathcal{A}_1^* \mathbf{1} = |\mathcal{D}| \Sigma_{xy}(q, p), \quad (2.71)$$

so that by substituting the expressions in formula (2.56), we obtain equation (2.66) By analogy with Section 2.3.1, the parameter ξ is viewed here as the strain rate $\dot{\gamma}$ defined by the relation (2.65). The definition of the shear viscosity with the above formula require some care, in particular with the boundary conditions of the system considered in [107]. The choice of the underlying flow Φ_t requires also some care. From the physical viewpoint, Hamiltonian flow seems the natural choice since the particles are expected to be Newtonian. The mathematical counterpart is less obvious since we are not aware of any result concerning integrability of the self-correlation functions generated with the Hamiltonian flow, the latter having an infinitesimal generator lacking a spectral gap.

Practical implementation

Practitioners often run a very long canonical simulation and compute the shear viscosity by computing self-correlation function their unique simulation. This approach can be heuristically justified for large systems, by taking the thermodynamic limit, for which the thermodynamic ensembles are equivalent. Another approach to compute self-correlation functions, based on fast Fourier transform (FFT), is also considered, see [107, Section 13.4] for a discussion on these methods.

The direct method (and most rigorous) to compute a self-correlation function is to proceed as follow: Fix a number of replicas $N_{\text{replica}} \in \mathbb{N}$, for $k \in \{1, \dots, N_{\text{replica}}\}$ do

- i Initialize with $(q_0^k, p_0^k) \in \mathcal{M} \times \mathbb{R}^{dN}$;
- ii Fix a time step $\delta\tau_{\text{eq}}$ and a simulation time τ_{eq} and run an equilibrium Langevin trajectory;
- iii Fix a time step δt_{dyn} and a simulation time τ_{dyn} and run the dynamics associated with the infinitesimal generator \mathcal{A}_0 (either Langevin or Hamiltonian) starting from canonical initial condition, then compute the approximation of (2.69) being

$$\mathcal{C}_{\delta t_{\text{dyn}}}(j) := \frac{1}{N_{\text{replica}}} \sum_{k=1}^{N_{\text{replica}}} \Sigma_{xy}(q_j^k, p_j^k) \Sigma_{xy}(q_0^k, p_0^k), \quad j = 0, \dots, N_{\text{dyn}} = \left\lfloor \frac{\tau_{\text{dyn}}}{\delta t_{\text{dyn}}} \right\rfloor. \quad (2.72)$$

Note that step (ii) could be replaced by Monte Carlo sampling of the canonical measure, the use of the Langevin dynamic to generate canonical initial condition is a convenient choice when using a molecular dynamics simulation code. In the case of the Green-Kubo formula (2.66), an estimator of the shear viscosity is for instance given by

$$\eta \approx \frac{1}{N_{\text{replica}}} \sum_{k=1}^{N_{\text{replica}}} \sum_{j=0}^{N_{\text{dyn}}} \delta t_{\text{dyn}} \mathcal{C}_{\delta t_{\text{dyn}}}(j). \quad (2.73)$$

The time τ_{dyn} as to be taken large enough to capture the long tail of the self-correlation function while in practice the number N_{replica} has to be extremely large because of the variance intrinsic to the problem. Note that integration in infinite time can easily be improved by using sharper quadrature rules, since by using the simple integration rule in (2.73) we observed a bias of a few percent. We will see in Chapter 3 an application of another Green-Kubo type formula and its corresponding nonequilibrium version.

The setting of the present paragraph can be illustrated by the following numerical application for a 2D Lennard–Jones system of 225 particles. The reduced number density and temperatures are chosen to be $(\rho, T) = (0.69, 2.5)$ so that the square box is of size $L = 18$. There are basically three types of error in such a simulation: (i) the truncature of the integral in infinite time to an integral in $(0, \tau_{\text{dyn}})$; (ii) the discretization time-step δt_{dyn} ; (iii) the statistical error linked to the number of replica N_{replica} . We reproduced 20 times the above protocol with a time-step $\delta t_{\text{dyn}} = 10^{-3}$ and a number of replica N_{replica} equal to 6.2×10^4 in the Hamiltonian case and 10^5 in Langevin case, the friction parameter being $\gamma = 1$.

We performed those computations by using both the Hamiltonian and Langevin flow to compute self-correlation of the off-diagonal term of the stress tensor. The time of equilibration was chosen to be $\tau_{\text{eq}} = 10$. The shear viscosity has been estimated by integrating the averaged self-correlation function on the time interval $(0, 1.5)$. Results and error bar can be found in Table 2.2 for both Hamiltonian flow and Langevin flow. Observe in Figure 2.3 that after a short transient time, the self-correlation function fluctuate around zero. Nevertheless, the statistical error coming out from those computations is large and require a huge number of independent replica. Figure 2.4 shows these variations by taking the logarithm of the self-correlation function for several independent replicas. We observe that the resulting viscosity slightly deviate (in dashed line in the right picture) from its mean value (in bold line in the right picture).

Dynamics	η
Hamiltonian	1.707 ± 0.101
Langevin	1.63 ± 0.06

Table 2.2. Shear viscosity evaluated with the Green-Kubo formula.

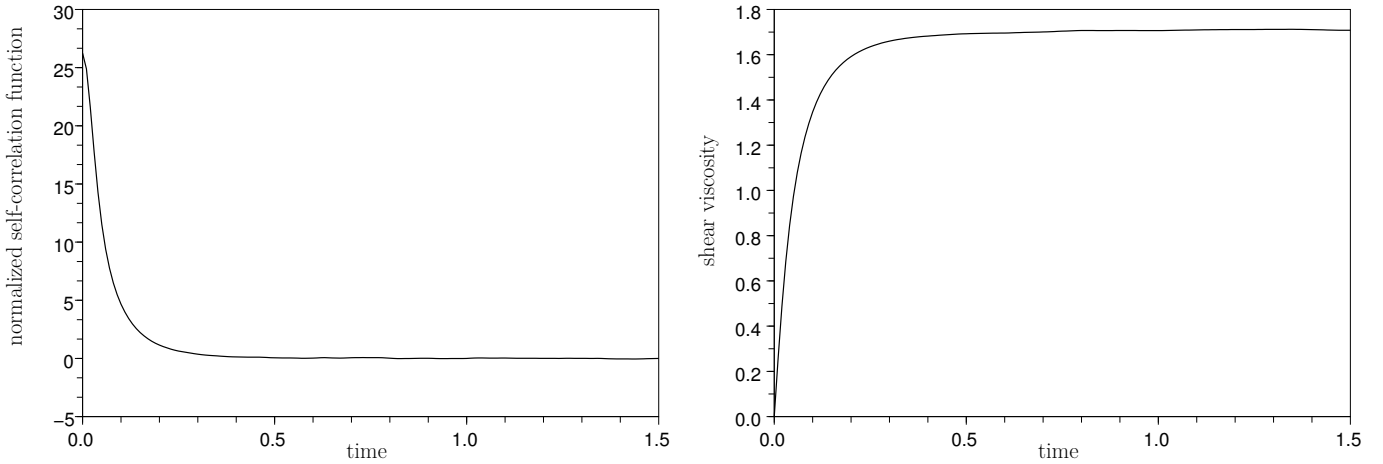


Fig. 2.3. Left: Self-correlation function multiplied by $\beta |\mathcal{D}|$; Right: Integral of the self-correlation function (shear viscosity).

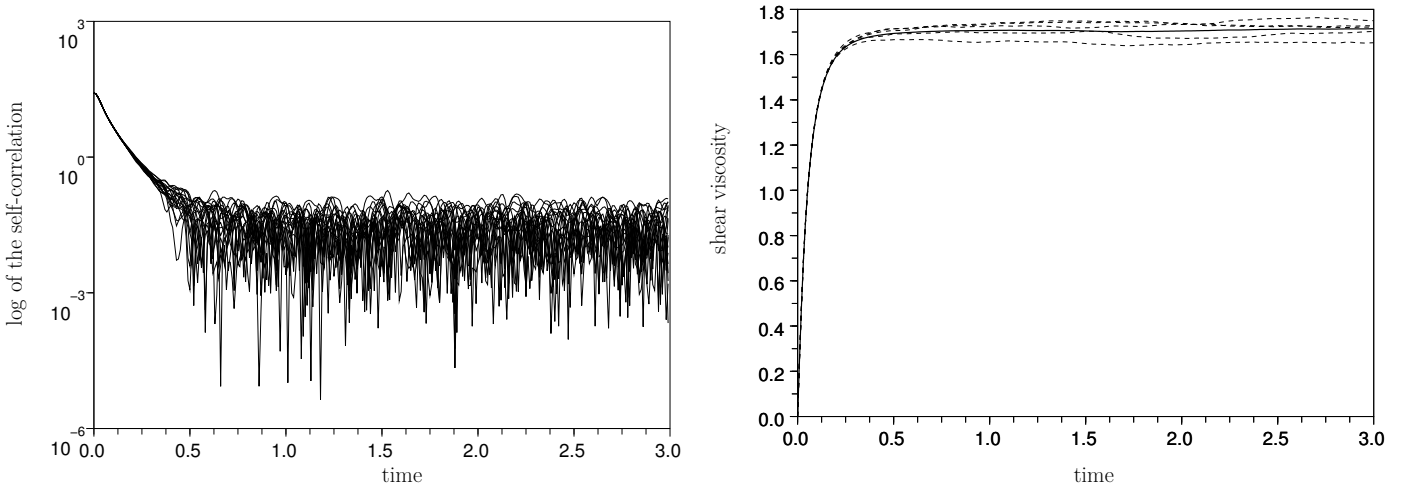


Fig. 2.4. Left: Log plot of the self-correlation function for several replicas; Right: Shear viscosity as a function of time for several replicas.

2.3.3 Steady state nonequilibrium

In steady state nonequilibrium methods, the system is characterized by the existence of stationary fluxes and spatial gradients of some quantities. These fluxes and gradients can be controlled by forcing terms acting on the boundaries of the system (for instance, a velocity profile can be obtained by fixing the average velocity in the extremal slabs of a fluid, see the early review [50], or subsequent works such as [106]), or by a bulk process where fictitious forces act on all particles (the so-called synthetic molecular dynamics approach [28]).

These are the main two approaches (i) boundary driven techniques where the external forcing is imposed only in boundary regions of the phase space, and (ii) bulk driven dynamics where all the particles of the system experience an external perturbation. Boundary driven methods are usually numerically less efficient than bulk-driven methods since there is more correlations in the system and the convergence to a steady-state starting from some reference equilibrium state

is slower. Besides, existence and uniqueness results are, in general, not available. Bulk driven method are often numerically more efficient, and from a theoretical viewpoint more tractable than boundary driven methods. Finally, let us mention that nonequilibrium methods are closely linked to the linear response theory in the sense that to each nonequilibrium method, one can associate a Green-Kubo formula, as we have seen in § 2.3.2.

Example of Boundary driven nonequilibrium method

Let us now describe a numerical illustration of a boundary driven method. One might consider the following nonequilibrium Langevin dynamics with non constant friction matrices:

$$\begin{cases} dq_t = M^{-1}p_t dt, \\ dp_t = -\nabla V(q_t)dt - \gamma(q_t) \left(M^{-1}p_t - \mathcal{V}(q_t) \right) dt + \sigma dW_t, \end{cases} \quad (2.74)$$

where the diagonal friction matrix γ has the entries

$$\gamma_{i,i}(q) = \begin{cases} 1 - q_y R^{-1} & q_y \leq R, \\ 1 - \left| q_y - \frac{L}{2} \right| R^{-1} & \left| q_y - \frac{L}{2} \right| \leq R, \\ \frac{q_y - L}{R} + 1 & q_y > L - R, \\ 0 & \text{elsewhere.} \end{cases} \quad (2.75)$$

and \mathcal{V} is the velocity function defined by

$$\mathcal{V}(q) = \begin{cases} -\mathcal{U} & q_y \leq R, \\ \mathcal{U} & \left| q_y - \frac{L}{2} \right| \leq R, \\ -\mathcal{U} & q_y > L - R, \\ 0 & \text{elsewhere.} \end{cases} \quad (2.76)$$

for a positive real number R such that $4R < L$ and a velocity \mathcal{U} . This choice of dynamics consists to impose a velocity field in the region where the friction is active while the other regions are governed by the standard Hamiltonian dynamics. We expect that a velocity profile settles down in the system. This allows to measure the susceptible thermodynamic flux, namely the off-diagonal term of the Cauchy stress-tensor (see Section 2.3.1). In particular, since there is a portion of the phase space ruled by the Hamiltonian dynamics, we expect the velocity profile to be affine in the concerned zone, so that the corresponding off-diagonal term is expected to be constant, so that a Couette flow is observed in the region where $\gamma = 0$. An issue with the lack of thermostating is that the local kinetic temperature can fluctuate in the system and local equilibrium is only ensured by the energy exchange with the zone ruled by the Langevin dynamics.

As a numerical example, we propose to simulate the dynamics (2.74) for the 2D Lennard-Jones system at state point $(\rho, T) = (0.69, 2.5)$. The simulation cell is a rectangle $18\mathbb{T} \times 360\mathbb{T}$. We performed computations for two forcing parameters $\mathcal{U} = 0.05, 0.1$ and for friction parameters

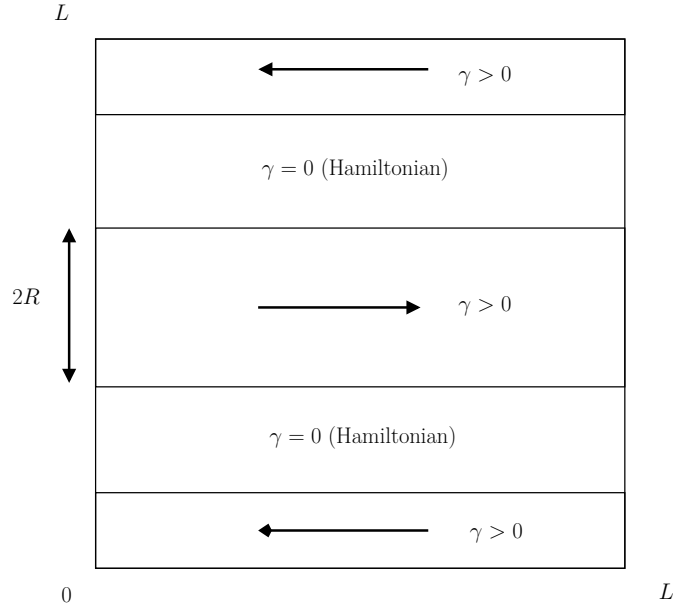


Fig. 2.5. Computation cell for the boundary driven flow

$\gamma_x = \gamma_y = 1$. We can monitor a spatially localized version of the off-diagonal term of the stress tensor (the method to compute such a quantity is described in detail in Chapter 3). Upon postulating that the Newton law for the shear viscosity (2.60) holds true, the shear viscosity of the fluid can be extracted by analyzing the Fourier mode of the velocity profile and the pressure profile extracted from the simulations (the method to compute such quantities is detailed in Chapter 3). Indeed, assuming

$$\sigma_{xy}(Y) = -\eta u'_x(Y), \quad Y \in L_y \mathbb{T}, \quad (2.77)$$

we see that we can obtain the shear viscosity η by simply taking the quotient of the Fourier mode of σ_{xy} and u'_x (in practice we compute the Fourier mode of u_x , reducing the numerical and statistical error). We verified that linear response holds, by remarking that the Fourier modes for $\mathcal{U} = 0.05, 0.1$, are approximatively proportional. Figure 2.6 depicts the localized velocity and pressure profiles. Estimated values and error bar for the imaginary part of the first Fourier coefficient $\widehat{\sigma}_{xy}, \widehat{u}'_x$, and the shear viscosity can be found in Table 2.3 for both computations. The simulation time was chosen extremely large ($N_{\text{iter}} > 3 \times 10^6$) in order to diminish the statistical uncertainty. We evaluated the variance by running several independent replicas.

\mathcal{U}	$\widehat{\sigma}_{xy}/\mathcal{U}$	$-\widehat{u}'_x/\mathcal{U}$	η
0.05	0.260 ± 0.0031	0.156 ± 0.0015	1.664 ± 0.02
0.1	0.264 ± 0.0043	0.154 ± 0.005	1.71 ± 0.04

Table 2.3. Shear viscosity evaluated with the boundary driven dynamics.

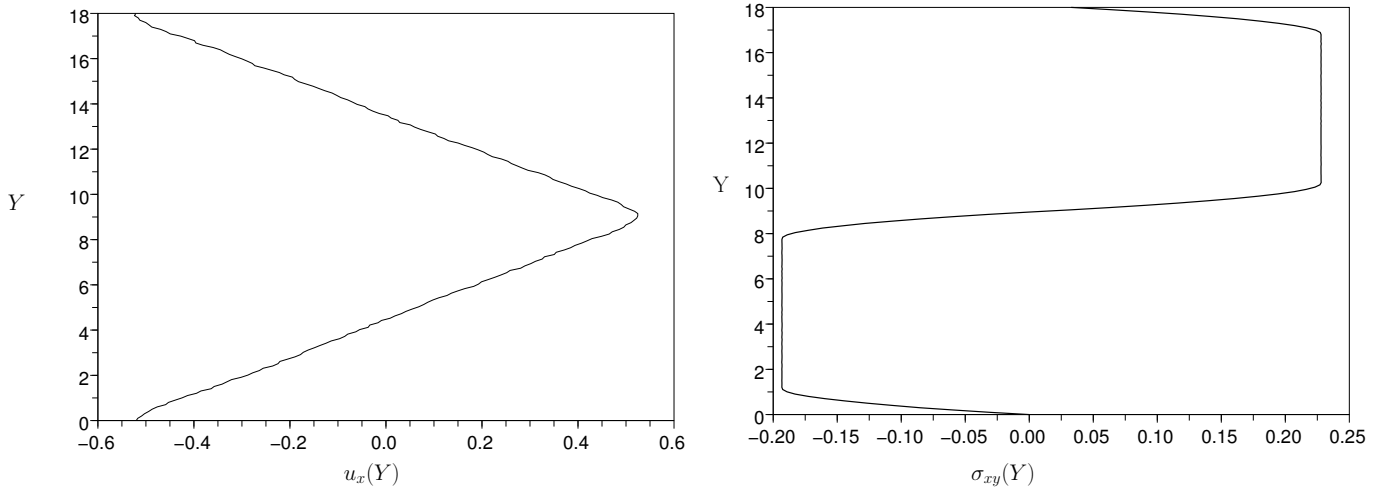


Fig. 2.6. Left: Velocity profile for $\mathcal{U} = 0.1$; Right: Off-diagonal term of the stress tensor for $\mathcal{U} = 0.1$.

Example of bulk driven nonequilibrium method

We focus in this section on bulk-driven nonequilibrium molecular dynamics techniques. One popular method is to use a version of the SLLOD algorithm in conjunction with Lees-Edwards boundary condition (see the references in [104]), which are consistent with a constant shear rate and linear velocity profiles. However, a mathematical study of the linear response in this framework is cumbersome since the boundary conditions for the operators at hand are time-dependent and also depend on the shear rate. It is easier to study techniques relying on periodic nongradient forcings. In this case, standard periodic boundary conditions can be resorted to. This is the path we follow in this thesis. Let us also mention that in methods using the Lees-Edwards boundary conditions, the velocity profile is known (linear), and the viscosity is extracted from the ratio of the total off-diagonal stress tensor and the shear rate; whereas in the method studied in this thesis, some form of spatial localization is needed to obtain velocity profiles, and the viscosity can be obtained directly from the velocity profile.

One of the seminal works using this technique is the article by Gosling and Mac Donald [33]. It consists in adding a periodic nongradient perturbation in the system and to measuring the response in the velocity profile. The viscosity is then computed by postulating a macroscopic equation for the velocity. The original method is formulated as follow, assuming that the volume force has the form $F := F(y)$, where F is a one real variable function defined on $L_y\mathbb{T}$ and neglecting pressure gradients, the Navier–Stokes equation (2.58) with periodic boundary conditions can be written

$$-\eta u_x''(y) = \rho F(y), \quad y \in L_y\mathbb{T}, \quad (2.78)$$

so that the shear viscosity of the fluid can be identified owing to Fourier series expansion of the solution u_x and the force profile F (see Chapter 3 for a precise discussion of the method). In fact, in the original work of Gosling and Mac Donald, a sinusoidal velocity force acts on all the particles and in this simple case, the viscosity can be estimated by simply fitting the resulting velocity profile (in this case a sinusoid proportional to F). An issue with the original method was the lack of thermostating in the system since the authors considered the Hamiltonian dynamics as

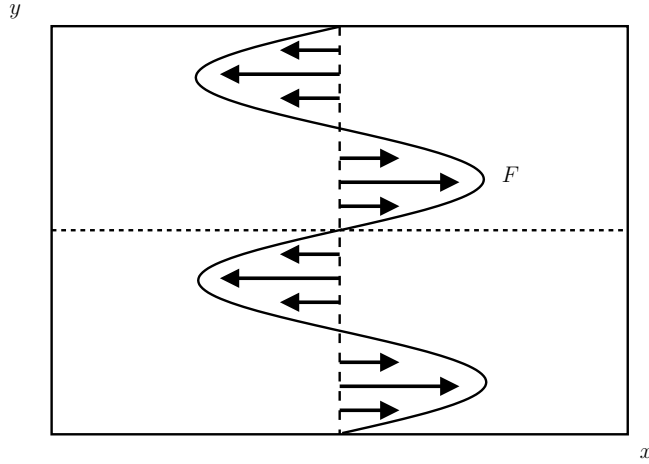


Fig. 2.7. Computation cell for the Bulk driven flow with sinusoidal forcing

the reference dynamics, the existence of a steady state in this setting being false. The equations of motion we propose (written in 2D for simplicity, the extension to 3D being straightforward) are a linear perturbation of the Langevin equations, with some additional nongradient external force in the x -direction (the direction of the flow). The dynamics reads (for $i = 1, \dots, N$):

$$\begin{cases} dq_{i,t} = \frac{p_{i,t}}{m} dt, \\ dp_{xi,t} = -\nabla_{q_{xi}} V(q_t) dt + \xi F(q_{yi,t}) dt - \gamma_x \frac{p_{xi,t}}{m} dt + \sqrt{\frac{2\gamma_x}{\beta}} dW_t^{xi}, \\ dp_{yi,t} = -\nabla_{q_{yi}} V(q_t) dt - \gamma_y \frac{p_{yi,t}}{m} dt + \sqrt{\frac{2\gamma_y}{\beta}} dW_t^{yi}, \end{cases} \quad (2.79)$$

where $(W_t^x, W_t^y)_{t \geq 0}$ is a $2N$ -dimensional standard Brownian motion, and the friction coefficients γ_x, γ_y are real positive numbers. The purpose of Chapter 3 is to study theoretically (when it is possible) and numerically (to go beyond what theories allow) the behavior of the transport coefficient extracted with dynamics (2.79). In particular, we will derive an equation analogous (2.78) that depends on the parameter γ_x .

2.3.4 Transient nonequilibrium dynamics

Finally, another class of method consists in monitoring the relaxation of some observable after a local initial disturbance, using a transient (nonequilibrium) dynamics. Macroscopic coefficients are obtained by fitting the observed response to the evolution predicted by a macroscopic evolution equation. For instance, in the case of thermal transport, a local temperature hot spot is initially created in the middle of a homogeneous material, and, assuming that the heat equation describes well the evolution of the kinetic temperature field, the diffusion of the energy allows to estimate the thermal conductivity of the material (see for instance [52, 100]). An example of such calculation has been carried in [48, Section iv: Periodic perturbation method] for the shear viscosity. A periodic one-dimensional velocity profile is imposed at time 0 and by monitoring the return to equilibrium, the shear viscosity is deduced from the instationary Navier–Stokes

equation. Note that we did not consider this class of method in this thesis, and a deeper look in these approaches may be a perspective of future work.

Nonequilibrium shear viscosity computations with Langevin dynamics

3.1	Aim of the study	41
3.2	The nonequilibrium Langevin dynamics	42
3.2.1	Existence and uniqueness of an invariant measure	42
3.3	Mathematical analysis of the viscosity	43
3.3.1	Linear response	43
3.3.2	Local conservation of the longitudinal velocity	44
3.3.3	Definition and closure relation for shear viscosity computations	46
3.3.4	Asymptotic behaviour of the viscosity for large frictions	46
3.4	Numerical results for the Lennard–Jones fluid	49
3.4.1	Numerical implementation	49
3.4.2	Numerical results	52
3.5	Proof of the results	60
3.5.1	Proof of Theorem 4	60
3.5.2	Proof of Proposition 1	62
3.5.3	Proof of Theorem 5	64
3.5.4	Proof of Theorem 6	68

3.1 Aim of the study

As discussed in Section 2.3.3 we decided to use a standard Langevin dynamics as the underlying dynamics of the system since this dynamics is ergodic and has many nice mathematical properties, while still being close enough to the Hamiltonian dynamics. In essence, the nonequilibrium dynamics we propose is obtained from the standard Langevin dynamics by adding a nongradient force, which can be interpreted as some fictitious external forcing term. The effect of this term is to create a velocity profile in the direction of the forcing, and the viscosity of the fluid can be extracted from this profile. The novelty of this work with respect to the (numerous) existing studies on the computation of shear viscosity is the rigor of the mathematical arguments used to prove linear response results and obtain the effective equation on the observed velocity profile in terms of the applied external force. In particular, we benefited from recent developments on hypocoercivity [109]. Besides, one of our main concern is the dependence of the viscosity as a function of the parameters of the underlying dynamics, in particular the friction. We analyzed the large friction asymptotics by extending and adapting mathematical studies

of the auto-diffusion coefficient [38, 88]. For the low friction dependence, we rely on numerical simulations.

In Section 3.2, we show the existence and uniqueness of the stationary state. The mathematical properties of this stationary state are studied in Section 3.3 (with the proofs postponed to Section 3.5). In particular, we give a rigorous proof of the linear response. We then show how to compute the viscosity, and characterize its asymptotic behavior for large frictions by determining the limiting behavior of the velocity profile. We finally present some numerical illustrations of the theoretical results in Section 3.4.

3.2 The nonequilibrium Langevin dynamics

In order to avoid irrelevant technical issues, we recall the assumption:

Assumption 2 *The potential V and the external force F belong respectively to $C^\infty(\mathcal{D}^N)$ and $C^\infty(L_y\mathbb{T})$.*

3.2.1 Existence and uniqueness of an invariant measure

When $\xi \neq 0$, there is no obvious invariant probability measure, and the very existence of such a measure is not guaranteed *a priori*. However, in the case when $\gamma_x, \gamma_y > 0$, standard techniques based on Lyapunov functions and hypoellipticity arguments can be resorted to to prove the existence and uniqueness of an invariant measure which has a smooth density with respect to the Lebesgue measure.

We can then state the following result being a special case of Theorem 2.1.

Theorem 4 *Consider $\gamma_x, \gamma_y > 0$ and suppose that Assumption 2 holds. Then, for any $\xi \in \mathbb{R}$, the dynamics (2.79) has a unique smooth invariant probability measure with density $\psi_\xi \in C^\infty(\mathcal{D}^N \times \mathbb{R}^{2N})$. Besides, there exists $\xi^* > 0$ such that, for any $\xi \in (-\xi^*, \xi^*)$, the following expansion holds in $L^2(\psi_0)$:*

$$\psi_\xi = f_\xi \psi_0, \quad f_\xi = 1 + \sum_{k \geq 1} \xi^k \mathfrak{f}_k, \quad (3.1)$$

where $\mathfrak{f}_k \in \mathcal{H}$ is such that $\|\mathfrak{f}_k\|_{L^2(\psi_0)} \leq C(\xi^*)^{-k}$ for some constant $C > 0$ independent of ξ .

Note that the measure (3.1) is indeed a probability measure (its integral over $\mathcal{D}^N \times \mathbb{R}^{2N}$ is equal to 1) since $\mathfrak{f}_k \in \mathcal{H}$ for all $k \geq 1$ and ψ_0 is appropriately normalized. In particular, the normalization constant for ψ_ξ does not depend on ξ .

The proof is presented in Section 3.5.1. The existence and uniqueness of an invariant measure in the case when either $\gamma_x = 0$ or $\gamma_y = 0$ is a much more difficult question. To obtain such a result, more precise assumptions on the potential are required (see Remark 3 in Section 3.5.1).

3.3 Mathematical analysis of the viscosity

3.3.1 Linear response

Linear response results allow to compute the average of some property with respect to the nonequilibrium measure in terms of equilibrium averages, in the limit when the parameter giving the strength of the nonequilibrium forcing vanishes. To describe the result more precisely, we recall the definitions of the infinitesimal generator associated to the equilibrium Langevin process (*i.e.* (2.79) in the case when $\xi = 0$):

$$\mathcal{A}_0 = \mathcal{A}_{\text{ham}} + \mathcal{A}_{\text{thm}},$$

where

$$\mathcal{A}_{\text{ham}} = \frac{p}{m} \cdot \nabla_q - \nabla V(q) \cdot \nabla_p,$$

and

$$\mathcal{A}_{\text{thm}} = \sum_{\alpha=x,y} \gamma_{\alpha} \left(-\frac{p_{\alpha}}{m} \cdot \nabla_{p_{\alpha}} + \frac{1}{\beta} \Delta_{p_{\alpha}} \right) = \frac{e^{\beta H}}{\beta} \sum_{\alpha=x,y} \gamma_{\alpha} \operatorname{div}_{p_{\alpha}} \left(e^{-\beta H} \nabla_{p_{\alpha}} \cdot \right).$$

It can be proved (see Section 3.5.1) that \mathcal{A}_0^{-1} is a well defined operator on \mathcal{H} .

The generator of the nonequilibrium perturbation reads

$$\mathcal{B} = \sum_{i=1}^N F(q_{yi}) \partial_{p_{xi}},$$

and its adjoint on $L^2(\psi_0)$ is

$$\mathcal{B}^* = -\sum_{i=1}^N F(q_{yi}) \partial_{p_{xi}} + \frac{\beta}{m} p_{xi} F(q_{yi}).$$

The generator of the dynamics (2.79) is therefore

$$\mathcal{A}_{\xi} = \mathcal{A}_0 + \xi \mathcal{B},$$

with adjoint $\mathcal{L}_{\xi} = \mathcal{L}_0 + \xi \mathcal{B}^*$.

Linear response is an easy consequence of Theorem 4:

Corollary 1 *Under the same assumptions as in Theorem 4, and for any function h regular enough,*

$$\lim_{\xi \rightarrow 0} \frac{\langle \mathcal{A}_0 h \rangle_{\xi}}{\xi} = -\frac{\beta}{m} \left\langle h, \sum_{i=1}^N p_{xi} F(q_{yi}) \right\rangle_{L^2(\psi_0)}. \quad (3.2)$$

Besides, for any function $h \in \mathcal{H}$,

$$\lim_{\xi \rightarrow 0} \frac{\langle h \rangle_{\xi}}{\xi} = -\frac{\beta}{m} \left\langle \mathcal{A}_0^{-1} h, \sum_{i=1}^N p_{xi} F(q_{yi}) \right\rangle_{L^2(\psi_0)}. \quad (3.3)$$

Using the identity

$$-\mathcal{A}_0^{-1} = \int_0^{+\infty} e^{t\mathcal{A}_0} dt$$

as operators on \mathcal{H} (see [38, 39, 87] for a precise justification of this equality, obtained as a limit of a Laplace transform of the semi-group), the linear response statement (3.3) can be rewritten as a time correlation

$$\begin{aligned} \lim_{\xi \rightarrow 0} \frac{\langle h \rangle_\xi}{\xi} &= \frac{\beta}{m} \int_0^{+\infty} \left\langle e^{t\mathcal{A}_0} h, \sum_{i=1}^N p_{xi} F(q_{yi}) \right\rangle_{L^2(\psi_0)} dt \\ &= \frac{\beta}{m} \int_0^{+\infty} \mathbb{E} \left(h(q_t, p_t) \sum_{i=1}^N p_{xi,0} F(q_{yi,0}) \right) dt \end{aligned}$$

where the expectation is taken over all initial condition distributed according to the equilibrium measure ψ_0 , and over all realizations of the equilibrium dynamics with generator \mathcal{A}_0 . This rewriting allows to make contact with Green-Kubo type formulas.

Proof. Since $\langle \mathcal{A}_0 h, 1 \rangle_{L^2(\psi_0)} = \langle h, \mathcal{L}_0 1 \rangle_{L^2(\psi_0)} = 0$, it holds

$$\langle \mathcal{A}_0 h \rangle_\xi = \langle \mathcal{A}_0 h, f_\xi \rangle_{L^2(\psi_0)} = \xi \langle \mathcal{A}_0 h, f_1 \rangle_{L^2(\psi_0)} + O(\xi^2) = \xi \langle h, \mathcal{L}_0 f_1 \rangle_{L^2(\psi_0)} + O(\xi^2).$$

Now, in the proof of Theorem 4, we show that (see (3.26))

$$\mathcal{L}_0 f_1 = -\mathcal{B}^* 1 = -\frac{\beta}{m} \sum_{i=1}^N p_{xi} F(q_{yi}),$$

which gives the expected result. \diamond

3.3.2 Local conservation of the longitudinal velocity

We prove in this section a conservation equation for velocities in the x -direction, when spatial averages over small windows in the transverse direction y are considered. This allows to state an equation relating the off-diagonal term of the stress tensor and the nongradient force acting on the system, see (3.8) below. Our derivation may be seen as a mathematically rigorous counterpart to the seminal work of Irving and Kirkwood [53]. We assume from now on that the potential energy is given by a sum of pairwise interactions:

$$V(q_1, \dots, q_N) = \sum_{1 \leq i < j \leq N} v(|q_i - q_j|), \quad (3.4)$$

for some given smooth potential v .

Consider the following average longitudinal velocity:

$$U_x^\varepsilon(Y, q, p) = \frac{L_y}{Nm} \sum_{i=1}^N p_{xi} \chi_\varepsilon(q_{yi} - Y), \quad (3.5)$$

where χ_ε (with $0 < \varepsilon \leq 1$) is an approximation of the identity on $L_y \mathbb{T}$. More precisely,

$$\chi_\varepsilon(s) = \sum_{n \in \mathbb{Z}} \frac{1}{\varepsilon} \chi\left(\frac{s - nL_y}{\varepsilon}\right),$$

where $\chi \in C^\infty(\mathbb{R})$ has support in $[0, L_y]$ and $\int_0^{L_y} \chi = 1$. The factor L_y in (3.5) accounts for the fact that χ_ε has units of inverse lengths: in fact,

$$\frac{1}{L_y} \int_0^{L_y} U_x^\varepsilon(Y, q, p) dY = \frac{1}{Nm} \sum_{i=1}^N p_{xi}$$

is the average velocity of the system. In practice, averages such as (3.5) are computed with bin indicator functions (see Section 3.4.1).

We also need a spatially localized (with respect to the altitude Y) version of the off-diagonal term of the stress tensor. This quantity is given by the following expression:

$$\begin{aligned} & \Sigma_{xy}^\varepsilon(Y, q, p) \\ &= \frac{1}{L_x} \left(\sum_{i=1}^N \frac{p_{xi} p_{yi}}{m} \chi_\varepsilon(q_{yi} - Y) - \sum_{1 \leq i < j \leq N} v'(|q_i - q_j|) \frac{q_{xi} - q_{xj}}{|q_i - q_j|} \int_{q_{yj}}^{q_{yi}} \chi_\varepsilon(s - Y) ds \right). \end{aligned} \quad (3.6)$$

The fact that it can be interpreted as some stress tensor is motivated below by the limiting spatial average (3.7) as well as the conservation law (3.8). Note that the spatial average over Y

$$\begin{aligned} & \frac{1}{L_y} \int_0^{L_y} \Sigma_{xy}^\varepsilon(Y, q, p) dY \\ &= \frac{1}{L_x L_y} \left(\sum_{i=1}^N \frac{p_{xi} p_{yi}}{m} - \sum_{1 \leq i < j \leq N} v'(|q_i - q_j|) \frac{(q_{xi} - q_{xj})(q_{yi} - q_{yj})}{|q_i - q_j|} \right) \end{aligned} \quad (3.7)$$

is the standard expression encountered for the off-diagonal term of the pressure tensor without spatial localization. The expression (3.6) comes out naturally from the mathematical analysis (see the proof of Proposition 1), and was already proposed in [105] (where it is called the 'method of planes').

The relationship between the local longitudinal velocity and the off-diagonal term of the stress tensor is made precise in the following proposition.

Proposition 1 *The limits*

$$u_x(Y) = \lim_{\varepsilon \rightarrow 0} \lim_{\xi \rightarrow 0} \frac{\langle U_x^\varepsilon(Y, \cdot) \rangle_\xi}{\xi}$$

and

$$\sigma_{xy}(Y) = \lim_{\varepsilon \rightarrow 0} \lim_{\xi \rightarrow 0} \frac{\langle \Sigma_{xy}^\varepsilon(Y, \cdot) \rangle_\xi}{\xi}$$

belong to $C^\infty(L_y \mathbb{T})$ and

$$\frac{d\sigma_{xy}(Y)}{dY} + \gamma_x \bar{\rho} u_x(Y) = \bar{\rho} F(Y), \quad (3.8)$$

where $\bar{\rho} = \rho/m$ is the particle density.

The proof is based on an application of Corollary 1 with (3.5) as a test function h . The order of the limits $\varepsilon \rightarrow 0$ and $\xi \rightarrow 0$ cannot be inverted since the linear response result of Corollary 1 cannot be applied with h replaced by the limit of χ_ε (which is a Dirac mass).

Equations similar to (3.8) could be written down for other quantities such as the transverse velocity U_y or longitudinal and transverse energy fluxes (see [53] for the original derivation of the corresponding equations).

3.3.3 Definition and closure relation for shear viscosity computations

We now discuss a closure relation for (3.8), which allows to obtain an equation on the average velocity only, from which the viscosity can be extracted.

By analogy with continuum fluid mechanics, we *define* the shear viscosity η as follows:

$$\sigma_{xy}(Y) := -\eta(Y) \frac{du_x(Y)}{dY}. \quad (3.9)$$

This definition leads to the following equation on u_x :

$$-\frac{d}{dY} \left(\eta(Y) \frac{du_x(Y)}{dY} \right) + \gamma_x \bar{\rho} u_x(Y) = \bar{\rho} F(Y).$$

In bulk homogeneous fluids, the simplest closure is to assume that

$$\eta(Y) = \eta > 0, \quad (3.10)$$

so that the following equation on u_x is obtained:

$$-\eta u_x''(Y) + \gamma_x \bar{\rho} u_x(Y) = \bar{\rho} F(Y). \quad (3.11)$$

In order to ensure the uniqueness of the solution when $\gamma_x = 0$, an additional condition on u_x should be added (such as a vanishing integral over the domain $L_y \mathbb{T}$).

The equation (3.11) obtained with the help of the closure relation is the basis for numerical methods to compute the shear viscosity given a potential energy function V . We were not able to justify mathematically the assumption (3.10). We nonetheless provide a numerical validation of this assumption in Section 3.4.2.

3.3.4 Asymptotic behaviour of the viscosity for large frictions

An important issue is the dependence of the viscosity on the parameters of the dynamics. For the Langevin dynamics (2.79), this means understanding the dependence of the viscosity on the friction parameters γ_x, γ_y . The limits $\gamma_x \rightarrow 0$ or $\gamma_y \rightarrow 0$ are very difficult to study mathematically without strong assumptions on the potential and/or the geometry of the system (see Remark 3). We therefore rely on numerical simulations for these cases (see Sections 3.4.2 and 3.4.2).

On the other hand, the limit when one of the friction parameters goes to infinity can be studied. To this end, we have to understand the limit of the velocity field u_x as either γ_x or γ_y goes to infinity. This is done by rigorous asymptotic analysis. Thanks to (3.11), limiting behaviors of the viscosity may be inferred from the limiting behaviors of the velocity profiles. The key result to obtain the limiting velocity profile is to characterize the limit of some averages with respect to specific solutions of the Poisson equation (see (3.13) and (3.15) below).

Infinite transverse friction

We start with the case $\gamma_y \rightarrow +\infty$, for a fixed value $\gamma_x > 0$.

Theorem 5 (Infinite transverse friction) *Consider a given smooth function G and a longitudinal friction $\gamma_x > 0$. Define $\mathcal{A}_0(\gamma_y) := \mathcal{A}_0 = \mathcal{A}_{\text{ham}} + \gamma_x \mathcal{A}_{x,\text{thm}} + \gamma_y \mathcal{A}_{y,\text{thm}}$, with*

$$\mathcal{A}_{\alpha,\text{thm}} = -\frac{p_\alpha}{m} \cdot \nabla_{p_\alpha} + \frac{1}{\beta} \Delta_{p_\alpha}, \quad (3.12)$$

and denote by f_{γ_y} the unique solution in \mathcal{H} of the equation

$$-\mathcal{A}_0(\gamma_y) f_{\gamma_y} = \sum_{i=1}^N p_{xi} G(q_{yi}). \quad (3.13)$$

Then, there exist $f^0 \in H^1(\psi_0)$ and a constant $C > 0$ such that, for all $\gamma_y \geq \gamma_x$,

$$\|f_{\gamma_y} - f^0\|_{H^1(\psi_0)} \leq \frac{C}{\gamma_y}. \quad (3.14)$$

Besides, the function f^0 is of the general form

$$f^0(q, p) = \sum_{i=1}^N G(q_{yi}) \phi_i(q_x, q_y, p_x),$$

where the functions ϕ_i are C^∞ .

The proof can be read in Section 3.5.3. The above result can be used to understand the limit of $u_x(Y)$ as $\gamma_y \rightarrow +\infty$. Indeed, by Proposition 1,

$$u_x^{\gamma_y, \varepsilon}(Y) := \lim_{\xi \rightarrow 0} \frac{\langle U_x^\varepsilon(Y, \cdot) \rangle_\xi}{\xi} = \frac{\beta}{m} \left\langle \mathcal{W}_{\gamma_y}^\varepsilon(Y, q, p), \sum_{i=1}^N p_{xi} F(q_{yi}) \right\rangle_{L^2(\psi_0)},$$

where $-\mathcal{A}_0(\gamma_y) \mathcal{W}_{\gamma_y}^\varepsilon(Y, \cdot) = U_x^\varepsilon(Y, \cdot)$ is a Poisson equation of the form (3.13) (with $G(y)$ proportional to $\chi_\varepsilon(y - Y)$). The convergence result (3.14) shows that $\mathcal{W}_{\gamma_y}^\varepsilon(Y, \cdot)$ has a limit as $\gamma_y \rightarrow +\infty$, and the limiting velocity field reads

$$u_x^{\infty, \varepsilon}(Y) = \frac{\beta L_y}{N m^2} \left\langle \sum_{j=1}^N \chi_\varepsilon(q_{yj} - Y) \phi_j(q_x, q_y, p_x), \sum_{i=1}^N p_{xi} F(q_{yi}) \right\rangle_{L^2(\psi_0)}.$$

The latter quantity has a limit as $\varepsilon \rightarrow 0$, so that the velocity field converges to some limiting field u_x^∞ . Therefore, the viscosity extracted from (3.11) also has a finite limit. These theoretical considerations are illustrated by numerical simulations in Section 3.4.2.

Infinite longitudinal friction

We now consider the limit $\gamma_x \rightarrow +\infty$, for a fixed value $\gamma_y > 0$. In this case, the leading term of the expansion in inverse powers of γ_x is 0, and a refined convergence result is needed to discuss the limit of the velocity profile.

Theorem 6 (Infinite longitudinal friction) *Consider a given smooth function G and a transverse friction $\gamma_y > 0$. Define $\mathcal{A}_0(\gamma_x) := \mathcal{A}_0 = \mathcal{A}_{\text{ham}} + \gamma_x \mathcal{A}_{x,\text{thm}} + \gamma_y \mathcal{A}_{y,\text{thm}}$, and denote by f_{γ_x} the unique solution in \mathcal{H} of the equation*

$$-\mathcal{A}_0(\gamma_x) f_{\gamma_x} = \sum_{i=1}^N p_{xi} G(q_{yi}). \quad (3.15)$$

Then, there exist $f^1 \in H^1(\psi_0)$ and a constant $C > 0$ such that, for all $\gamma_x \geq \gamma_y$,

$$\|f_{\gamma_x} - \gamma_x^{-1} f^1\|_{H^1(\psi_0)} \leq \frac{C}{\gamma_x^2}. \quad (3.16)$$

Besides, the dependence of the function f^1 in the variable p_x can be written explicitly as

$$f^1(q, p) = m \sum_{i=1}^N p_{xi} G(q_{yi}) + \tilde{f}^1(q, p_y).$$

The proof can be read in Section 3.5.4. To obtain asymptotics on the velocity field, we apply the above convergence result with $G(y)$ proportional to $\chi_\varepsilon(y - Y)$ (denoting by f_ε^1 the first term in the expansion in inverse powers of γ_x):

$$\begin{aligned} u_x^\varepsilon(Y) &:= \lim_{\xi \rightarrow 0} \frac{\langle U_x^\varepsilon(Y, \cdot) \rangle_\xi}{\xi} = \frac{\beta L_y}{Nm^2 \gamma_x} \left\langle \sum_{i=1}^N p_{xi} F(q_{yi}), f_\varepsilon^1(q, p) \right\rangle_{L^2(\psi_0)} + \mathcal{O}\left(\frac{1}{\gamma_x^2}\right) \\ &= \frac{\beta L_y}{Nm \gamma_x} \left\langle \sum_{i=1}^N p_{xi} F(q_{yi}), \sum_{j=1}^N p_{xj} \chi_\varepsilon(q_{yj} - Y) \right\rangle_{L^2(\psi_0)} + \mathcal{O}\left(\frac{1}{\gamma_x^2}\right) \\ &= \frac{L_y}{\gamma_x} \int_0^{L_y} F(y) \chi_\varepsilon(y - Y) dy + \mathcal{O}\left(\frac{1}{\gamma_x^2}\right), \end{aligned}$$

where we have used the fact that $\langle p_{xi}, \tilde{f}_\varepsilon^1 \rangle_{L^2(\psi_0)} = 0$ since \tilde{f}_ε^1 does not depend on p_x . This shows that the following limit is well defined:

$$\bar{u}_x(Y) = \lim_{\varepsilon \rightarrow 0} \lim_{\gamma_x \rightarrow +\infty} \gamma_x u_x^\varepsilon(Y) = F(Y). \quad (3.17)$$

The limiting velocity profile \bar{u}_x does not depend on the specific interaction potential v , and is the same for all systems with pairwise interactions. Besides, the viscosity η cannot be extracted from (3.11) since $(u_x^\varepsilon)''$ is of order γ_x^{-1} while F and $\gamma_x^\varepsilon u_x$ are of order 1. The limit $\gamma_x \rightarrow +\infty$ is therefore somewhat degenerate from a theoretical viewpoint. Numerical simulations however allow to investigate the large γ_x asymptotics, see Section 3.4.2.

3.4 Numerical results for the Lennard–Jones fluid

We present in this section some numerical illustrations of the theoretical results obtained in Section 3.3.

3.4.1 Numerical implementation

Description of the system

We consider a Lennard–Jones fluid, which is a standard test case for shear flow computations, in a 2-dimensional setting (in order to limit the number of degrees of freedom and henceforth obtain results with lower statistical uncertainties). The potential energy is of the form (3.4), with

$$v_{\text{LJ}}(r) = 4\varepsilon_{\text{LJ}} \left(\left(\frac{d_{\text{LJ}}}{r} \right)^{12} - \left(\frac{d_{\text{LJ}}}{r} \right)^6 \right). \quad (3.18)$$

Actually, it is numerically more convenient to work with a truncated potential, which reads:

$$v(r) = \begin{cases} v_{\text{LJ}}(r) & \text{if } r \leq r_{\text{spline}}, \\ v_{\text{spline}}(r) & \text{if } r_{\text{spline}} \leq r \leq r_{\text{cut}}, \\ 0 & \text{if } r \geq r_{\text{cut}}. \end{cases}$$

The function v_{spline} is a polynomial of order 3 which is such that the potential is C^1 on $(0, +\infty)$. Note that there is a singularity at $r = 0$ so that the potential v does not satisfy Assumption 2. It seems that this singularity does not show up in the numerical simulations. Any problem related to this singularity could be overcome by modifying appropriately the potential for the very small values of r . We use $r_{\text{cut}} = 3d_{\text{LJ}}$ and $r_{\text{spline}} = 0.9r_{\text{cut}}$.

All the results presented below are in reduced units, which are determined by setting to 1 the energy ε_{LJ} , the length d_{LJ} , and the mass m . The remaining tunable parameters of the model are the force amplitude ξ and the friction parameters γ_x, γ_y .

The thermodynamic state of the system is determined by the fluid mass density ρ and the temperature T . In the numerical illustrations below, we set $\beta = 0.4$, $\rho = 0.69$ and consider $L_x = 360$ and $L_y = 18$. The number of simulated particles is therefore $N = 4500$.

We have checked that the thermodynamic limit is attained for the systems we simulate, *i.e.* that the values of the viscosity and the profiles we present are converged with respect to increasing values of L_x, L_y (at fixed density).

Nongradient forces

We consider three different external perturbations, which are all normalized so that $-1 \leq F(y) \leq 1$:

- (i) sinusoidal perturbation: $F(y) = \sin\left(\frac{2\pi y}{L_y}\right)$;

$$\begin{aligned}
\text{(ii) piecewise linear perturbation: } F(y) &= \begin{cases} \frac{4}{L_y} \left(y - \frac{L_y}{4} \right), & 0 \leq y \leq \frac{L_y}{2}, \\ \frac{4}{L_y} \left(\frac{3L_y}{4} - y \right), & \frac{L_y}{2} \leq y \leq L_y; \end{cases} \\
\text{(iii) piecewise constant constant perturbation: } F(y) &= \begin{cases} 1, & 0 < y < \frac{L_y}{2}, \\ -1, & \frac{L_y}{2} < y < L_y. \end{cases}
\end{aligned}$$

Note that only the sinusoidal force satisfies Assumption 2. This shape of perturbation, introduced in [33], is the most popular choice for shear viscosity computations.

Integration of the dynamics

The dynamics (2.79) is discretized using a standard splitting scheme, similar to the schemes proposed in [68]. The evolution is decomposed as the superposition of (i) a Hamiltonian part, which is integrated with the standard Verlet scheme [37, 108]; and (ii) a fluctuation/dissipation part containing also the nongradient force, which can be integrated analytically since it is an Ornstein-Uhlenbeck process with a constant drift. The numerical scheme reads

$$\left\{ \begin{array}{l} p^{n+1/2} = p^n - \frac{\Delta t}{2} \nabla V(q^n), \\ q^{n+1} = q^n + \Delta t p^{n+1/2}, \\ \tilde{p}^{n+1} = p^{n+1/2} - \frac{\Delta t}{2} \nabla V(q^{n+1}), \\ p_{xi}^{n+1} = \alpha_x \tilde{p}_{xi}^{n+1} + \sqrt{\frac{1}{\beta} (1 - \alpha_x^2)} G_{xi}^n + (1 - \alpha_x) \frac{\xi}{\gamma_x} F(q_{yi}^{n+1}), \quad i = 1, \dots, N \\ p_y^{n+1} = \alpha_y \tilde{p}_y^{n+1} + \sqrt{\frac{1}{\beta} (1 - \alpha_y^2)} G_y^n, \end{array} \right. \quad (3.19)$$

where $\alpha_{x,y} = \exp(-\gamma_{x,y} \Delta t)$, and G_x^n, G_y^n are independent and identically distributed standard Gaussian random variables. Note that this scheme is well behaved in the limits $\gamma_x \rightarrow +\infty$ and/or $\gamma_y \rightarrow +\infty$, as well as in the limits $\gamma_y \rightarrow 0$ or $\gamma_x \rightarrow 0$ (the well posedness of the latter case is a consequence of the limit $(1 - \alpha_x)/\gamma_x \rightarrow \Delta t$ as $\gamma_x \rightarrow 0$). It reduces to the standard Verlet scheme when $F = 0$ and $\gamma_x = \gamma_y = 0$.

We use $\Delta t = 0.005$ in all the simulations below. This time step ensures that the relative error in energy is about 1% for the Verlet scheme.

Numerical localization

To analyze the various fields which can be constructed from the numerical data generated by the simulation (longitudinal velocity, off-diagonal component of the stress tensor, kinetic temperatures, etc), we use a binning procedure in the Y variable. More precisely, we introduce a mesh with a uniform spacing ΔY , centered on the altitudes $Y_s = (s + 1/2)\Delta Y$ (with $0 \leq s \leq S - 1$ and $S\Delta Y = L_y$).

The microscopic observables we wish to average are either the longitudinal velocity (3.5) or the off diagonal stress tensor (3.6). Both functions are of the general form

$$A^\varepsilon(Y, q, p) = \sum_{i=1}^N a_i(q, p) \Phi_\varepsilon(q_{yi} - Y),$$

where Φ_ε is either χ_ε or an integral of this function. Averages of such functions over each cell are computed as

$$\mathcal{A}_s^\varepsilon = \frac{1}{\xi \Delta Y} \int_{Y_s - \Delta Y/2}^{Y_s + \Delta Y/2} \langle A(Y, \cdot) \rangle_\xi dY = \frac{1}{\xi \Delta Y} \left\langle \int_{Y_s - \Delta Y/2}^{Y_s + \Delta Y/2} A^\varepsilon(Y, \cdot) dY \right\rangle_\xi.$$

Taking advantage of the integration in the Y variable, it is possible to take the limit $\varepsilon \rightarrow 0$ in the latter expression. This amounts to computing ensemble averages with respect to bin indicator functions (or their integrals). For instance, the average normalized longitudinal velocity in the s th bin is

$$\mathcal{U}_s = \frac{L_y}{\xi N m \Delta Y} \left\langle \sum_{i=1}^N p_{xi} \mathbf{1}_{[Y_s - \Delta Y/2, Y_s + \Delta Y/2]}(q_{yi}) \right\rangle_\xi.$$

In practice, the ensemble average $\langle \cdot \rangle_\xi$ is computed as a time average over numerical trajectories $(q^n, p^n)_{n=1, \dots, N_{\text{iter}}}$.

Estimation of the viscosity

The solutions of Equation (3.11) are periodic in the Y -variable and are hence most easily analyzed using Fourier series (see for instance the discussion in [28, 42]). We consider the Fourier coefficients of the the average longitudinal velocity u_x and the force F , given respectively for $k \in \mathbb{Z}$ by

$$U_k = \frac{1}{L_y} \int_0^{L_y} u_x(y) \exp\left(\frac{2ik\pi y}{L_y}\right) dy, \quad F_k = \frac{1}{L_y} \int_0^{L_y} F(y) \exp\left(\frac{2ik\pi y}{L_y}\right) dy. \quad (3.20)$$

The coefficients U_k can be estimated numerically using trajectory averages as

$$U_k^{N_{\text{iter}}} = \frac{1}{N_{\text{iter}} \xi N} \sum_{n=1}^{N_{\text{iter}}} \sum_{j=1}^N \frac{p_{xj}^n}{m} \exp\left(\frac{2ik\pi q_{yj}^n}{L_y}\right). \quad (3.21)$$

This is a valid estimation provided the particle density is uniform, *i.e.* when the marginal distribution in the position variable of one particle is the uniform law on the domain. By translation invariance, this is true when no external force is present. It remains approximately true when ξ is not too large. We checked that this approximation has no influence on the presented numerical results.

The shear viscosity is obtained from a Fourier analysis of (3.11). The value of η should be independent of $k \in \mathbb{Z}$. It should also satisfy the following equation:

$$U_k = \frac{F_k}{\frac{\eta}{\bar{\rho}} \left(\frac{2\pi}{L_y}\right)^2 k^2 + \gamma_x}. \quad (3.22)$$

The shear viscosity is finally obtained as

$$\eta = \bar{\rho} \left(\frac{F_k}{U_k} - \gamma_x \right) \left(\frac{L_y}{2k\pi} \right)^2. \quad (3.23)$$

A confidence interval on the value of U_k can straightforwardly be obtained from the estimator (3.21) using block averaging procedures. The statistical uncertainty on the viscosity is then obtained with (3.23). Since the coefficients U_k decrease very rapidly as $|k|$ increases, the relative statistical errors increase rapidly as well. We therefore restricted ourselves to $|k| = 1$ in our numerical simulations.

3.4.2 Numerical results

In all cases, time averages were computed over $N_{\text{iter}} \simeq 10^7$ iterations.

Linear response

We first verify numerically the linearity of the amplitude of the longitudinal velocity as a function of the magnitude ξ of the nongradient force. More precisely, we check that $|U_1|$ is constant, for the three forces F at hand, in the case when $(\gamma_x, \gamma_y) = (1, 1)$ (see Figure 3.1). In the sequel, unless otherwise stated, the numerical results are obtained with $\xi = 0.1$.

ξ	U_1	η
0.03	0.788 ± 0.05	1.53 ± 0.5
0.1	0.788 ± 0.01	1.52 ± 0.14
0.3	0.781 ± 0.0049	1.59 ± 0.04
1	0.780 ± 0.00148	1.60 ± 0.01

Table 3.1. Fourier coefficient U_1 and shear viscosity for various ξ in the case of the sinusoidal force.

Validation of the closure

We present in Figures 3.2, 3.3 and 3.4 the numerical approximations of the longitudinal velocity u_x and the off-diagonal term of the stress tensor σ_{xy} . The latter function is compared to the quantity $-\eta u'_x$, where η is obtained from (3.23), and u'_x is evaluated using a second order finite difference. The good agreement between σ_{xy} and $-\eta u'_x$ validates the assumption (3.10), the discrepancies resulting from statistical fluctuations magnified by the numerical derivative, and also, for the piecewise constant force, from the singularity at $L_y/2$.

Besides, the velocity profile is consistent with (3.11) (as can be checked by comparing the numerical solution and the solution of (3.11) computed with the value of η estimated from the simulation).

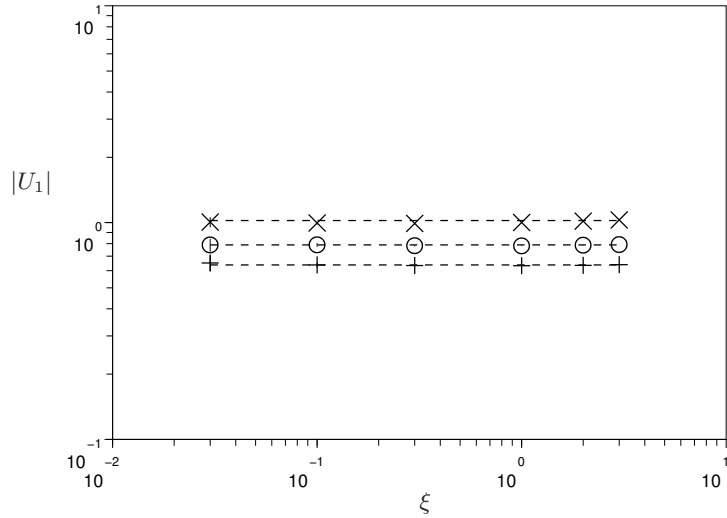


Fig. 3.1. Value of $|U_1|$ as a function of ξ , for $(\gamma_x, \gamma_y) = (1, 1)$ and the three nongradient forces at hand (piecewise constant perturbation \times ; piecewise linear perturbation $+$; sinusoidal perturbation \circ).

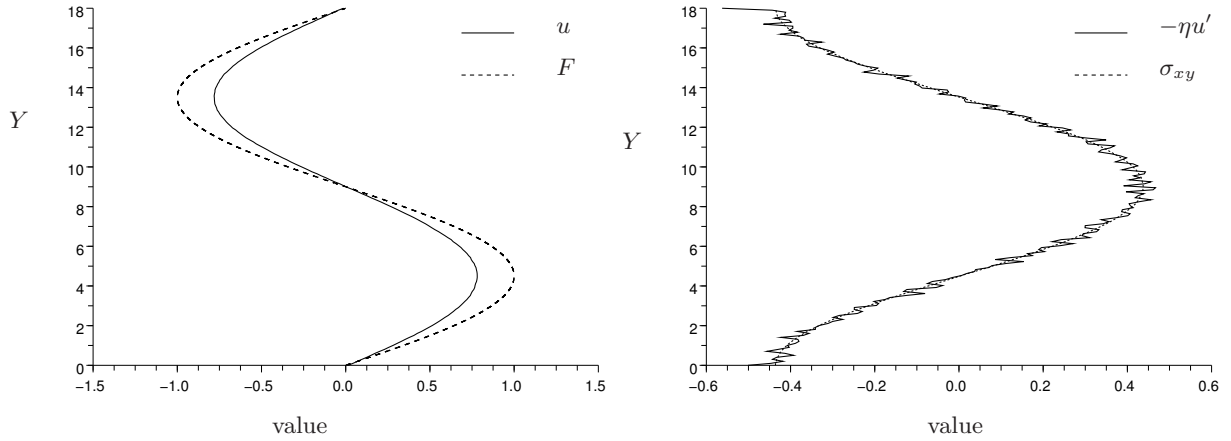


Fig. 3.2. Velocity profile and off diagonal component of the stress tensor for the sinusoidal nongradient force.

Nonlinear effects

The numerical results show that the linear response for the velocity is valid even for larger values of ξ . In fact, a more refined analysis shows that, even if no nonlinear effect can be observed on the longitudinal velocity for the values of ξ we considered, nonlinear effects on the kinetic temperature cannot be ignored for values of $|\xi| \geq 0.1$ as depicted in Figure 3.5 and 3.6. More precisely, Figure 3.5 shows spatial variation of small amplitude of the densities profiles around the constant density imposed in the system ($\rho = 0.69$) while in Figure 3.6 we observe a bias in temperature, which deviates significantly from the temperature of the Langevin bath ($T = \beta^{-1} = 2.5$), a phenomenon that is not observed for small ξ .

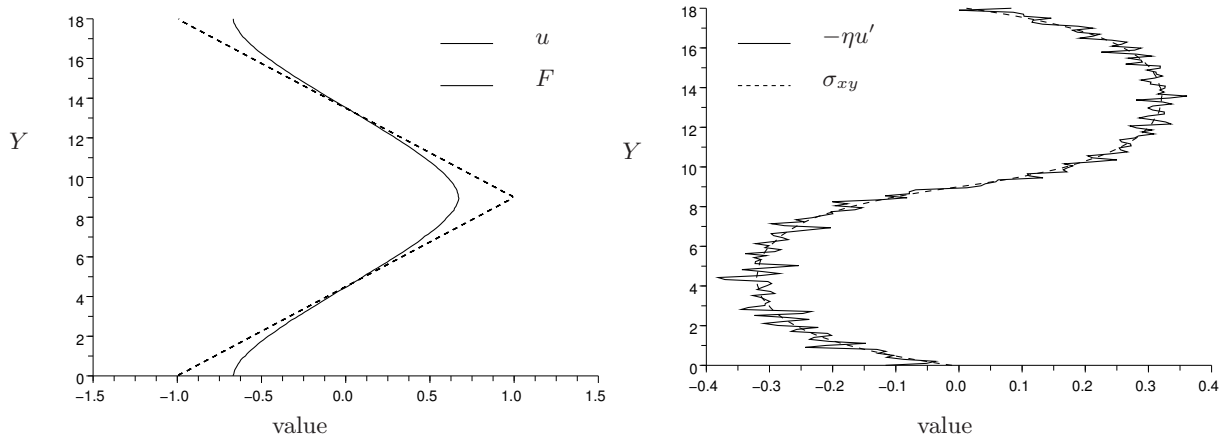


Fig. 3.3. Velocity profile and off diagonal component of the stress tensor for the piecewise linear nongradient force.

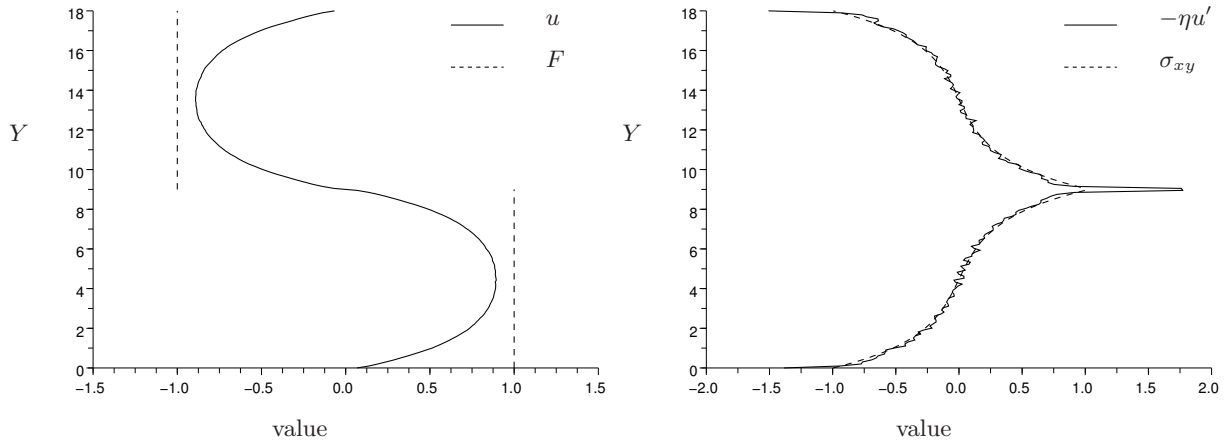


Fig. 3.4. Velocity profile and off diagonal component of the stress tensor for the piecewise constant force.

Vanishing friction parameter

The mathematical analysis presented in this chapter does not cover the case where one of the friction parameter vanishes. This consideration is relevant since the presence of the noise is somewhat artificial. We tested numerically a case where $\gamma_x = 0$, and observed that the system reach a steady state owing to the dissipation in the y -direction. Figure 3.7 shows that linear response result for the velocity seem to hold in the case where the longitudinal friction is set to 0. Note that the amplitude of the response is much more sensitive than in the case of positive γ_x . Though, the relative statistical error seems to be diminished which is natural since the noise is less present in the system. Concerning the shear viscosity, a plateau value seems to be achieved as $\gamma_x \rightarrow 0$, as we will see in § 3.4.2, and formula (3.23) seems to be valid even in the limit $\gamma_x \rightarrow 0$. In contrast, taking both friction parameters γ_x and γ_y equal to 0 do not allow to recover the linear response since the system does not reach a steady state.

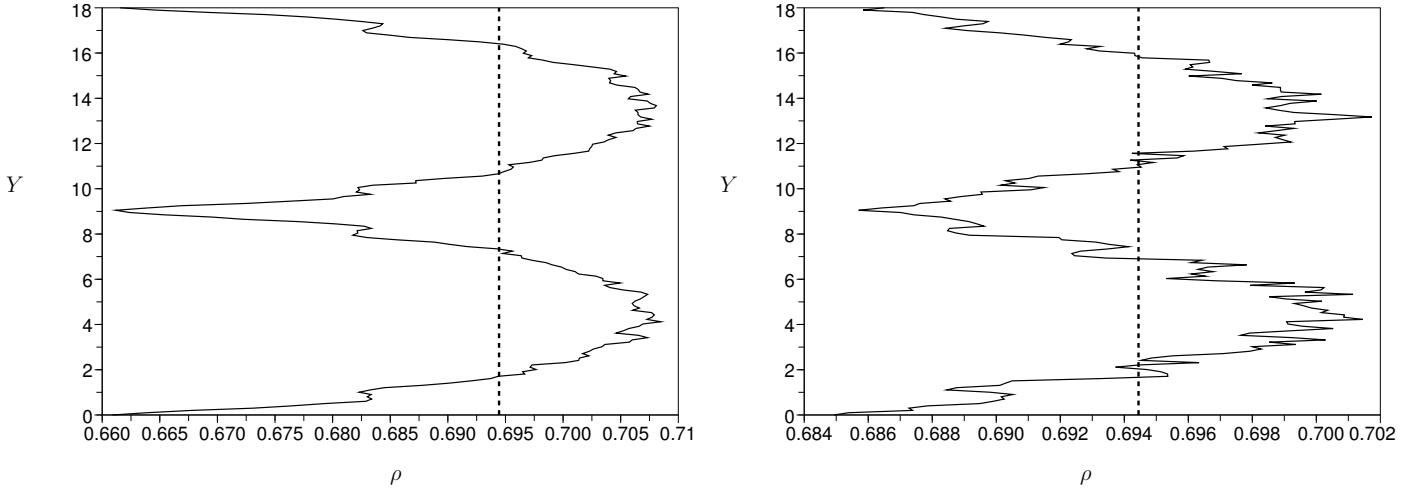


Fig. 3.5. Density profile evaluated with binning method. Left: $(\gamma_x, \xi, U_1) = (1, 2, 2.03)$; Right: $(\gamma_x, \xi, U_1) = (0, 0.3, 1.34)$. The dashed line indicate the value of the constant density of the corresponding equilibrium system ($\rho = 0.69$).

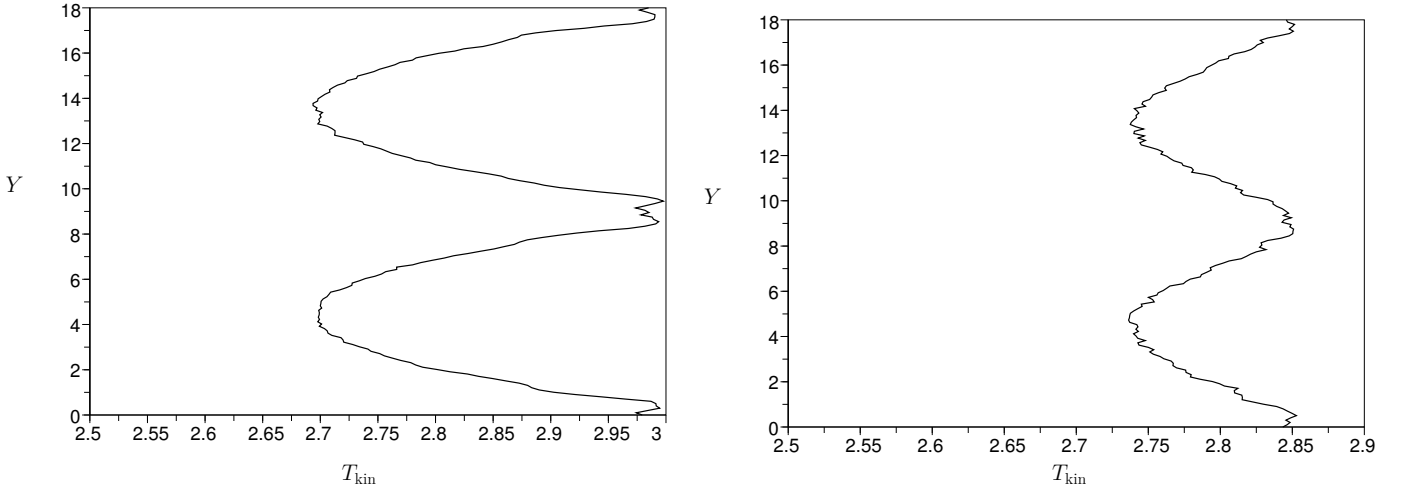


Fig. 3.6. Kinetic temperature profiles evaluated with binning method: Left $(\gamma_x, \xi, U_1) = (1, 2, 2.03)$; Right: $(\gamma_x, \xi, U_1) = (0, 0.3, 1.34)$. The kinetic temperature of the equilibrium system is $T = 2.5$.

Linear response via the Green-Kubo formula

As we have seen in Chapter 2 and § 3.3.1, the linear response can be evaluated owing to the Green-Kubo formula:

$$\begin{aligned} \lim_{\xi \rightarrow 0} \frac{\langle h \rangle_\xi}{\xi} &= \frac{\beta}{m} \int_0^{+\infty} \left\langle e^{tA_0} h, \sum_{i=1}^N p_{xi} F(q_{yi}) \right\rangle_{L^2(\psi_0)} dt \\ &= \frac{\beta}{m} \int_0^{+\infty} \mathbb{E} \left(h(q_t, p_t) \sum_{i=1}^N p_{xi,0} F(q_{yi,0}) \right) dt \end{aligned}$$

By considering the sinusoidal perturbation $F(y) = \sin\left(\frac{2\pi y}{L_y}\right)$ and the observable

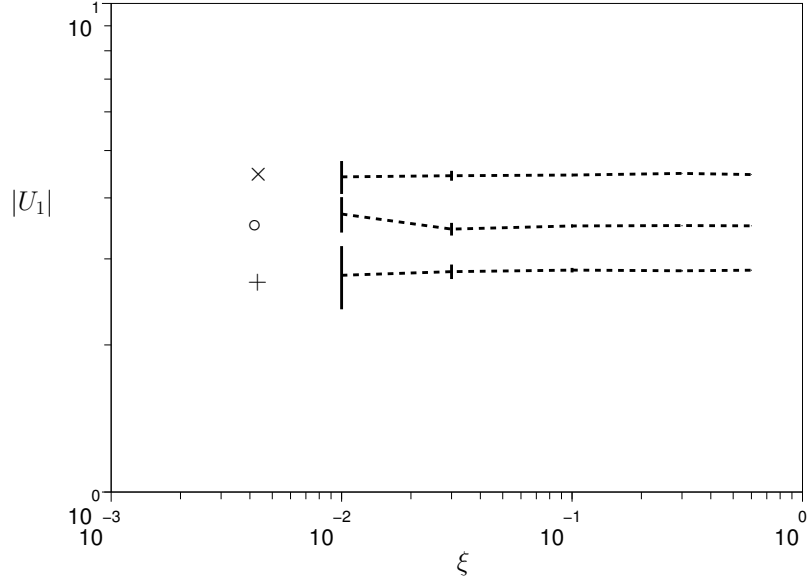


Fig. 3.7. Value of $|U_1|$ as a function of ξ , for $(\gamma_x, \gamma_y) = (0, 1)$ and the three nongradient forces at hand (piecewise constant perturbation \times ; piecewise linear perturbation $+$; sinusoidal perturbation \circ).

$$\mathcal{U}_1(q, p) = \frac{1}{N} \sum_{j=1}^N \frac{p_{xj}}{m} \sin\left(\frac{2\pi q_{yj}}{L_y}\right),$$

which is the first Fourier mode of the expected velocity profile in the nonequilibrium steady state, we obtain the following Green-Kubo formula for U_1

$$U_1 = \lim_{\xi \rightarrow 0} \frac{\langle \mathcal{U}_1 \rangle_{\xi}}{\xi} = \frac{\beta}{m} \int_0^{+\infty} \left\langle \mathcal{U}_1(q_t, p_t) \sum_{i=1}^N p_{xi,0} F(q_{yi,0}) \right\rangle_{\text{eq}} dt, \quad (3.24)$$

Now, we can identify the integrand as the canonical average of the following self-correlation function:

$$\mathcal{C}_{U_1}(t, q, p) = \left\langle \sum_{i=1}^N p_{xi,t} F(q_{yi,t}) \sum_{i=1}^N p_{xi,0} F(q_{yi,0}) \right\rangle_{\text{eq}}. \quad (3.25)$$

We are now in position to compute the linear response coefficient of the velocity profile with the Green-Kubo algorithm presented in Chapter 2. The shear viscosity can be deduced from the closure relationship leading to formula (3.23). Note that herein, we also use formula (3.23) in the case $\gamma_x = 0$. To illustrate numerically this method we consider the same protocol as in Chapter 2, Section 2.3.2, for a system of 225 particles at state point $(\rho, T) = (0.69, 2.5)$ with $N_{\text{replica}} = 20 \times 10^7$. We also investigated the behaviour of the self-correlation function in the case where the flow used to generate the time-dependant Fourier coefficient is the Hamiltonian flow. Results with statistical error are reported in Table 3.2. Figure 3.8 depicts the behaviour of the correlation functions for $(\gamma_x, \gamma_y) = (1, 1)$ (Langevin flow) and $(\gamma_x, \gamma_y) = (0, 0)$ (Hamiltonian flow). Observe that the decorrelation time is much longer in the case of Hamiltonian flow but the integral seems to converge. More precisely we can observe that the self-correlation function seems to behave like $\exp(-\lambda t)$ for $\lambda > 0$ depending on the friction parameters. Finally, we observed that the value of the Fourier coefficient evaluated by this method are in good agreement with the

results obtained with the nonequilibrium method (see Table 3.1). Though, the computational time to achieve the same levels of accuracy is much longer.

Dynamics	U_1	η	t_{dyn}
Langevin	0.781 ± 0.01	1.59 ± 0.168	10
Hamiltonian	3.41 ± 0.094	1.67 ± 0.048	30

Table 3.2. Fourier coefficient U_1 evaluated with the Green-Kubo formula and resulting shear viscosity.

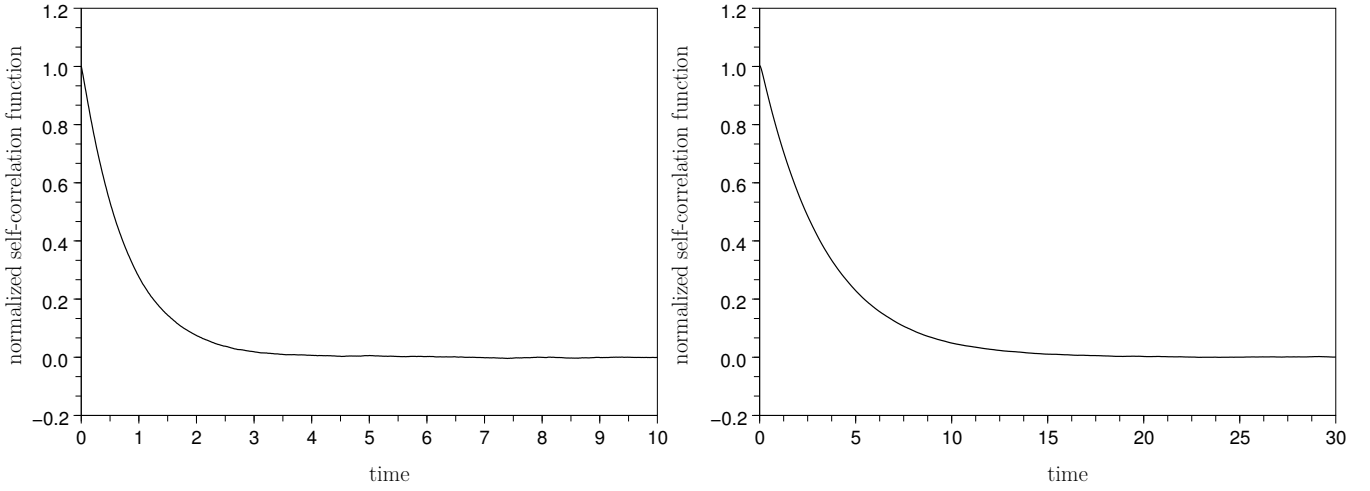


Fig. 3.8. Normalized self-correlation \mathcal{C}_{U_1} . Left: Langevin flow; Right: Hamiltonian flow.

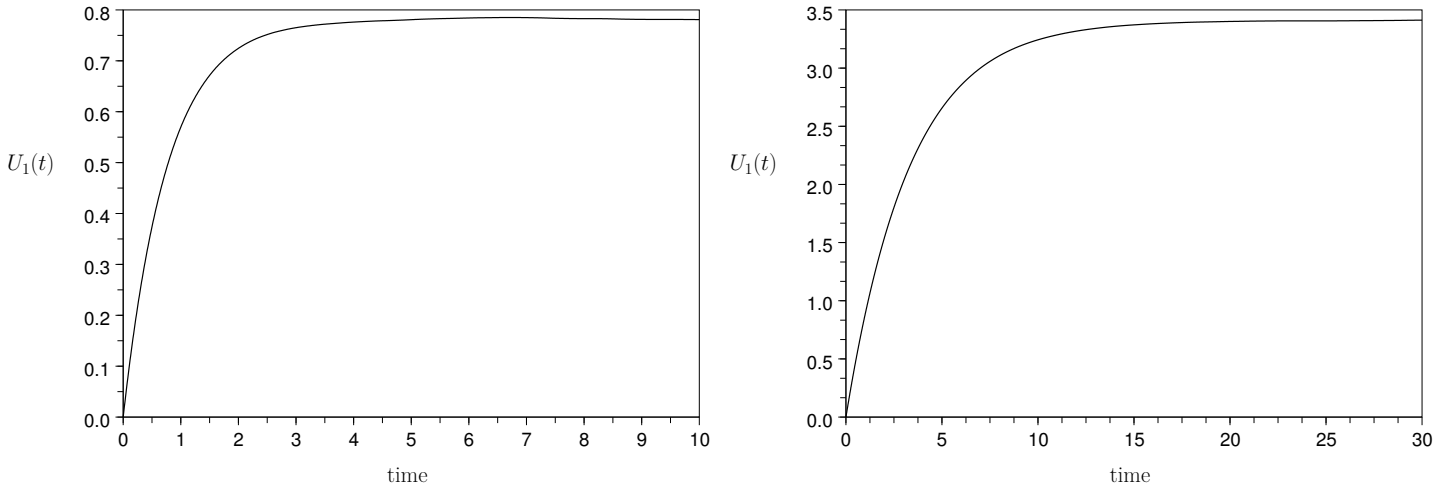


Fig. 3.9. Normalized U_1 as a function of time. Left: Langevin flow; Right: Hamiltonian flow.

Dependence and asymptotics in γ_y

We first verify numerically that the velocity profiles converge to some limiting profile as $\gamma_y \rightarrow +\infty$ with γ_x fixed, and in fact that U_1 converges to some limiting value U_1^∞ (see Figure 3.10). We estimated U_1^∞ by long time simulations with $\alpha_y = 0$ in (3.19) (which amounts to formally setting γ_y to $+\infty$), and computed the distance $|U_1^{\gamma_y} - U_1^\infty|$ as a function of γ_y . A least square fit on the last computed values (in log-log scale) gives $|U_1^{\gamma_y} - U_1^\infty| \sim \gamma_y^{-2.6}$.

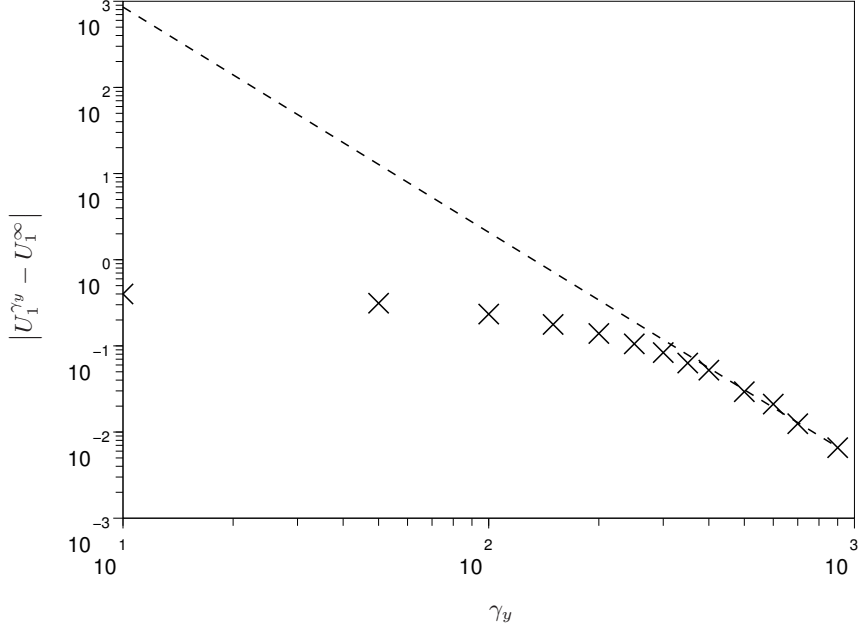


Fig. 3.10. Convergence of the velocity profile for increasing values of the transverse friction γ_y . The dashed line represents an affine fit in log-log scale.

We present in Figure 3.11 the dependence of the viscosity on the friction parameter γ_y , for a fixed value $\gamma_x = 1$. A mild dependence on γ_y is observed in the limit $\gamma_y \rightarrow 0$. The value obtained for $\gamma_y \rightarrow +\infty$ is on the other hand very different from the limit obtained as $\gamma_y \rightarrow 0$. Note also that the viscosity seems to be an increasing function of the transverse friction, which makes sense from a physical viewpoint.

Dependence and asymptotics in γ_x

The discussion after Theorem 6 suggests that the longitudinal velocity decreases as $1/\gamma_x$ as $\gamma_x \rightarrow +\infty$. To observe numerically this behavior, it is necessary to increase the magnitude of the nongradient force. Otherwise, the response is very small (indeed, proportional to γ_x^{-1}) and relative statistical errors are too large to obtain meaningful results. We therefore computed the linear response of the velocity for values of ξ proportional to γ_x . This is done by modifying the evolution on p_x in (2.79) as follows:

$$dp_{xi,t} = -\nabla_{q_{xi}} V(q_t) dt - \gamma_x \left(\frac{p_{xi,t}}{m} - \bar{\xi} F(q_{yi,t}) \right) dt + \sqrt{\frac{2\gamma_x}{\beta}} dW_t^{xi}.$$

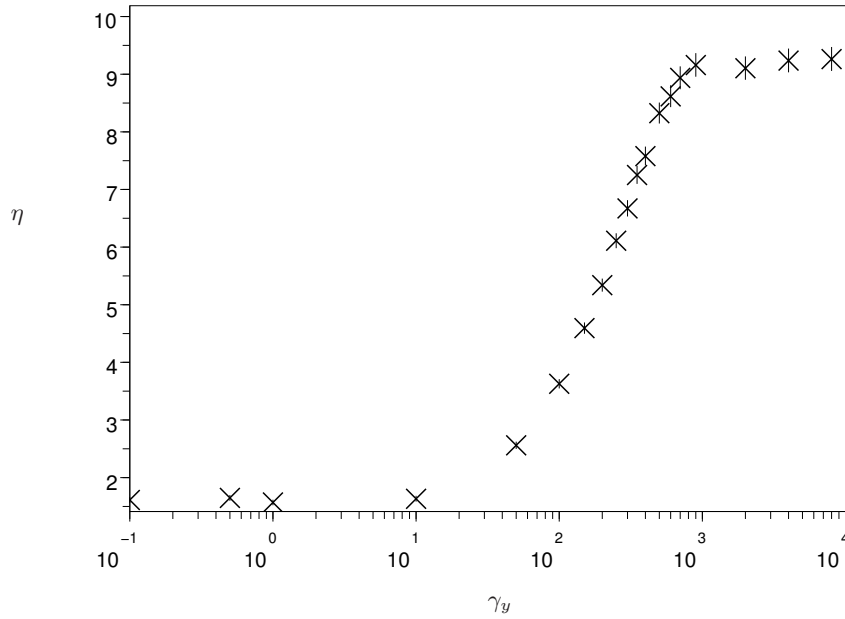


Fig. 3.11. Shear viscosity η as function of γ_y in the case $\gamma_x = 1$, for the sinusoidal nongradient force.

This amounts to replacing ξ in (2.79) by $\xi = \gamma_x \bar{\xi}$. The resulting average velocity profile is $\gamma_x u_x$ at first order in $\bar{\xi}$.

The results depicted in Figure 3.12 show that the average velocity, properly rescaled by γ_x , converges to the nongradient force, as predicted by (3.17). The estimated convergence rate is $|\gamma_x U_1^{\gamma_x} - F_1| \sim \gamma_x^{-0.9}$.

The behavior of the corresponding viscosities cannot be predicted from the results of Theorem 6 (see the discussion at the end of Section 3.3.4). We therefore investigated numerically this dependence, see Figure 3.13. The viscosity is more or less constant for low values of γ_x , and increases for larger ones.

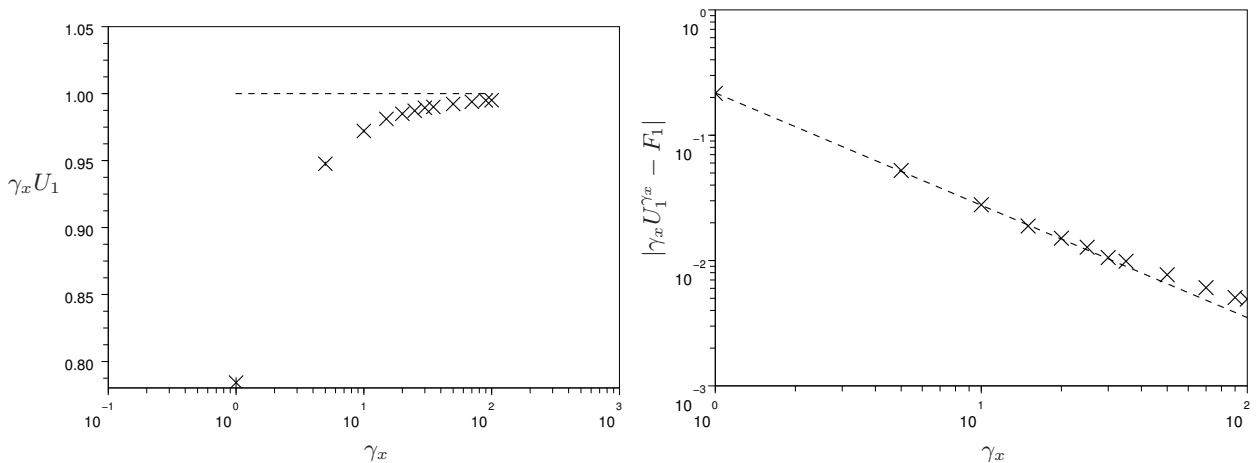


Fig. 3.12. Convergence of the velocity profile for increasing values of the friction γ_x . The dashed line on the right picture represents an affine fit in log-log scale.

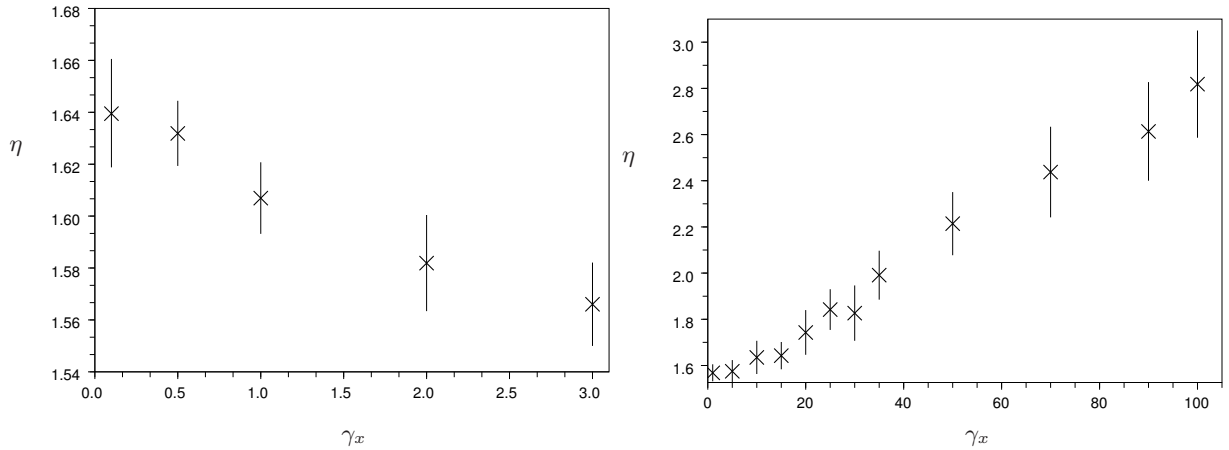


Fig. 3.13. Shear viscosity η as function of γ_x in the case $\gamma_y = 1$, for the sinusoidal nongradient force. Left: behavior for small values of γ_x . Right: large γ_x asymptotics.

3.5 Proof of the results

Unless otherwise stated, the norm $\|\cdot\|$ refers to the norm induced by the canonical scalar product on $L^2(\psi_0)$. Recall from Chapter 2 that the operator $\mathcal{A}_{\alpha,\text{thm}}$ ($\alpha = x, y$), defined in (3.12), can be rewritten as

$$\mathcal{A}_{\alpha,\text{thm}} = -\frac{1}{\beta} \sum_{i=1}^N (\partial_{p_{\alpha i}})^* \partial_{p_{\alpha i}}.$$

Note also that

$$[\partial_{p_{\alpha i}}, \mathcal{A}_{\text{ham}}] = \frac{1}{m} \partial_{q_{\alpha i}},$$

where $[A, B] = AB - BA$ is the commutator of two operators.

3.5.1 Proof of Theorem 4

The existence and the uniqueness of the invariant measure which has a smooth density with respect to the Lebesgue measure for any $\xi \in \mathbb{R}$ is a standard result since the position space is compact and the forces are smooth. It suffices to use hypoellipticity arguments and take the kinetic energy as a Lyapunov function (see for instance [93] for the general strategy, and [88, Appendix A] for the specific case under consideration). As a consequence, and recalling the definitions of the operators given in Section 3.3.1,

$$\text{Ker}(\mathcal{L}_0) = \text{Span}(1) = \{c\psi_0, c \in \mathbb{R}\},$$

the vector space of constant functions on $L^2(\psi_0)$. Note also that $\text{Ker}(\mathcal{A}_0) = \text{Span}(1)$ by [109, Proposition 15].

The key result to prove the expansion (3.1) is the following lemma (proved below).

Lemma 1 *The operators \mathcal{L}_0^{-1} and $\mathcal{L}_0^{-1}\mathcal{B}^*$ are bounded operator on \mathcal{H} (endowed with the $L^2(\psi_0)$ scalar product).*

In view of this result, we can introduce

$$\xi^* = \left\| \mathcal{L}_0^{-1}\mathcal{B}^* \Big|_{\mathcal{H}} \right\|^{-1},$$

and define, for $k \geq 1$,

$$f_{k+1} = -\mathcal{L}_0^{-1}\mathcal{B}^*f_k,$$

with

$$f_1 = -\mathcal{L}_0^{-1}(\mathcal{B}^*1) = -\frac{\beta}{m}\mathcal{L}_0^{-1}\left(\sum_{i=1}^N p_{xi}F(q_{yi})\right), \quad (3.26)$$

which is well-defined since the function $(q, p) \mapsto p_{xi}F(q_{yi})$ belongs to \mathcal{H} for all $i = 1, \dots, N$. The function f_ξ in (3.1) is well defined for $|\xi| < \xi^*$ and a straightforward computation shows that

$$\mathcal{L}_\xi f_\xi = 0.$$

The uniqueness of the invariant measure allows to conclude.

We now write the

Proof of Lemma 1. We denote by $\|\cdot\|$ the $L^2(\psi_0)$ -norm. Standard results of hypocoercivity show that \mathcal{A}_0^{-1} is bounded on \mathcal{H} (and in fact compact by a treatment similar to [38, 39, 87]). Besides, for a smooth test function φ ,

$$\|\mathcal{B}\varphi\| \leq \|F\|_{L^\infty} \sum_{i=1}^N \|\partial_{p_{xi}}\varphi\|,$$

while

$$\langle \varphi, \mathcal{A}_0\varphi \rangle = -\frac{1}{\beta} \left(\gamma_x \|\nabla_{p_x}\varphi\|^2 + \gamma_y \|\nabla_{p_y}\varphi\|^2 \right).$$

This shows that there exists a constant $C > 0$ such that, for any smooth test function φ ,

$$\|\mathcal{B}\varphi\|^2 \leq C |\langle \varphi, \mathcal{A}_0\varphi \rangle| \leq C \|\varphi\| \|\mathcal{A}_0\varphi\|.$$

In conclusion, for any $\varphi \in \mathcal{H}$,

$$\|\mathcal{B}\mathcal{A}_0^{-1}\varphi\|^2 \leq C \|\mathcal{A}_0^{-1}\varphi\| \|\varphi\|.$$

Since $\text{Ran}(\mathcal{B}) \subset \mathcal{H}$, this shows that $\mathcal{B}\mathcal{A}_0^{-1}$ is a bounded operator on \mathcal{H} . The same holds true for $\mathcal{L}_0^{-1}\mathcal{B}^* \Big|_{\mathcal{H}}$, which is its adjoint on $\mathcal{H} \subset L^2(\psi_0)$. \diamond

Remark 3 *In the above proof, the fact that both γ_x and γ_y are non-zero is a crucial assumption. If for instance $\gamma_x = 0$, many arguments break down, and the proofs become much more technical and/or some results cannot be proved anymore. This is due to the fact that the the Lie algebra generated by $\{\mathcal{A}_{\text{ham}}, \partial_{p_{y1}}, \dots, \partial_{p_{yN}}\}$ may be different from the Lie algebra generated by $\{\mathcal{A}_{\text{ham}}, \partial_{p_{x1}}, \dots, \partial_{p_{xN}}, \partial_{p_{y1}}, \dots, \partial_{p_{yN}}\}$. Indeed,*

$$[\mathcal{A}_{\text{ham}}, \partial_{p_{yi}}] = \partial_{q_{yi}}, \quad [\mathcal{A}_{\text{ham}}, \partial_{q_{yi}}] = \sum_{j=1}^N \partial_{q_{yi}, q_{yj}}^2 V \cdot \partial_{p_{yj}} + \sum_{j=1}^N \partial_{q_{yi}, q_{xj}}^2 V \cdot \partial_{p_{xj}}.$$

Possibly, iterated commutators should be computed as well. Additional assumptions on the potential are required to infer that $\partial_{p_{xi}}$ is in the Lie algebra. This amounts to assuming that the coupling between the x and the y directions is strong enough. To our knowledge, the only cases where such arguments could be used are one-dimensional atom chains, for which the simple geometric structure of the system is of paramount importance to show that the Lie algebra has full rank. Obtaining hypocoercivity estimates is more challenging and imposes further restrictions on the interactions (see [26]).

3.5.2 Proof of Proposition 1

Corollary 1 shows that

$$\begin{aligned} \lim_{\xi \rightarrow 0} \frac{\langle \mathcal{A}_0 U_x^\varepsilon(Y, \cdot) \rangle_\xi}{\xi} &= -\frac{\beta}{m} \left\langle U_x^\varepsilon(Y, q, p), \sum_{i=1}^N p_{xi} F(q_{yi}) \right\rangle_{L^2(\psi_0)} \\ &= -\frac{L_y}{mN} \sum_{i=1}^N \int_{\mathcal{D}^N} \chi_\varepsilon(q_{yi} - Y) F(q_{yi}) \bar{\psi}_0(q) dq, \end{aligned}$$

where $\bar{\psi}_0(q) dq = Z_q^{-1} e^{-\beta V(q)} dq$ is the marginal of the canonical measure in the q variable. The integrand in the last equation depends only on one variable q_{yi} . By translation invariance of the system, the marginal distribution in the q_{yi} variable of $\bar{\psi}_0(q) dq$ is the uniform distribution on $L_y \mathbb{T}$. Therefore, for any $i = 1, \dots, N$,

$$\int_{\mathcal{D}^N} \chi_\varepsilon(q_{yi} - Y) F(q_{yi}) \bar{\psi}_0(q) dq = \frac{1}{L_y} \int_0^{L_y} \chi_\varepsilon(y - Y) F(y) dy \longrightarrow F(Y)$$

as $\varepsilon \rightarrow 0$, so that

$$\lim_{\varepsilon \rightarrow 0} \lim_{\xi \rightarrow 0} \frac{\langle \mathcal{A}_0 U_x^\varepsilon(Y, \cdot) \rangle_\xi}{\xi} = -\frac{1}{m} F(Y). \quad (3.27)$$

Now, a simple computation shows that

$$\begin{aligned} \mathcal{A}_0 U_x^\varepsilon(Y, q, p) &= \frac{1}{\rho L_x} \left(\sum_{i=1}^N \frac{p_{xi} p_{yi}}{m} \partial_{q_{yi}} \chi'_\varepsilon(q_{yi} - Y) - \chi_\varepsilon(q_{yi} - Y) \partial_{q_{xi}} V(q) \right) \\ &\quad - \frac{\gamma_x}{m} U_x^\varepsilon(Y, q, p). \end{aligned}$$

The sum on the right-hand side can be decomposed into two contributions, one proportional to the kinetic part of the off-diagonal part of the stress tensor, and the other one arising solely from interaction forces. The first contribution can be written as

$$-\frac{\partial \Sigma_{xy, \text{kin}}^\varepsilon(Y, q, p)}{\partial Y} = -\frac{d}{dY} \left(\frac{1}{\rho L_x} \sum_{i=1}^N \frac{p_{xi} p_{yi}}{m} \chi_\varepsilon(q_{yi} - Y) \right).$$

For the second part, we first use the pairwise character of the interactions to write

$$\partial_{q_{xi}} V(q) = \sum_{i \neq j} v'(|q_i - q_j|) \frac{q_{xi} - q_{xj}}{|q_i - q_j|},$$

and then symmetrize the resulting expression as

$$\begin{aligned} \sum_{i=1}^N \chi_\varepsilon(q_{yi} - Y) \partial_{q_{xi}} V(q) &= \sum_{i \neq j} \chi_\varepsilon(q_{yi} - Y) v'(|q_i - q_j|) \frac{q_{xi} - q_{xj}}{|q_i - q_j|}, \\ &= \sum_{1 \leq i < j \leq N} (\chi_\varepsilon(q_{yi} - Y) - \chi_\varepsilon(q_{yj} - Y)) v'(|q_i - q_j|) \frac{q_{xi} - q_{xj}}{|q_i - q_j|}. \end{aligned}$$

The second contribution finally reads

$$-\frac{\partial \Sigma_{xy, \text{pot}}^\varepsilon(Y, q, p)}{\partial Y} = \frac{d}{dY} \left(\frac{1}{\rho L_x} \sum_{1 \leq i < j \leq N} v'(|q_i - q_j|) \left(\frac{q_{xi} - q_{xj}}{|q_i - q_j|} \right) \int_{q_{yj}}^{q_{yi}} \chi_\varepsilon(s - Y) ds \right).$$

In conclusion, it holds

$$\mathcal{A}_0 U_x^\varepsilon(Y, q, p) = -\frac{1}{\rho} \frac{\partial \Sigma_{xy}^\varepsilon(Y, q, p)}{\partial Y} - \frac{\gamma_x}{m} U_x^\varepsilon(Y, q, p). \quad (3.28)$$

Combining the latter result and (3.27) leads to

$$\lim_{\varepsilon \rightarrow 0} \lim_{\xi \rightarrow 0} \frac{1}{\xi} \left(\frac{1}{\rho} \frac{\partial \langle \Sigma_{xy}^\varepsilon(Y, \cdot) \rangle_\xi}{\partial Y} + \frac{\gamma_x}{m} \langle U_x^\varepsilon(Y, \cdot) \rangle_\xi \right) = \frac{1}{m} F(Y). \quad (3.29)$$

Now, Corollary 1 shows that the limit

$$u_x^\varepsilon(Y) := \lim_{\xi \rightarrow 0} \frac{\langle U_x^\varepsilon(Y, \cdot) \rangle_\xi}{\xi} = \frac{L_y}{Nm} \sum_{i=1}^N \int_{\mathcal{D}^N \times \mathbb{R}^{2N}} p_{xi} \chi_\varepsilon(q_{yi} - Y) f_1(q, p) \psi_0(q, p) dq dp$$

is well defined. By hypoellipticity, the function f_1 belongs to $C^\infty(\mathcal{D}^N \times \mathbb{R}^{2N})$. The limit $\varepsilon \rightarrow 0$ of the right-hand side is therefore well defined and

$$u_x(Y) = \frac{L_y}{Nm} \sum_{i=1}^N \int_{\mathcal{D}^{N-1} \times L_x \mathbb{T} \times \mathbb{R}^{2N}} p_{xi} (f_1^1 \psi_0)(q_1, \dots, q_{i-1}, q_{xi}, Y, q_{i+1}, \dots, q_N, p) dq_{1:i:N} dq_{xi} dp,$$

where $dq_{1:i:N} = dq_1 \dots dq_{i-1} dq_{i+1} \dots dq_N$. A similar reasoning holds for σ_{xy} . Passing to the limit in (3.29),

$$\frac{1}{\rho} \frac{\partial \sigma_{xy}(Y)}{\partial Y} + \frac{\gamma_x}{m} u_x(Y) = \frac{1}{m} F(Y),$$

which is (3.8).

3.5.3 Proof of Theorem 5

To simplify the notation, we set $m = 1$ in this section, but the proof can be straightforwardly modified to account for more general masses. Note first that the solution of (3.13) is well defined for any $\gamma_y > 0$ by the Fredholm alternative (since $\mathcal{A}_0(\gamma_y)$ has a compact resolvent on $\mathcal{H} = L^2(\psi_0) \cap \{1\}^\perp$, and the right-hand side of the equation is orthogonal to $\text{Vect}(1)$).

We start by formal computations providing possible expressions of f^0, f^1 , and then prove rigorously the convergence result stated in Theorem 5. To this end, we need some intermediate uniform hypocoercivity result.

Formal asymptotic expansion in γ_y

We consider the following *ansatz* for the solution f_{γ_y} :

$$f_{\gamma_y} = f^0 + \frac{1}{\gamma_y} f^1 + \frac{1}{\gamma_y^2} f^2 + \dots$$

and rewrite the operator $\mathcal{A}_0(\gamma_y)$ as the sum $\mathcal{A}_0(\gamma_y) = T_0 + \gamma_y \mathcal{A}_{y,\text{thm}}$. The kernel of the operator $\mathcal{A}_{y,\text{thm}}$ on $L^2(\psi_0)$ is

$$\text{Ker}(\mathcal{A}_{y,\text{thm}}) = \left\{ g \in L^2(\psi_0) \mid g = g(q, p_x) \right\}.$$

This is a consequence of the equality

$$\langle g, \mathcal{A}_{y,\text{thm}} g \rangle_{L^2(\psi_0)} = -\frac{1}{\beta} \|\nabla_{p_y} g\|^2$$

and the fact that the Gaussian measure (in the p_y variable) satisfies a Poincaré inequality. Identifying terms with the same powers of γ_y in (3.13), the following hierarchy is obtained:

$$\begin{cases} \mathcal{A}_{y,\text{thm}} f^0 = 0, \\ T_0 f^0 + \mathcal{A}_{y,\text{thm}} f^1 = -\sum_{i=1}^N p_{xi} G(q_{yi}), \\ T_0 f^1 + \mathcal{A}_{y,\text{thm}} f^2 = 0. \end{cases} \quad (3.30)$$

The first equation shows that $f^0 \equiv f^0(q, p_x)$. The second equation can then be rewritten as

$$\mathcal{A}_{y,\text{thm}} f^1(q, p) = -p_y \cdot \nabla_{q_y} f^0(q, p_x) - \sum_{i=1}^N p_{xi} G(q_{yi}) - \mathcal{I}_{q_y} f^0(q, p_x).$$

where

$$\mathcal{I}_{q_y} = p_x \cdot \nabla_{q_x} - \nabla_{q_x} V(q_x, q_y) \cdot \nabla_{p_x} + \gamma_x \mathcal{A}_{x,\text{thm}}$$

is an operator parameterized by $q_y \in (L_y \mathbb{T})^N$, and acting on the Hilbert space $L^2(\Psi_{q_y})$, where

$$\Psi_{q_y}(q_x, p_x) = Z_{q_y}^{-1} \exp \left(-\beta \left(V(q_x, q_y) + \frac{p_x^2}{2m} \right) \right).$$

Setting

$$f^1 = \tilde{f}^1 + p_y \cdot \nabla_{q_y} f^0,$$

it holds

$$\mathcal{A}_{y,\text{thm}} \tilde{f}^1(q, p) = - \sum_{i=1}^N p_{xi} G(q_{yi}) - \mathcal{T}_{q_y} f^0(q, p_x).$$

Since the right-hand side does not depend on p_y , the solvability condition for this equation is that the right-hand side vanishes. Besides, by results from [39], the operator \mathcal{T}_{q_y} , considered as an operator on $L^2(\Psi_{q_y})$, has bounded resolvent on $\text{Ker}(\mathcal{T}_{q_y})^\perp = \{1\}^\perp$ (where the orthogonality is with respect to the canonical scalar product on $L^2(\Psi_{q_y})$; see [109, Proposition 15] for a proof of the latter equality). Therefore, $\mathcal{T}_{q_y}^{-1}(p_{xi})$ is well defined. By linearity,

$$f^0(q, p) = - \sum_{i=1}^N G(q_{yi}) \mathcal{T}_{q_y}^{-1}(p_{xi}),$$

and

$$f^1(q, p) = p_y \cdot \nabla_{q_y} f^0(q, p) + \tilde{f}^1(q, p_x),$$

provide admissible solutions for the first two levels of the hierarchy (3.30). The function \tilde{f}^1 will be made precise below (see (3.37)).

The function f^0 is in $H^1(\psi_0)$ since $\mathcal{T}_{q_y}^{-1}$ is bounded on $\{1\}^\perp$. To show that the function $f^1 - \tilde{f}^1$ is indeed well defined, it is enough to show that $\partial_{q_{yi}} [\mathcal{T}_{q_y}^{-1}(p_{xk})]$ is well defined. This, in turn, follows from the following equality for any function $\varphi = \varphi(q_x, p_x)$:

$$\partial_{q_{yi}} \left(\mathcal{T}_{q_y}^{-1} \right) \varphi = \left(\mathcal{T}_{q_y}^{-1} \right) \left[\sum_{j=1}^N \partial_{q_{yi}, q_{xj}}^2 V(q_x, q_y) \partial_{p_{xj}} \right] \left(\mathcal{T}_{q_y}^{-1} \right) \varphi. \quad (3.31)$$

The operators $\partial_{p_{xj}} \left(\mathcal{T}_{q_y}^{-1} \right)$ are bounded on $L^2(\Psi_{q_y}) \cap \{1\}^\perp$ for $j = 1, \dots, N$ since

$$\langle \varphi, \mathcal{T}_{q_y} \varphi \rangle_{L^2(\Psi_{q_y})} = - \frac{\gamma_x}{\beta} \|\nabla_{p_x} \varphi\|_{L^2(\Psi_{q_y})}^2,$$

which implies, for $\|\varphi\|_{L^2(\Psi_{q_y})} \leq 1$,

$$\left\| \nabla_{p_x} \left(\mathcal{T}_{q_y}^{-1} \right) \varphi \right\|_{L^2(\Psi_{q_y})}^2 \leq \frac{\beta}{\gamma_x} \|\varphi\|_{L^2(\Psi_{q_y})} \left\| \left(\mathcal{T}_{q_y}^{-1} \right) \varphi \right\|_{L^2(\Psi_{q_y})} \leq \frac{\beta}{\gamma_x} \left\| \mathcal{T}_{q_y}^{-1} \right\|.$$

In conclusion, $f^1 - \tilde{f}^1 \in H^1(\psi_0)$. In addition, by hypoellipticity, the functions $f^0, f^1 - \tilde{f}^1$ are C^∞ when G is smooth.

Uniform hypocoercivity estimates

Let us show that the operator $\mathcal{A}_0(\gamma_y)$ is uniformly hypocoercive for γ_y large enough (say, $\gamma_y \geq \gamma_x$), provided the domain of the operator is restricted to functions with vanishing average with respect to the Gibbs measure in the p_y variable. To this end, we decompose $\mathcal{A}_0(\gamma_y)$ as

$$\mathcal{A}_0(\gamma_y) = \mathcal{A}_0(\gamma_x) + (\gamma_y - \gamma_x)\mathcal{A}_{y,\text{thm}}.$$

Following the proof of Theorem 6.2 in [39], it can be shown that there exists $\kappa > 0$ such that, for all smooth functions $u \in \mathcal{H}$,

$$-\langle \langle u, \mathcal{A}_0(\gamma_x)u \rangle \rangle \geq \kappa \langle \langle u, u \rangle \rangle,$$

where the norm induced by $\langle \langle \cdot, \cdot \rangle \rangle$ is equivalent to the $H^1(\psi_0)$ norm

$$\|u\|_{H^1(\psi_0)}^2 = \|u\|^2 + \|\nabla_p u\|^2 + \|\nabla_q u\|^2.$$

More precisely, $\langle \langle \cdot, \cdot \rangle \rangle$ is the bilinear form defined by

$$\langle \langle u, v \rangle \rangle = a \langle u, v \rangle + b \langle \nabla_p u, \nabla_p v \rangle + \langle \nabla_p u, \nabla_q v \rangle + \langle \nabla_q u, \nabla_p v \rangle + b \langle \nabla_q u, \nabla_q v \rangle,$$

with appropriate coefficients $a \gg b \gg 1$. It follows that there exists $C > 0$ independent of γ_y such that

$$C \|u\|_{H^1(\psi_0)}^2 - (\gamma_y - \gamma_x) \langle \langle u, \mathcal{A}_{y,\text{thm}}u \rangle \rangle \leq -\langle \langle u, \mathcal{A}_0(\gamma_y)u \rangle \rangle.$$

Let us now show that

$$-\langle \langle u, \mathcal{A}_{y,\text{thm}}u \rangle \rangle \geq 0 \tag{3.32}$$

for functions u in an appropriate subspace of $H^1(\psi_0)$. Using the commutation relations $[\partial_{p_{\alpha,i}}, \partial_{p_{\alpha',j}}^*] = \beta \delta_{\alpha,\alpha'} \delta_{ij}$ ($\alpha, \alpha' \in \{x, y\}$), a simple computation shows

$$\begin{aligned} \left\langle \left\langle u, \sum_{i=1}^N (\partial_{p_{y_i}})^* \partial_{p_{y_i}} u \right\rangle \right\rangle &= \sum_{i=1}^N (a + \beta b) \|\partial_{p_{y_i}} u\|^2 + b \|\nabla_p \partial_{p_{y_i}} u\|^2 \\ &\quad + b \|\nabla_q \partial_{p_{y_i}} u\|^2 + 2 \langle \nabla_q \partial_{p_{y_i}} u, \nabla_p \partial_{p_{y_i}} u \rangle + \beta \langle \partial_{q_{y_i}} u, \partial_{p_{y_i}} u \rangle \\ &\geq \sum_{i=1}^N \left(a + \beta \left(b - \frac{1}{2} \right) \right) \|\partial_{p_{y_i}} u\|^2 + (b-1) \|\nabla_p \partial_{p_{y_i}} u\|^2 \\ &\quad + (b-1) \|\nabla_q \partial_{p_{y_i}} u\|^2 - \frac{\beta}{2} \|\partial_{q_{y_i}} u\|^2. \end{aligned}$$

Summing on $i \in \{1, \dots, N\}$, the quantity (3.32) is seen to be non-negative for an appropriate choice of constants $a \gg b \gg 1$ provided there exists a constant $A > 0$ such that, for all $i = 1, \dots, N$,

$$\|\partial_{q_{y_i}} u\| \leq A \|\nabla_p \partial_{q_{y_i}} u\|. \tag{3.33}$$

This indeed implies

$$\sum_{i=1}^N \|\partial_{q_{y_i}} u\|^2 \leq A \sum_{i,j=1}^N \|\partial_{p_{y_j}} \partial_{q_{y_i}} u\|^2 = A \sum_{j=1}^N \|\nabla_{q_y} \partial_{p_{y_j}}\|^2 \leq A \sum_{j=1}^N \|\nabla_q \partial_{p_{y_j}}\|^2.$$

Since the Gaussian measure satisfies a Poincaré inequality, the inequalities (3.33) hold provided

$$\forall i = 1, \dots, N, \quad \int_{\mathbb{R}^N} \partial_{q_{y_i}} u(q, p) \exp\left(-\beta \frac{p_y^2}{2}\right) dp_y = 0.$$

Defining the closed subspace of $L^2(\psi_0) \cap \{1\}^\perp$

$$\mathcal{H}_0 = \left\{ v \in H^1(\psi_0) \mid \bar{v}(q, p_x) = \left(\frac{2\pi}{\beta} \right)^{-N/2} \int_{\mathbb{R}^N} v(q, p) \exp \left(-\beta \frac{p_y^2}{2} \right) dp_y = 0 \right\} \subset \mathcal{H}, \quad (3.34)$$

we conclude that, for any $u \in \mathcal{H}_0 \cap H^2(\psi_0)$,

$$C \|u\|_{H^1(\psi_0)}^2 \leq -\langle u, \mathcal{A}_0(\gamma_y)u \rangle. \quad (3.35)$$

In particular, there exists a constant $K > 0$ such that, for any $\gamma_y \geq \gamma_x$ and for any $u \in \mathcal{H}_0 \cap H^2(\psi_0)$,

$$\left\| \mathcal{A}_0(\gamma_y)^{-1} u \right\|_{H^1(\psi_0)} \leq K \|u\|_{H^1(\psi_0)}.$$

In fact, this inequality can be extended to functions in \mathcal{H}_0 .

Proof of the limit (3.14)

To prove (3.14), we proceed as follows. Note first that

$$-\mathcal{A}_0(\gamma_y) (f_{\gamma_y} - f^0 - \gamma_y^{-1} f^1) = \frac{1}{\gamma_y} T_0 f^1,$$

so that

$$f_{\gamma_y} - f^0 - \gamma_y^{-1} f^1 = -\frac{1}{\gamma_y} \mathcal{A}_0(\gamma_y)^{-1} T_0 f^1. \quad (3.36)$$

Since $\mathcal{A}_0(\gamma_y)^{-1}$ is bounded on \mathcal{H}_0 , uniformly in γ_y (see (3.35)), it is sufficient to show that $T_0 f^1 \in \mathcal{H}_0$. The proof is then concluded by setting $\phi_i(q, p) = -\mathcal{T}_{q_y}^{-1}(p_{xi})$.

Let us first show that $\overline{T_0 f^1}(q, p_x) = 0$ (where \bar{v} is defined in (3.34)). This can be ensured by an appropriate choice of \tilde{f}^1 . Note first that

$$T_0 f^1 = p_y \cdot \nabla_{q_y} \tilde{f}^1 + \mathcal{T}_{q_y} f^1 + (p_y \cdot \nabla_{q_y} - \nabla_{q_y} V \cdot \nabla_{p_y}) f^1 + \mathcal{T}_{q_y} \tilde{f}^1.$$

The first two terms have a vanishing average with respect to $(2\pi)^{-N/2} \exp \left(-\beta \frac{p_y^2}{2} \right) dp_y$. Introducing

$$g(q, p_x) = -(2\pi)^{-N/2} \int_{\mathbb{R}^N} (p_y \cdot \nabla_{q_y} - \nabla_{q_y} V \cdot \nabla_{p_y}) f^1 \exp \left(-\beta \frac{p_y^2}{2} \right) dp_y,$$

the condition $\overline{T_0 f^1} = 0$ is satisfied provided

$$\mathcal{T}_{q_y} \tilde{f}^1 = g(q, p_x),$$

Seeing the function on the right-hand side as a function of (q_x, p_x) indexed by q_y allows to define \tilde{f}^1 pointwise in q_y as

$$\tilde{f}^1 = -(2\pi)^{-N/2} \mathcal{T}_{q_y}^{-1} g. \quad (3.37)$$

Let us now study the regularity of $T_0 f^1$. We only treat the term $T_0(f^1 - \tilde{f}^1)$ since the regularity of $T_0 \tilde{f}^1$ can be proved similarly. In fact, only the derivatives in the p variables have to be considered because the position space is compact. First, recall that by hypoellipticity all the functions (f, f^0, f^1) are in $C^\infty(\mathcal{D}^N \times \mathbb{R}^{2N})$

$$\begin{aligned}
f^1 - \tilde{f}^1 &= - \sum_i p_{yi} G'(q_{yi}) \mathcal{T}_{q_y}^{-1}(p_{xi}) \\
&\quad - \sum_{i,j,k} p_{yi} G(q_{yj}) \left\{ \left(\mathcal{T}_{q_y}^{-1} \right) \left[\partial_{q_{yi}, q_{xk}}^2 V(q_x, q_y) \partial_{p_{xk}} \right] \left(\mathcal{T}_{q_y}^{-1} \right) p_{xj} \right\}. \tag{3.38}
\end{aligned}$$

The p_y dependence is trivial in the above expression, so that only derivatives in p_x require some attention. Since $T_0 = \mathcal{A}_{y,\text{ham}} + \mathcal{T}_{q_y}$ where $\mathcal{A}_{y,\text{ham}} = p_y \cdot \nabla_{q_y} - \nabla_{q_y} V(q_x, q_y) \cdot \nabla_{p_y}$ is an operator in the q_y, p_y variables (parameterized by q_x), it suffices to consider $\mathcal{T}_{q_y} f^1$. This function is, in turn, a linear combination of terms of the form $p_{yi} p_{xi}$ (cf. the first term in the right-hand side of (3.38)) and $p_{yi} \partial_{p_{xk}} \mathcal{T}_{q_y}^{-1} p_{xj}$ (second term in the right-hand side of (3.38)). To prove that the latter functions are in $H^1(\psi_0)$, we use the results of [47, 103], which show that $\mathcal{T}_{q_y}^{-1}$ is a bounded operator on the Hilbert spaces

$$\left\{ f \in H^m(\Psi_{q_y}) \mid \int_{(L_x \mathbb{T})^N \times \mathbb{R}^N} f(q_x, p_x) \Psi_{q_y}(q_x, p_x) dq_x dp_x \right\} \subset L^2(\Psi_{q_y})$$

for any $m \geq 0$, with a bound uniform in q_y .

3.5.4 Proof of Theorem 6

The proof follows the same lines as the proof presented in Section 3.5.3, so we skip the parts of the argument which can be straightforwardly extended from there.

As in the previous section, we set $m = 1$ to simplify the notation, but the proof can be straightforwardly modified to account for more general masses. Note first that the solution of (3.15) is well defined for any $\gamma_x > 0$, for reasons similar to the ones exposed at the beginning of Section 3.5.3. Define

$$\mathcal{T}_{q_x} = p_y \cdot \nabla_{q_y} - \nabla_{q_y} V(q_x, q_y) \cdot \nabla_{p_y} + \gamma_y \mathcal{A}_{y,\text{thm}},$$

which is an operator parameterized by $q_x \in (L_x \mathbb{T})^N$, and acting on the Hilbert space $L^2(\Psi_{q_x})$, where

$$\Psi_{q_x}(q_y, p_y) = Z_{q_x}^{-1} \exp \left(-\beta \left(V(q_x, q_y) + \frac{p_y^2}{2m} \right) \right).$$

Its kernel is $\text{Vect}(1) = \{c \Psi_{q_x}, c \in \mathbb{R}\}$.

Formal asymptotic expansion in γ_x

We start by formal computations, with a discussion parallel to the corresponding one in Section 3.5.3. We consider the following *ansatz* for the solution f_{γ_x} :

$$f_{\gamma_x} = f^0 + \frac{1}{\gamma_x} f^1 + \frac{1}{\gamma_x^2} f^2 + \dots$$

and rewrite the operator $\mathcal{A}_0(\gamma_x)$ as the sum $\mathcal{A}_0(\gamma_x) = T_0 + \gamma_x \mathcal{A}_{x,\text{thm}}$. The kernel of the operator $\mathcal{A}_{x,\text{thm}}$ on $L^2(\psi_0)$ is

$$\text{Ker}(\mathcal{A}_{x,\text{thm}}) = \left\{ g \in L^2(\psi_0) \mid g = g(q, p_y) \right\}.$$

Identifying terms with the same powers of γ_x in (3.15), the following hierarchy is obtained:

$$\begin{cases} \mathcal{A}_{x,\text{thm}}f^0 = 0, \\ T_0f^0 + \mathcal{A}_{x,\text{thm}}f^1 = -\sum_{i=1}^N p_{xi}G(q_{yi}), \\ T_0f^1 + \mathcal{A}_{x,\text{thm}}f^2 = 0. \end{cases} \quad (3.39)$$

The first equation shows that $f^0 \equiv f^0(q, p_y)$. The second one can be rewritten as

$$\mathcal{A}_{x,\text{thm}}f^1(q, p) = -\sum_{i=1}^N p_{xi} \left(G(q_{yi}) + \partial_{q_{xi}}f^0(q, p_y) \right) - \mathcal{T}_{q_x}f^0(q, p_y),$$

so that

$$f^1 = \sum_{i=1}^N p_{xi} \left(G(q_{yi}) + \partial_{q_{xi}}f^0(q, p_y) \right) + \tilde{f}^1,$$

with

$$\mathcal{A}_{x,\text{thm}}\tilde{f}^1(q, p) = -\mathcal{T}_{q_x}f^0(q, p_y).$$

The solvability condition requires $\mathcal{T}_{q_x}f^0(q, p_y) = 0$, hence $f^0 \equiv f^0(q_x)$. Besides, \tilde{f}^1 does not depend on p_x . The solvability condition for the third equation in (3.39) is $T_0f^1 \in \text{Ker}(\mathcal{A}_{x,\text{thm}})$. Now,

$$\begin{aligned} T_0 \left(\sum_{i=1}^N p_{xi} \left(G(q_{yi}) + \partial_{q_{xi}}f^0(q_x) \right) \right) &= -\sum_{i=1}^N \partial_{q_{xi}}V(q_x, q_y) \left(G(q_{yi}) + \partial_{q_{xi}}f^0(q_x) \right) \\ &\quad + \sum_{i=1}^N p_{xi}p_{yi}G'(q_{yi}) + \sum_{i=1}^N p_{xi}^2 \partial_{q_{xi}}^2 f^0(q_x), \end{aligned}$$

and

$$T_0\tilde{f}^1 = \mathcal{T}_{q_x}\tilde{f}^1 + \sum_{i=1}^N p_{xi} \partial_{q_{xi}}\tilde{f}^1.$$

We therefore set

$$f^0 = 0, \quad \tilde{f}^1 = \mathcal{T}_{q_x}^{-1} \left(\sum_{i=1}^N \partial_{q_{xi}}V(q_x, q_y)G(q_{yi}) \right),$$

and

$$f^2(q, p) = \sum_{i=1}^N p_{xi} \left(p_{yi}G'(q_{yi}) + \partial_{q_{xi}}\tilde{f}^1 \right) + \tilde{f}^2,$$

so that

$$\mathcal{A}_{x,\text{thm}}f^2(q, p) = -\sum_{i=1}^N p_{xi} \left(p_{yi}G'(q_{yi}) + \partial_{q_{xi}}\tilde{f}^1 \right) = -T_0f^1.$$

The function \tilde{f}^2 is chosen such that T_0f^2 has a vanishing average with respect to the Gaussian measure in the p_x variable.

Note that \tilde{f}^1 is well defined since $\sum_{i=1}^N \partial_{q_{xi}}V(q_x, q_y)G(q_{yi}) \in \text{Ker}(\mathcal{T}_{q_x})^\perp = \{1\}^\perp$ (where the orthogonality is with respect to the scalar product on $L^2(\Psi_{q_x})$). Indeed,

$$\begin{aligned} \sum_{i=1}^N \partial_{q_{xi}} V(q_x, q_y) G(q_{yi}) &= \sum_{i=1}^N \sum_{j \neq i} v'(|q_i - q_j|) \frac{q_{xi} - q_{xj}}{|q_i - q_j|} G(q_{yi}) \\ &= \sum_{1 \leq i < j \leq N} v'(|q_i - q_j|) \frac{q_{xi} - q_{xj}}{|q_i - q_j|} (G(q_{yi}) - G(q_{yj})). \end{aligned}$$

The last line is antisymmetric with respect to the exchange of coordinates q_{yi} and q_{yj} , hence the average of the corresponding function with respect to Ψ_{q_x} , which is symmetric with respect to the exchange of coordinates q_{yi} and q_{yj} , vanishes.

A discussion similar to the one in Section 3.5.3 show also that $\partial_{q_{xi}} \tilde{f}^1$ is well defined, hence the definition of f^2 makes sense.

Proof of the limit (3.16)

The remainder of the proof follows the very same lines as the proof presented in Section 3.5.3, hence we omit it.

Continuous models for equilibrium eletrolytes

Modelling of non-ideal equilibrium electrolytes

4.1	Bibliography overview on ideal and non-ideal electrolytes	74
4.2	Mathematical statement of the electrochemical model	75
4.2.1	Geometry and equilibrium equations	75
4.2.2	First variational formulation	79
4.2.3	Second variational formulation	82
4.2.4	Modelling of non-ideality	83
4.2.5	Mild and strong non-ideality	85
4.2.6	Application: mechanical equilibrium and evaluation of the pressure	86
4.2.7	Previous mathematical results	87
4.3	The primitive model for homogeneous electrolytes	89
4.3.1	Hamiltonian of the isolated system	89
4.3.2	The ideal gas bulk free energy density	90
4.3.3	The non-ideal bulk free energy density	92
4.4	Derivation of the free energy functional \mathcal{F} for confined electrolytes	98
4.4.1	A microscopic model for confined electrolytes	98
4.4.2	Inhomogeneous Ornstein–Zernike equation	100
4.4.3	Ansatz for the free energy functional	102
4.4.4	Derivation of \mathcal{F}_{mf}	103
4.4.5	Approximations of $\mathcal{F}_{\text{corr}}$	104

The purpose of this chapter is to introduce the concepts developed in Chapters 5 and 6 dealing respectively with the mathematical analysis of a continuous model for confined equilibrium electrolytes when the underlying bulk free energy density is a convex function of the ionic concentrations (mild non-ideality setting) and with a numerical study of the case where the bulk free energy density is not a convex function of the ionic concentrations, leading in particular to phase separation (strong non-ideality).

This chapter is organized as follows. In Section 4.1, we present a bibliography review stemming from the chemical physicist community. Section 4.2 states the mathematical framework that will be used in the two next Chapters and summarizes the previous mathematical results concerning the present setting. The end of the Chapter is devoted to a formal derivation of the model introduced in Section 4.2 starting from a microscopic description. In Section 4.3, we present the primitive model for electrolytes and we derive the bulk free energy density for this model. Finally, in Section 4.4, we present a microscopic model for confined electrolytes and a derivation of the density functional theory for this microscopic model and the various approximations and closures that are used to derive the model presented in Section 4.2. Chapters 5

and 6 are independent of Sections 4.3 and 4.4 so that these sections can be omitted in a first reading.

4.1 Bibliography overview on ideal and non-ideal electrolytes

In continuum models, equilibrium electrolytes (steady state and no flow) can be described by the electrostatic potential and the ionic concentrations. The properties of such systems constitute the first step to understand more complex chemical and mechanical behaviours, for instance within clays.

For nanometric confinements, the classical Poisson–Boltzmann theory, where the electrostatic potential ψ solves a Poisson equation while the ionic concentrations $(c_i)_{i=\pm}$ of the two species follow the Boltzmann distribution, is valid at low ionic concentrations, that is in the infinite dilute limit. Multivalent ions and electrolytes near highly charged objects of various geometries may behave very differently from the ideal behaviour of infinitely diluted solutions, leading in some cases to phase separation. Phase separation can be defined as the phenomenon occurring when the physical domain is partitioned in (at least) two regions where the ionic concentrations take values in distinct sets, typically leading to a diluted phase (low ionic concentrations) and a condensed phase (moderately high concentrations). The non-ideality is encountered even in bulk solutions, that is, in unconfined geometries and arises mainly from two types of effects, which both play a larger role as the ionic concentration increases: electrostatic correlations and short-range excluded volume effects (also referred to as hard-sphere repulsion). Since the early theories which treat the former at the mean-field level and ignore the latter, such as the pioneering work of Debye and Hückel (DH) [22], which is valid at relatively low ionic concentrations, most of the work on the phase behaviour in electrolytes has been performed within the framework of the primitive models of charged hard spheres in a continuous solvent characterized only by its dielectric constant. The structural and thermodynamic properties of more concentrated solutions can then be predicted using integral equation theories, such as the Mean Spherical Approximation (MSA) [10, 11, 63, 64].

In the case of inhomogeneous electrolytes in contact with charged solid surfaces, *e.g.* in confined geometries, electrostatic interactions also control the structure and the phase behaviour of the solution [30, 89, 90]. In some cases, such as clay minerals, the counterions compensating the charge of the surface may even be the only ions present in the confined fluid, resulting in a situation similar to the One Component Plasma (for a review, see [9]). For highly charged surfaces or multivalent counterions, a large fraction of the counterions occupies a condensed phase near the charged surface, as suggested by Stern to generalize the Gouy and Chapman description of charged surfaces. The remaining ions then feel a much weaker effective charge, which can be described within the Poisson–Boltzmann theory. Nevertheless, the determination of the fraction of condensed ions and the corresponding effective charge is not straightforward.

A number of approaches have been proposed to incorporate correlations neglected in the Poisson–Boltzmann theory. In the particular case where counterions are the only ions present, a perturbative correction to the Poisson–Boltzmann theory has been established [7]. Furthermore, the so-called "Strong Coupling" theory allows to investigate regimes where the interaction with the charged surface is stronger than that between ions [36, 80, 83, 95] and to explain the origin

of the attraction between like-charged surfaces observed under certain conditions. Another successful development for the description of the inhomogeneous primitive model, considered in this thesis in Section 4.3, is the use of density functional theory (DFT), which determines structural thermodynamic properties of an inhomogeneous fluid from the Helmholtz free energy and its functional dependence on the local densities of particles [13, 31, 35, 40, 73, 78, 84]. Finally, Molecular Dynamics and Monte Carlo simulations have been used to study the properties of bulk and confined electrolytes, described either within the primitive model or from a molecular point of view, thus providing a more realistic description of these complex systems.

In density functional theory, the free energy is decomposed into the sum of an ideal term and various non-ideal terms and is minimized with respect to the ionic concentrations under some constraints. In this thesis, in order to take into account correlations between counterions, we have included electrostatic and hard-sphere contributions in the free energy, calculated with the MSA and corresponding to *Local Density Approximation* [61] where the correction is obtained from the correlation function evaluated for a bulk solution (where there is no external field). However, within this type of model, the interaction of the ions with the charged solid is still treated at the mean-field level (thereby neglecting an excluded volume effect between the solid and the ions).

The problem is formulated in terms of the ionic concentrations c and the electrostatic potential ψ which is computed self-consistently by the Poisson equation relating the electric field to the charge density. This free energy functional takes the form

$$\mathcal{F}(c) = \mathcal{F}_{\text{bulk}}(c) + \mathcal{F}_{\text{mf}}(c). \quad (4.1)$$

The term $\mathcal{F}_{\text{bulk}}$ contains the ideal and non-ideal effects in the bulk solution regardless of the presence of a negatively charged solid object, while the mean-field term \mathcal{F}_{mf} accounts for the mean-field electrostatic potential between the ions and the negatively charged solid object. The equilibrium state of the system is determined by minimizing \mathcal{F} under suitable constraints (such as a fixed average in space of the ionic concentrations c).

4.2 Mathematical statement of the electrochemical model

We now formalize mathematically the problem of determining the thermodynamic equilibrium of a system consisting in an electrolyte surrounded by a negatively charged object. First, we describe the geometry, the physical setting and write the equation expressing the thermodynamic equilibrium. Second, we describe the properties of the free energy functional (4.1) and show formally that a minimizer of this functional solves the equilibrium equations. Third, we introduce another functional \mathcal{E} depending on the ionic concentrations c and the electrostatic potential ψ and show formally that a critical point of \mathcal{E} solves the equilibrium equation. The end of this section is devoted to the methodology to compute the pressure of the system. Finally, a bibliography overview of the mathematical and numerical results available is discussed.

4.2.1 Geometry and equilibrium equations

We focus on binary electrolytes (which means electrolytes composed of two species, cations and anions), and consider a periodic setting with elementary cell $[0, L_*]^d$, $d \in \{2, 3\}$, with length

scale L_* (expressed in m). The elementary cell contains inclusions Ω_S whose boundary $\partial\Omega_S$ (see Figure 4.1 left) contains negative charges with surface density $\Sigma_S > 0$ (expressed in Cm^{-2}). Our approach also applies to other settings, *e.g.*, confined electrolytes in nanochannels (see Figure 4.1 right). The problem is posed in the domain $\Omega := [0, L_*]^d \setminus \Omega_S$ and consists in finding

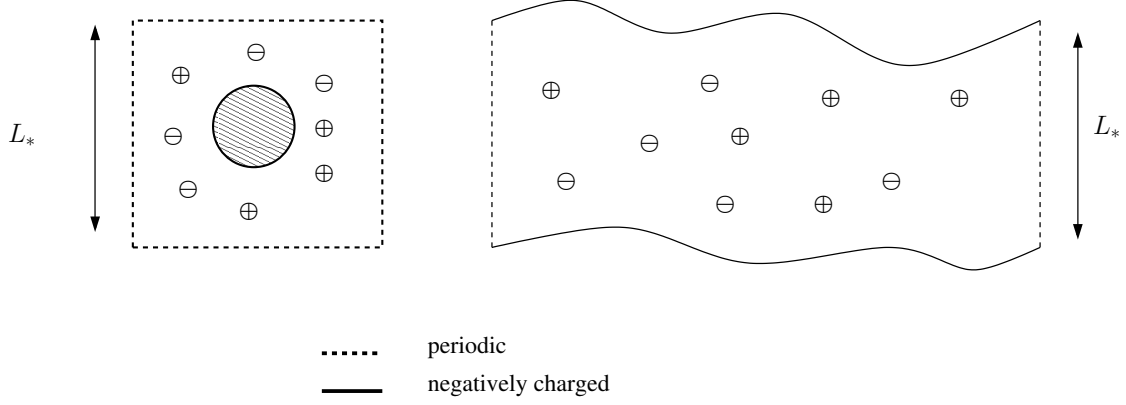


Fig. 4.1. Geometries for Ω : periodic media with negatively charged inclusions (left); nanochannel with negatively charged walls (right)

the electrostatic potential ψ (expressed in V) and the ionic concentrations $c = (c_+, c_-)$ (each concentration is expressed in m^{-3}) such that

$$-\Delta\psi = \frac{e}{\varepsilon} \sum_{i=\pm} Z_i c_i \quad \text{in } \Omega, \quad (4.2a)$$

$$\mu_+^{\text{el}}(\psi, c) \text{ and } \mu_-^{\text{el}}(\psi, c) \text{ are constant in } \Omega, \quad (4.2b)$$

where e is the elementary charge (expressed in C), $\varepsilon = \varepsilon_0 \varepsilon_r$ the solvent permittivity with ε_0 the vacuum permittivity (expressed in $\text{CV}^{-1}\text{m}^{-1}$) and ε_r the solvent relative permittivity (dimensionless), and Z_i the valence (dimensionless) of species $i = \pm$. The electrochemical potentials $\mu_{\pm}^{\text{el}}(\psi, c)$ depend on the chemical potentials $\mu_{\pm}(c)$ and the electrostatic potential ψ as follow:

$$\mu_i^{\text{el}}(\psi, c) := \mu_i(c) + Z_i e \psi, \quad \mu_i(c) = \frac{1}{\beta} \log(\Lambda_i^3 c_i) + \frac{1}{\beta} \log(\gamma_i(c)), \quad i = \pm, \quad (4.3)$$

where $\frac{1}{\beta} = k_B T$, k_B is the Boltzmann constant (expressed in JK^{-1}), T the temperature (expressed in K), Λ_i the de Broglie thermal wavelength, and $\gamma_i(c)$ the dimensionless activity coefficient of species $i = \pm$ accounting for non-ideal behaviour ($\gamma_i(c) \equiv 1$, $i = \pm$, in the ideal case). Since we consider electrolytes surrounded by a negatively charged solid object, the counterions concentration is c_+ and the coions concentration is c_- . A first consequence of equation (4.3) is that the ionic concentrations have to be sought in the set of non-negative functions (owing to the presence of the logarithm of the ionic concentrations in the definition of μ_i).

The presence of the de Broglie thermal wavelength Λ_i originates from the kinetic contribution to the microscopic Hamiltonian function (see Section 4.4) and ensures that the product $\Lambda_i^3 c_i$ is non-dimensional. Changing the value of Λ_i (which can be interpreted as modifying artificially the masses of the ions) only shifts the chemical potential by a constant. In particular, such a shift does not affect the equilibrium properties (such as the equilibrium ionic concentrations c).

Thus, in what follows, we suppose (without loss of generality) that the value of the de Broglie wavelength is

$$A_i = \sigma, \quad i = \pm, \quad (4.4)$$

where σ is the mean ion diameter (expressed in m), so that

$$\mu_i(c) = \frac{1}{\beta} \log(\sigma^3 c_i) + \frac{1}{\beta} \log(\gamma_i(c)), \quad i = \pm. \quad (4.5)$$

Boundary conditions enforce that

$$\psi \text{ is periodic on } \partial\Omega \setminus \partial\Omega_S, \quad (4.6a)$$

$$\nabla\psi \cdot \mathbf{n} = -\frac{1}{\varepsilon} \Sigma_S \quad \text{on } \partial\Omega_S, \quad (4.6b)$$

where \mathbf{n} denotes the unit outward normal to $\partial\Omega_S$. The Neumann boundary condition on ψ hinges on the physical assumption that the solid Ω_S is infinitely conducting. Indeed, the natural boundary condition is that

$$[\nabla\psi] \cdot \mathbf{n} = -\frac{1}{\varepsilon} \Sigma_S \quad \text{on } \partial\Omega_S, \quad (4.7)$$

where $[g]$ denote the jump of a function g across $\partial\Omega_S$. This condition reduces to (4.6) whenever the normal derivative of $\psi|_{\Omega_S}$ is much smaller than $\varepsilon^{-1} \Sigma_S$ (see discussion in Section 4.4). Additionally, considering canonical constraints, we prescribe the mean ionic concentrations in the form

$$\langle c_i \rangle_\Omega = c_i^{\text{bulk}}, \quad i = \pm, \quad (4.8)$$

where c_+^{bulk} and c_-^{bulk} are given nonnegative real numbers and where, for any function $g \in L^1(\Omega)$, $\langle g \rangle_\Omega$ denote its mean value in Ω given by

$$\langle g \rangle_\Omega := \frac{1}{|\Omega|} \int_\Omega g. \quad (4.9)$$

We assume that the data c_\pm^{bulk} satisfy the global electroneutrality condition

$$\sum_{i=\pm} Z_i c_i^{\text{bulk}} = \frac{1}{|\Omega|} \int_{\partial\Omega_S} \frac{1}{e} \Sigma_S, \quad (4.10)$$

which is a necessary and sufficient condition for the solvability of the Poisson equation (4.2a) together with the boundary conditions (4.6) for the electrostatic potential ψ given the ionic concentrations c . Finally, since the electrostatic potential is determined up to an additive constant, we require that

$$\langle \psi \rangle_\Omega = 0. \quad (4.11)$$

Remark 4 (Minimal value for L_* .) *The present model does not incorporate the hard-sphere repulsion between the ions and the charged object Ω_S , so that the ions are pointwise particles from the perspective of Ω_S . We will assume implicitly that at least one particle fits in the volume Ω . In the case of a periodic medium without inclusion, the volume Ω is the cube $[0, L_*]^3$ and assuming the ions are spherical, this hypothesis amounts to the condition $\sigma < L_*$. More generally, in a box of length L_* , the maximum number of spheres N is such that*

$$\frac{\pi\sigma^3}{6}N = \alpha L_*^3, \quad (4.12)$$

with $\alpha \approx 0.74$ (for a face-centered cubic lattice). Requiring at least N_0 particles in the box leads to the condition

$$\sigma \left(\frac{\pi N_0}{6\alpha} \right)^{\frac{1}{3}} \leq L_*, \quad (4.13)$$

e.g. $L_* \geq 3.367$ nm for $N_0 = 1000$ spheres of diameter $\sigma = 3$ Å.

To summarize, the problem we consider can be formulated as:

Given a surface charge density Σ_S and constant ionic concentrations $\{c_i^{\text{bulk}}\}_{i=\pm}$ satisfying (4.10), find a set of ionic concentrations $c = (c_+, c_-)$, an electrostatic potential ψ , and constant chemical potentials $\{\mu_i^{\text{bulk}}\}_{i=\pm}$ such that

$$-\varepsilon \Delta \psi = \sum_{i=\pm} Z_i e c_i, \text{ in } \Omega, \quad (4.14a)$$

$$\mu_i^{\text{el}}(\psi, c) = \frac{1}{\beta} \log(\sigma^3 c_i) + \frac{1}{\beta} \log(\gamma_i(c)) + Z_i e \psi = \mu_i^{\text{bulk}}, \text{ in } \Omega, i = \pm, \quad (4.14b)$$

$$\langle c_i \rangle_\Omega = c_i^{\text{bulk}}, \quad (4.14c)$$

$$\psi \text{ is periodic on } \partial\Omega \setminus \partial\Omega_S, \quad (4.14d)$$

$$\nabla \psi \cdot \mathbf{n} = -\frac{1}{\varepsilon} \Sigma_S \text{ on } \partial\Omega_S, \quad (4.14e)$$

$$\langle \psi \rangle_\Omega = 0. \quad (4.14f)$$

Remark 5 (Poisson–Boltzmann equation.) The so-called Poisson–Boltzmann equation is obtained in the ideal case, namely when $\gamma_i(c) \equiv 1$. In this case, one can invert exactly the equilibrium equation satisfied by the electrochemical potential (4.14b) yielding

$$\sigma^3 c_i = e^{\beta \mu_i^{\text{bulk}}} e^{-\beta Z_i e \psi}, i = \pm. \quad (4.15)$$

It is then more convenient to impose the value of the bulk chemical potentials rather than the average of the ionic concentrations. To find the equilibrium, one needs to solve the following nonlinear Poisson equation for the electrostatic potential:

$$-\Delta \psi = \frac{e}{\varepsilon} \sum_{i=\pm} \sigma^{-3} Z_i e^{\beta \mu_i^{\text{bulk}}} e^{-\beta Z_i e \psi}, i = \pm, \quad (4.16)$$

with the boundary conditions (4.14d), (4.14e) and the mean-value condition (4.14f). A strictly convex functional depending only on ψ can be introduced, and its unique minimizer solves the Poisson–Boltzmann equation (4.16) with boundary conditions (4.14d), (4.14e) and the mean-value condition (4.14f). This problem was considered by Looker [72] who performed the mathematical analysis of the Poisson–Boltzmann equation (4.16) with inhomogeneous Neumann boundary conditions, while Allaire, Mikelić, and Piatniski [3] considered this setting in the context of homogenization. In fact, Allaire et al. consider this approach also in the non-ideal case in [2]. We remark that this procedure is applicable as long as the map $(c_+, c_-) \mapsto (\mu_+(c), \mu_-(c))$ is invertible.

4.2.2 First variational formulation

We now turn to a first variational formulation of the problem (4.14). Recall the free energy functional

$$\mathcal{F}(c) = \mathcal{F}_{\text{bulk}}(c) + \mathcal{F}_{\text{mf}}(c), \quad (4.17)$$

which decomposes into two terms: the bulk free energy functional $\mathcal{F}_{\text{bulk}}$ and the mean-field free energy functional \mathcal{F}_{mf} .

Bulk free energy functional

The first term, namely the bulk free energy functional, is given as the integral over the volume Ω of the bulk free energy density f

$$\mathcal{F}_{\text{bulk}}(c) = \int_{\Omega} f(c), \quad (4.18)$$

where f , defined by

$$f(c) := \left(\sum_{i=\pm} f_{\text{id}}(c_i) \right) + f_{\text{corr}}(c), \quad (4.19)$$

is the sum of the ideal term ($\sum_{i=\pm} f_{\text{id}}(c_i)$) and the non-ideal term $f_{\text{corr}}(c)$. The ideal term is an entropic term and the function $f_{\text{id}} : \mathbb{R}_{\geq 0} \rightarrow \mathbb{R}$ is such that, for all $u \in \mathbb{R}_{\geq 0}$,

$$f_{\text{id}}(u) := \begin{cases} \frac{1}{\beta} u (\log(\sigma^3 u) - 1), & u > 0, \\ 0, & u = 0. \end{cases} \quad (4.20)$$

For the moment, we do not make precise the analytic form of f_{corr} . We note only that f_{corr} is related to the activity coefficients (introduced in (4.3)) by the equation

$$\log(\gamma_i(c)) = \beta \frac{\partial f_{\text{corr}}}{\partial c_i}(c), \quad i = \pm. \quad (4.21)$$

For convenience we decompose $\mathcal{F}_{\text{bulk}}$ as

$$\mathcal{F}_{\text{bulk}}(c) = \mathcal{F}_{\text{id}}(c) + \mathcal{F}_{\text{corr}}(c), \quad (4.22)$$

where

$$\mathcal{F}_{\text{id}}(c) := \int_{\Omega} \left(\sum_{i=\pm} f_{\text{id}}(c_i) \right), \quad \mathcal{F}_{\text{corr}}(c) := \int_{\Omega} f_{\text{corr}}(c), \quad (4.23)$$

so that

$$\mathcal{F}(c) = \mathcal{F}_{\text{id}}(c) + \mathcal{F}_{\text{corr}}(c) + \mathcal{F}_{\text{mf}}(c). \quad (4.24)$$

Mean-field free energy functional

In order to define the mean-field free energy functional \mathcal{F}_{mf} , we introduce the affine operator Ψ_{Σ_S} such that, for all $g \in L^2(\Omega)$, $\Psi_{\Sigma_S}(g)$ solves

$$-\varepsilon \Delta \Psi_{\Sigma_S}(g) = g - \langle g \rangle_{\Omega} + |\Omega|^{-1} \int_{\partial\Omega_S} \Sigma_S, \text{ in } \Omega, \quad (4.25a)$$

$$\Psi_{\Sigma_S}(g) \text{ is periodic on } \partial\Omega \setminus \partial\Omega_S, \quad (4.25b)$$

$$\nabla \Psi_{\Sigma_S}(g) \cdot \mathbf{n} = -\frac{1}{\varepsilon} \Sigma_S \text{ on } \partial\Omega_S, \quad (4.25c)$$

$$\langle \Psi_{\Sigma_S}(g) \rangle_{\Omega} = 0. \quad (4.25d)$$

For later use, we also introduce Ψ_0 as the linear operator associated with homogeneous Neumann boundary conditions ($\Sigma_S = 0$ in (4.25)). Introducing the charge density ρ defined by

$$\rho(c) = \sum_{i=\pm} Z_i e c_i, \quad (4.26)$$

it is clear that $\psi = \Psi_{\Sigma_S}(\rho(c))$ is the unique solution of (4.14a) with boundary conditions (4.14d), (4.14e) and the mean-value condition (4.14f).

The mean-field free energy functional, is given by

$$\mathcal{F}_{\text{mf}}(c) = \frac{1}{2} \left(\int_{\Omega} \rho(c) \Psi_{\Sigma_S}(\rho(c)) - \int_{\partial\Omega_S} \Sigma_S \Psi_{\Sigma_S}(\rho(c)) \right), \quad (4.27)$$

or, equivalently, by

$$\mathcal{F}_{\text{mf}}(c) = \frac{\varepsilon}{2} \left(\int_{\Omega} |\nabla \Psi_{\Sigma_S}(\rho(c))|^2 \right). \quad (4.28)$$

Indeed, for any function $\varphi \in H_{\text{per}}^1(\Omega)$ with $\langle \varphi \rangle_{\Omega} = 0$, there holds, owing to the global electroneutrality condition (4.10),

$$\varepsilon \int_{\Omega} \nabla \Psi_{\Sigma_S}(\rho(c)) \cdot \nabla \varphi = \int_{\Omega} \rho(c) \varphi - \int_{\partial\Omega_S} \Sigma_S \varphi, \quad (4.29)$$

so that the equality (4.28) is obtained from (4.29) by testing with $\varphi = \Psi_{\Sigma_S}(\rho(c))$. From a modelling viewpoint, this contribution is called mean-field free energy since it is the energy in an electrolyte where the ions experience the mean-field potential ψ .

Remark 6 (Convexity of \mathcal{F}_{mf} .) *It is easy to verify that \mathcal{F}_{mf} is a convex functional (but not strictly convex in general). Indeed, for any test functions u, v such that $\langle u \rangle_{\Omega} = 0$ and $\langle v \rangle_{\Omega} = 0$, we can write the Hessian of \mathcal{F}_{mf} as*

$$\left[\partial_{c_i, c_j}^2 \mathcal{F}_{\text{mf}}(c) \right] (u, v) = \varepsilon Z_i Z_j e^2 \int_{\Omega} \nabla \Psi_0(u) \cdot \nabla \Psi_0(v), \quad i = \pm, j = \pm, \quad (4.30)$$

and observe that this bilinear form is positive semi-definite. When there is only one species (as considered in Chapter 6), the functional \mathcal{F}_{mf} is strictly convex.

Partial derivative of \mathcal{F}

Let us now turn to the evaluation of the partial derivative of the bulk free energy functional (needed to establish a variational principle). Formally (see Chapter 5 for precise statements), the partial Gâteaux derivative of \mathcal{F} at point $c = (c_+, c_-)$ is given by

$$\langle \partial_{c_i} \mathcal{F}(c), \phi_i \rangle_{L^2} = \int_{\Omega} (\mu_i(c) + Z_i e \Psi_{\Sigma_S}(\rho(c))) \phi_i = \int_{\Omega} \mu_i^{\text{el}}(\Psi_{\Sigma_S}(\rho(c)), c) \phi_i, \quad (4.31)$$

for any function $\phi_i \in L^2(\Omega)$ such that $\langle \phi_i \rangle_{\Omega} = 0$. This computation is only formal since we did not precise the regularity of f_{corr} . The first thing to notice to obtain formally the result is that

$$\mu_i(c) = \frac{\partial f(c)}{\partial c_i}, \quad i = \pm, \quad (4.32)$$

owing to equality (4.21) and the definition of the ideal bulk free energy density (4.20). The second thing lies in the following Lemma, that delivers the partial Gâteaux derivative of \mathcal{F}_{mf} .

Lemma 2 *The partial Gâteaux derivative of \mathcal{F}_{mf} with respect to c_i is given by*

$$\langle \partial_{c_i} \mathcal{F}_{\text{mf}}(c), \phi_i \rangle_{L^2} = \int_{\Omega} Z_i e \Psi_{\Sigma_S}(\rho(c)) \phi_i, \quad (4.33)$$

for any function $\phi_i \in L^2(\Omega)$ with $\langle \phi_i \rangle_{\Omega} = 0$.

For convenience we provide a short proof of this Lemma.

Proof. We compute the partial Gâteaux derivative with respect to the variable c_+ (the case of c_- is treated similarly). For any function $\phi_+ \in L^2(\Omega)$ with $\langle \phi_+ \rangle_{\Omega} = 0$, setting $\phi = (\phi_+, 0)$, by taking a variation $c + \phi$ in \mathcal{F}_{mf} , we obtain for the quadratic contribution of \mathcal{F}_{mf}

$$\begin{aligned} \int_{\Omega} \rho(c + \phi) \Psi_{\Sigma_S}(\rho(c + \phi)) &= \int_{\Omega} (\rho(c) + \rho(\phi)) (\Psi_{\Sigma_S}(\rho(c)) + \Psi_0(\rho(\phi))) \\ &= \int_{\Omega} \rho(c) \Psi_{\Sigma_S}(\rho(c)) + \int_{\Omega} \rho(c) \Psi_0(\rho(\phi)) + \rho(\phi) \Psi_{\Sigma_S}(\rho(c)) \\ &\quad + \int_{\Omega} \rho(\phi) \Psi_0(\rho(\phi)), \end{aligned} \quad (4.34)$$

where we made use of the identity

$$\Psi_{\Sigma_S}(\rho(c + \phi)) = \Psi_{\Sigma_S}(\rho(c)) + \Psi_0(\rho(\phi)). \quad (4.35)$$

It follows easily that the partial Gâteaux derivative of \mathcal{F}_{mf} with respect to c_+ is given by

$$\langle \partial_{c_+} \mathcal{F}_{\text{mf}}(c), \phi_+ \rangle_{L^2} = \frac{1}{2} \left(\int_{\Omega} \rho(c) \Psi_0(\rho(\phi)) + \rho(\phi) \Psi_{\Sigma_S}(\rho(c)) - \int_{\partial\Omega_S} \Sigma_S \Psi_0(\rho(\phi)) \right), \quad (4.36)$$

and since $\rho(\phi) = Z_+ e \phi_+$, we obtain

$$\langle \partial_{c_+} \mathcal{F}_{\text{mf}}(c), \phi_+ \rangle_{L^2} = \frac{1}{2} \left(\int_{\Omega} \rho(c) \Psi_0(Z_+ e \phi_+) + Z_+ e \phi_+ \Psi_{\Sigma_S}(\rho(c)) - \int_{\partial\Omega_S} \Sigma_S \Psi_0(Z_+ e \phi_+) \right). \quad (4.37)$$

The conclusion follows from the fact that

$$\begin{aligned} \int_{\Omega} \rho(c) \Psi_0(Z_+ e \phi_+) - \int_{\partial\Omega_S} \Sigma_S \Psi_0(Z_+ e \phi_+) &= \varepsilon \int_{\Omega} \nabla \Psi_{\Sigma_S}(\rho(c)) \cdot \nabla \Psi_0(Z_+ e \phi_+) \\ &= \int_{\Omega} Z_+ e \phi_+ \Psi_{\Sigma_S}(\rho(c)), \end{aligned} \quad (4.38)$$

by definition of Ψ_0 . ◇

The minimization problem and equivalence with (4.14)

We now motivate the introduction of the free energy functional \mathcal{F} by deriving formally the variational principle allowing to solve problem (4.14).

The mathematical problem we want to solve concerning \mathcal{F} can be formulated as follows: *Given a surface charge density Σ_S and constant ionic concentrations $\{c_i^{\text{bulk}}\}_{i=\pm}$ satisfying (4.10), find a set of ionic concentrations $c = (c_+, c_-)$ such that*

$$\mathcal{F}(c) = \min \left\{ \mathcal{F}(\tilde{c}) \mid \tilde{c} \text{ s.t. } \langle \tilde{c}_i \rangle_{\Omega} = c_i^{\text{bulk}}, \tilde{c}_i \geq 0, i = \pm \right\}, \quad (4.39)$$

(the precise functional space where c is sought will be made precise in Chapter 5). Then, if \mathcal{F} is differentiable at point c , c is a critical point of \mathcal{F} and is therefore such that,

$$\mu_i^{\text{el}}(\Psi_{\Sigma_S}(\rho(c)), c) = \mu_i^{\text{bulk}}, \quad i = \pm, \quad (4.40)$$

owing to (4.31), where $\{\mu_i^{\text{bulk}}\}_{i=\pm}$ are the Lagrange multipliers resulting from the constraint $\langle \tilde{c}_i \rangle_{\Omega} = c_i^{\text{bulk}}$, $i = \pm$. Under a convexity assumption on $\mathcal{F}_{\text{bulk}}$ (so that \mathcal{F} is convex since \mathcal{F}_{mf} is always convex), we prove that solving the problem (4.39) is equivalent to solving (4.14), so that critical points are minimizers. Note that in the situation where $\Sigma_S = 0$ and the ionic concentrations $c = (c_+^{\text{bulk}}, c_-^{\text{bulk}})$ are constant, owing to the global electroneutrality condition (4.10), we find that $\psi = 0$ is the unique solution of (4.14a) with boundary conditions (4.14d), (4.14e) and the mean-value condition (4.14f). In the case where the bulk free energy density is a strictly convex function of the ionic concentrations, we verify easily that $c = (c_+^{\text{bulk}}, c_-^{\text{bulk}})$ is the unique minimizer of \mathcal{F} .

4.2.3 Second variational formulation

For the mathematical and numerical study, in order to avoid the use of the nonlocal operator Ψ_{Σ_S} , we adopt the following reformulation by introducing the two variables functional

$$\mathcal{E}(\psi, c) = \mathcal{U}(\psi) - \mathcal{B}(\psi, c) - \mathcal{F}_{\text{bulk}}(c), \quad (4.41)$$

with

$$\mathcal{U}(\psi) = \frac{\varepsilon}{2} \int_{\Omega} |\nabla \psi|^2 + \int_{\partial\Omega_S} \Sigma_S \psi, \quad (4.42a)$$

$$\mathcal{B}(\psi, c) = \sum_{i=\pm} \int_{\Omega} Z_i e c_i \psi = \int_{\Omega} \rho(c) \psi. \quad (4.42b)$$

Working either with the functional \mathcal{E} or \mathcal{F} is essentially equivalent since \mathcal{E} is strictly convex in the variable ψ . Moreover, whenever $\mathcal{F}_{\text{bulk}}$ is convex in the variable c (as assumed in Chapter 5), \mathcal{E} is concave in the variable c . Within this setting, we will be searching for a saddle-point (ψ, c) of the functional \mathcal{E} (*i.e.* a minmax in (ψ, c)).

The saddle-point problem and equivalence with (4.14)

We now motivate the use of functional \mathcal{E} . The mathematical problem we address is the following:

Given a surface charge density Σ_S and constant ionic concentrations $\{c_i^{\text{bulk}}\}_{i=\pm}$ satisfying (4.10), find a set of ionic concentrations $c = (c_+, c_-)$ and an electrostatic potential ψ such that (ψ, c) is the saddle-point of \mathcal{E} :

$$\mathcal{E}(\psi, c) = \min \max \left\{ \mathcal{E}(\tilde{\psi}, \tilde{c}) \mid (\tilde{\psi}, \tilde{c}) \text{ s.t. } \langle \tilde{\psi} \rangle_{\Omega} = 0, \langle \tilde{c}_i \rangle_{\Omega} = c_i^{\text{bulk}}, \tilde{c}_i \geq 0, i = \pm \right\}, \quad (4.43)$$

(the precise functional spaces where ψ and c are sought will be made precise in Chapter 5).

If \mathcal{E} is differentiable at (ψ, c) , then (ψ, c) is a critical point of \mathcal{E} . Differentiating \mathcal{E} with respect to its first argument shows that ψ solves the Poisson problem (4.14a), (4.14d)-(4.14f), while differentiating \mathcal{E} with respect to its second argument shows that the electrochemical potentials $\mu_{\pm}^{\text{el}}(\psi, c)$ are constant in Ω with $\mu_i^{\text{el}}(\psi, c) = \mu_i^{\text{bulk}}$, $i = \pm$, where the μ_i^{bulk} 's are the Lagrange multipliers associated with the constraints on the mean ionic concentrations. Under a convexity assumption (so that \mathcal{E} is concave in the c variable), we can verify that formulations (4.14) and (4.43) are equivalent so that critical points are saddle-points.

The main issue with the above statements is that in practice, we need to prove that either \mathcal{F} or \mathcal{E} are differentiable at the point c respectively minimizer of \mathcal{F} / maximizer of $\mathcal{E}(\psi, \cdot)$. This property depends on the hypothesis made for the non-ideal bulk free energy density f_{corr} , but also on the ideal free energy density f_{id} that forbids negative ionic concentrations. The strategy of proof to differentiate the functionals is to obtain uniform upper and positive lower bounds on the ionic concentrations. These questions are treated in detail in Chapter 5 with a precise mathematical setting for f_{corr} .

4.2.4 Modelling of non-ideality

We now describe the model of bulk free energy density f_{corr} that we consider in this thesis. The non-ideal term f_{corr} has the general form

$$f_{\text{corr}}(c) := f_{\text{Coul}}(c) + f_{\text{HS}}(c). \quad (4.44)$$

Following (4.44) and (4.21), the activity coefficient $\gamma_i(c)$, $i = \pm$, is correspondingly split into two parts in such a way that

$$\log(\gamma_i(c)) = \log(\gamma_i^{\text{Coul}}(c)) + \log(\gamma_{\text{HS}}(c)), \quad i = \pm. \quad (4.45)$$

where

$$\beta \frac{\partial f_{\text{Coul}}}{\partial c_i}(c) = \log(\gamma_i^{\text{Coul}}(c)), \quad i = \pm, \quad \beta \frac{\partial f_{\text{HS}}}{\partial c_i}(c) = \log(\gamma_{\text{HS}}(c)) \quad (4.46)$$

We note that in the case of the activity coefficient γ_{HS} , there is no dependence in $i = \pm$ (owing to the fact that we consider the mean ion diameter σ). Furthermore, in many models (MSA, Debye-Hückel), the density f_{Coul} depends on c only through the ionic strength $I : \mathbb{R}_{\geq 0}^2 \rightarrow \mathbb{R}_{\geq 0}$ (expressed in m^{-3}) such that, for all $c \in \mathbb{R}_{\geq 0}^2$,

$$I(c) := \sum_{i=\pm} \eta_i c_i, \quad \eta_i := \frac{1}{2} Z_i^2. \quad (4.47)$$

Then, it is convenient to introduce the function $f_0 : \mathbb{R}_{\geq 0} \rightarrow \mathbb{R}$ such that

$$f_{\text{Coul}}(c) = 2f_0(I(c)). \quad (4.48)$$

Following this path, we also define the function $\gamma_0 : \mathbb{R}_{\geq 0} \rightarrow \mathbb{R}_{> 0}$ such that

$$\log(\gamma_i^{\text{Coul}}(c)) = Z_i^2 \log(\gamma_0(I(c))), \quad i = \pm. \quad (4.49)$$

For example, the MSA model introduces a screening parameter Γ_{MSA} given by $\Gamma_{\text{MSA}} = \Upsilon_{\text{MSA}}(I(c))$ with the function $\Upsilon_{\text{MSA}} : \mathbb{R}_{\geq 0} \rightarrow \mathbb{R}_{\geq 0}$ such that, for all $\theta \in \mathbb{R}_{\geq 0}$,

$$\Upsilon_{\text{MSA}}(\theta) := \frac{1}{2\sigma} \left(\sqrt{2\sigma(4\pi L_B)^{1/2} (2\theta)^{1/2} + 1} - 1 \right). \quad (4.50)$$

The function f_0 is then given by

$$f_0(\theta) := -\frac{L_B}{\beta\sigma} \left(\theta - \frac{2\sigma}{3\pi L_B} (\Upsilon_{\text{MSA}}(\theta))^3 - \frac{1}{2\pi L_B} (\Upsilon_{\text{MSA}}(\theta))^2 \right), \quad (4.51)$$

so that

$$\log(\gamma_0(\theta)) = -\frac{L_B \Upsilon_{\text{MSA}}(\theta)}{1 + \sigma \Upsilon_{\text{MSA}}(\theta)}. \quad (4.52)$$

Concerning the hard-sphere term, further discussed in Section 4.3.3, we remark that in most models (Percus-Yevick, Carnahan-Starling), f_{HS} only depends on the concentration through the packing number $\xi(c) := \sum_{i=\pm} \vartheta c_i$ where $\vartheta := \frac{\pi\sigma^3}{6}$, so that

$$f_{\text{HS}}(c) = \frac{1}{\vartheta} f_1(\xi(c)), \quad (4.53)$$

for some function $f_1 : \mathbb{R}_{\geq 0} \rightarrow \mathbb{R}$. It follows that the activity coefficient γ_{HS} is of the form

$$\log(\gamma_{\text{HS}}(c)) = \log(\gamma_1(\xi(c))), \quad (4.54)$$

for a function $\gamma_1 : \mathbb{R}_{\geq 0} \rightarrow \mathbb{R}_{> 0}$. For example, in the case of the Carnahan-Starling (CS) activity coefficient, we have

$$\log(\gamma_1^{\text{CS}}(t)) := (8t - 9t^2 + 3t^3)(1-t)^{-3}, \quad t < 1, \quad +\infty, \quad t \geq 1, \quad (4.55)$$

while its linearized version (CS1) (valid at low ionic concentrations) is

$$\log(\gamma_1^{\text{CS1}}(t)) := 8t, \quad t \geq 0. \quad (4.56)$$

The bulk free energy density for (CS) is obtained by integration of (4.54) with respect to the ionic concentrations, yielding

$$f_1(t) := -\frac{1}{\beta\vartheta} \frac{t^2(3t-4)}{(1-t)^2}, \quad t < 1, \quad +\infty, t \geq 1, \quad (4.57)$$

while the bulk free energy density for (CS1) is

$$f_1(t) := \frac{4t^2}{\beta\vartheta}, \quad t \geq 0. \quad (4.58)$$

In summary, when the bulk free energy density is evaluated with the MSA model with (CS1) for the hard-sphere repulsion term, there holds

$$f_{\text{corr}}(c) := -\frac{2L_B}{\beta\sigma} \left(I(c) - \frac{2\sigma}{3\pi L_B} (\Upsilon_{\text{MSA}}(I(c)))^3 - \frac{1}{2\pi L_B} (\Upsilon_{\text{MSA}}(I(c)))^2 \right) + \frac{4}{\beta\vartheta} \xi(c)^2, \quad (4.59)$$

while using (CS) for the hard-sphere repulsion term, there holds

$$\begin{aligned} f_{\text{corr}}(c) := & -\frac{2L_B}{\beta\sigma} \left(I(c) - \frac{2\sigma}{3\pi L_B} (\Upsilon_{\text{MSA}}(I(c)))^3 - \frac{1}{2\pi L_B} (\Upsilon_{\text{MSA}}(I(c)))^2 \right) \\ & - \frac{1}{\beta\vartheta} \frac{\xi(c)^2(3\xi(c)-4)}{(1-\xi(c))^2}, \quad \xi(c) < 1, \quad +\infty, \xi(c) \geq 1. \end{aligned} \quad (4.60)$$

4.2.5 Mild and strong non-ideality

In view of the mathematical analysis of the problems (4.39) and (4.43), an important question is the convexity of the functional $\mathcal{F}_{\text{bulk}}$. This question reduces to the convexity of the bulk free energy density f defined by (4.19).

We can see in the above examples of bulk free energy densities that f_{Coul} is a concave function of c that behaves like $-c_i^{\frac{3}{2}}$ when $c_i \rightarrow 0$ and that f_0 is continuous on $\mathbb{R}_{\geq 0}$ and C^∞ on $\mathbb{R}_{> 0}$. Concerning the hard-sphere term, f_{HS} is a convex function of c on its domain, the domain of a function g being defined as the set

$$\text{dom}(g) := \left\{ c \in \mathbb{R}_{\geq 0}^2, g(c) < +\infty \right\}. \quad (4.61)$$

For the examples given above we obtain

- $\text{dom}f_{\text{HS}} := \{c_+ \geq 0, c_- \geq 0\}$ in the case of (CS1);
- $\text{dom}f_{\text{HS}} := \{c_+ \geq 0, c_- \geq 0, \xi(c) < 1\}$ in the case of (CS).

It turns out that in general f_1 is C^∞ on $\mathbb{R}_{\geq 0}$ (as for (CS1)) or C^∞ on $[0, 1)$ (as for (CS)). Finally, the ideal bulk free energy density f_{id} defined by (4.20) is convex and continuous on $\mathbb{R}_{\geq 0}$ and strictly convex and C^∞ on $\mathbb{R}_{> 0}$. These qualitative behaviours for the bulk free energy densities are common to other models [41, 75, 84].

When studying mathematically and numerically the behaviour of the bulk free energy density f , we identify two physical settings. The first setting is the case where the convexity of

the ideal term f_{id} and the steric exclusion term f_{HS} compensate the concavity of the electrostatic correlations modelled by f_{Coul} so that f is altogether a convex function of the ionic concentrations (this behaviour corresponds generally to a sufficiently large ion diameter at fixed temperature). We refer to this setting as *mildly non-ideal*. The second setting is the case where at relatively low ionic concentrations, the non-ideal term accounting for electrostatic correlations f_{Coul} dominates the two other terms $\sum_{i=\pm} f_{\text{id}}(c_i)$ and f_{HS} , so that the bulk free energy density f is a non convex function of the ionic concentrations (this behaviour corresponds generally to a sufficiently small ion diameter at fixed temperature). For example, for a system with one species, the bulk free energy density f has the shape of a double-well potential (see Chapter 6). A physical consequence of the lack of convexity is the possible appearance of phase separation. This phenomenon has been widely studied in the past two decades, in particular in a work of Levin and Fisher [69] and in the work of Groh *et al* [35] who computed the phase diagram for the bulk free energy density defined by (4.60). The mathematical counter-part is the ill-posedness of the problems (4.14), (4.39), (4.43) since uniqueness is lost. In this thesis, this last setting is referred to as *strongly non-ideal*.

Remark 7 (Debye–Hückel limit) *For extremely low values of the mean ion diameter, $\sigma \rightarrow 0$, we recover the expression derived in the Debye–Hückel theory, namely $\log(\gamma_0(\theta)) = -(2\pi L_{\text{B}}^3 \theta)^{1/2}$. Noticing that both (CS) and (CS1) goes to zero when $\sigma \rightarrow 0$ we infer that the bulk free energy density for the Debye–Hückel theory is a non convex function of the concentration for a wide range of physical parameter.*

4.2.6 Application: mechanical equilibrium and evaluation of the pressure

We have seen that thermodynamic equilibrium allows to find the spatial distribution of the ionic concentrations and the electrostatic potential. In view of applications in mechanics, a key quantity is the pressure of the system [1, 59, 97]. The pressure p of the electrolyte is a useful quantity to characterize mechanical equilibrium in a confined ionic system. In the absence of any external forcing, there holds

$$-\nabla p = \sum_{i=\pm} Z_i e c_i \nabla \psi, \quad (4.62)$$

expressing the fact that the spatial pressure gradient balances the Coulomb force. Assuming the ionic concentrations to be smooth enough, since we have $\nabla(\mu_i(c) + Z_i e \psi) = 0$, $i = \pm$, then

$$\begin{aligned} \nabla p &= \sum_{i=\pm} c_i \nabla(\mu_i(c)) \\ &= \nabla(p_{\text{osm}}(c)), \end{aligned} \quad (4.63)$$

where p_{osm} is the osmotic pressure, satisfying the Gibbs-Duhem relation

$$p_{\text{osm}}(c) := \left(\sum_{i=\pm} c_i \mu_i(c) \right) - f(c), \quad (4.64)$$

so that p and p_{osm} differ only by an additive constant. Moreover, denoting $E = -\nabla \psi$ the electric field, we observe that

$$\begin{aligned}
\nabla p &= (\varepsilon \Delta \psi) E \\
&= \varepsilon (\nabla \cdot E) E \\
&= \frac{\varepsilon}{2} \nabla \cdot (2E \otimes E - |E|^2 \mathbf{I}_d) \\
&= \nabla \cdot \tau_m(\psi),
\end{aligned} \tag{4.65}$$

where

$$\tau_m := \frac{\varepsilon}{2} (2E \otimes E - |E|^2 \mathbf{I}_d), \tag{4.66}$$

is the Maxwell tensor and \mathbf{I}_d the identity tensor. Thus, it is convenient to introduce the total pressure tensor Π defined by

$$\Pi := -\tau_m(\psi) + p_{\text{osm}}(c) \mathbf{I}_d. \tag{4.67}$$

The mechanical equilibrium (4.62) can then be expressed equivalently by

$$\operatorname{div}(\Pi) = 0. \tag{4.68}$$

4.2.7 Previous mathematical results

Let us now turn to the mathematical results available concerning the study of the free energy functional (4.1). We start by briefly reviewing the mathematical results available concerning ideal models and the Poisson–Boltzmann equation (4.16). The work of Looker [72] establishes existence and uniqueness of the solution of the Poisson–Boltzmann equation with inhomogeneous Neumann boundary conditions, formulated in terms of the electrostatic potential ψ . The same model is considered by Allaire, Mikelić, and Piatniski [3] in view of homogenization of confined electrolytes coupled with Stokes flow.

Generalizations of the ideal setting have been addressed previously in the literature. In [71], Li analyzes the generalized Poisson–Boltzmann theory with implicit solvent. This formulation, also considered by Borukhov, Andelman, and Orland [13], accounts for steric exclusion effects, but not for electrostatic correlations. For an electrolyte with M species, the solvent concentration c_0 is introduced such that

$$\sigma^3 c_0 := 1 - \sum_{i=1}^M \sigma^3 c_i,$$

where $\sigma > 0$ represents the mean ion diameter, and the ideal contribution of the solvent concentration, $c_0(\log(\sigma^3 c_0) - 1)$, is included in the free energy functional. The mathematical analysis has been extended to different ion diameters by Li [70]. The critical points of the free energy are sought in a convex set enforcing $c_i \geq 0$ for all $0 \leq i \leq M$, so that the ionic concentrations are a priori bounded from above. One important result in the analysis of [70, 71] is the proof that these constraints are not active, that is, that all the c_i 's, $0 \leq i \leq M$, are bounded uniformly away from zero. The technique of proof, which consists in further optimizing the free energy by modifying the ionic concentrations at extreme values if the above bounds are not satisfied, will be extended in Chapter 5 for f_{corr} defined by (4.59). This extension is not straightforward owing to the model we consider for f_{corr} that couples in a more intricate way all the ionic concentrations.

Furthermore, the work of Carlen *et al.* [17] considers nonlinearities of the same kind as those described by the implicit solvent. The authors analyze long-range interactions by incorporating a nonlocal term with long-range Kac type potentials. The mathematical analysis shows that L^∞ -bounds on the ionic concentrations can be enforced in the convex set where the minimization is taken, but also that under a condition on both the ideal and steric exclusion terms, L^∞ -bounds can be achieved [17, Theorem B.1]. The authors also address mathematically the question of phase separation, vapor-liquid coexistence and segregation of species, in systems with long-range interactions.

In the strongly non-ideal case, phase separation is expected to take place owing to the non convexity of the bulk free energy density as discussed in Section 4.1. There is an extensive bibliography concerning the theoretical and numerical study of phase separation phenomena in other settings than confined electrolytes. In general, the free energy density used in such phase field theory is a double well potential inducing a partition of the state space into two phases. Most of the studies have been performed in bulk situations where no external field perturbs the constant ionic concentrations profiles in each phase. The first mathematical difficulty comes from the fact that the underlying free energy density f is a non convex function of the ionic concentrations, *e.g.* f is typically a double-well potential. Results have been achieved by considering a regularized free energy functional of the form

$$\mathcal{F}_{\kappa,\text{bulk}}(c) = \int_{\Omega} \left\{ \frac{\kappa^2 L_*^3}{2\beta} |\nabla c|^2 + f(c) \right\}, \quad (4.69)$$

with $\kappa > 0$ the regularization parameter, *e.g.*, in the seminal work of Modica [79] without nonlocal term. References on phase transition and links with Γ -convergence can also be found in the book of Braides [15]. Other recent results concerning the study of the Ohta-Kawasaki model (modelling diblock copolymer systems) are relevant here owing to the similarity of the mathematical problem. Let us mention, without exhaustivity, the mathematical and numerical works of Muratov [81], Choksi [18], and more recently Goldman, Muratov and Serfaty [32] who studied Γ -convergence properties and Γ -expansions of a functional similar to $\mathcal{F}_{\kappa,\text{bulk}}$ when a nonlocal operator accounting for Coulomb interaction is added.

The situation we consider in this thesis is slightly different since our nonlocal operator takes into account the mean field internal energy of the ions and also the presence of a charged inclusion or of a surrounding charged wall. In general, under those conditions, we do not expect piecewise constant ionic concentrations profiles, but phase separation between a diluted phase and a condensed phase with inhomogeneous ionic concentrations profiles in both phases, induced by the gradient of the electrostatic potential in the system. In Chapter 6, we propose a numerical approach to solve this phase separation problem in the case where a single counterion compensates the negative surface charge. The method is based on two regularizations of the initial model: using the convex hull of the bulk free energy instead of the free energy itself and adding a gradient perturbation that penalizes the oscillation of the ionic concentrations (such as (4.69)). These regularizations can be motivated by Γ -convergence arguments (sketched at the end of Chapter 6).

Finally, we mention some work on the time-dependent setting and nonequilibrium situations that we do not consider in this thesis. We refer to the work of Schmuck [96] and Prohl and Schmuck [91] who studied the time dependent Navier–Stokes–Poisson–Nernst–Planck (NSPNP)

system and its numerical analysis, noting that steady-state solutions of the homogeneous NSPNP system (for example with periodic boundary conditions and no source term) solve the Poisson–Boltzmann equation. This mathematical and numerical analysis has been performed for models that do not incorporate non-ideal effects. In fact, when considering transport within time-dependent settings, in addition to the non-ideal terms in the electro-chemical potential (that are relevant at equilibrium), additional corrections due to non-ideality appear in the diffusion Onsager tensor [2, 23].

4.3 The primitive model for homogeneous electrolytes

We now turn to the derivation of the model presented in Section 4.2 starting from a model at the molecular level. The present material is a formal derivation and collects existing results and methods from various fields of Statistical physics (equilibrium thermodynamics, integral equations, inhomogeneous DFT, partial differential equations, mean-field theory). The calculations are formal (unless mentioned), and the mathematical justification of the derivation is definitely a challenge. We start by presenting the bulk theory in Section 4.3 where we derive the expression of the ideal bulk free energy density f_{id} and the non-ideal bulk free energy density f_{corr} . In Section 4.4, we introduce a microscopic description of confined electrolytes and derive a density functional theory for this model. We also present various approximations leading to the model considered in Section 4.2 and in particular to the free energy functional \mathcal{F} defined by (4.17) and the bulk free energy density defined by (4.59).

We refer to the textbooks [41, 75] for further insight into the physical background. We consider a simplified description of electrolytes which is the *primitive model* of electrolytes. This model attempts to describe the behaviour of ions in solution by considering ions as charged hard spheres of diameter σ_{\pm} (expressed in m) and to consider the water as a continuous medium of uniform dielectric constant $\varepsilon = \varepsilon_0 \varepsilon_r$. In this thesis, we consider the restricted primitive model for electrolytes where all ions have the same diameter $\sigma_{\pm} = \sigma$. The primitive model has been considered historically for an isolated system, so that we may consider that the space of position is \mathbb{R}^3 . This situation is referred to as the “bulk” situation, where the system is homogeneous (in opposition to the confined situation, where the system is inhomogeneous).

4.3.1 Hamiltonian of the isolated system

In the primitive model, for binary electrolytes (two species) the ions are described by $N = N_+ + N_-$ particles of position and momenta $(q, p) \in \mathbb{R}^{3N} \times \mathbb{R}^{3N}$ and the energy of the system is given by the Hamiltonian

$$\mathcal{H}(q, p) = \frac{1}{2} p^T M^{-1} p + \mathcal{V}(q), \quad (4.70)$$

with $M = \text{diag}(m_+, m_-)$ the mass matrix, thereby considering that all the ions of same type have the same mass. As we consider a two-species model, we can make more tractable the form of the potential energy by collecting the positions of the ions of same type:

$$q = (q^+, q^-) \in \mathbb{R}^{3N_+} \times \mathbb{R}^{3N_-},$$

and in the same fashion, we suppose that all the ions of the same type have the same valence $Z_+ \in \mathbb{Z}^+ \setminus \{0\}$ or $Z_- \in \mathbb{Z}^- \setminus \{0\}$. We write all the expressions of the potential energy by distinguishing the contribution only through the species type. We start with the interaction potential energy

$$\mathcal{V}(q) = \sum_{k=\pm} \mathcal{V}^k(q), \quad (4.71)$$

where we defined the potentials

$$\mathcal{V}^k(q) = \sum_{1 \leq i \leq N_k} \left(\sum_{i < j \leq N_k} v_{k,k}(q_k^i - q_k^j) + \frac{1}{2} \sum_{1 \leq j \leq N_{-k}} v_{k,-k}(q_k^i - q_{-k}^j) \right), \quad k = \pm. \quad (4.72)$$

The pair potential is defined by

$$v_{k,l}(r) := \begin{cases} +\infty, & r \leq \sigma, \\ Z_k Z_l \left(\frac{L_B}{\beta} \right) r^{-1}, & r > \sigma, \quad k, l = \pm, \end{cases} \quad (4.73)$$

where the Bjerrum length L_B is defined by

$$L_B := \frac{\beta e^2}{4\pi\epsilon}. \quad (4.74)$$

The Bjerrum length measures the distance at which the interaction between two charged particles equals the thermal energy $\frac{1}{\beta} = k_B T$. The pairwise potential defined by (4.73) describes the hardcore repulsion between the ions for distances lower than the ionic diameter and the Coulomb interaction between the ions for distances larger than the ionic diameter.

4.3.2 The ideal gas bulk free energy density

We now present the derivation of thermodynamics quantities with the help of the microscopic Hamiltonian defined by (4.70). We consider that the particles live in a bounded domain Ω and are isolated from any external perturbation so that the system is homogeneous. We consider a canonical setting (NVT) where the number of particles N , the occupied volume V and the temperature T are fixed.

For completeness, we start by deriving the standard thermodynamic properties of the ideal gas. Assume that the particles are confined in a volume Ω . Then, the expression of the canonical measure for a system of N particles (with $N = N_+ + N_-$) at fixed temperature T is given by

$$\psi_{\text{eq}}(q, p) = \frac{1}{N_+! N_-! \hbar^{3N}} \frac{e^{-\beta \mathcal{H}(q, p)}}{Z}, \quad (4.75)$$

where the partition function is given by

$$Z = \frac{1}{N_+! N_-! \hbar^{3N}} \int_{\Omega^N \times \mathbb{R}^{3N}} e^{-\beta \mathcal{H}(q, p)} dq dp < +\infty, \quad (4.76)$$

for \hbar the reduced Planck constant. In classical thermodynamics, it is convenient to introduce the Helmholtz free energy of the system which is the thermodynamical potential defined by

$$F = -\frac{1}{\beta} \log(Z), \quad (4.77)$$

which is minimal at equilibrium for a system at fixed number of particles N , volume V , and temperature T . The free energy of the system is commonly written as

$$F = U - TS, \quad (4.78)$$

where U is the internal energy and S is the entropy defined through the relations

$$S = -\left(\frac{\partial F}{\partial T}\right)_{N,V}, \quad U = \left(\frac{\partial(\beta F)}{\partial \beta}\right)_{N,V}. \quad (4.79)$$

Another useful quantity for the following derivation is the notion of bulk free energy density, the latter being the rescaling of the free energy by the occupied volume:

$$f = \frac{F}{|\Omega|}. \quad (4.80)$$

These equations make the link between classical thermodynamics and statistical mechanics.

Pursuing the analysis, using the separated form of the Hamiltonian, we can make more explicit the partition function remarking that integration with respect to the momenta yields

$$Z = \frac{1}{\Lambda_+^{3N_+} \Lambda_-^{3N_-} N_+! N_-!} \int_{\Omega^N} e^{-\beta \mathcal{V}(q)} dq, \quad (4.81)$$

since the distribution of momenta are Gaussians. When the potential energy is $\mathcal{V} = 0$, we obtain the partition function of the ideal gas:

$$Z^{\text{id}} = \frac{|\Omega|^N}{N_+! N_-! \Lambda_+^{3N_+} \Lambda_-^{3N_-}}, \quad (4.82)$$

where we recall the definition of the de Broglie wavelength

$$\Lambda_i = \left(\frac{2\pi\beta\hbar^2}{m_i}\right)^{\frac{1}{2}}, \quad i = \pm. \quad (4.83)$$

For nonzero \mathcal{V} , we write

$$Z = Z^{\text{id}} Z^{\text{ex}}, \quad (4.84)$$

with

$$Z^{\text{ex}} = \frac{1}{|\Omega|^N} \int_{\Omega^N} e^{-\beta \mathcal{V}(q)} dq. \quad (4.85)$$

We can turn back to the expression of the Helmholtz free energy, splitting F into ideal (F_{id}) and excess component (F_{ex}) by taking the logarithm of (4.84). This yields

$$F = F_{\text{id}} + F_{\text{ex}}, \quad (4.86)$$

where

$$F_{\text{id}} := -\frac{1}{\beta} \log(Z^{\text{id}}), \quad F_{\text{ex}} := -\frac{1}{\beta} \log(Z^{\text{ex}}). \quad (4.87)$$

We can write

$$F_{\text{id}} = \frac{1}{\beta} \left[\log \left(\frac{N_+! \Lambda_+^{3N_+}}{|\Omega|^{N_+}} \right) + \log \left(\frac{N_-! \Lambda_-^{3N_-}}{|\Omega|^{N_-}} \right) \right],$$

and using the Stirling approximation

$$\log(k!) \sim_{k \rightarrow \infty} \int_0^k \log(n) dn = k(\log(k) - 1),$$

we can approximate the ideal gas free energy as

$$F_{\text{id}}^N = \frac{1}{\beta} \sum_{i=\pm} \left(N_i \log(\Lambda_i^3 c_i) - 1 \right), \quad (4.88)$$

where we introduced the bulk ionic concentrations $c = (c_+, c_-)$ (expressed in m^{-3}) defined as

$$c_i = \frac{N_i}{|\Omega|}, \quad i = \pm. \quad (4.89)$$

In the thermodynamic limit, that is, $c_i = \frac{N_i}{|\Omega|}$ fixed and $|\Omega| \rightarrow +\infty$, we obtain the ideal gas free energy density

$$\lim_{\text{thermo}} \frac{F_{\text{id}}^N}{|\Omega|} = \sum_{i=\pm} f_{\text{id}}(c_i), \quad (4.90)$$

where the function f_{id} is defined by

$$f_{\text{id}}(c_i) := \frac{1}{\beta} c_i (\log(\Lambda_i^3 c_i) - 1), \quad i = \pm, \quad c_i \geq 0. \quad (4.91)$$

Note that this ideal gas contribution to the free energy density is purely entropic remarking that, for fixed c_i , we have

$$\frac{\partial(\beta f_{\text{id}}(c_i))}{\partial \beta} = 0, \quad i = \pm, \quad (4.92)$$

so that the corresponding internal energy is 0.

4.3.3 The non-ideal bulk free energy density

We now present a method to obtain the bulk free energy density f_{corr} which is, in general, an approximation of F_{ex} defined by (4.87). We do not reproduce all the tedious explicit calculations but only the key ideas and will mostly refer to the bibliography.

Distribution functions theory and the homogeneous Ornstein–Zernike equation

As detailed in the textbook [41], the key quantity to describe properties of bulk electrolytes is the so-called pair distribution function $g_{i,j}$ defined by

$$g_{i,j}(x, y) = (c_i c_j)^{-1} \rho_{i,j}^2(x, y), \quad i, j = \pm, \quad (4.93)$$

where x, y are positions in Ω and where

$$\rho_{i,i}^2(q_i^1, q_i^2) = \frac{N_i(N_i - 1)}{|\Omega|^N} \int_{\Omega^{N-2}} (Z_{\text{ex}})^{-1} e^{-\beta\mathcal{V}(q)} dq_i^3 : dq_i^{N_i} dq_{-i}, \quad i = \pm, \quad (4.94a)$$

$$\rho_{i,j}^2(q_i^1, q_j^1) = \frac{N_i N_j}{|\Omega|^N} \int_{\Omega^{N-2}} (Z_{\text{ex}})^{-1} e^{-\beta\mathcal{V}(q)} dq_i^2 : dq_i^{N_i} dq_j^2 : dq_j^{N_j}, \quad i = \pm, j = -i, \quad (4.94b)$$

recalling that the $c_i = \frac{N_i}{|\Omega|}$ are the constant ionic concentrations. Notice that we have $\rho_{i,j}^2 = \rho_{j,i}^2$. Owing to translation invariance and isotropy, we have in fact

$$g_{i,j}(x, y) \equiv g_{i,j}(|x - y|), \quad (4.95)$$

so that $g_{i,j}$ is also referred to as the radial pair distribution function. The physical interpretation of the quantity $g_{i,j}(|x - y|)$ is that it is proportional to the probability of finding an ion of type j at distance $|x - y|$ of an ion of type i . The interest of the function $g_{i,j}$ is that it is directly measurable by experiments (radiation-scattering experiments).

Let us introduce some notions and notation about the Ornstein–Zernike equation. The Ornstein–Zernike equation is an integral equation relating the so-called direct pair correlation function $\mathcal{C}_{i,j}$ to the so-called indirect pair correlation function $h_{i,j}$. The indirect pair correlation function $h_{i,j}$ is simply given by

$$h_{i,j} := g_{i,j} - 1, \quad (4.96)$$

while the direct pair correlation function $\mathcal{C}_{i,j}$ is defined by the Ornstein–Zernike equation:

$$h_{i,j}(|x - y|) = \mathcal{C}_{i,j}(|x - y|) + \sum_{k=\pm} c_k \int_{\Omega} \mathcal{C}_{i,k}(|x - x'|) h_{k,j}(|y - x'|) dx'. \quad (4.97)$$

For convenience, we denote $r = |x - y| > 0$. The Ornstein–Zernike equation has a simple physical interpretation since it splits the correlation between the ions in a direct contribution $\mathcal{C}_{i,j}$ (the correlation between ion i and ion j) and an indirect correlation (the interaction of ion i and ion j through a third one k). The practical interest of equation (4.97) is that it seems easier to make an approximation of $g_{i,j}$ with the help of the direct pair correlation function $\mathcal{C}_{i,j}$ solving (4.97). Indeed, the difficulty is that even in this bulk situation, the function $g_{i,j}$ is a complex function of the high dimensional interaction potential \mathcal{V} (and so is $h_{i,j} = g_{i,j} - 1$). The idea is then to introduce a closure (either exact or approximate) specifying $\mathcal{C}_{i,j}$ for $r > \sigma$ and $g_{i,j}$ for $r \leq \sigma$ in order to solve (4.97) and find both $g_{i,j}$ and $\mathcal{C}_{i,j}$ for all $r > 0$ (analytically or numerically).

Remark 4.1. (*Well posedness of the Ornstein–Zernike equation.*) *The Ornstein–Zernike equation (4.97) is formulated in the grand-canonical ensemble. In this thesis, we consider a canonical setting and modifications of the Ornstein–Zernike theory are required to take into*

account the thermodynamics constraints, see White and Velasco [110]. In the homogeneous case (considered above), it is stated in [110] and [92] that the equations of the canonical and grand canonical settings only differ through an additive factor that goes to zero in the thermodynamic limit.

The Mean Spherical Approximation

We now turn to the approximation leading to the non-ideal bulk free energy density considered in this thesis. The goal is to obtain a suitable approximation of $g_{i,j}$ and $\mathcal{C}_{i,j}$ satisfying (4.97).

There is a wide variety of closures. We consider mostly the *Mean Spherical Approximation* (MSA) introduced by Waisman and Lebowitz in [63] and [64]. Blum generalised this model to asymmetric electrolytes [10] with ions of different ionic diameters. The interest of the MSA is that it provides semi-analytical expressions of most of the thermodynamic quantities of interest (internal energy, free energy density, osmotic pressure). The MSA requires global electroneutrality in the form:

$$\sum_{i=\pm} Z_i e c_i = 0, \quad (4.98)$$

where we recall that c_i are the bulk (constant) ionic concentrations. The closure is to postulate

$$h_{i,j}(r) = -1, \quad r \leq \sigma, \quad (4.99a)$$

$$\mathcal{C}_{i,j}(r) = -Z_i Z_j L_B r^{-1}, \quad r > \sigma. \quad (4.99b)$$

The physical interpretation of the MSA is the following: the exact closure relation for $h_{i,j}$ indicates that the ions cannot overlap each other, while the approximate closure for $\mathcal{C}_{i,j}$ supposes an asymptotic behaviour matching that of the long-range potential. We define the short-range part of the direct pair correlation function $\mathcal{C}_{i,j}$ by

$$\mathcal{C}_{i,j}^{\text{SR}}(r) := \mathcal{C}_{i,j}(r) + Z_i Z_j L_B r^{-1}, \quad (4.100)$$

so that in the case of MSA we have

$$\mathcal{C}_{i,j}^{\text{SR}}(r) = \begin{cases} \mathcal{C}_{i,j}(r) + Z_i Z_j L_B r^{-1}, & r \leq \sigma, \\ 0, & r > \sigma. \end{cases} \quad (4.101)$$

Another remark of interest (observed in [64]) is that we can split the direct correlation function calculated with the MSA into a hard-sphere component \mathcal{C}^{HS} and an electrostatic component $\mathcal{C}_{i,j}^{\text{Coul}}$ so that

$$\mathcal{C}_{i,j}^{\text{SR}}(r) := \mathcal{C}^{\text{HS}}(r) + \mathcal{C}_{i,j}^{\text{Coul}}(r), \quad (4.102)$$

for which we will give analytic expressions in the next sections. In bulk homogeneous fluids, the correlation functions only depend on the distance between the atoms. The function \mathcal{C}^{HS} is the direct-correlation function calculated with the Percus–Yevick closure for a pure hard-sphere interaction potential, while the correlation function $\mathcal{C}_{i,j}^{\text{Coul}}$ contains the electrostatic contribution at distances lower than the ionic diameter [64]. These correlation functions have only a short-range contribution owing to (4.101).

Thermodynamics relationships

For a bulk system, we can derive exact expressions of various thermodynamics quantities such as internal energy, compressibility, entropy and deduce formulas for derived or integrated quantities (thermodynamic integration, virial theorem, Gibbs–Duhem equation). These formulas depend generally on the pairwise potential energy $v_{i,j}$ and the radial distribution functions $g_{i,j}$. For example, the formula for the internal energy (per unit of volume) is given by

$$\frac{U_{\text{ex}}}{|\Omega|} = \frac{1}{2} \sum_{i,j=\pm} c_i c_j \left(\int_{\Omega} v_{i,j}(x) g_{i,j}(x, \beta) dx \right). \quad (4.103)$$

In general, the free energy is obtained by thermodynamic integration of a thermodynamic quantity derived from the excess free energy. For example, thermodynamic integration of the excess internal energy with respect to the inverse temperature β yields

$$\beta F_{\text{ex}}(\beta) = \int_0^{\beta} U_{\text{ex}}(\beta') d\beta', \quad (4.104)$$

from definition (4.79). Another useful formula relates the pressure to the free energy, for example for a one-component mixture, we have

$$\frac{\beta F_{\text{ex}}}{|\Omega|} = c \int_0^{\xi} \left(\frac{\beta P(\xi)}{c} - 1 \right) \frac{d\xi'}{\xi'}, \quad (4.105)$$

where ξ is the packing number (defined by (4.109)) and using the thermodynamic relationship

$$P = - \left(\frac{\partial F}{\partial V} \right)_{T,N}. \quad (4.106)$$

There also is a formula linking the free energy to the direct correlation function, which is (see [41, Eq. 3.5.25])

$$\frac{\beta F_{\text{ex}}}{|\Omega|} = \sum_{i,j=\pm} c_i c_j \int_0^1 (\lambda - 1) \int_{\Omega} \mathcal{C}_{i,j}(x, \lambda c_+, \lambda c_-) dx d\lambda. \quad (4.107)$$

When the function $g_{i,j}$ is defined by (4.93) and (4.94) and $\mathcal{C}_{i,j}$ is defined by (4.97), then (4.104) is equivalent to (4.107). This equivalence does not hold when using approximate closures (such as MSA) so that $g_{i,j}$ does no longer satisfy (4.93) and (4.94). This phenomenon is the so-called *thermodynamic inconsistency*.

In the next sections, we present the examples of the Percus–Yevick bulk free energy density and the electrostatic component of the MSA bulk free energy density.

Hard-Sphere bulk free energy density for MSA

We now reproduce the derivation of the Hard-Sphere bulk free energy density used within the MSA, the latter resulting from the decomposition of short-range steric exclusion effect and

short-range Coulomb interaction. The Percus–Yevick direct correlation function is given by the approximation of the solution of the Ornstein–Zernike equation in the form (see *e.g.* [41, Section 4.4] and the proof therein):

$$\mathcal{C}^{\text{HS}}(r, c) = \begin{cases} -\lambda_1(\xi(c)) - 6\xi(c)\lambda_2(\xi(c)) \left(\frac{r}{\sigma}\right) - \frac{1}{2}\xi(c)\lambda_1(\xi(c)) \left(\frac{r}{\sigma}\right)^3, & r \leq \sigma, \\ 0, & r > \sigma, \end{cases} \quad (4.108)$$

where $\xi(c)$ stands for the packing fraction and is defined through

$$\xi(c) := \sum_{i=\pm} \vartheta c_i, \quad \vartheta := \frac{\pi\sigma^3}{6}, \quad (4.109)$$

and $r = |x|$. The functions λ_1 and λ_2 are defined, for $0 \leq t < 1$, by

$$\lambda_1(t) = \frac{(1+2t)^2}{(1-t)^4}, \quad \lambda_2(t) = -\frac{(1+\frac{t}{2})}{(1-t)^4}. \quad (4.110)$$

Using this solution of the Ornstein–Zernike equation, two equations of state relating the pressure (defined by (4.106)) to the concentration can be obtained by the so-called “virial route” or the so-called “compressibility route”. One obtain (see [41, Section 4.4])

$$\frac{\beta P_v(c)}{c} = \frac{1 + 2\xi(c) + 3\xi(c)^2}{(1 - \xi(c))^2}, \quad \frac{\beta P_{\text{comp}}(c)}{c} = \frac{1 + \xi(c) + \xi(c)^2}{(1 - \xi(c))^3}, \quad (4.111)$$

where $P_{v/\text{comp}}$ is the pressure evaluated respectively *via* the virial route and compressibility route. An interesting observation is that one obtain the Carnahan–Starling equation of state [74] by considering a particular linear combination of the equations of state obtained through the Percus–Yevick solution of the Ornstein–Zernike equation. There holds

$$\frac{\beta P_{\text{CS}}(c)}{c} = \frac{\beta}{3c} (2P_{\text{comp}}(c) + P_v(c)). \quad (4.112)$$

The bulk free energy density accounting for the hard-sphere potential is obtained by using formula (4.105) for the various pressure given above. In the applications, we do not consider a Percus–Yevick expression of the hard-sphere free energy but rather two alternatives that are the Carnahan–Starling given by

$$f_{\text{CS}}(c) = \begin{cases} -\frac{1}{\beta\vartheta} \frac{\xi(c)^2 (3\xi(c) - 4)}{(1 - \xi(c))^2}, & \xi(c) < 1, \\ +\infty, & \xi(c) \geq 1. \end{cases} \quad (4.113)$$

and the linearized expression being obtained by a Taylor expansion of f_{CS} at second order:

$$f_{\text{CS}}(c) = \frac{4\xi(c)^2}{\beta\vartheta} + O(c^3) = f_{\text{CS1}}(c) + O(c^3).$$

In what follows, we refer to f_{HS} when considering the hard-sphere component of the bulk free energy density. This derivation justifies the definition of the bulk free energy density (CS) and (CS1) previously defined by (4.57) and (4.58).

Electrostatic correlations bulk free energy density for MSA

We now turn to the evaluation of the bulk free energy density accounting for electrostatic correlations. From previous work ([63], [64] and [10]), we can obtain an analytical expression of the direct correlation function solution of (4.97) with the MSA closure (4.99). We express the short-range direct correlation function in the form presented in [64] that reads

$$\mathcal{C}_{i,j}^{\text{Coul}}(r) = \begin{cases} -L_B Z_i Z_j \left(\frac{2B}{\sigma} - \left(\frac{B}{\sigma} \right)^2 r - \frac{1}{r} \right), & r \leq \sigma, \\ 0, & r > \sigma, \end{cases} \quad (4.114)$$

the only difference with [64] being the last term proportional to r^{-1} coming from the fact we subtracted this contribution in equation (4.100). In fact, following [35], this term can be omitted. At this stage, the non-dimensional parameter B remains to be defined and is a function of the ionic concentrations. To this end, we introduce the screening parameter Γ_{MSA} (expressed in m^{-1}) derived in [10] as the solution of

$$\Gamma_{\text{MSA}}^2 = \pi L_B \sum_{i=\pm} \frac{Z_i^2 c_i}{(1 + \sigma \Gamma_{\text{MSA}})^2}, \quad (4.115)$$

For convenience, we introduce the ionic strength (expressed in m^{-3}) such that,

$$I(c) = \frac{1}{2} \sum_{i=\pm} Z_i^2 c_i, \quad (4.116)$$

The algebraic equation (4.115) can be easily solved when considered for equal ionic diameters and the solution is

$$\Gamma_{\text{MSA}}(c, \beta) = \frac{1}{2\sigma} \left(\sqrt{2\sigma(4\pi L_B)^{1/2} (2I(c))^{1/2} + 1} - 1 \right) \quad (4.117)$$

Finally, the non-dimensional parameter B derived in [64] is given by

$$B(c, \beta) = -\frac{\sigma \Gamma_{\text{MSA}}(c, \beta)}{1 + \sigma \Gamma_{\text{MSA}}(c, \beta)}. \quad (4.118)$$

The method of derivation of the thermodynamics quantities is of paramount importance. For example, for a bulk solution, where the ionic concentrations $c = (c_+, c_-)$ are constant and satisfy the electroneutrality condition (4.98), evaluating the integral (4.107) yields the value 0. However, as mentioned in [11], the most reliable formula for the free energy density of the MSA is obtained through the internal energy by computing U_{ex} defined by (4.103) and thermodynamic integration, applying formula (4.104). An issue is that even with the approximations performed, the $g_{i,j}$ computed owing to the MSA are complex functions of Γ_{MSA} (see [35, equation 10]) and as explained in [64], some tricks of the analytic resolution of (4.97) with the approximations (4.99) must be used to compute the integral (4.103). We mention the result derived in [64] where the excess free energy density accounting for electrostatic correlations obtained by thermodynamic integration of the internal energy is given by

$$u_{\text{Coul}}(c, \beta) := \left(\frac{2L_B}{\beta\sigma} \right) I(c)B(c, \beta), \quad (4.119)$$

so that, using

$$\int_0^\beta u_{\text{Coul}}(c, \beta') d\beta' = \beta f_{\text{Coul}}(c, \beta), \quad (4.120)$$

we get

$$f_{\text{Coul}}(c, \beta) = f_{\text{Coul}}(c) := -\frac{2L_B}{\beta\sigma} \left(I(c) - \frac{2\sigma}{3\pi L_B} (\Gamma_{\text{MSA}}(c))^3 - \frac{1}{2\pi L_B} (\Gamma_{\text{MSA}}(c))^2 \right). \quad (4.121)$$

Note that the electrostatic correlation bulk free energy density is a function only depending on the ionic strength and is *a priori* only valid on the set

$$\left\{ c_i \geq 0, \sum_{i=\pm} Z_i c_i = 0 \right\} \subset \mathbb{R}^2.$$

Nonetheless, in the applications, we will not restrict ourselves to this bulk setting and use this expression for any couple of positive ionic concentrations. Moreover, the free energy density given by (4.121) is the sum of a non-zero internal energy and a non-zero entropy (as opposed to the ideal and hard-sphere bulk free energy densities for which we have seen that the internal energy is 0).

Eventually, all these calculations lead to the following bulk free energy density:

$$f(c) := \left(\sum_{i=\pm} f_{\text{id}}(c_i) \right) + f_{\text{corr}}(c), \quad f_{\text{corr}}(c) := f_{\text{Coul}}(c) + f_{\text{HS}}(c). \quad (4.122)$$

which was the first task of the derivation.

Remark 8 (Thermodynamic limit) *As in the case of the ideal bulk free energy density, the non-ideal bulk free energy density has to be understood in the thermodynamic limit [94].*

4.4 Derivation of the free energy functional \mathcal{F} for confined electrolytes

4.4.1 A microscopic model for confined electrolytes

We now turn to the description of a microscopic model for confined inhomogeneous fluids at the molecular level. In what follows, we still consider thermodynamic properties in the canonical ensemble, that is the number of particles N , the volume V , and the temperature T are fixed. This section shares a lot of elements with Section 4.3, and we try to emphasize the differences caused by the inhomogeneity and the confinement. In order to derive the continuous model, the space of positions is required to be a three-dimensional torus of the form

$$\mathcal{D} = \ell_{x_1} \mathbb{T} \times \ell_{x_2} \mathbb{T} \times \ell_{x_3} \mathbb{T}, \quad (4.123)$$

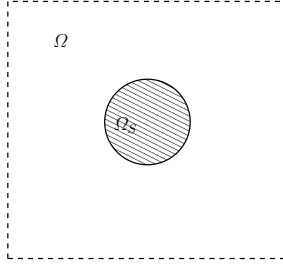


Fig. 4.2. Geometry for this derivation.

for length scales $(\ell_{x_1}, \ell_{x_2}, \ell_{x_3}) \in \mathbb{R}^3$. To simplify the notation, we set $\ell_{x_1} = \ell_{x_2} = \ell_{x_3} = L_*$ and we recall the minimal assumption $L_* > \sigma$, so that a single cell $[0, L_*]^3$ contains at least one particle. We introduce the subset Ω_S of \mathcal{D} being the solid object whose boundary is negatively charged and $\Omega = \mathcal{D} \setminus \Omega_S$. Here we assume that $\Omega_S \subset\subset \mathcal{D}$, see Figure 4.2. We consider a system of N ions of positions and momenta $(q, p) \in \mathcal{D}^N \times \mathbb{R}^{3N}$. The energy of the system is now described by the Hamiltonian

$$H(q, p) = \frac{1}{2} p^T M^{-1} p + V(q), \quad V(q) = V_{\text{inter}}(q) + V_{\text{ext}}(q),$$

with M the mass matrix as before. The internal potential V_{inter} is the sum of the pair interactions in the form

$$V(q) = \sum_{k=\pm} \left\{ V_{\text{inter}}^k(q) + V_{\text{ext}}^k(q) \right\}. \quad (4.124)$$

We define the potential

$$V_{\text{inter}}^k(q) = \sum_{1 \leq i \leq N_k} \left(\sum_{i < j \leq N_k} v_{k,k}(q_k^i - q_k^j) + \frac{1}{2} \sum_{1 \leq j \leq N_{-k}} v_{k,-k}(q_k^i - q_{-k}^j) \right), \quad k = \pm, \quad (4.125)$$

with pairwise potential for $x \in \mathcal{D}$,

$$v_{i,j}(x) := \begin{cases} +\infty, & |x| \leq \sigma, \\ Z_i Z_j v_{\text{Coul}}(x), & i, j = \pm, \text{ elsewhere,} \end{cases} \quad (4.126)$$

with the same conventions as in Section 4.3. To define the periodic version of the Coulomb potential, v_{Coul} , we consider G , the Green function for \mathcal{D} , such that $\varphi = (G \star (g - \langle g \rangle_{\mathcal{D}}))$ solves

$$-\Delta \varphi = g - \langle g \rangle_{\mathcal{D}}, \quad \varphi \text{ } L_*\text{-periodic}, \quad \langle \varphi \rangle_{\mathcal{D}} = 0, \quad (4.127)$$

where $\langle g \rangle_{\mathcal{D}}$ denote the average of g over the volume \mathcal{D} . In general, the function G is not a function only depending on the distance to the origin (as opposed to the case of the whole space where $G_{\mathbb{R}^3}$ is invariant with respect to the rotations). The potential v_{Coul} is defined by

$$v_{\text{Coul}}(x) := \frac{4\pi L_B}{\beta} G(x), \quad x \in \mathcal{D}. \quad (4.128)$$

The external potentials V_{ext}^k are of the form

$$V_{\text{ext}}^k := \begin{cases} (Z_k e) \psi_S(x), & x \in \Omega, k = \pm, \\ +\infty, & x \in \Omega_S. \end{cases} \quad (4.129)$$

This potential describes the Coulomb interaction and the hardcore repulsion between the ions and the solid object Ω_S negatively charged on its surface. The present setting can be adapted to the case of nanochannels or cylindrical inclusions.

The definition of the electrostatic potential ψ_S relating the charged solid Ω_S to the other particles requires some care. We introduce the surface charge density $\Sigma_S > 0$ (expressed in Cm^{-2}) carried by the boundary of Ω_S . For convenience, we also define the permittivity of the domain \mathcal{D} as the piecewise constant function

$$\varepsilon_{\mathcal{D}}(x) = \begin{cases} \varepsilon, & x \in \Omega, \\ \varepsilon_S, & x \in \Omega_S, \end{cases} \quad (4.130)$$

where $\varepsilon_S > 0$ is the permittivity of the solid Ω_S . The last definition allows us to consider ψ_S as the solution (up to an additive constant) of the following boundary value problem on \mathcal{D} :

$$\begin{cases} -\operatorname{div}(\varepsilon_{\mathcal{D}} \nabla \psi_S) = \frac{\mathbf{1}_{\Omega}}{|\Omega|} \int_{\partial\Omega_S} \Sigma_S, & \text{in } \mathcal{D}, \\ \psi_S \text{ periodic on } \partial\mathcal{D}, \\ [\varepsilon_{\mathcal{D}} \nabla \psi_S] \cdot \mathbf{n} = -\Sigma_S, & \text{on } \partial\Omega_S, \end{cases} \quad (4.131)$$

where $[g]_{\partial\Omega_S}$ is the jump of the function g across the boundary $\partial\Omega_S$ in the direction of the normal vector \mathbf{n} which is oriented outward to $\partial\Omega_S$. A simplification of the problem (4.131) is to consider that

$$\varepsilon_S (\nabla \psi_S \cdot \mathbf{n})|_{\Omega_S} \ll \Sigma_S, \quad (4.132)$$

so that we consider that ψ_S is the unique solution of the problem

$$\begin{cases} -\varepsilon \Delta \psi_S = \frac{1}{|\Omega|} \int_{\partial\Omega_S} \Sigma_S, & \text{in } \Omega, \\ \psi_S \text{ periodic on } \partial\Omega \setminus \partial\Omega_S, \\ \nabla \psi_S \cdot \mathbf{n} = -\frac{\Sigma_S}{\varepsilon}, & \text{on } \partial\Omega_S, \quad \langle \psi_S \rangle_{\Omega} = 0, \end{cases} \quad (4.133)$$

where the last condition fixes the additive constant on ψ_S .

At this level of description, the system consisting of discrete ions and the solid object is still high-dimensional and requires a statistical mechanics treatment. Since the charged object has hard repulsion, we consider the problem posed on the volume accessible to the ions that is, $\Omega = \mathcal{D} \setminus \Omega_S$, and we denote $|\Omega|$ the volume of Ω that is $L_*^3 - |\Omega_S|$. We now attempt to derive macroscopic thermodynamics quantities for the system confined system, following the same ideas as in the bulk theory derived in Section 4.3.

4.4.2 Inhomogeneous Ornstein–Zernike equation

We define the probability density ρ_{eq} of positions defined by

$$\rho_{\text{eq}}(q) := Z_{\text{ex}}^{-1} e^{-\beta V(q)}, \quad Z_{\text{ex}} := \frac{1}{|\Omega|^N} \int_{\Omega^N} e^{-\beta V(q)} dq. \quad (4.134)$$

By analogy with Section 4.3, we perform partial integrations of the equilibrium probability density ρ_{eq} with respect to all the positions of the ions of each species except one or two particles allowing us to define the one-body and two-body macroscopic densities

$$\rho_i^1(q_i^1) = \frac{N_i}{|\Omega|^N} \int_{\Omega^{N-1}} \rho_{\text{eq}}(q) dq_i^2 : dq_i^{N_i} dq_{-i}, \quad i = \pm, \quad (4.135a)$$

$$\rho_{i,i}^2(q_i^1, q_i^2) = \frac{N_i(N_i-1)}{|\Omega|^N} \int_{\Omega^{N-2}} \rho_{\text{eq}}(q) dq_i^3 : dq_i^{N_i} dq_{-i}, \quad i = \pm, \quad (4.135b)$$

$$\rho_{i,j}^2(q_i^1, q_j^1) = \frac{N_i N_j}{|\Omega|^N} \int_{\Omega^{N-2}} \rho_{\text{eq}}(q) dq_i^2 : dq_i^{N_i} dq_j^2 : dq_j^{N_j}, \quad i = \pm, j = -i. \quad (4.135c)$$

Notice that we still have $\rho_{i,j}^2 = \rho_{j,i}^2$. The function ρ_i^1 is the one-body macroscopic density and $\rho_{i,j}^2$ is the two-body macroscopic density. We integrated over Ω , since $\text{supp}(\rho_{\pm}^1) = \bar{\Omega}$ and $\text{supp}(\rho_{\pm,\pm}^2) = \bar{\Omega} \times \bar{\Omega}$. This is in fact a consequence of the presence of the hard-sphere term (4.129) excluding the ions from the volume Ω_S . Indeed, we notice that the equilibrium distribution ρ_{eq} satisfies

$$\rho_{\text{eq}}(q) = Z_{\text{ex}}^{-1} e^{-\beta V_{\text{inter}}(q)} \prod_{1 \leq k \leq N} e^{-\beta V_{\text{ext}}^k(q_k)} = 0, \quad \forall q \in \bigcup_{1 \leq k \leq N} \{q_k \in \Omega_S\}. \quad (4.136)$$

In what follows, we define the (inhomogeneous) ionic concentrations by

$$c_i(x) = \rho_i^1(x), \quad x \in \Omega, \quad c_i(x) = 0, \quad x \in \Omega_S. \quad (4.137)$$

Still by analogy with the homogeneous theory, an inhomogeneous Ornstein–Zernike theory can be derived. We recall that in this framework, the indirect pair correlation function is defined by

$$h_{i,j} = g_{i,j} - 1, \quad i, j = \pm, \quad (4.138)$$

where $g_{i,j}$ is the so-called pair distribution function

$$g_{i,j}(x, y) := \frac{\rho_{i,j}^2(x, y)}{c_i(x)c_j(y)}, \quad i, j = \pm, \quad (4.139)$$

so that $g_{i,j}$ and $h_{i,j}$ are well defined through the knowledge of ρ_{eq} . The direct correlation function $\mathcal{C}_{i,j}$ is defined by the following integral equation:

$$h_{i,j}(x, y) = \mathcal{C}_{i,j}(x, y) + \sum_{k=\pm} \int_{\Omega} c_k(x') \mathcal{C}_{i,k}(x, x') h_{k,j}(x', y) dx'. \quad (4.140)$$

We assume that the solution of (4.140) exists and is uniquely determined by $h_{i,j}$ and c_{\pm} . The direct correlation function allows us to define the following free energy functional:

$$\mathcal{F}_{\text{inter}}(c) = \frac{1}{\beta} \sum_{i,j=\pm} \int_{\Omega \times \Omega} c_i(x) c_j(y) \int_0^1 (\lambda - 1) \mathcal{C}_{i,j}(x, y, \lambda c_+, \lambda c_-) d\lambda dx dy, \quad (4.141)$$

by analogy with formula (4.107). This free energy functional is motivated for example in [29].

4.4.3 Ansatz for the free energy functional

We assume that the following ansatz for the free energy functional \mathcal{F} holds true:

$$\mathcal{F}(c) = \mathcal{F}_{\text{id}}(c) + \mathcal{F}_{\text{inter}}(c) + \mathcal{F}_{\text{ext}}(c). \quad (4.142)$$

We will define \mathcal{F}_{ext} and \mathcal{F}_{id} , while $\mathcal{F}_{\text{inter}}$ has been defined by (4.141). In Section 4.2, the free energy functional \mathcal{F} has been written as

$$\mathcal{F}(c) = \mathcal{F}_{\text{id}}(c) + \mathcal{F}_{\text{corr}}(c) + \mathcal{F}_{\text{mf}}(c). \quad (4.143)$$

For the derivation, the formula (4.142) is more convenient and we will see that some contribution of $\mathcal{F}_{\text{inter}}$ distributes in $\mathcal{F}_{\text{corr}}$ while the remainder contributes to \mathcal{F}_{mf} .

The ideal contribution \mathcal{F}_{id} is obtained by integration over the volume Ω of the ideal bulk free energy density derived in Section 4.3.2:

$$\mathcal{F}_{\text{id}}(c) := \sum_{i=\pm} \int_{\Omega} f_{\text{id}}(c_i), \quad (4.144)$$

where f_{id} is defined by (4.91).

We define the external free energy functional by

$$\mathcal{F}_{\text{ext}}(c) := \int_{\Omega} \rho(c) \psi_S, \quad (4.145)$$

with

$$\rho(c(x)) := \sum_{i=\pm} Z_i e c_i(x), \quad x \in \Omega, \quad \rho(c(x)) := 0, \quad x \in \Omega_S, \quad (4.146)$$

the charge density and by definition of V_{ext}^k for $x \in \Omega$, see (4.129).

It remains to derive the functional $\mathcal{F}_{\text{inter}}$. To this purpose, we make approximations of the function $\rho_{i,j}^2$. The rewriting in terms of the direct-correlation function $\mathcal{C}_{i,j}$ is still motivated by the fact that it is easier to make approximations on $\mathcal{C}_{i,j}$ rather than on $\rho_{i,j}^2$. This is the purpose of the remainder of this section.

Anticipating the approximation to be performed on $\mathcal{C}_{i,j}$, we define the so-called short-range contribution

$$\mathcal{C}_{i,j}^{\text{SR}}(x, y) = \mathcal{C}_{i,j}(x, y) + Z_i Z_j 4\pi L_B G_{\text{lr}}(x, y), \quad (4.147)$$

analogous to the decomposition we performed in § 4.3.3. The function G_{lr} is the Green function for the operator $-\Delta$ on Ω with homogeneous Neumann boundary condition on $\partial\Omega_S$ and periodic boundary conditions on $\partial\Omega \setminus \partial\Omega_S$. This rewriting defines in fact a first closure relation for $\mathcal{C}_{i,j}$, thereby assuming that the long-ranged contributions on $\mathcal{C}_{i,j}$ can be written as $-Z_i Z_j 4\pi L_B G_{\text{lr}}(x, y)$. This is motivated by the analogy with the bulk where $G_{\text{lr}}(x, y) = \frac{1}{4\pi|x-y|}$. Then, we define

$$\psi_{\text{inter}}(x) = \frac{1}{\varepsilon} \int_{\Omega} \rho(c(y)) G_{\text{lr}}(x, y) dy, \quad (4.148)$$

so that using (4.141), (4.147), (4.145), and the definition of G_{lr} , we get

$$\frac{1}{2\beta} \sum_{i,j=\pm} \int_{\Omega \times \Omega} c_i(x)c_j(y) \left(\frac{\beta e^2}{\varepsilon} \right) G_{\text{lr}}(x,y) dx dy = \frac{1}{\varepsilon} \int_{\Omega \times \Omega} \rho(c(x))\rho(c(y))G_{\text{lr}}(x,y) dx dy, \quad (4.149)$$

(recalling $L_{\text{B}} = \frac{\beta e^2}{4\pi\varepsilon}$). It follows that

$$\begin{aligned} \mathcal{F}_{\text{inter}}(c) &= \frac{1}{\varepsilon} \int_{\Omega \times \Omega} \rho(c(x))\rho(c(y))G_{\text{lr}}(x,y) dx dy - \\ &\quad \frac{1}{\beta} \sum_{i,j=\pm} \int_{\Omega \times \Omega} c_i(x)c_j(y) \int_0^1 (\lambda - 1) \mathcal{C}_{i,j}^{\text{SR}}(x,y, \lambda c_+, \lambda c_-) d\lambda dx dy, \end{aligned} \quad (4.150)$$

so that, re-arranging the terms, we infer

$$\begin{aligned} \mathcal{F}_{\text{inter}}(c) + \mathcal{F}_{\text{ext}}(c) &= \frac{1}{2} \int_{\Omega} \rho(c) (\psi_{\text{inter}} + 2\psi_{\text{S}}) \\ &\quad - \frac{1}{\beta} \sum_{i,j=\pm} \int_{\Omega \times \Omega} c_i(x)c_j(y) \int_0^1 (\lambda - 1) \mathcal{C}_{i,j}^{\text{SR}}(x,y, \lambda c_+, \lambda c_-) d\lambda dx dy. \end{aligned} \quad (4.151)$$

For further purpose we introduce the functional $\tilde{\mathcal{F}}_{\text{mf}}$ as

$$\tilde{\mathcal{F}}_{\text{mf}}(c) := \frac{1}{2} \int_{\Omega} \rho(c) (\psi_{\text{inter}} + 2\psi_{\text{S}}), \quad (4.152)$$

(we will see in § 4.4.4 that $\tilde{\mathcal{F}}_{\text{mf}}$ and \mathcal{F}_{mf} defined by (4.27) only differ by an irrelevant additive constant). The correlation free energy functional is given by

$$\mathcal{F}_{\text{corr}}(c) := -\frac{1}{2\beta} \sum_{i,j=\pm} \int_{\Omega \times \Omega} c_i(x)c_j(y) \int_0^1 (\lambda - 1) \mathcal{C}_{i,j}^{\text{SR}}(x,y, \lambda c_+, \lambda c_-) d\lambda dx dy. \quad (4.153)$$

The mean-field term contains the internal Coulomb energy coupled with the external contribution \mathcal{F}_{ext} while the term $\mathcal{F}_{\text{corr}}$ contains correlations coming from the interaction between the ions, including Coulomb interaction and hard-sphere repulsion. The superscript SR indicates that the removal of the Coulomb potential on the total correlation function $\mathcal{C}_{i,j}$ allows to consider $\mathcal{C}_{i,j}^{\text{SR}}$ as a short-range function. This statement is motivated in section 4.4.5.

4.4.4 Derivation of \mathcal{F}_{mf}

We now derive the mean-field free energy functional related to the equation satisfied by the electrostatic potential ψ defined on Ω . We start by imposing global electroneutrality of the system

$$\int_{\Omega} \rho(c) = \int_{\partial\Omega_{\text{S}}} \Sigma_{\text{S}}, \quad (4.154)$$

Let us recall that the ionic concentrations c_i are such that

$$\text{supp}(c_i) \subset \overline{\Omega}, \quad i = \pm, \quad (4.155)$$

meaning the ions are excluded from the volume Ω_{S} . By definition of ψ_{inter} , see (4.148), ψ_{inter} is the solution of the boundary value problem on Ω

$$\begin{cases} -\varepsilon\Delta\psi_{\text{inter}} = \rho(c) - \langle\rho(c)\rangle_{\Omega}, & \text{in } \Omega, \\ \psi_{\text{inter}} \text{ is periodic on } \partial\Omega \setminus \partial\Omega_S, \nabla\psi_{\text{inter}} \cdot \mathbf{n} = 0 & \text{on } \partial\Omega_S, \text{ and } \langle\psi_{\text{inter}}\rangle_{\Omega} = 0, \end{cases} \quad (4.156)$$

and we recall that ψ_S is the unique solution of

$$\begin{cases} -\varepsilon\Delta\psi_S = \frac{1}{|\Omega|} \int_{\partial\Omega_S} \Sigma_S, & \text{in } \Omega, \\ \psi_S \text{ is periodic on } \partial\Omega \setminus \partial\Omega_S, \nabla\psi_S \cdot \mathbf{n} = -\frac{\Sigma_S}{\varepsilon} & \text{on } \partial\Omega_S, \text{ and } \langle\psi_S\rangle_{\Omega} = 0. \end{cases} \quad (4.157)$$

It follows that $\psi = \psi_{\text{inter}} + \psi_S$ is the solution of the following boundary value problem on Ω :

$$-\varepsilon\Delta\psi = \rho(c) \quad \text{in } \Omega, \quad (4.158a)$$

$$\psi \text{ is periodic on } \partial\Omega \setminus \partial\Omega_S, \nabla\psi \cdot \mathbf{n} = -\frac{\Sigma_S}{\varepsilon} \text{ on } \partial\Omega_S, \text{ and } \langle\psi\rangle_{\Omega} = 0. \quad (4.158b)$$

We are now in a position to define the mean-field component of the electrostatic excess free energy as

$$\mathcal{F}_{\text{mf}}(c) := \frac{1}{2} \left(\int_{\Omega} \rho(c) \Psi_{\Sigma_S}(\rho(c)) - \int_{\partial\Omega_S} \Sigma_S \Psi_{\Sigma_S}(\rho(c)) \right), \quad (4.159)$$

with $\psi = \Psi_{\Sigma_S}(\rho)$, where Ψ_{Σ_S} is defined by (4.25) in Section 4.2.

Let us rewrite the second contributions in $\tilde{\mathcal{F}}_{\text{mf}}$. Using the weak formulation for the boundary value problem for ψ and ψ_S , we have that

$$\begin{aligned} \int_{\Omega} \rho(c) \psi_S &= \int_{\Omega} \nabla\psi \cdot \nabla\psi_S + \int_{\partial\Omega_S} \psi_S \Sigma_S \\ &= - \int_{\partial\Omega_S} (\psi - \psi_S) \Sigma_S. \end{aligned} \quad (4.160)$$

The term $\int_{\partial\Omega_S} \psi_S \Sigma_S$ is independent of c so that we can forget it; a constant shift in the functional being transparent in view of minimization. It follows that $\tilde{\mathcal{F}}_{\text{mf}}$ and \mathcal{F}_{mf} differ only by an irrelevant additive constant. This constant is in fact the free energy accounting for the solid-solid interaction.

4.4.5 Approximations of $\mathcal{F}_{\text{corr}}$

We now present the final approximation that we need to end up with the derivation of \mathcal{F} . For completeness, we start by presenting the Mean-field approximation in the ideal case yielding the Poisson–Boltzmann equation, and then we present the two approximations needed to derive the functional $\mathcal{F}_{\text{corr}}$ defined by (4.23).

Mean-field approximation of $\mathcal{F}_{\text{corr}}$ in the ideal case

We start by the Mean-field approximation yielding the Poisson–Boltzmann equation. The simplest approximation consists in setting

$$g_{i,j} \equiv 1 \text{ and } \sigma \equiv 0, \quad (4.161)$$

thereby neglecting the correlations between the particles and the size of the particles (assuming the ions are pointwise).

This approximation has two consequences. At the continuous level, the ions experience the same mean-field potential ψ . The second consequence is that the hard-sphere potential energy is now 0. Since $\mathcal{C}_{i,j} = 0$ is, in this particular case, the unique solution of (4.140), it follows that

$$\mathcal{F}_{\text{corr}}(c) \equiv 0. \quad (4.162)$$

Within this approximation, the free energy functional \mathcal{F} is then the sum of the ideal and mean-field term

$$\mathcal{F}(c) := \mathcal{F}_{\text{id}}(c) + \mathcal{F}_{\text{mf}}(c), \quad (4.163)$$

The Poisson–Boltzmann theory is a mean-field theory in the sense that approximation (4.161) is an assumption of independence of the particles in the system. We have seen in Section 4.2 that a minimizer c of \mathcal{F} under the canonical constraints is such that $\psi = \Psi_{\Sigma_S}(\rho(c))$ solves the Poisson–Boltzmann equation

$$-\varepsilon \Delta \psi = \sum_{i=\pm} e \Lambda_i^{-3} Z_i e^{\beta \mu_i^{\text{bulk}}} e^{-\beta Z_i e \psi}, \quad (4.164)$$

with inhomogeneous Neumann boundary conditions and for some constant chemical potential μ_i^{bulk} .

Remark 9 (Mean-field limit theory.) *In fact, the assumption of independence of the particles in the system can be rigorously proved in some cases using probabilistic tools and the theory of mean-field limits [102]. Such a rigorous mathematical treatment of the mean-field limit is not covered in this thesis; we refer to previous work that studied similar problems in the bulk for systems with Coulomb interactions in 2D [12, 16].*

Local Density Approximation of $\mathcal{F}_{\text{corr}}$

We now present the approximations made on $\mathcal{F}_{\text{corr}}$ allowing to finish the derivation of \mathcal{F} . The first approximation that we make is to postulate that

$$\mathcal{C}_{i,j}^{\text{SR}}(x, y) \equiv \mathcal{C}_{i,j}^{\text{SR}}(|x - y|), \quad (4.165)$$

where $\mathcal{C}_{i,j}^{\text{SR}}$ is the short-range direct correlation solution of the homogeneous Ornstein–Zernike equation (4.97). In particular, the consequence of this approximation is that the correlations between the ions and the charged surface $\partial\Omega_S$ are neglected so that the interaction between the ions and the solid Ω_S are only treated at a mean-field level through the free energy functional \mathcal{F}_{mf} .

The second approximation is the so-called Local Density Approximation (LDA) introduced by Kohn and Sham [61] in the context of Hartree–Fock models. Nevertheless, the key ideas are similar to the present framework. The LDA consists in assuming that

$$\mathcal{F}_{\text{corr}}(c) \equiv \int_{\Omega} f_{\text{corr}}(c), \quad (4.166)$$

where f_{corr} is the exact bulk free energy density accounting for non-ideality evaluated for a bulk solution (without approximations either on $g_{i,j}$ or $\mathcal{C}_{i,j}$). In practice, we use the approximations derived in Section 4.3, so that f_{corr} is given by formula (4.122). As mentioned in [61], this approach may be valid for slowly varying ionic concentrations. From a numerical viewpoint, the functional

$$\mathcal{F}_{\text{corr}}(c) = \int_{\Omega} f_{\text{corr}}(c), \quad (4.167)$$

is much more tractable than the original functional involving the evaluation of non-local operators.

In comparison with the Mean-field approximation in the ideal case, yielding the Poisson–Boltzmann free energy (4.163), we observe that the LDA yields a functional similar to the Poisson–Boltzmann functional with corrections on the bulk free energy density coming from the microscopic theory. This derivation is a first step towards models closer to the microscopic description. Improvement of the approximations of the functional $\mathcal{F}_{\text{corr}}$ is still an active topic of research.

Mild non-ideality: convex bulk free energy

5.1	Introduction	107
5.2	Mathematical analysis	108
5.2.1	Non-dimensionalization	108
5.2.2	Assumptions	110
5.2.3	Main result and main steps of its proof	111
5.2.4	Technical results	113
5.3	Numerical aspects	118
5.3.1	Physical input	118
5.3.2	Verification of assumptions for MSA	119
5.3.3	Numerical methods	120
5.3.4	Validation of the approach: flat nanochannel	121
5.3.5	Periodic medium with charged inclusions	122

5.1 Introduction

In this chapter, we undertake the mathematical analysis of the model describing equilibrium binary electrolytes surrounded by charged solid walls. Our main result, Theorem 7 below, states that there is a unique saddle point (ψ, c) of the functional (4.41) for an equilibrium binary electrolyte surrounding a charged inclusion or confined by charged walls. The electrostatic potential ψ is sought in the Sobolev space H^1 with zero mean-value, while the ionic concentrations $c = (c_+, c_-)$ are sought in the closed convex subset of $L^2 \times L^2$ consisting of nonnegative ionic concentrations with prescribed mean-value (canonical constraint). Moreover, we prove that ψ and c_{\pm} are in $L^\infty(\Omega)$, and that c_{\pm} are uniformly bounded away from zero. Theorem 7 is established under four main assumptions stated in §5.2.2. The first two assumptions are the classical global electroneutrality condition on the prescribed mean ionic concentrations and elliptic regularity for the Poisson problem governing the electrostatic potential (with non-homogeneous Neumann boundary conditions). The other two conditions are formulated in an abstract setting for the activity coefficient $\log(\gamma_0)$ describing non-ideal electrostatic correlations. These conditions, which in particular encompass the MSA setting, require a sublinear growth condition at large ionic concentrations for $\log(\gamma_0)$, and a lower bound on the derivative of $\log(\gamma_0)$ with respect to the ionic strength. This last condition is important to assert the convexity of the bulk free energy.

This convexity condition is derived here using the linear expression (4.54) for the activity coefficient related to steric exclusion. The main idea is that the ideal and hard-sphere contributions, which dominate respectively at very low and large ionic concentrations, are both convex, but the electrostatic correlations lead to a non convex contribution to the bulk free energy. Furthermore, we observe that we do not need to enforce a priori L^∞ -bounds on the concentrations. To the best of our knowledge, the present analysis, together with the ongoing work [2] investigating the role of non-ideality for homogenized ion transport in porous media, is the first to address mathematically the critical points of the free energy in the presence of electrostatic correlations.

This chapter is organized as follows. In §5.2, we state the mathematical assumptions together with our main result, we present first the main steps of its proof for more clarity, and then we prove various technical lemmas, dealing in particular with the convexity of the bulk free energy and the a priori bounds on the electrostatic potential and ionic concentrations. Finally, we focus on numerical aspects in §5.3, providing details about the numerical method employed to solve the conservation equations and some numerical illustrations of the physical setting.

5.2 Mathematical analysis

In this section, following the mathematical framework of Section 4.2, we prove that, under the assumptions stated below, the functional \mathcal{E} defined by (4.41) admits a unique saddle point (ψ, c) . Moreover, we establish some a priori bounds on (ψ, c) and show that ψ solves the Poisson problem (4.14a), (4.14d)-(4.14f) while the electrochemical potentials $\mu_i^{\text{el}}(\psi, c)$, $i = \pm$, defined by (4.5) are constant in Ω . In what follows, we consider an abstract setting for the one-real variable function $\log(\gamma_0)$ which can be chosen arbitrarily provided assumptions (H3)-(H4) below are satisfied. The MSA case where $\log(\gamma_0)$ is defined by (4.52) is a special case of application, for which the verification of assumptions (H3)-(H4) is discussed in §5.3. We use the expression (CS1) given by (4.56) for the steric exclusion term.

5.2.1 Non-dimensionalization

We start by making the equations non-dimensional. There are three length scales in the problem: the characteristic size of the elementary cell L_* , the mean ion diameter σ , and the Bjerrum length $L_B = \frac{\beta e^2}{4\pi\epsilon}$. It is convenient to introduce the reference Debye length L_D^* and the non-dimensional ratio λ such that

$$L_D^* := \sqrt{\frac{L_*^3}{4\pi L_B}}, \quad \lambda := \left(\frac{L_D^*}{L_*}\right)^2 = \frac{L_*}{4\pi L_B}. \quad (5.1)$$

The reference Debye length represents the scale over which the ions screen out the electric field at the reference concentration L_*^{-3} .

In what follows, we use L_* as the reference length. Moreover, the reference electrostatic potential is the so-called Zeta potential $\psi_* := k_B T/e$, the reference electrochemical potential is $\mu_* := k_B T$, the reference surface charge density is $\Sigma_{S_*} := k_B T \epsilon / (e L_*)$, and the reference ionic concentration is $c_* := L_*^{-3}$. Typical values for these quantities are provided in §5.3. With these reference values, the governing equations are recast into non-dimensional form, and to alleviate the notation, we use the same symbols for non-dimensional quantities.

The Poisson problem for the electrostatic potential ψ takes the form

$$-\lambda \Delta \psi = \sum_{i=\pm} Z_i c_i \quad \text{in } \Omega, \quad (5.2a)$$

$$\psi \text{ is periodic on } \partial\Omega \setminus \partial\Omega_S, \quad (5.2b)$$

$$\nabla \psi \cdot \mathbf{n} = -\Sigma_S \quad \text{on } \partial\Omega_S, \quad (5.2c)$$

$$\langle \psi \rangle_\Omega = 0. \quad (5.2d)$$

The mean ionic concentrations c_\pm^{bulk} satisfy the global electroneutrality condition

$$\sum_{i=\pm} Z_i c_i^{\text{bulk}} = \frac{\lambda}{|\Omega|} \int_{\partial\Omega_S} \Sigma_S, \quad (5.3)$$

and the electrochemical potentials are such that

$$\mu_i^{\text{el}}(\psi, c) = \log(\sigma^3 c_i) + \log(\gamma_i(c)) + Z_i \psi, \quad i = \pm. \quad (5.4)$$

The functional \mathcal{E} is now

$$\mathcal{E}(\psi, c) = \mathcal{U}(\psi) - \mathcal{B}(\psi, c) - \mathcal{F}_{\text{bulk}}(c), \quad (5.5)$$

where

$$\mathcal{B}(\psi, c) = \sum_{i=\pm} \int_\Omega Z_i c_i \psi, \quad (5.6a)$$

$$\mathcal{U}(\psi) = \frac{\lambda}{2} \int_\Omega |\nabla \psi|^2 + \lambda \int_{\partial\Omega_S} \Sigma_S \psi. \quad (5.6b)$$

The bulk free energy density functional $\mathcal{F}_{\text{bulk}}$ is such that

$$\mathcal{F}_{\text{bulk}}(c) = \mathcal{F}_{\text{id}}(c) + \mathcal{F}_{\text{corr}}(c), \quad (5.7)$$

with

$$\mathcal{F}_{\text{id}}(c) := \sum_{i=\pm} \int_\Omega f_{\text{id}}(c_i), \quad \mathcal{F}_{\text{corr}}(c) := \int_\Omega f_{\text{corr}}(c). \quad (5.8)$$

The nondimensional ideal free energy density is given by

$$f_{\text{id}}(u) := \begin{cases} u(\log(\sigma^3 u) - 1), & u > 0, \\ 0, & u = 0, \end{cases} \quad (5.9)$$

while the excess free energy density $f_{\text{corr}} : \mathbb{R}_{\geq 0}^2 \rightarrow \mathbb{R}$ is now given by

$$f_{\text{corr}}(c) := f_0(I(c)) + \frac{2\pi\sigma^3}{3} (c_+ + c_-)^2, \quad (5.10)$$

where $I(c) = \sum_{i=\pm} \eta_i c_i$, $\eta_i = \frac{1}{2} Z_i^2$, is the ionic strength. In the MSA case, there holds, for all $\theta \in \mathbb{R}_{\geq 0}$,

$$f_0(\theta) := -\frac{1}{4\pi\sigma\lambda} \left(\theta - \frac{8\lambda\sigma}{3} (\Upsilon_{\text{MSA}}(\theta))^3 - 2\lambda (\Upsilon_{\text{MSA}}(\theta))^2 \right). \quad (5.11)$$

The ideal bulk free energy density f_{id} is continuous in $\mathbb{R}_{\geq 0}$ and continuously differentiable in $\mathbb{R}_{> 0}$, while the excess bulk free energy density f_{corr} is continuously differentiable in $\mathbb{R}_{\geq 0}^2$ with

$$\frac{\partial f_{\text{corr}}}{\partial c_i}(c) = \log(\gamma_i(c)), \quad i = \pm. \quad (5.12)$$

The rescaled activity coefficients $\gamma_{\pm}(c)$ are decomposed as in (4.45). The Coulomb term is still given in the form (4.49) in terms of the function $\gamma_0 : \mathbb{R}_{\geq 0} \rightarrow \mathbb{R}_{\geq 0}$. In the MSA case, there holds, for all $\theta \in \mathbb{R}_{\geq 0}$,

$$\log(\gamma_0(\theta)) := -\frac{1}{4\pi\lambda} \frac{\Upsilon_{\text{MSA}}(\theta)}{1 + \sigma\Upsilon_{\text{MSA}}(\theta)}, \quad (5.13)$$

with the function $\Upsilon_{\text{MSA}} : \mathbb{R}_{\geq 0} \rightarrow \mathbb{R}_{\geq 0}$ such that,

$$\Upsilon_{\text{MSA}}(\theta) := \frac{1}{2\sigma} \left(\sqrt{2\sigma\lambda^{-1/2}(2\theta)^{1/2} + 1} - 1 \right). \quad (5.14)$$

Finally, the steric exclusion term is simply given by

$$\log(\gamma_{\text{HS}}(c)) = \log(\gamma_1(\xi(c))) = 8\xi(c) = \frac{4\pi}{3}\sigma^3(c_+ + c_-). \quad (5.15)$$

5.2.2 Assumptions

We consider the sets

$$\mathfrak{H} := \left\{ \phi \in H_{\text{per}}^1(\Omega), \langle \phi \rangle_{\Omega} = 0 \right\}, \quad (5.16)$$

$$\mathfrak{K} := \left\{ c = (c_+, c_-) \in [L^2(\Omega)]^2, c_{\pm} \geq 0 \text{ a.e. in } \Omega, \langle c_{\pm} \rangle_{\Omega} = c_{\pm}^{\text{bulk}} \right\}, \quad (5.17)$$

where the functional spaces $H_{\text{per}}^1(\Omega)$ and $L^2(\Omega)$ are, respectively, the closure of $C_{\text{per}}^{\infty}(\overline{\Omega})$, the space of periodic and infinitely differentiable functions in $\overline{\Omega}$, for the canonical norms $\|\cdot\|_{H^1(\Omega)}$ and $\|\cdot\|_{L^2(\Omega)}$. It is clear that \mathfrak{H} is a closed subspace of $H_{\text{per}}^1(\Omega)$ and that \mathfrak{K} is a closed convex subset of $[L^2(\Omega)]^2$.

In what follows, we make the following assumptions:

- (H1) $\Sigma_S \in H^{1/2}(\partial\Omega_S)$, the real numbers c_{\pm}^{bulk} are positive and satisfy the global electroneutrality condition (5.3).
- (H2) The affine operator $\Psi_{\Sigma_S} : L^2(\Omega) \rightarrow \mathfrak{H}$ (in nondimensional form) such that, for all $g \in L^2(\Omega)$, $\Psi_{\Sigma_S}(g) \in \mathfrak{H}$ solves $-\Delta\Psi_{\Sigma_S}(g) = g - \langle g \rangle_{\Omega} + |\Omega|^{-1} \int_{\partial\Omega_S} \Sigma_S$ in Ω with the Neumann boundary condition $\nabla\Psi_{\Sigma_S}(g) \cdot \mathbf{n} = -\Sigma_S$ on $\partial\Omega_S$ and $\langle \Psi_{\Sigma_S}(g) \rangle_{\Omega} = 0$, is bounded from $L^2(\Omega)$ to $H^2(\Omega)$.
- (H3) The function $\theta \mapsto \log(\gamma_0(\theta))$ is continuous on $\mathbb{R}_{\geq 0}$; moreover, there is $\beta \in [0, 1)$ and $(C_1, C_2) \in \mathbb{R}_{\geq 0}^2$ such that

$$\forall \theta \in \mathbb{R}_{\geq 0}, \quad |\log(\gamma_0(\theta))| \leq C_1 + C_2\theta^{\beta}. \quad (5.18)$$

- (H4) The function $\theta \mapsto \log(\gamma_0(\theta))$ is non-increasing and continuously differentiable on $\mathbb{R}_{>0}$ and there holds, for all $\theta \in \mathbb{R}_{>0}$,

$$\frac{\eta_{\sharp}}{\theta} + \frac{4\pi\sigma^3}{3} + \left(2\eta_{\sharp}^2 + \frac{2\pi\sigma^3}{3\eta_{\flat}}\theta(\eta_{\sharp} - \eta_{\flat})^2\right) (\log(\gamma_0))'(\theta) > 0, \quad (5.19)$$

where $\eta_{\sharp} := \max(\eta_+, \eta_-)$ and $\eta_{\flat} := \min(\eta_+, \eta_-)$.

An important consequence of assumption (H3) is that the excess bulk free energy f_{corr} is a nondecreasing function of both its arguments if at least one ionic concentration is large enough.

Lemma 3 *Assume (H3). Then, there is $\kappa_{\gamma} \in \mathbb{R}_{\geq 0}$ such that, for all $c \in \mathbb{R}_{\geq 0}^2$ satisfying $c_+ \geq \kappa_{\gamma}$ or $c_- \geq \kappa_{\gamma}$, there holds*

$$\frac{\partial f_{\text{corr}}}{\partial c_+}(c) \geq 0, \quad \frac{\partial f_{\text{corr}}}{\partial c_-}(c) \geq 0. \quad (5.20)$$

Proof. Recall that

$$\frac{\partial f_{\text{corr}}}{\partial c_{\pm}}(c) = \log(\gamma_{\pm}(c)) = 2\eta_{\pm} \log(\gamma_0(I(c))) + \frac{4\pi}{3}\sigma^3(c_+ + c_-).$$

Invoking assumption (H3), we infer that for suitable constants C_3 and C_4 , there holds

$$\frac{\partial f_{\text{corr}}}{\partial c_{\pm}}(c) \geq \frac{4\pi}{3}\sigma^3(c_+ + c_-) - C_3 - C_4(c_+^{\beta} + c_-^{\beta}).$$

Since $\beta \in [0, 1)$, the conclusion is straightforward. \diamond

5.2.3 Main result and main steps of its proof

It is readily verified that the functional \mathcal{E} maps $\mathfrak{H} \times \mathfrak{K}$ to \mathbb{R} . We recall that $(\psi, c) \in \mathfrak{H} \times \mathfrak{K}$ is a saddle point of \mathcal{E} if

$$\forall \tilde{c} \in \mathfrak{K}, \quad \mathcal{E}(\psi, \tilde{c}) \leq \mathcal{E}(\psi, c) \leq \mathcal{E}(\phi, c), \quad \forall \phi \in \mathfrak{H}. \quad (5.21)$$

We can now state the main result of this chapter.

Theorem 7 *Assume (H1), (H2), (H3) and (H4). Then, the functional \mathcal{E} has a unique saddle point $(\psi, c) \in \mathfrak{H} \times \mathfrak{K}$. Moreover, $\psi \in L^{\infty}(\Omega)$ and there are $0 < c_m \leq c_M < +\infty$ such that, for a.e. $x \in \Omega$, $c_m \leq c_i(x) \leq c_M$, $i = \pm$. Finally, ψ solves the Poisson problem (5.2), and the electrochemical potentials $\mu_i^{\text{el}}(\psi, c)$, $i = \pm$, defined by (5.4) are constant in Ω .*

Remark 10 (Minimizer of \mathcal{F}) *Under the same technical assumptions (H1), (H2), (H3) and (H4), we can prove that the problem (4.39) admits a unique minimizer solving (4.14).*

Proof. The proof is decomposed into several steps.

Existence of a saddle point

For any $\bar{c} \in \mathfrak{K}$, the functional $\mathfrak{H} \ni \psi \mapsto \mathcal{E}(\psi, \bar{c}) \in \mathbb{R}$ is strictly convex, continuous, and satisfies, for all $\psi \in \mathfrak{H}$ with $\|\psi\|_{H^1(\Omega)} \rightarrow +\infty$, $\mathcal{E}(\psi, \bar{c}) \rightarrow +\infty$. Furthermore, in Lemma 4 below, we use assumption (H4) to prove that the bulk free energy functional $\mathcal{F}_{\text{bulk}}$ is convex on \mathfrak{K} , while in Lemma 5, we use assumption (H3) to prove that the bulk free energy functional $\mathcal{F}_{\text{bulk}}$ is continuous on \mathfrak{K} . Hence, for any $\bar{\psi} \in \mathfrak{H}$, the functional $\mathfrak{K} \ni c \mapsto \mathcal{E}(\bar{\psi}, c) \in \mathbb{R}$ is concave and continuous. Additionally, for all $c \in \mathfrak{K}$ with $\|c\|_{[L^2(\Omega)]^2} \rightarrow +\infty$, $\mathcal{F}_{\text{bulk}}(c) \rightarrow +\infty$ and $\mathcal{E}(\bar{\psi}, c) \rightarrow -\infty$ since, at high concentrations, the hard-sphere contribution to the activity coefficient dominates. As a result, we can apply the Ky Fan–Von Neumann theorem [27, Prop. 2.2, p. 161] to infer the existence of a saddle point (ψ, c) of the functional \mathcal{E} .

Characterization of, and bound on electrostatic potential

Let $(\psi, c) \in \mathfrak{H} \times \mathfrak{K}$ be a saddle point of the functional \mathcal{E} . Since \mathcal{E} is differentiable with respect to ψ and since \mathfrak{H} is a vector space, there holds

$$\langle \partial_\psi \mathcal{E}(\psi, c), \phi \rangle = \lambda \int_\Omega \nabla \psi \cdot \nabla \phi + \lambda \int_{\partial\Omega_S} \Sigma_S \phi - \sum_{i=\pm} \int_\Omega Z_i c_i \phi = 0, \quad \forall \phi \in \mathfrak{H}.$$

This shows that ψ solves the Poisson problem (5.2). Moreover, recalling the affine operator $\Psi_{\Sigma_S} : L^2(\Omega) \rightarrow \mathfrak{H}$ introduced in assumption (H2) and using the global electroneutrality condition (5.3), we infer

$$\psi = \Psi_{\Sigma_S} \left(\frac{1}{\lambda} \sum_{i=\pm} Z_i c_i \right).$$

As a result, $\psi \in H^2(\Omega)$, and owing to the Sobolev embedding theorem, $\psi \in L^\infty(\Omega)$.

Characterization of, and bound on ionic concentrations

Using assumption (H3), we prove in Lemmas 6 and 7 below that there are $0 < c_m \leq c_M < +\infty$ such that, for a.e. $x \in \Omega$, $c_m \leq c_i(x) \leq c_M$, $i = \pm$. Finally, owing again to the uniform lower bound on the ionic concentrations and using Lemma 5, we infer that the functional \mathcal{E} is Gâteaux-differentiable at (ψ, c) with respect to c_\pm along any direction $v \in C_{\text{per}}^\infty(\bar{\Omega})$ with $\langle v \rangle_\Omega = 0$, and there holds

$$\langle \partial_{c_\pm} \mathcal{E}(\psi, c), v \rangle = \int_\Omega \mu_\pm^{\text{el}}(\psi, c) v,$$

where $\mu_\pm^{\text{el}}(\psi, c)$ are the electrochemical potentials defined by (5.4). Let now $v \in C_{\text{per}}^\infty(\bar{\Omega})$. Since (ψ, c) is a saddle point, there holds $\langle \partial_{c_\pm} \mathcal{E}(\psi, c), \tilde{v} \rangle = 0$ with $\tilde{v} = v - \langle v \rangle_\Omega$, whence $\int_\Omega \{\mu_\pm^{\text{el}}(\psi, c) - \langle \mu_\pm^{\text{el}}(\psi, c) \rangle_\Omega\} v = 0$. By density of $C_{\text{per}}^\infty(\bar{\Omega})$ in $L^2(\Omega)$, this shows that the electrochemical potentials are constant in Ω .

Uniqueness

The functional \mathcal{E} is strictly convex in its first argument. Moreover, owing to the uniform lower bound on the ionic concentrations, the bulk free energy is strictly convex in c (see, again, Lemma 4 below). This yields uniqueness of the saddle point. \diamond

Remark 11 (Critical points are saddle points) *It is readily verified using convexity arguments that if (ψ, c) (with c uniformly bounded from above and below) is a critical point of the free energy functional \mathcal{E} , then (ψ, c) is a saddle point of \mathcal{E} . In §5.3, we will compute an approximation of the saddle point by solving the Euler–Lagrange equations satisfied by the critical point.*

5.2.4 Technical results

We prove the various lemmas invoked in the proof of our main result, Theorem 7. Our first result concerns the convexity of the bulk free energy functional $\mathcal{F}_{\text{bulk}}$.

Lemma 4 (Convexity of the bulk free energy) *Assume (H4). Then, the functional $\mathcal{F}_{\text{bulk}}$ is convex on \mathfrak{K} and strictly convex on the subset $\mathfrak{K}_{>0} := \{c \in \mathfrak{K}; c_+ > 0 \text{ and } c_- > 0 \text{ a.e. in } \Omega\}$.*

Proof. It suffices to show that the bulk free energy density $f : \mathbb{R}_{\geq 0}^2 \rightarrow \mathbb{R}$ such that, for all $c = (c_+, c_-) \in \mathbb{R}_{\geq 0}^2$,

$$f(c) := f_{\text{id}}(c_+) + f_{\text{id}}(c_-) + f_{\text{corr}}(c)$$

is convex on $\mathbb{R}_{\geq 0}^2$ and strictly convex on $\mathbb{R}_{>0}^2$. The convexity of f on $\mathbb{R}_{\geq 0}^2$ follows from the strict convexity of f on $\mathbb{R}_{>0}^2$ and the continuity of f . Hence, it is sufficient to address the strict convexity of f on $\mathbb{R}_{>0}^2$. Set $\eta_{\#} := \max(\eta_+, \eta_-)$, $\eta_b := \min(\eta_+, \eta_-)$, and $\bar{\eta} := \frac{1}{2}(\eta_+ + \eta_-)$. The Hessian associated with f is given by

$$\text{Hess}(f) = \begin{pmatrix} \frac{1}{c_+} + A + B\eta_+^2 & A + B\eta_+\eta_- \\ A + B\eta_+\eta_- & \frac{1}{c_-} + A + B\eta_-^2 \end{pmatrix},$$

where $A := \frac{4\pi}{3}\sigma^3$ and $B := 2(\log(\gamma_0))'(\theta)$ with $\theta = I(c)$. We verify that the trace and the determinant of $\text{Hess}(f)$ are positive. We obtain

$$c_+c_- \det \text{Hess}(f) = 1 + A(c_+ + c_-) + (\eta_+^2c_+ + \eta_-^2c_- + Ac_+c_-(\eta_+ - \eta_-)^2)B.$$

Since $c_+ + c_- \geq \theta/\eta_{\#}$, $\eta_+^2c_+ + \eta_-^2c_- \leq \eta_{\#}\theta$, $c_+c_- \leq \theta^2/(4\eta_-\eta_+)$, and $B \leq 0$, we infer that, under condition (5.19), that is,

$$\frac{\eta_{\#}}{\theta} + A + \left(\eta_{\#}^2 + \frac{A}{4\eta_b} \theta (\eta_{\#} - \eta_b)^2 \right) B > 0, \quad (5.22)$$

there holds $\det \text{Hess}(f) > 0$. Furthermore,

$$\frac{1}{2} \text{tr} \text{Hess}(f) = \frac{1}{2} \left(\frac{1}{c_+} + \frac{1}{c_-} \right) + A + \frac{1}{2}(\eta_+^2 + \eta_-^2)B.$$

Since $(c_+^{-1} + c_-^{-1})/2 \geq \bar{\eta}/\theta$, we infer that, under the condition

$$\frac{\bar{\eta}}{\theta} + A + \frac{1}{2}(\eta_{\#}^2 + \eta_b^2)B > 0, \quad (5.23)$$

there holds $\text{tr} \text{Hess}(f) > 0$. Finally, it is readily verified that, for all $\theta \in \mathbb{R}_{>0}$, $(\frac{\eta_{\#}}{\theta} + A)\frac{1}{2}(\eta_+^2 + \eta_-^2) \leq (\frac{\bar{\eta}}{\theta} + A)(\eta_{\#}^2 + \frac{A}{4\eta_b}\theta(\eta_{\#} - \eta_b)^2)$, so that (5.22) implies (5.23). \diamond

Remark 12 (Convexity condition for symmetric electrolytes) *In the case of symmetric electrolytes, that is, $\eta_+ = \eta_- = \eta$, condition (5.19) reduces to*

$$\frac{\eta}{\theta} + \frac{4\pi\sigma^3}{3} + 2\eta^2(\log(\gamma_0))'(\theta) > 0, \quad (5.24)$$

and this condition is also necessary for convexity of the bulk free energy. Condition (5.19) is also necessary and sufficient for electrolytes with M species, all with the same coefficient η .

Our second result deals with the continuity and Gâteaux-differentiability of the bulk free energy functional $\mathcal{F}_{\text{bulk}}$.

Lemma 5 (Continuity and differentiability of the free energy) *Assume (H3). Then, the bulk free energy functional $\mathcal{F}_{\text{bulk}}$ is continuous on $[L^2(\Omega)]^2$. Moreover, for all $c \in [L^2(\Omega)]^2$ such that there is $c_m > 0$ with $c_i(x) \geq c_m$ for a.e. $x \in \Omega$ and all $i = \pm$, $\mathcal{F}_{\text{bulk}}$ is Gâteaux-differentiable at c along any direction $v \in C_{\text{per}}^\infty(\bar{\Omega})$, and there holds*

$$\langle \partial_{c_\pm} \mathcal{F}_{\text{bulk}}(c), v \rangle = \int_{\Omega} \{\log(\sigma^3 c_\pm) + \log(\gamma_\pm(c))\} v.$$

Proof. A classical result of nonlinear analysis [57, Lemma 16.2, p. 61] states that, if $F : \mathbb{R} \rightarrow \mathbb{R}$ is a continuous function satisfying the growth condition

$$\exists a, b \in \mathbb{R}, \quad \forall u \in \mathbb{R}, \quad |F(u)| \leq a + b|u|^{p/q},$$

with $1 \leq p, q < +\infty$ then, for all $v \in L^p(\Omega)$, there holds $F(v) \in L^q(\Omega)$, and the superposition operator $L^p(\Omega) \ni v \mapsto F(v) \in L^q(\Omega)$ is continuous. This result can be applied to the function $F_1(x) = f_{\text{id}}(x)$ (extended by zero for $x \leq 0$) showing that $\mathcal{F}_{\text{id}}(c)$ is continuous from $[L^2(\Omega)]^2$ to $L^1(\Omega)$. The result can also be applied to the function $F_2(x) = 2f_0(x)$ (extended by zero for $x \leq 0$) since, owing to assumption (H3), F_2 satisfies the above growth condition with exponent $1 + \beta < 2$. Since the function $c \mapsto I(c)$ maps continuously $[L^2(\Omega)]^2$ to $L^2(\Omega)$, we infer that the functional $c \mapsto f_0(I(c))$ is continuous from $[L^2(\Omega)]^2$ to $L^1(\Omega)$. Finally, the continuity of the hard-sphere contribution $c \mapsto \frac{2\pi\sigma^3}{3} (c_+ + c_-)^2$ from $[L^2(\Omega)]^2$ to $L^1(\Omega)$ is obvious.

Gâteaux-differentiability

Let now $c \in [L^2(\Omega)]^2$ be such that there is $c_m > 0$ with $c_i(x) \geq c_m$ for a.e. $x \in \Omega$ and all $i = \pm$. We treat the partial derivative with respect to c_+ ; the other case is treated similarly. Let $v \in C_{\text{per}}^\infty(\bar{\Omega})$ with $\langle v \rangle_{\Omega} = 0$. There is $t_0 > 0$ such that, for all $t \in [-t_0, t_0]$, $c_+(x) + tv(x) \geq \frac{1}{2}c_m$ for a.e. $x \in \Omega$. Since the function $F_3(x) = \log(\sigma^3 x)$ for $x \geq \frac{1}{2}c_m$ extended by the constant value $\log(\frac{1}{2}\sigma^3 c_m)$ for $x \leq \frac{1}{2}c_m$ satisfies a linear growth condition, we can show, using the proof of [57, Lemma 17.1, p. 64], that the ideal bulk free energy is Gâteaux-differentiable with

$$\langle \partial_{c_+} \mathcal{F}_{\text{id}}(c), v \rangle = \int_{\Omega} \log(\sigma^3 c_+) v.$$

Gâteaux-differentiating the excess free energy is simpler. We use the growth condition in assumption (H3) to infer

$$\left\langle \partial_{c_+} \left(\int_{\Omega} 2f_0(I(c)) \right), v \right\rangle = \int_{\Omega} 2\eta_+ \log(\gamma_0(I(c)))v = \int_{\Omega} \log(\gamma_+^{\text{Coul}}(c))v,$$

while Gâteaux-differentiating the hard-sphere term $\frac{2\pi\sigma^3}{3}(c_+ + c_-)^2$ is straightforward. \diamond

Our third result delivers an a priori L^∞ -bound on the ionic concentrations $c = (c_+, c_-)$.

Lemma 6 (Upper bound on c) *Assume (H3). Let $(\psi, c) \in \mathfrak{H} \times \mathfrak{K}$ be a saddle point of the functional \mathcal{E} . Then, there is $c_M < +\infty$ such that, for a.e. $x \in \Omega$, $c_i(x) \leq c_M$ for all $i = \pm$.*

Proof. Let $(\psi, c) \in \mathfrak{H} \times \mathfrak{K}$ be a saddle point of the functional \mathcal{E} . Proceeding by contradiction, we assume that there is $i = \pm$ such that, for all $n \in \mathbb{N}$, the set

$$A_i^n := \{x \in \Omega; c_i(x) > 2^n\}$$

has positive measure. We then construct modified ionic concentrations $\tilde{c} \in \mathfrak{K}$ such that $\mathcal{E}(\psi, \tilde{c}) > \mathcal{E}(\psi, c)$, thereby providing the desired contradiction with (5.21). As a result, for all $i = \pm$, there is $n_i \in \mathbb{N}$ such that the set $A_i^{n_i}$ has zero measure, yielding the statement of Lemma 6 with $c_M = \max_{i=\pm} 2^{n_i}$. The principle of the construction is that, by diminishing the ionic concentration where it is very large, the bulk free energy can be decreased, and thus the functional \mathcal{E} . Both the ideal term and the steric exclusion term are large enough at high concentrations to lead to a bulk free energy decrease. We choose to work with the ideal term since, in the proof of Lemma 7 below, the ideal term is the only one leading to the bulk free energy decrease at small concentrations; thus, the two proofs are similar. Furthermore, we observe that some care is needed when perturbing the ionic concentrations since it is necessary to preserve their mean values.

Without loss of generality, we assume that, for all $n \in \mathbb{N}$, the set A_+^n has positive measure. We first observe that there is $k \in \mathbb{N}$ such that the set

$$\Omega_+^k := \{x \in \Omega; 2^{-k} \leq c_+(x) \leq 2^k\} \quad (5.25)$$

has positive measure (otherwise, c_+ is zero or infinity a.e. in Ω which contradicts the fact that $\langle c_+ \rangle_{\Omega} = c_+^0 > 0$). In what follows, we fix such $k \in \mathbb{N}$, and, without loss of generality, we assume that $n \geq k$ so that the sets A_+^n and Ω_+^k are disjoint. Moreover, since $\langle c_- \rangle_{\Omega} = c_-^0$ and $c_-(x) \geq 0$ for a.e. $x \in \Omega$, we infer that, for all $m \in \mathbb{N}$, $c_-^0 \geq \frac{1}{|\Omega|} 2^m |A_-^m|$, which shows that $|A_-^m| \rightarrow 0$ as $m \rightarrow \infty$. As a result, there is $m \in \mathbb{N}$ such that the set $\Omega^{k,m} := \Omega_+^k \cap (\Omega \setminus A_-^m)$ has positive measure. In what follows, we fix such $m \in \mathbb{N}$. We observe that in $\Omega^{k,m}$, both ionic concentrations c_{\pm} are bounded by $C_{k,m} := \max(2^k, 2^m)$. We now define the function \tilde{c}_+^n as follows:

$$\tilde{c}_+^n(x) = \begin{cases} 0, & x \in A_+^n, \\ c_+(x) + \delta^n, & x \in \Omega^{k,m}, \\ c_+(x), & x \in \Omega \setminus (A_+^n \cup \Omega^{k,m}), \end{cases}$$

with $\delta^n = \frac{1}{|\Omega^{k,m}|} \int_{A_+^n} c_+$. It is readily verified that $\langle \tilde{c}_+^n \rangle_{\Omega} = c_+^0$ so that $\tilde{c}^n := (\tilde{c}_+^n, c_-) \in \mathfrak{K}$. We observe that the real number δ^n is uniformly bounded since $\delta^n \leq \delta := \frac{1}{|\Omega^{k,m}|} |\Omega| c_+^0$ for all $n \in \mathbb{N}$. It is important to modify c_+ only in the set $\Omega^{k,m}$ to preserve its mean value (and not in the

larger set Ω_+^k); indeed, a bound on c_- is needed to control the variation of the non-ideal terms between c and \tilde{c}^n .

To conclude the proof, we show that it is possible to choose n large enough so that

$$\Delta\mathcal{E} := \mathcal{E}(\psi, \tilde{c}^n) - \mathcal{E}(\psi, c) > 0.$$

There holds

$$\Delta\mathcal{E} = -\Delta\mathcal{F}_{\text{id}} - \Delta\mathcal{F}_{\text{corr}} - \Delta\mathcal{B}$$

with $\Delta\mathcal{F}_{\text{id}} := \mathcal{F}_{\text{id}}(\tilde{c}^n) - \mathcal{F}_{\text{id}}(c)$, $\Delta\mathcal{F}_{\text{corr}} := \mathcal{F}_{\text{corr}}(\tilde{c}^n) - \mathcal{F}_{\text{corr}}(c)$, and $\Delta\mathcal{B} := \mathcal{B}(\psi, \tilde{c}^n) - \mathcal{B}(\psi, c)$. We estimate the three terms separately. Since

$$\Delta\mathcal{B} = -Z_+ \int_{A_+^n} c_+ \psi + Z_+ \int_{\Omega^{k,m}} \delta^n \psi,$$

we infer, since $\psi \in L^\infty(\Omega)$ owing to the second step in the proof of Theorem 7, that

$$|\Delta\mathcal{B}| \leq 2Z_+ \|\psi\|_{L^\infty(\Omega)} \int_{A_+^n} c_+.$$

Since

$$\Delta\mathcal{F}_{\text{id}} = \int_{A_+^n} -f_{\text{id}}(c_+) + \int_{\Omega^{k,m}} \{f_{\text{id}}(c_+ + \delta^n) - f_{\text{id}}(c_+)\} =: T_1 + T_2,$$

we infer that

$$\begin{aligned} T_1 &\leq -(\log(\sigma^3 2^n) - 1) \int_{A_+^n} c_+, \\ |T_2| &\leq \delta^n \int_{\Omega^{k,m}} m(c_+, c_+ + \delta^n) \leq m(2^{-k}, 2^k + \delta) \int_{A_+^n} c_+, \end{aligned}$$

where we have used the fact that $c_+ \geq 0$, $\delta^n \leq \delta$, and that, for $b \in \mathbb{R}_{>0}$ and $a \in \mathbb{R}_{\geq 0}$, there holds $|f_{\text{id}}(b) - f_{\text{id}}(a)| \leq |b - a|m(a, b)$ with $m(a, b) := \max(|\log(\sigma^3 a)|, |\log(\sigma^3 b)|)$. Turning next to $\Delta\mathcal{F}_{\text{corr}}$, recall that the excess bulk free energy density f_{corr} is continuously differentiable in $\mathbb{R}_{\geq 0}^2$ and that $\frac{\partial f_{\text{corr}}}{\partial c_+}(u) \geq 0$ for all $u = (u_+, u_-) \in \mathbb{R}_{\geq 0}^2$ such that $u_+ \geq \kappa_\gamma$ or $u_- \geq \kappa_\gamma$ as shown in Lemma 3. Let $C_\gamma := \max_{u \in K_\gamma} |\frac{\partial f_{\text{corr}}}{\partial c_+}(u)|$ with the compact set $K_\gamma := [0, \max(2^k + \delta, \kappa_\gamma)] \times [0, \max(2^m, \kappa_\gamma)]$. We decompose $\Delta\mathcal{F}_{\text{corr}}$ into

$$\Delta\mathcal{F}_{\text{corr}} = \int_{A_+^n} \{f_{\text{corr}}(\tilde{c}_+^n, c_-) - f_{\text{corr}}(c_+, c_-)\} + \int_{\Omega^{k,m}} \{f_{\text{corr}}(\tilde{c}_+^n, c_-) - f_{\text{corr}}(c_+, c_-)\} =: T_3 + T_4.$$

Observing that $f_{\text{corr}}(\tilde{c}_+^n, c_-) - f_{\text{corr}}(c_+, c_-) = \left(\int_{c_+}^{\tilde{c}_+^n} \frac{\partial f_{\text{corr}}}{\partial c_+}(u_+, c_-) du_+ \right)$, we obtain

$$|T_4| \leq \int_{\Omega^{k,m}} C_\gamma \delta^n = C_\gamma \int_{A_+^n} c_+,$$

since for all $x \in \Omega^{k,m}$ and for all $u_+ \in [c_+(x), \tilde{c}_+^n(x)]$, $(u_+, c_-(x)) \in K_\gamma$. Moreover, owing to Lemma 3,

$$\begin{aligned}
 T_3 &\leq \int_{A_+^n} \{f_{\text{corr}}(0, c_-) - f_{\text{corr}}(\min(\kappa_\gamma, c_+), c_-)\} \\
 &\leq \int_{A_+^n \cap \{c_- \leq \kappa_\gamma\}} \{f_{\text{corr}}(0, c_-) - f_{\text{corr}}(\min(\kappa_\gamma, c_+), c_-)\} =: T'_3,
 \end{aligned}$$

since for $c_- > \kappa_\gamma$, $f_{\text{corr}}(0, c_-) - f_{\text{corr}}(\min(\kappa_\gamma, c_+), c_-) \leq 0$. Moreover,

$$\begin{aligned}
 |T'_3| &\leq \int_{A_+^n \cap \{c_- \leq \kappa_\gamma\}} \left(\int_0^{\min(\kappa_\gamma, c_+)} \left| \frac{\partial f_{\text{corr}}}{\partial c_+}(u_+, c_-) \right| du_+ \right) \\
 &\leq \int_{A_+^n \cap \{c_- \leq \kappa_\gamma\}} C_\gamma \min(\kappa_\gamma, c_+) \leq C_\gamma \int_{A_+^n} c_+.
 \end{aligned}$$

Collecting the above bounds, we infer

$$\Delta \mathcal{E} \geq (\log(\sigma^3 2^n) - 1 - C) \int_{A_+^n} c_+,$$

with $C = 2Z_+ \|\psi\|_{L^\infty(\Omega)} + m(2^{-k}, 2^k + \delta) + 2C_\gamma$. Taking n large enough so that $\log(\sigma^3 2^n) \geq 1 + C$ and since A_+^n has positive measure, we infer $\Delta \mathcal{E} > 0$. \diamond

Our last result delivers a uniform positive lower bound on the ionic concentrations.

Lemma 7 (Uniform positive lower bound on c) *Assume (H3). Let $(\psi, c) \in \mathfrak{H} \times \mathfrak{K}$ be a saddle point of the functional \mathcal{E} . Then, there is $c_m > 0$ such that, for a.e. $x \in \Omega$, $c_i(x) \geq c_m$ for all $i = \pm$.*

Proof. Let $(\psi, c) \in \mathfrak{H} \times \mathfrak{K}$ be a saddle point of the functional \mathcal{E} . The structure of the proof is similar to that of Lemma 6, though a bit simpler since we already have upper bounds on c_\pm . Proceeding by contradiction, we assume that there is $i = \pm$ such that, for all $n \in \mathbb{N}$, the set

$$B_i^n := \{x \in \Omega; c_i(x) < 2^{-n}\}$$

has positive measure. We then construct modified ionic concentrations $\tilde{c} \in \mathfrak{K}$ such that $\mathcal{E}(\psi, \tilde{c}) > \mathcal{E}(\psi, c)$, thereby providing the desired contradiction with (5.21). As a result, for all $i = \pm$, there is $n_i \in \mathbb{N}$ such that the set $B_i^{n_i}$ has zero measure, yielding the statement of Lemma 7 with $c_m = \min_{i=\pm} 2^{-n_i}$.

Without loss of generality, we assume that, for all $n \in \mathbb{N}$, the set B_+^n has positive measure. We fix $k \in \mathbb{N}$ such that the set Ω_+^k defined by (5.25) has positive measure, and, without loss of generality, we assume that n is large enough so that $2^{-n} \leq \frac{1}{|\Omega|} |\Omega_+^k| 2^{-k}$. Since this implies $2^{-n} \leq 2^{-k}$, the sets B_+^n and Ω_+^k are disjoint. We now define the function \tilde{c}_+^n as follows:

$$\tilde{c}_+^n(x) = \begin{cases} c_+(x) + 2^{-n}, & x \in B_+^n, \\ c_+(x) - \delta^n, & x \in \Omega_+^k, \\ c_+(x), & x \in \Omega \setminus (B_+^n \cup \Omega_+^k), \end{cases}$$

with $\delta^n = \frac{1}{|\Omega_+^k|} |B_+^n| 2^{-n}$. It is readily verified that $\langle \tilde{c}_+^n \rangle_\Omega = c_+^0$. Moreover, since $|B_+^n| < |\Omega|$, $\delta^n < \frac{1}{|\Omega_+^k|} |\Omega| 2^{-n} \leq 2^{-k}$, so that $\tilde{c}_+^n \geq 0$ in Ω . Hence, $\tilde{c}^n := (\tilde{c}_+^n, c_-) \in \mathfrak{K}$.

To conclude the proof, we show that it is possible to choose n large enough so that

$$\Delta\mathcal{E} := \mathcal{E}(\psi, \tilde{c}^n) - \mathcal{E}(\psi, c) > 0.$$

As in the proof of Lemma 6, we write $\Delta\mathcal{E} = -\Delta\mathcal{F}_{\text{id}} - \Delta\mathcal{F}_{\text{corr}} - \Delta\mathcal{B}$. Since $\psi \in L^\infty(\Omega)$ owing to the second step in the proof of Theorem 7, we infer

$$|\Delta\mathcal{B}| \leq 2Z_+ \|\psi\|_{L^\infty(\Omega)} 2^{-n} |B_+^n|.$$

Moreover,

$$\Delta\mathcal{F}_{\text{id}} = \int_{B_+^n} \{f_{\text{id}}(c_+ + 2^{-n}) - f_{\text{id}}(c_+)\} + \int_{\Omega_+^k} \{f_{\text{id}}(c_+ - \delta^n) - f_{\text{id}}(c_+)\} =: T_1 + T_2,$$

with

$$\begin{aligned} T_1 &\leq \int_{B_+^n} 2^{-n} \log(\sigma^3 2^{-n+1}) = \log(\sigma^3 2^{-n+1}) 2^{-n} |B_+^n|, \\ |T_2| &\leq \int_{\Omega_+^k} \delta^n m(c_+ - \delta^n, c_+) \leq m(2^{-k} - \delta, 2^k) 2^{-n} |B_+^n|. \end{aligned}$$

Finally, let $C'_\gamma := \max_{u \in K'_\gamma} \left| \frac{\partial f_{\text{corr}}}{\partial c_+}(u) \right|$ with the compact set $K'_\gamma := [0, 2^k] \times [0, c_M]$. We obtain

$$|\Delta\mathcal{F}_{\text{corr}}| \leq \int_{B_+^n \cup \Omega_+^k} \left(\int_{c_+}^{\tilde{c}_+^n} \left| \frac{\partial f_{\text{corr}}}{\partial c_+}(u_+, c_-) \right| du_+ \right) \leq C'_\gamma \int_{B_+^n \cup \Omega_+^k} |\tilde{c}_+^n - c_+| \leq 2C'_\gamma 2^{-n} |B_+^n|,$$

since for all $x \in B_+^n \cup \Omega_+^k$ and for all $u_+ \in [c_+(x), \tilde{c}_+^n(x)]$, $(u_+, c_-(x)) \in K'_\gamma$. Collecting the above bounds, we infer

$$\Delta\mathcal{E} \geq (\log(\sigma^{-3} 2^{n-1}) - C) 2^{-n} |B_+^n|,$$

with $C = 2Z_+ \|\psi\|_{L^\infty(\Omega)} + m(2^{-k} - \delta, 2^k) + 2C'_\gamma$. Taking n large enough so that $\log(\sigma^{-3} 2^{n-1}) \geq C$ and since B_+^n has positive measure, we infer $\Delta\mathcal{E} > 0$. \diamond

5.3 Numerical aspects

This section presents numerical experiments in the case where the activity coefficient $\log(\gamma_0)$ is evaluated using the MSA (5.13) and the steric exclusion term using the (CS1), linearized version of (CS), given by (5.15).

5.3.1 Physical input

The physical input parameters are the temperature T , the surface charge density Σ_S , the ion diameter σ , the relative permittivity of the solvent ε_r , and the geometric length scale L_* . A convenient way to specify the mean ionic concentrations while satisfying the global electroneutrality condition is to choose a concentration of added salt c^{salt} and to set

$$c_+^{\text{bulk}} := c^{\text{salt}} + \frac{1}{Z_+ |\Omega|} \int_{\partial\Omega_S} \frac{1}{e} \Sigma_S, \quad c_-^{\text{bulk}} = -\frac{Z_+}{Z_-} c^{\text{salt}}.$$

In the case where there is no added salt, the mean concentration of co-ion is $c_-^{\text{bulk}} = 0$ while the mean concentration of counterions is only ruled by global electroneutrality and given by $c_+^{\text{bulk}} = \frac{1}{Z_+ |\Omega|} \int_{\partial\Omega_S} \frac{1}{e} \Sigma_S$.

5.3.2 Verification of assumptions for MSA

We verify the abstract assumptions (H3)-(H4) in the context of the MSA, that is, when $\log(\gamma_0)$ is defined by (5.13) with the screening parameter \mathcal{Y}_{MSA} defined by (5.14). Assumption (H3) is straightforward to verify, so that we focus on (H4). For all $\theta > 0$, setting $y := \sqrt{2\sigma\lambda^{-1/2}(2\theta)^{1/2} + 1}$, we obtain

$$(\log(\gamma_0))'(\theta) = -\frac{\sigma}{\pi\lambda^2} \frac{1}{y(y+1)^2(y^2-1)},$$

and a simple calculation shows that (H4) is equivalent to the fact that the sixth degree polynomial

$$\begin{aligned} P(y) = & y(y-1)^2(y+1)^3 - \frac{(\eta_{\#} - \eta_b)^2}{16\pi\lambda\sigma\eta_b} (y^2-1)^2(y-1) \\ & + \left(\frac{6\eta_{\#}}{\pi\lambda\sigma}\right) y(y+1) - \frac{3}{2} \left(\frac{\eta_{\#}}{\pi\lambda\sigma}\right)^2 (y-1) \end{aligned}$$

takes positive values for all $y > 1$. This condition, in turn, can be checked numerically. It holds under a condition of the form $\sigma\lambda > v_0$, where the threshold v_0 , which depends on the species valences Z_{\pm} , is reported in the second column of Table 5.1 for several values of Z_{\pm} . Recalling the definition (5.1) of the non-dimensional parameter λ and reverting to dimensional length scales, the above condition can be expressed as $\sigma/L_B > 4\pi v_0$. Using the values $e = 1.60 \times 10^{-19}$ C, $\varepsilon_0 = 8.85 \times 10^{-12}$ CV $^{-1}$ m $^{-1}$, and $k_B = 1.38 \times 10^{-23}$ JK $^{-1}$, the Bjerrum length can be evaluated as a function of the temperature T (yielding $L_B = 7.1$ Å at $T = 300$ K with $\varepsilon_r = 78.3$ and $L_B = 7.7$ Å at $T = 350$ K with $\varepsilon_r = 62.0$ [6]), and a minimal value σ_0 for the mean ion diameter can be computed so that (H4) holds true for $\sigma > \sigma_0$. The threshold σ_0 is reported in the third and fourth columns of Table 5.1. We observe that σ_0 takes slightly higher values as the temperature is increased. The condition $\sigma > \sigma_0$ is also more stringent for 2:1 and 2:2 electrolytes than for 1:1 electrolytes, and becomes difficult to fulfill for 3:1 and 3:3 electrolytes. Interestingly, the condition $\sigma > \sigma_0$ shows that the mean ion diameter cannot take extremely low values within the present physical model if convexity of the bulk free energy is to be asserted (in particular, the Debye–Hückel limit $\sigma \rightarrow 0$ does not yield a convex bulk free energy).

$Z_+ : Z_- $	v_0	σ_0 (Å)	
		$T = 300$ K	$T = 350$ K
-	-		
1 : 1	6.263×10^{-3}	0.560	0.606
2 : 1	2.605×10^{-2}	2.329	2.521
2 : 2	2.505×10^{-2}	2.239	2.424
3 : 3	5.637×10^{-2}	5.039	5.454
3 : 1	8.224×10^{-2}	7.352	7.958

Table 5.1. Threshold values above which assumption (H4) holds true.

5.3.3 Numerical methods

Let us now turn to the approximation of the ionic concentrations and of the electrostatic potential. The saddle point of the functional \mathcal{E} is computed numerically by solving the associated Euler–Lagrange conditions approximately using finite elements for space discretization (using the `FreeFEM++` library [44]) in conjunction with a Newton–Raphson algorithm to solve the discrete set of coupled nonlinear equations. The constraints on the mean value of the electrostatic potential and of the ionic concentrations are handled using three additional Lagrange multipliers.

Finite element discretization

We start by discussing the weak variational formulation of the system coupling the Poisson equation and the constancy of the electrochemical potential. The solution (ψ, c) provided by Theorem 7 lives in a convex subset of $H_{\text{per}}^1(\Omega) \times [L^2(\Omega)]^2$. We introduce two finite-dimensional subspaces $V_h \subset H_{\text{per}}^1(\Omega)$ and $P_h \subset L^2(\Omega)$ and solve the nonlinear variational formulation (we omit the indices h on the discrete solution) *Find* $(\psi, c, \lambda_{\text{el}}, \mu_+^{\text{bulk}}, \mu_-^{\text{bulk}}) \in V_h \times P_h^2 \times \mathbb{R}^3$ *such that*: $\forall (u_h, v_h, w_h, p, q, r) \in V_h \times P_h^2 \times \mathbb{R}^3$,

$$\left\{ \begin{array}{l} \int_{\Omega} \lambda \nabla \psi \cdot \nabla u_h + \lambda_{\text{el}} \langle u_h \rangle_{\Omega} = \int_{\Omega} (Z_+ c_+ + Z_- c_-) u_h - \lambda \int_{\partial\Omega_S} \Sigma_S u_h, \\ p \langle \psi \rangle_{\Omega} = 0, \\ \int_{\Omega} (\partial_{c_+} f(c) + Z_+ \psi) v_h = \int_{\Omega} \mu_+^{\text{bulk}} v_h, \\ q \langle c_+ \rangle_{\Omega} = q c_+^{\text{bulk}}, \\ \int_{\Omega} (\partial_{c_-} f(c) + Z_- \psi) w_h = \int_{\Omega} \mu_-^{\text{bulk}} w_h, \\ r \langle c_- \rangle_{\Omega} = r c_-^{\text{bulk}}. \end{array} \right. \quad (5.26)$$

In our simulations, we use either \mathbb{P}_0 piecewise constant finite elements or conforming continuous \mathbb{P}_1 finite elements for the concentrations and conforming \mathbb{P}_1 finite elements for the electrostatic potential. The constants $(\lambda_{\text{el}}, \mu_+^{\text{bulk}}, \mu_-^{\text{bulk}}) \in \mathbb{R}^3$ are the Lagrange multipliers mentioned above. Periodic boundary conditions are enforced strongly in the finite element space. Nevertheless, for various shapes of the domain Ω , we exploit symmetries of the solution and simply enforce natural boundary conditions on symmetry boundaries.

A Newton–Raphson algorithm

The main difficulty with the system of equations (5.26) is its nonlinear character since there is a quadratic coupling between c and ψ and since the equation on c is nonlinear. This discrete system can be solved by means of a Newton–Raphson algorithm. Let us recall the basic steps of the method. Consider the system (5.26) in the abstract form

$$\mathcal{J}(y_h) = 0, \quad y_h = (\psi, c, \lambda_{\text{el}}, \mu_+^{\text{bulk}}, \mu_-^{\text{bulk}}) \in V_h \times P_h^2 \times \mathbb{R}^3. \quad (5.27)$$

The Newton–Raphson algorithm can be written as follows:

- (i) Fix a small positive tolerance $\text{tol} > 0$ and an initial condition y_h^0 such that c^0 satisfies the global electroneutrality condition and set $\psi^0 = \Psi_{\Sigma_S}(\lambda^{-1} \sum_{i=\pm} Z_i c_i^0)$; set $k = 0$;
- (ii) Update $y_h^{k+1} = y_h^k - \left(\nabla \mathcal{J}(y_h^k)\right)^{-1} \left(\mathcal{J}(y_h^k)\right)$;
- (iii) Check convergence; if satisfied stop, else set $k = k + 1$ and return to step (ii).

The convergence of the algorithm can be checked by monitoring the evolution of three quantities, at iteration $k \geq 0$,

- (a) The norm of the residual of the problem $\mathcal{E}_{\text{cvg}}^{1,k} := \|\mathcal{J}(y_h^k)\|$, where $\|\cdot\|$ is the Euclidean norm;
- (b) The norm of the difference between two successive iterates $\mathcal{E}_{\text{cvg}}^{2,k} := \|y_h^{k+1} - y_h^k\|$;
- (c) The discrete free energy $\mathcal{E}_{\text{cvg}}^{3,k} := -\mathcal{E}\left(\Psi_{\Sigma_S}\left(\lambda^{-1}\rho(c^k)\right), c^k\right)$ with

$$\rho(c) := \sum_{i=\pm} Z_i c_i \quad (5.28)$$

the nondimensional charge density;

Convergence of the iterative process is achieved if we have $\mathcal{E}_{\text{cvg}}^{1,k} < \left(\mathcal{E}_{\text{cvg}}^{1,0}\text{tol}\right)$ and $\mathcal{E}_{\text{cvg}}^{2,k} < \left(\mathcal{E}_{\text{cvg}}^{2,0}\text{tol}\right)$. Monitoring the quantity $\mathcal{E}_{\text{cvg}}^{3,k}$ is motivated by the fact that, if (ψ, c) is a saddle point of \mathcal{E} , c minimizes the functional $-\mathcal{E}\left(\Psi_{\Sigma_S}\left(\lambda^{-1}\rho(\cdot)\right), \cdot\right)$ under the canonical constraints.

In practice, the matrix $\nabla \mathcal{J}(y_h)$ and the vector $\mathcal{J}(y_h)$ are computed with the analytical formulas of the chemical potential $\mu_i(c) = \partial_{c_i} f(c)$ and its first derivative $\partial_{c_j} \mu_i(c) = \partial_{c_i, c_j}^2 f(c)$. The components of the 6×6 block matrix $[\nabla \mathcal{J}(y_h)]_{i,j}$ are thus obtained by differentiating the operator $y \mapsto \mathcal{J}(y)$. The right-hand side of the linear system to be inverted is given by

$$b_h^k = -\mathcal{J}(y_h^k), \quad (5.29)$$

and the linear system $[\nabla \mathcal{J}(y_h^k)] \left(y_h^{k+1} - y_h^k\right) = b_h^k$ is solved iteratively using the UMFPAK library called by FreeFem++ (see [44] and [21]).

5.3.4 Validation of the approach: flat nanochannel

In the ideal case, for a 1D geometry such as a nanochannel with parallel negatively charged flat walls and in the one-species case, there is an analytical solution to the Poisson-Boltzmann equation for the electrostatic potential, see [24]. The concentration of counterions is given by

$$c_+(x) = \frac{a}{\cos\left(Z_+ \sqrt{\frac{a}{2\lambda}} \left(x - \frac{1}{2}\right)\right)^2}, \quad x \in [0, 1], \quad (5.30)$$

where the parameter a satisfies the nonlinear equation

$$\tan\left(Z_+ \sqrt{\frac{a}{8\lambda}}\right) = \Sigma_S \sqrt{\frac{\lambda}{2a}}, \quad (5.31)$$

resulting from the global electroneutrality condition. We verified that our computational code produces an accurate approximation of this analytical solution. In the non-ideal case, there is, a priori, no analytical result available. We ran simulations for a 1:1 electrolyte in a flat nanochannel with physical parameters $T = 300\text{K}$, $\Sigma_S = 0.1\text{Cm}^{-2}$, $L_* = 10\text{Å}$, and $\sigma = 3\text{Å}$. The concentration of added salt is set to $c^{\text{salt}} = 0.1\text{mol/l}$ so that the canonical constraints are $c^{\text{bulk}} = (c_+^{\text{bulk}}, c_-^{\text{bulk}}) = (2.17, 0.1)\text{mol/l}$. The problem is solved on the half interval exploiting the symmetry of the problem with a constant discretization parameter $\delta x = 0.001$. The algorithm is initialized with concentrations satisfying the canonical constraints while we set $\psi^0 = \Psi_{\Sigma_S}(\lambda^{-1}\rho(c^0))$. Figure 5.1 depicts the behaviour of the Newton–Raphson algorithm in this situation. Convergence is achieved extremely fast for the two indicators. As expected, the indicator related to the functional \mathcal{E} decreases along the iterations of the Newton–Raphson algorithm, and in fact is almost stationary after the third iteration. We will see in Chapter 6 that the situation is much more complex when dealing with a non convex bulk free energy density.

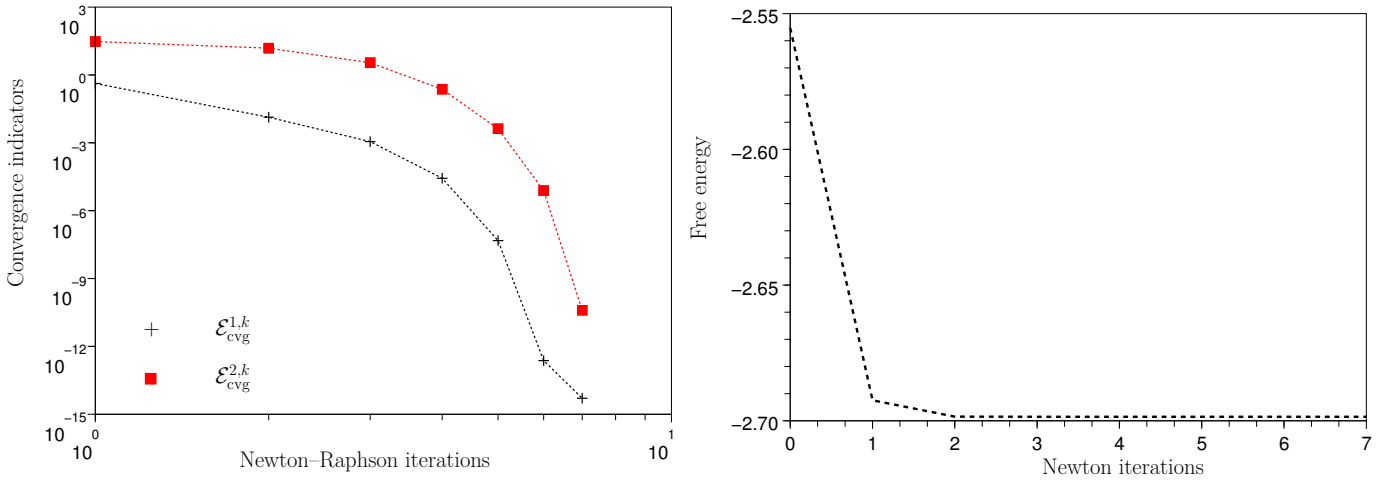


Fig. 5.1. Convergence indicators for the Newton–Raphson algorithm. Left: convergence indicator; Right: Decrease of the free energy.

5.3.5 Periodic medium with charged inclusions

We consider a two-dimensional setting where the inclusion Ω_S is a disk of radius $R = 0.3L_*$ whose center coincides with that of the elementary cell $[0, L_*]^2$. We take $L_* \in \{1, 10\}\text{nm}$, $T = 300\text{K}$, and $\Sigma_S = 0.13\text{Cm}^{-2}$. With these values, the Debye length is in the range $[3.345, 105.8]\text{Å}$. We consider a 1:1 electrolyte. We set the concentration of added salt to $c^{\text{salt}} = 0.15\text{mol/l}$. In particular, since the disk is negatively charged, there is always an excess of counterions to ensure the global electroneutrality of the system. It is readily seen that assumptions (H1)-(H2) hold true. Moreover, the ion diameter is set to $\sigma \in \{3, 4, 5\}\text{Å}$, so that assumptions (H3)-(H4) also hold true (see Table 5.1). Figure 5.2 (left) depicts the activity coefficient $\log(\gamma_0)$ as a function of ionic strength for the various values of the parameter σ , whereas Figure 5.2 (right) depicts the hard-sphere activity coefficient γ_{HS} as a function of total concentration. This figure illustrates that electrostatic correlations have a more pronounced effect for small values of σ , whereas the

opposite effect is observed for steric exclusion. For completeness, we also present the steric exclusion activity coefficient for the (CS) expression (4.56).

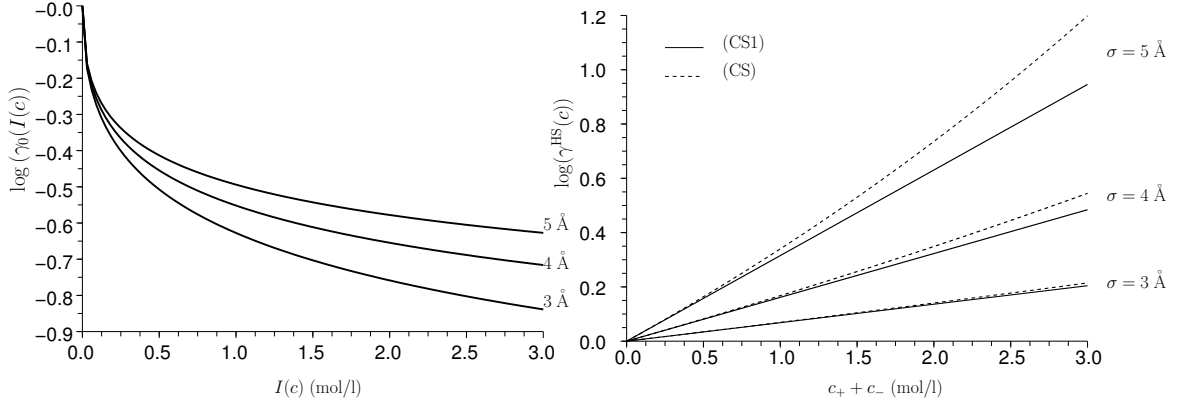


Fig. 5.2. Left: activity coefficient $\log(\gamma_0)$ as a function of ionic strength $I(c)$ (mol/l); Right: hard-sphere activity coefficient γ_{HS} as a function of total concentration $(c_+ + c_-)$ (mol/l)

Figure 5.3 depicts iso-values of the counterion concentration for the two values of the reference length L_* and for a ion diameter equal to 3 \AA (the elementary cell is rescaled to $[0, 1]^2$ in the figure so that the two plots have the same size). We observe that for large L_* , boundary layers appear near the charged walls: counterion concentrations exhibit a steep gradient close to the charged surface and take almost constant values in the region far from the disk.

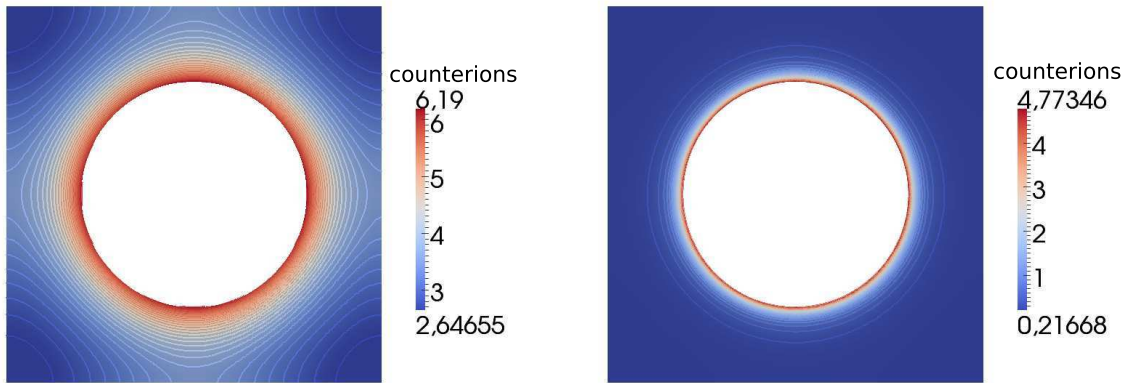


Fig. 5.3. Counterion concentration (mol/l) for a 1:1 electrolyte with parameters $c^{\text{salt}} = 0.15 \text{ mol/l}$ and $\sigma = 3 \text{ \AA}$. Left: $L_* = 1 \text{ nm}$; Right: $L_* = 10 \text{ nm}$.

To gain further insight, we compare the solutions obtained for the three values of the ion diameter $\sigma \in \{3, 4, 5\} \text{ \AA}$ and for the two values of $L_* \in \{1, 10\} \text{ nm}$. We focus on the results obtained on the horizontal line $[0.8L_*, L_*] \times [0.5L_*, L_*]$ joining the rightmost part of the disk to the right vertical side of the elementary cell. Figure 5.4 depicts the values of the activity coefficient $\log(\gamma_{\pm}(c))$ (note that $\log(\gamma_+(c)) = \log(\gamma_-(c))$ for a symmetric electrolyte), while Figure 5.5 depicts those of the counterion concentration; for completeness, concentrations values obtained

in the ideal Poisson–Boltzmann case ($\gamma_{\pm}(c) = 1$) are also reported. We observe three different behaviors in Figure 5.4: electrostatic correlations dominate for $\sigma = 3 \text{ \AA}$ ($\log(\gamma_{\pm}(c)) < 0$), steric exclusion effects dominate for $\sigma = 5 \text{ \AA}$ ($\log(\gamma_{\pm}(c)) > 0$), or both effects play a role for $\sigma = 4 \text{ \AA}$. In Figure 5.5, we observe the influence of the non-ideality on the counterion concentration close to the charged disk, especially when comparing the concentrations to those obtained within the Poisson–Boltzmann theory. The main effect of non-ideality is to lower the counterion concentration close to the charged surface. Interestingly, the ideal predictions are more accurate for larger cell sizes ($L_* = 10 \text{ nm}$). Finally, we notice that for $L_* = 1 \text{ nm}$ and $\sigma = 5 \text{ \AA}$, the packing number defined as $\xi(c) = \frac{\pi}{6} \sum_{i=\pm} \sigma^3 c_i$ takes values of the order of 0.2 close to the disk. The hard-sphere contribution can also be evaluated using the Carnahan–Starling expression $\log(\gamma_1^{\text{CS}}(\xi(c))) := (8\xi - 9\xi^2 + 3\xi^3)(1 - \xi)^{-3}$ instead of its first-order approximation (6.7). With this expression for $\log(\gamma_{\text{HS}}(c))$, the counterion concentration near the charged disk is lowered by about 10%. Notice that assumption (H4) still provides a sufficient condition for convexity in this case. Indeed, recalling the setting of Section 4.2.4, $\log(\gamma^{\text{HS}}(c)) = \log(\gamma_1(\xi(c)))$ is solely a function of the packing number such that, for all $t \in [0, 1)$,

$$\left[\log(\gamma_1^{\text{CS}}(t))\right]' = \left[(8t - 9t^2 + 3t^3)(1 - t)^{-3}\right]' \geq \left[\log(\gamma_1^{\text{CS1}}(t))\right]' = 8. \quad (5.32)$$

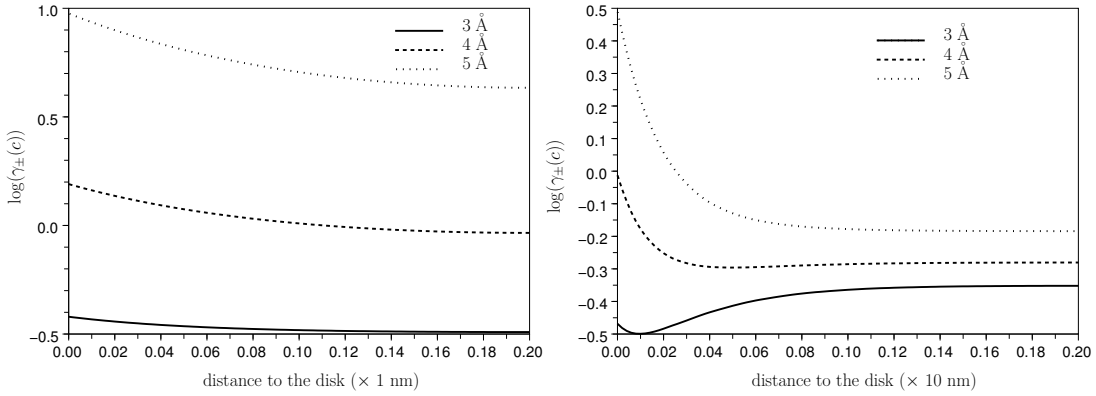


Fig. 5.4. $\log(\gamma_{\pm}(c))$ for a 1:1 electrolyte with parameters $c^{\text{salt}} = 0.15 \text{ mol/l}$ and $\sigma \in \{3, 4, 5\} \text{ \AA}$. Left: $L_* = 1 \text{ nm}$; Right: $L_* = 10 \text{ nm}$.

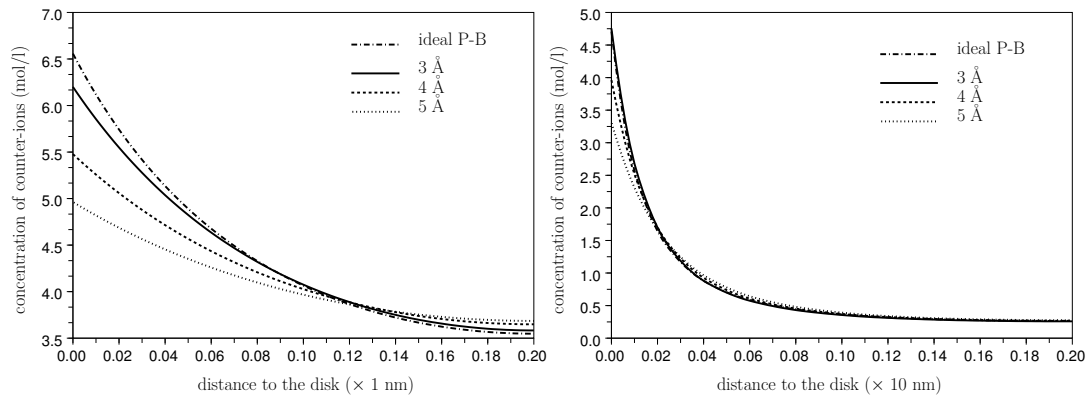


Fig. 5.5. Counterion concentrations (mol/l) for a 1:1 electrolyte with parameters $c^{\text{salt}} = 0.15$ mol/l and $\sigma \in \{3, 4, 5\}$ Å. Left: $L_* = 1$ nm; Right: $L_* = 10$ nm.

Strong non-ideality: non convex bulk free-energy and phase separation

6.1 Bulk thermodynamics of the one-species setting	127
6.1.1 Chemical potential	128
6.1.2 Free energy density	129
6.1.3 Osmotic pressure	129
6.1.4 Phase separation	130
6.1.5 The Maxwell equal area rule	130
6.1.6 Convex hull: numerical illustrations	131
6.2 Confined electrolytes: Theory and method	132
6.2.1 Canonical constraints and thermodynamic equilibrium	133
6.2.2 Mechanical equilibrium	133
6.2.3 Regularizations	134
6.2.4 Discretization and nonlinear solver	135
6.2.5 Validation test cases	137
6.3 Confined electrolytes: Numerical results	139
6.3.1 Flat nanochannel	140
6.3.2 Periodic network of charged inclusions and wavy channel	142
6.4 An approach for symmetric salts	144
6.5 Some mathematical aspects	146
6.5.1 Minimizing properties of \mathcal{F}^{**}	147
6.5.2 Minimizing properties of \mathcal{F}_κ^{**}	148
6.5.3 Existing Γ -convergence results	148

This chapter is organized as follows: in Section 6.1 we restate the electrochemical model in the bulk focusing on the one-species setting. The reason for this choice is that phase separation in the bulk can be treated using the Maxwell equal area rule, analogous to the Van der Waals model of liquid-vapor phase transition. In Section 6.2, we detail the confined setting and the numerical methods that we used to solve the phase separation problem. Numerical results are presented in Section 6.3. A possible approach to treat binary symmetric electrolytes is proposed in Section 6.4. Finally, a discussion on the mathematical aspects underlying the minimizing properties of the free energy functional in the non convex case is presented in Section 6.5.

6.1 Bulk thermodynamics of the one-species setting

We consider equilibrium electrolytes described by the electrostatic potential ψ and the concentration of counterions c . The electrochemical potential is defined by

$$\mu^{\text{el}}(\psi, c) := \mu(c) + Ze\psi = \frac{1}{\beta} \left(\log(\sigma^3 c) + \log(\gamma(c)) \right) + Ze\psi, \quad (6.1)$$

σ , Z , e standing respectively for the ion diameter, the positive valence of the counterion, and the elementary charge, while $\beta = (k_B T)^{-1}$ is proportional to the inverse of the temperature T . Here, μ is the chemical potential and γ the activity coefficient. We start by describing the form of the chemical potential, the free energy of the electrolyte solution, and the osmotic pressure. Then, we deal with phase separation.

6.1.1 Chemical potential

The chemical potential μ splits into the ideal part

$$\mu_{\text{id}}(c) = \frac{1}{\beta} \log(\sigma^3 c), \quad (6.2)$$

and the non-ideal part

$$\mu_{\text{corr}}(c) = \frac{1}{\beta} \log(\gamma(c)). \quad (6.3)$$

The activity coefficient $\gamma(c)$ is split into two parts in such a way that

$$\log(\gamma(c)) = \log(\gamma_{\text{Coul}}(c)) + \log(\gamma_{\text{HS}}(c)). \quad (6.4)$$

The first contribution accounts for Coulomb interactions, while the second contribution is a hard-sphere term introducing steric effects which dominate at high ionic concentrations.

For the Coulomb term, we consider the *mean spherical approximation* (MSA) valid for a neutral binary electrolyte, which we use in this one-species setting without modifications accounting for a neutralizing background of negatively charged constituents. The MSA hinges on the screening parameter Γ_{MSA} (expressed in m^{-1}) defined by

$$\Gamma_{\text{MSA}}(c) := \frac{1}{2\sigma} \left(\sqrt{2\sigma(4\pi L_B)^{1/2} Z \sqrt{c} + 1} - 1 \right), \quad (6.5)$$

where L_B is the Bjerrum length defined by $L_B := \frac{\beta e^2}{4\pi\epsilon}$, where $\epsilon = \epsilon_0 \epsilon_r$ is the permittivity of the solvent. Then, the activity coefficient $\gamma_{\text{Coul}}(c)$ is given by

$$\log(\gamma_{\text{Coul}}(c)) = -Z^2 \frac{L_B \Gamma_{\text{MSA}}(c)}{1 + \sigma \Gamma_{\text{MSA}}(c)}. \quad (6.6)$$

For the hard-sphere contribution, we consider the Carnahan–Starling expression

$$\log(\gamma_{\text{HS}}(c)) := \log(\gamma_1^{\text{CS}}(\xi(c))) = \begin{cases} \frac{8\xi(c) - 9\xi(c)^2 + 3\xi(c)^3}{(1 - \xi(c))^3}, & \xi(c) < 1, \\ +\infty, & \xi(c) \geq 1, \end{cases} \quad (6.7)$$

where $\xi(c)$ stands for the packing number defined as

$$\xi(c) := \vartheta c, \quad (6.8)$$

and $\vartheta = \frac{1}{6}\pi\sigma^3$. For low values of $\xi(c)$, we recover the linearized hard-sphere contribution (CS1) considered in Chapter 5,

$$\log(\gamma_{\text{HS}}(c)) \approx \log(\gamma_1^{\text{CS1}}(\xi(c))) = 8\xi(c) = \frac{4}{3}\pi\sigma^3 c. \quad (6.9)$$

6.1.2 Free energy density

We can now write the bulk free energy density by integrating the chemical potentials with respect to the ionic concentration. We write the free energy density as the sum of the ideal contribution

$$f_{\text{id}}(c) := \frac{1}{\beta} c (\log(\sigma^3 c) - 1), \quad (6.10)$$

the Coulomb contribution

$$f_{\text{Coul}}(c) := -\frac{2L_{\text{B}}}{\beta\sigma} \left(I(c) - \frac{2\sigma}{3\pi L_{\text{B}}} (\Gamma_{\text{MSA}}(c))^3 - \frac{1}{2\pi L_{\text{B}}} (\Gamma_{\text{MSA}}(c))^2 \right), \quad (6.11)$$

and the hard-sphere contribution

$$f_{\text{HS}}(c) := \begin{cases} -\frac{1}{\beta\vartheta} \left(\frac{\xi(c)^2 (3\xi(c) - 4)}{(1 - \xi(c))^2} \right), & \xi(c) < 1, \\ +\infty, & \xi(c) \geq 1. \end{cases} \quad (6.12)$$

Collecting the contributions, we write the bulk free energy density as

$$f := f_{\text{id}} + f_{\text{corr}} := f_{\text{id}} + f_{\text{Coul}} + f_{\text{HS}}. \quad (6.13)$$

The bulk free energy functional is the integral of the free energy density over the volume Ω occupied by the electrolyte:

$$\mathcal{F}_{\text{bulk}}(c) := \int_{\Omega} f(c). \quad (6.14)$$

In a canonical setting that consists in fixing the space-average of the counterion concentration, minimizing the thermodynamic potential $\mathcal{F}_{\text{bulk}}$ with canonical constraint yields thermodynamic equilibrium expressed by the constancy of the electro-chemical potential over the domain.

6.1.3 Osmotic pressure

Owing to the Gibbs-Duhem relation, see Section 4.2.6, we write the pressure of the system (up to an additive constant) as

$$p_{\text{osm}}(c) := (c\mu(c) - f(c)). \quad (6.15)$$

6.1.4 Phase separation

For a wide range of physical parameters, the bulk free energy density f is not a convex function of its argument, see Chapter 5 for explicit bounds in the case of the linearized hard-sphere contribution. This is a consequence of the presence of the Coulombic excess free energy which is concave in c , whereas the ideal and steric exclusion terms are convex in c . This phenomenon is illustrated by the behaviour of the chemical potential depicted in Figure 6.1. We observe that at fixed temperature and for large ion diameters σ , the chemical potential remains an increasing function of the concentration while for smaller ion diameters, the chemical potential can decrease locally. The same phenomenon is observed when fixing the ion diameter and letting the temperature vary. By assuming that the solvent under consideration is bulk water at ambient conditions of observation, we assign a permittivity constant to each temperature in the range $T \in [300, 350]$ K by following [6]. We then observe that for higher temperatures, the bulk free energy density is no longer convex. The conclusion of this study is that for a wide range of situations, thermodynamic equilibrium cannot be determined by simply minimizing the bulk free energy since there might be multiple equilibria.

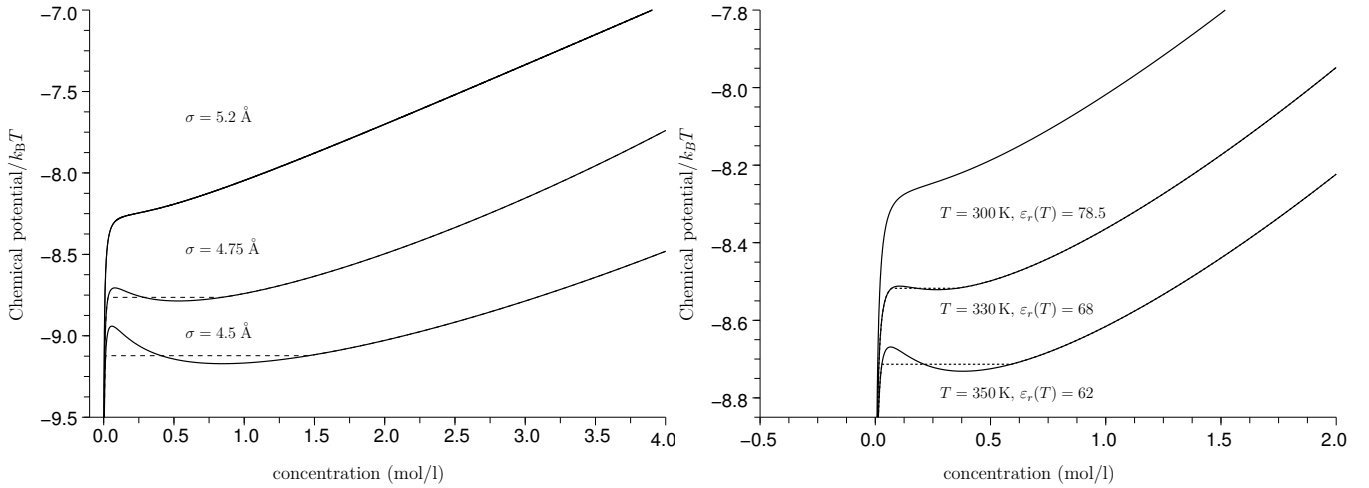


Fig. 6.1. Left: Chemical potential for $Z = 3$ with varying ionic diameter at fixed temperature $T = 300$ K. Right: chemical potential at various temperatures $T \in [300, 350]$ K for $Z = 2$ and $\sigma = 5.2$ Å. Dashed lines indicate the chemical potential resulting from a convexified bulk free energy density as described in §6.1.5.

6.1.5 The Maxwell equal area rule

When the bulk free energy density is not convex, it takes the form of a double-well potential, with two roots for its second derivative. The convex hull of f (denoted f^{**}) can be calculated analytically owing to the Maxwell equal area rule. This construction consists in determining binodal concentrations c_b, c_{\sharp} and an equilibrium chemical potential μ^* such that

$$\mu(c_b) = \mu(c_{\sharp}) = \mu^* \text{ and } \int_{c_b}^{c_{\sharp}} \mu(c) = \mu^* (c_{\sharp} - c_b), \quad (6.16)$$

as depicted in Figure 6.2. In addition to the binodal concentrations, we consider the spinodal concentrations $c_b, c_\#$ defined as the two roots of f'' . Then, concentrations outside $(c_b, c_\#)$ are deemed stable, those inside $(c_b, c_\#)$ unstable, and concentrations inside $(c_b, c_b) \cup (c_\#, c_\#)$ metastable.

The first derivative of the convex hull f^{**} is given by

$$\mu^{**}(c) = \begin{cases} \mu(c), & c \notin (c_b, c_\#), \\ \mu^*, & c \in [c_b, c_\#]. \end{cases}$$

The explicit formula for the convex hull of f is

$$f^{**}(c) = \begin{cases} f(c), & c \notin (c_b, c_\#), \\ (c - c_b) \mu^* + f(c_b), & c \in [c_b, c_\#]. \end{cases}$$

We observe that the osmotic pressure associated with the convex hull f^{**} satisfies the relation

$$p_{\text{osm}}^{**}(c_b) = p_{\text{osm}}^{**}(c_\#),$$

and moreover,

$$p_{\text{osm}}^{**}(c) \geq 0, \quad \forall c \geq 0, \quad (6.17)$$

since

$$(p_{\text{osm}}^{**})'(c) = c(f^{**})''(c) \geq 0, \quad \text{for almost every } c \geq 0, \quad (6.18)$$

$p_{\text{osm}}^{**}(0) = 0$, and p_{osm}^{**} is continuous. This result is important in view of the applications of this theoretical setting to confined electrolytes (see Section 6.3).

The Maxwell equal area rule is only applicable to univariate functions. For bivariate functions (as in the case of two species with counterions and coions), the convex hull of the free energy density can be obtained by means of the double Legendre transform, but analytical results are not available in general, so that that the transform has to be performed numerically (see *e.g.* Helluy and Mathis [45]).

6.1.6 Convex hull: numerical illustrations

To illustrate this theoretical setting, we compute values of $(\mu^*, c_b, c_\#)$ by combined Newton and dichotomy algorithms. Figure 6.3 depicts the behaviour of the binodal concentrations for divalent counterions and ion diameters in $[1.8, 2.23]$ Å at a fixed temperature $T = 300$ K. Furthermore, Table 6.1 collects values for the binodal and spinodal concentrations for divalent and trivalent ions at selected diameters. We also report the value of the packing number $\xi(c_\#)$ to illustrate the fact that its values are still relatively far away from 1 at the highest binodal concentration.

Remark 6.1. *Figure 6.3 is in fact the phase diagram for the bulk free energy density of a ionic fluid evaluated using the bulk free energy density (6.13). We can see in [Pr1] that the phase diagram computed in this thesis is in very good agreement with [35].*

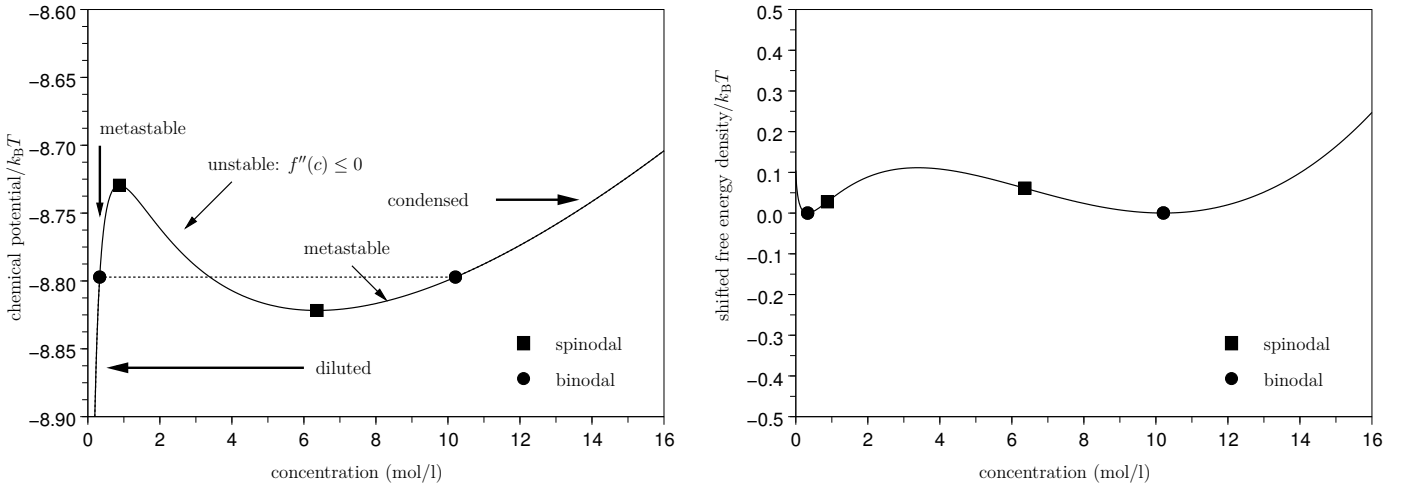


Fig. 6.2. Left: Chemical potential as a function of the concentration c with ionic diameter of $\sigma = 2.1 \text{ \AA}$ at $T = 300 \text{ K}$, $Z = 2$; Right: Affine shift of the bulk free energy density $\tilde{f}(c) = f(c) - ((c - c_b)\mu^* + f(c_b))$ illustrating the double-well form of f .

$Z = 2$						$Z = 3$					
$\sigma(\text{\AA})$	c_b	c_s	$c_{\#}$	$\xi(c_{\#})$		$\sigma(\text{\AA})$	c_b	c_s	$c_{\#}$	$\xi(c_{\#})$	
2	0.15	0.66	9.62	16.60	0.041	4.5	0.01	0.05	0.84	1.45	0.041
2.1	0.32	0.87	6.35	10.20	0.029	4.75	0.03	0.07	0.52	0.84	0.028
2.2	0.92	1.37	3	4.70	0.014	5	0.12	0.15	0.24	0.28	0.011

Table 6.1. Computed values of the binodal ($c_b, c_{\#}$) and spinodal concentrations ($c_s, c_{\#}$) (mol/l) for various ion diameters (\AA) at $T = 300 \text{ K}$.

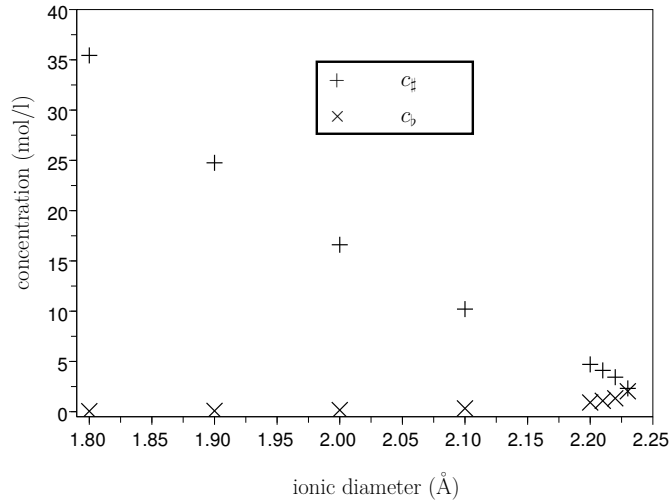


Fig. 6.3. Binodal values ($c_b, c_{\#}$) (mol/l) for $Z = 2$ at $T = 300 \text{ K}$ for various ion diameter.

6.2 Confined electrolytes: Theory and method

We now turn to confined electrolytes. As in the previous chapters, the physical domain containing the counterions is denoted Ω with reference length scale L_* , and we suppose that there is a

negatively charged surface $\partial\Omega_S$. We consider two geometries: a nanochannel with flat (1D) or wavy walls (2D) and a network of inclusions (2D). In the case of flat nanochannel, $\Omega := [0, L_*]$ so that $\partial\Omega_S = \{0, L_*\}$. The nanochannel with wavy walls is described in § 6.3.2. The second 2D case consists in a reference cell minus a disk $D(R)$ of radius R so that $\Omega := [0, L_*]^2 \setminus D(R)$ with $\partial\Omega_S = \partial D(R)$.

We now describe the variational setting in which we solve the conservation equations involving the electrochemical potential depending on the electrostatic potential ψ and the ionic concentration c . In the situations where the bulk free energy of the system is non convex, we expect to observe a separation between a diluted and a condensed phase. A regularization is then needed to make precise the mathematical and numerical setting.

6.2.1 Canonical constraints and thermodynamic equilibrium

The physical setting can be described by a thermodynamic potential which is the free energy functional of the system. In a canonical setting, the mean ionic concentration is prescribed in the form

$$\langle c \rangle_\Omega = c^{\text{bulk}}, \quad (6.19)$$

where $\langle \cdot \rangle_\Omega$ denotes the mean value over Ω . The thermodynamic potential we consider is given by

$$\mathcal{F}(c) := \mathcal{F}_{\text{bulk}}(c) + \mathcal{F}_{\text{mf}}(c). \quad (6.20)$$

The bulk free energy $\mathcal{F}_{\text{bulk}}$ functional is defined by (6.14). Moreover, letting $\rho(c) := Zec$ denote the charge density, there holds for the mean-field energy \mathcal{F}_{mf} ,

$$\mathcal{F}_{\text{mf}}(c) = \frac{1}{2} \left(\int_\Omega \rho(c) \Psi_{\Sigma_S}(\rho(c)) - \int_{\partial\Omega_S} \Sigma_S \Psi_{\Sigma_S}(\rho(c)) \right) = \frac{\varepsilon}{2} \int_\Omega |\nabla \Psi_{\Sigma_S}(\rho(c))|^2, \quad (6.21)$$

as discussed in Section 4.2. The non-local affine operator Ψ_{Σ_S} is defined by (4.25) in Section 4.2, while Ψ_0 denotes the linear operator associated with homogeneous Neumann boundary conditions. We assume that the datum c^{bulk} in the canonical constraint (6.19) satisfies the global electroneutrality condition

$$Zc^{\text{bulk}} = \frac{1}{|\Omega|} \int_{\partial\Omega_S} \frac{1}{e} \Sigma_S. \quad (6.22)$$

As discussed in Section 4.2, a minimizer of the free energy functional under the canonical constraint (6.22) solves (at least formally)

$$\mu(c) + Ze\Psi_{\Sigma_S}(\rho(c)) = \mu^{\text{bulk}} \quad \text{in } \Omega, \quad \langle c \rangle_\Omega = c^{\text{bulk}}, \quad (6.23)$$

for a suitable constant μ^{bulk} . A major issue of the above statement is that without convexity properties of the functional $\mathcal{F}_{\text{bulk}}$, uniqueness of a solution to the minimization problem is lost.

6.2.2 Mechanical equilibrium

We briefly recall the notion of mechanical equilibrium in a confined ionic system, see Section 4.2.6. Mechanical equilibrium can be described by the fact that the gradient of the osmotic pressure balances the Coulomb force:

$$-\nabla p_{\text{osm}}(c) = Zec\nabla\psi, \quad (6.24)$$

Denoting $E = -\nabla\psi$, the electric field, it is convenient to introduce the total pressure tensor Π defined by

$$\Pi := -\frac{\varepsilon}{2} \left(2E \otimes E - |E|^2 \text{I}_d \right) + p_{\text{osm}}(c) \text{I}_d. \quad (6.25)$$

Mechanical equilibrium is then expressed by the fact that the tensor Π is divergence free. If there is phase separation, the normal component of Π remains continuous at the interface between the two phases, and the zero divergence condition is understood in the distributional sense.

6.2.3 Regularizations

We now present two regularizations needed to carry the numerical study of the model. The first regularization is to consider the convex hull of the bulk free energy density leading to

$$\mathcal{F}_{\text{bulk}}^{\star\star}(c) := \int_{\Omega} f^{\star\star}(c), \quad \mathcal{F}^{\star\star}(c) := \mathcal{F}_{\text{bulk}}^{\star\star}(c) + \mathcal{F}_{\text{mf}}(c). \quad (6.26)$$

By construction of $f^{\star\star}$, the functional $\mathcal{F}_{\text{bulk}}^{\star\star}$ is convex in the variable c , but not strictly convex in c since the second derivative of $f^{\star\star}$ cancels for $c \in [c_{\flat}, c_{\sharp}]$.

Remark 13 (*Computation of the convex hull of the functional $\mathcal{F}_{\text{bulk}}$*). *The definition of $\mathcal{F}_{\text{bulk}}^{\star\star}$ by (6.26) is a priori only a definition. We can verify that we have the identity*

$$(\mathcal{F}_{\text{bulk}}(c))^{\star\star} = \mathcal{F}_{\text{bulk}}^{\star\star}(c), \quad (6.27)$$

for the $L^2(\Omega)$ -weak topology. This result is obtained under mild-assumptions on the function f that are fulfilled in our case (positivity up to a trivial shift, growth conditions, and regularity) as we have seen in Section 6.1.5 (see [27, Chap. IX, Sec. 2, Prop. 2.3]).

From a physical viewpoint, finding a minimizer of $\mathcal{F}^{\star\star}$ seems more pertinent since we expect that a single sharp interface will separate Ω into a diluted and a condensed phase, so that c will not take values in the interval (c_{\flat}, c_{\sharp}) .

From the numerical viewpoint, finding a minimizer of $\mathcal{F}^{\star\star}$ under the canonical constraint (6.22) or solving the corresponding Euler–Lagrange equations is not an easy task since we do not know a priori where the sharp interface is located in Ω . In order to circumvent this difficulty, we introduce a second regularization, which penalizes in a least-squares way the gradient of the concentration. This leads to the modified free energy functional

$$\mathcal{F}_{\kappa}^{\star\star}(c) := \mathcal{F}^{\star\star}(c) + \mathcal{F}_{\kappa}(c), \quad \mathcal{F}_{\kappa}(c) := \left(\frac{\kappa^2 L_*^3}{2\beta} \right) \int_{\Omega} |\nabla c|^2, \quad (6.28)$$

with $\kappa > 0$ a length parameter (expressed in m). The role the gradient term is to penalize the oscillations that can appear in a minimizer of the functional $\mathcal{F}^{\star\star}$. This type of regularization is commonly introduced in phase-field theory, and there is an extensive bibliography about the $\kappa \rightarrow 0$ process in bulk environment, process also known as the sharp interface limit. The situation here is different owing to the presence of the gradient of the electrostatic potential resulting from the surface charge density carried by the walls. We also introduce the non-dimensional number

$$\ell = \left(\frac{\kappa}{L_*} \right)^2, \quad (6.29)$$

that will be used in the numerical studies. In what follows, we denote c_κ a solution of the constrained minimization problem of \mathcal{F}_κ^{**} under the constraint (6.22), and we also set $\psi_\kappa := \Psi_{\Sigma_S}(\rho(c_\kappa))$.

The equilibrium equation after both regularizations is expressed as

$$\begin{cases} - \left(\frac{\kappa^2 L_*^3}{\beta} \right) \Delta c_\kappa + \mu^{**}(c_\kappa) + Ze\psi_\kappa = \mu_\kappa^{\text{bulk}} & \text{in } \Omega, \\ \nabla c_\kappa \cdot \mathbf{n} = 0 & \text{on } \partial\Omega, \quad \langle c_\kappa \rangle_\Omega = c^{\text{bulk}}. \end{cases} \quad (6.30)$$

Remark 14 (*Boundary condition on c_κ*). *The homogeneous Neumann boundary condition enforced on c_κ results from the penalty term and induces a boundary layer of the concentration since the gradient of the concentration near the boundary is not expected to be zero. It is possible to enforce a nonlinear boundary condition that corrects this phenomenon. Indeed, the equation that we expect for (6.30) when $\kappa \rightarrow 0$ expresses the constancy of the convexified chemical potential, so that (assuming that c_κ is smooth near the boundary), we have*

$$\nabla(\mu^{**}(c_\kappa) + Ze\psi_\kappa) \cdot \mathbf{n} = 0, \quad \text{on } \partial\Omega_S,$$

Using the boundary condition satisfied by ψ_κ leads to the boundary condition

$$\mu^{**'}(c_\kappa) \nabla c_\kappa \cdot \mathbf{n} = \frac{Z\Sigma_S \varepsilon}{e}, \quad \text{on } \partial\Omega_S.$$

Using this condition, we have to verify that $(\mu^{**}')'(c_\kappa)$ actually does not cancel on $\partial\Omega_S$. This is generally the case in our numerical simulations (see Section 6.3) since the interface is located at a positive distance of $\partial\Omega_S$ for $\kappa > 0$. After this verification, the nonlinear boundary condition can be enforced by a fixed point iterative process. The interest of this condition is to obtain the correct behaviour of the concentration near the boundary for $\kappa > 0$. Of course, the artificial boundary layer disappears in the sharp interface limit. In what follows, we use the simpler homogeneous Neumann boundary condition in (6.30).

Mathematical issues concerning the minimizers of the various above functionals are discussed in Section 6.5. In the next sections, we carry a numerical study of the limit behaviour $\kappa \rightarrow 0$.

6.2.4 Discretization and nonlinear solver

For the discretization, we adopt a conforming finite element formulation both for the electrostatic potential and the concentration. The discrete variational formulation can be written: Find $(c_\kappa, \psi_\kappa, \lambda_\kappa^{\text{el}}, \mu_\kappa^{\text{bulk}}) \in (X_h)^2 \times \mathbb{R}^2$ such that $\forall(\varphi, v, p, q) \in (X_h)^2 \times \mathbb{R}^2$:

$$\begin{cases} \int_\Omega \varepsilon \nabla \psi_\kappa \cdot \nabla \varphi + \lambda_\kappa^{\text{el}} \langle \varphi \rangle_\Omega = \int_\Omega \rho(c_\kappa) \varphi - \int_{\partial\Omega_S} \Sigma_S \varphi, \\ p \langle \psi_\kappa \rangle_\Omega = 0, \\ \int_\Omega \left(\frac{\kappa^2 L_*^3}{\beta} \right) \nabla c_\kappa \cdot \nabla v + (\mu^{**}(c_\kappa) + Ze\psi_\kappa) v = \int_\Omega \mu_\kappa^{\text{bulk}} v, \\ q \langle c_\kappa \rangle_\Omega = qc^{\text{bulk}}. \end{cases} \quad (6.31)$$

The finite dimensional vector space X_h is typically the space of conforming piecewise \mathbb{P}_1 functions.

To solve the discrete algebraic system of nonlinear equations that we cast into the form

$$\mathcal{J}(y_h) = 0, \quad y_h = (c_\kappa, \psi_\kappa, \lambda_\kappa^{\text{el}}, \mu_\kappa^{\text{bulk}}),$$

we use a Newton–Raphson algorithm by computing analytically the Jacobian of \mathcal{J} (analogous to the one introduced in Chapter 5). The Newton–Raphson algorithm is initialized with a ionic concentration c_κ^0 (such that the constraint of global electroneutrality is fulfilled) and $\psi_\kappa^0 = \Psi_{\Sigma_S}(\rho(c_\kappa^0))$. The convergence of the algorithm can be checked by monitoring the evolution of three quantities, at iteration $k \geq 0$:

- (i) The norm of the residual of the problem $\mathcal{E}_{\text{cvg}}^{1,k} = \|\mathcal{J}(y_h^k)\|$;
- (ii) The norm of the difference between two successive iterates $\mathcal{E}_{\text{cvg}}^{2,k} = \|y_h^{k+1} - y_h^k\|$;
- (iii) The discrete free energy $\mathcal{F}_\kappa^{\text{**}}(c_\kappa^k)$;

By fixing a tolerance value $0 < \text{tol} \ll 1$, convergence of the iterative process is achieved if we have $\mathcal{E}_{\text{cvg}}^{1,k} < (\mathcal{E}_{\text{cvg}}^{1,0} \text{tol})$ and $\mathcal{E}_{\text{cvg}}^{2,k} < (\mathcal{E}_{\text{cvg}}^{2,0} \text{tol})$. The main difference with the setting of Chapter 5 is that, in practice, the value of the parameter κ is of paramount importance regarding the convergence properties of the method since the problem is harder to solve for small κ when initialized with a constant value. In general, a continuation process has to be performed to achieve the sharp interface limit $\kappa \rightarrow 0$ by diminishing progressively the value of κ . Another numerical issue is that the second derivative of $f^{\text{**}}$ is discontinuous at the binodal points so that the Newton–Raphson algorithm is non-smooth. Additionally, a phenomenon that can occur in practice is that the concentration c_κ^k takes negative values or values such that the packing number $\xi(c_\kappa^k) > 1$. A correction is then needed leading to the following clipping

$$s_{c_{\min}, c_{\max}}(c) = \begin{cases} c_{\min}, & c \leq c_{\min}, \\ c, & c_{\min} < c \leq c_{\max}, \\ c_{\max}, & c_{\max} < c. \end{cases} \quad (6.32)$$

with concentrations c_{\min} and c_{\max} carefully chosen depending on the state of the system (mildly or highly charged). In practice, we can chose c_{\max} such that $\xi(c_{\max}) \leq 0.7$ to remain in the domain of validity of the Carnahan–Starling formula. By using this correction, we are able to obtain convergence of the Newton–Raphson algorithm in all the studies considered in this work.

The general Newton–Raphson algorithm is then performed as follows:

- (i) Initialize with a chosen y_h^0 (typically y_h^{old} coming from a previous successful computation for a larger value of κ); set $k = 0$;
- (ii) For $k \geq 0$, iterate in the Newton–Raphson algorithm $y_h^k \rightarrow y_h^{k+1}$:
 - ii(a) Solve the linear system;
 - ii(b) Clip the concentration by setting: $\tilde{c}_\kappa^{k+1} = s_{c_{\min}, c_{\max}}(c_\kappa^{k+1})$;
 - ii(c) Rescale the concentrations to enforce the global electroneutrality condition;

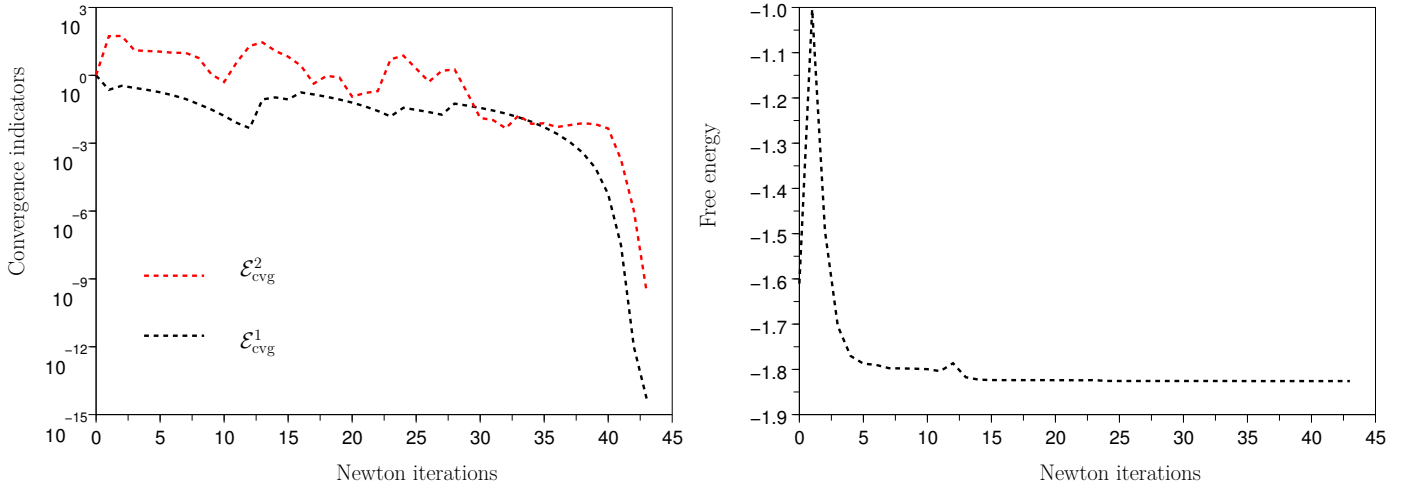


Fig. 6.4. Convergence indicators for the Newton–Raphson algorithm.

(iii) Check convergence; if satisfied stop, else set $k = k + 1$ and return to step (ii).

In practice, the first initialization in step (i) of the Newton–Raphson algorithm is done with the constant value $c_\kappa^0 = c^{\text{bulk}}$. Figure 6.4 depicts the convergence process of the Newton algorithm. The physical parameters were chosen to be $L_* = 10^{-9}$ m, $\Sigma_S = 0.1$ Cm⁻², $T = 300$ K, $Z = 3$, and $\sigma = 4.5$ Å. We chose κ so that the value of the nondimensional parameter defined by (6.29) is $\ell = 10^{-6}$. The energy curve is a decreasing function of the number of iterations until the 6th iteration where the clipping makes the energy increase locally. This behaviour happens here only at this iteration, and more generally, we observed that it happens only at a very few iterations. This is confirmed by the behaviour of the convergence indicators both going to zero. Notice also that with the above physical parameters, the maximal packing number is approximately equal to $0.08 \ll 1$.

6.2.5 Validation test cases

In this section, we provide a numerical assessment of the sharp interface limit (that is $\kappa \rightarrow 0$) to solve the phase separation problem. The protocol consists in computing approximations of the function c_κ obtained at convergence of the Newton–Raphson algorithm and to monitor, as κ goes to 0, the convergence of the quantity

$$E_\kappa^X := \|c_\kappa - c_{\kappa \rightarrow 0}\|_X,$$

where X denotes a functional space (*e.g.* $L^p(\Omega)$ functions for $p \in [1, \infty]$), and $c_{\kappa \rightarrow 0}$ is a solution actually computed with $\kappa = 0$, after the continuation process. The meshes used for these computations are adapted to the presence of the sharp interface and are smoothly refined in order to capture the steep variation of the concentrations for $\kappa > 0$. We consider the same geometric settings as in Section 5.3. Recall that owing to symmetries, we discretize only the half interval for the 1D case and a quarter of the domain for the 2D case with inclusions. Mesh resolution is increased using local adaptation around the interface. For example, in 1D, the numerical protocol for this procedure is as follows:

- (i) Fix $\kappa > 0$ and a coarse mesh $\mathcal{T}_{\delta x}$ with nodes $x_0 = 0 < \dots < x_N = 0.5L_*$ with $x_k = k\delta x$ and $\delta x = \frac{L_*}{2N}$;
- (ii) Compute the discrete solution in the space of conforming piecewise \mathbb{P}_1 functions $\{c_\kappa^k, 0 \leq k \leq N\}$;
- (iii) Determine x_{inter} by sorting c_κ^k (in descending order) and finding

$$x_{\text{inter}} = \operatorname{argmin}_{0 \leq k \leq N} \left\{ c_\kappa^k \leq \frac{c_b + c_\#}{2} \right\};$$

- (iv) Adaptive mesh generation: local refinement around x_{inter} by defining three types of nodes:
- N_{inter} nodes in the interval $(x_{\text{inter}} - \delta, x_{\text{inter}} + \delta)$ (diffuse interface zone);
 - N_{bulk} nodes in the interval $(x_{\text{inter}} + \delta, 0.5L_*)$ (diluted phase);
 - $N_{\partial\Omega_S}$ nodes in the interval $(0, x_{\text{inter}} - \delta)$ (condensed phase);
- for a real number $\delta > 0$ small enough and regularize the nodes distribution *e.g* by solving a Laplace equation $-\nu\Delta u + u = f$ with f the bijective node distribution function, and $0 < \nu \ll 1$ a small real parameter.

In practice, the integers $(N_{\text{inter}}, N_{\text{bulk}}, N_{\partial\Omega_S})$ are such that $N_{\text{bulk}} < N_{\partial\Omega_S} < N_{\text{inter}}$ and can be computed adaptively from the knowledge of the discrete derivatives of c_κ . The procedure can be reproduced in the 2D case for more complex geometries by using adaption tools of the FreeFEM++ library. Figures 6.5 depicts the meshes typically generated by the above protocol and that we used in our numerical studies.

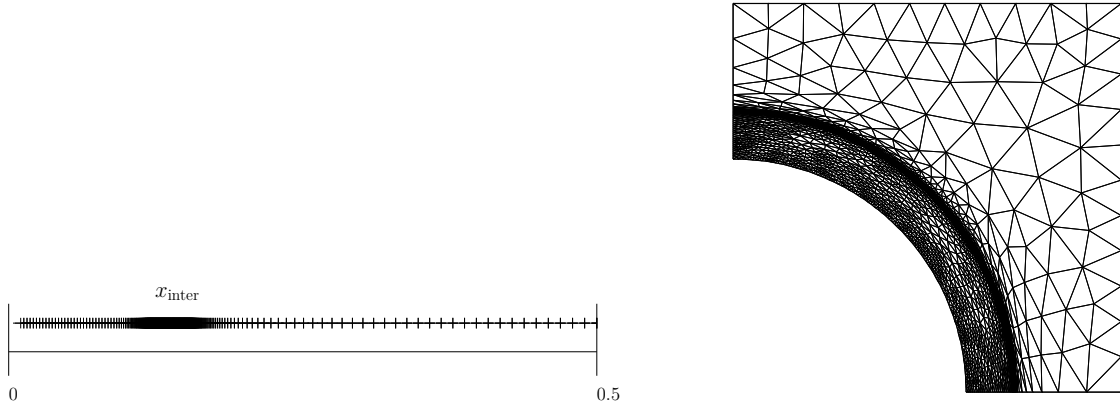


Fig. 6.5. Left: 1D refined mesh; Right: 2D refined mesh.

Asymptotic $\kappa \rightarrow 0$: convex case

Let us consider a convex case for the 1D setting, for example divalent counterions of diameter equal to 4.5 \AA , for which $f^{**}(c) = f(c)$. We choose $L_* = 10^{-9} \text{ m}$, $\Sigma_S = 0.1 \text{ Cm}^{-2}$, $T = 300 \text{ K}$ for

the physical parameters defining the state of the system. Figure 6.6 depicts the convergence of $E_\kappa^{L^\infty}$ to 0 with an estimated rate $\alpha \sim 1$. The horizontal axis uses the nondimensional parameter ℓ defined by (6.29). This kind of behaviour is expected since the solution of (6.23) does not present any discontinuity in this case.

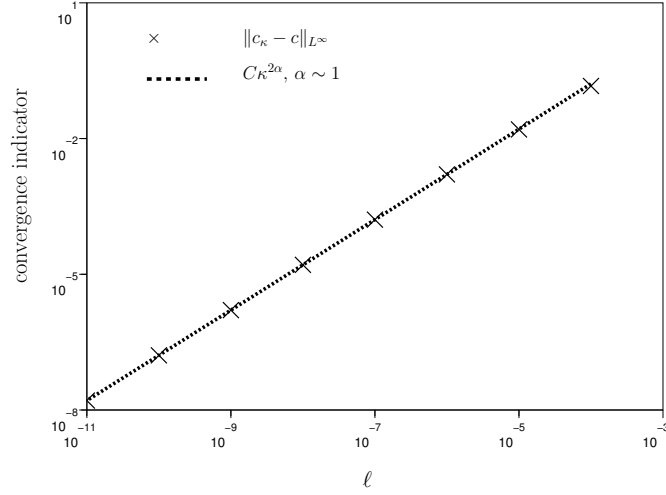


Fig. 6.6. Asymptotic $\kappa \rightarrow 0$ for $E_\kappa^{L^\infty}$: convex case with divalent counterions of diameter 4.5 Å.

Asymptotic $\kappa \rightarrow 0$: non convex case

We choose now $L_* = 10^{-9}$ m, $\Sigma_S = 0.1 \text{Cm}^{-2}$, $T = 300$ K, $Z = 3$, and $\sigma = 4.5$ Å (resulting in a non convex bulk free energy density). We consider both the 1D setting (flat nanochannel) and the 2D setting (cylindrical inclusions). For the 2D case, the radius of the disk is chosen equal to $R = 0.3L_*$. The results are presented in Figure 6.7 for the 1D and 2D cases. We observe numerically a convergence of the quantity $E_\kappa^{L^1}$ with an estimated rate $\alpha \sim \frac{1}{3}$ (the quantity $E_\kappa^{L^\infty}$ does not converge to 0 as expected for discontinuous solutions). We observe in Figure 6.8 (flat nanochannel) that the quantity L^∞ -error concentrates in the interface zone, whereas the solutions coincide almost exactly outside this part of the domain for all values of κ (reasonably small).

6.3 Confined electrolytes: Numerical results

We investigate the dependence on the geometric length scale L_* of the equilibrium properties such as concentration and pressure. To do so, we fix a surface charge density Σ_S and we study the dependence of the computed solutions versus L_* . Simulations are performed for $L_* > \sigma$ (although values of L_* close to σ are not realistic in a continuous modelling, see Remark 4). We recall that there are three length scales in the problem: the characteristic size of the elementary cell L_* , the ion diameter σ , and the Bjerrum length L_B . We also recall the definition of a reference Debye length L_D^* and the non-dimensional ratio λ such that

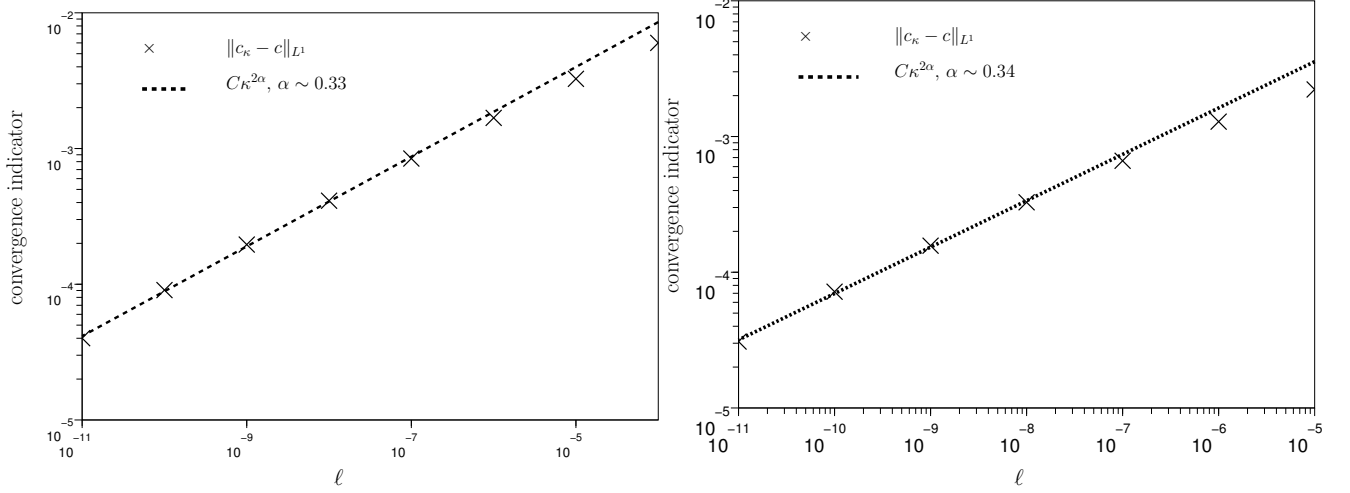


Fig. 6.7. Asymptotic $\kappa \rightarrow 0$ for $E_\kappa^{L^1}$: non convex case for trivalent counterion of diameter 4.5 \AA . Left: Flat nanochannel; Right: Cylindrical inclusion.

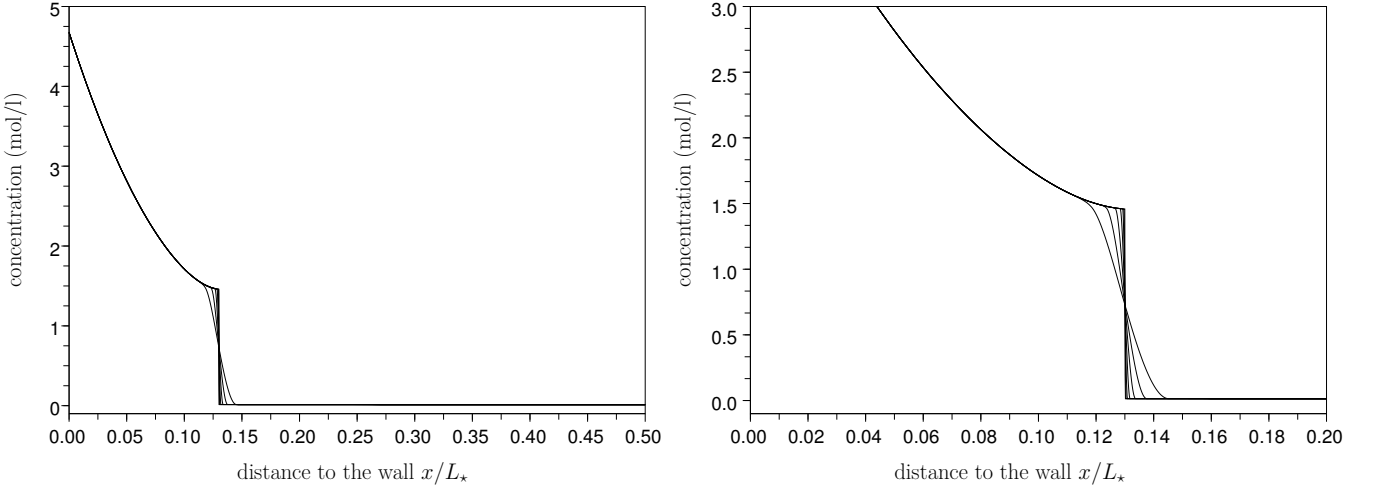


Fig. 6.8. Asymptotic $\kappa \rightarrow 0$ in the non convex case. Concentrations profiles for trivalent counterions of diameter 4.5 \AA ; Left: Concentration profiles for various values of κ in the domain Ω (1D); Right: Zoom close to the interface.

$$L_D^* := \sqrt{\frac{L_*^3}{4\pi L_B}}, \quad \lambda := \left(\frac{L_D^*}{L_*}\right)^2 = \frac{L_*}{4\pi L_B}, \quad (6.33)$$

the reference Debye length L_D^* corresponding to the choice of L_*^{-3} for the reference concentration. The Debye length represents the scale over which the ions screen out the electric field, while the Bjerrum length measures the length below which thermal effects are negligible.

6.3.1 Flat nanochannel

We start by considering the case of the flat nanochannel, for which L_* is the spacing between the two charged planes. For this simple geometry, we can determine an interval $[L_\sharp, L_b]$ for which

we know *a priori* there will be a phase separation. This interval corresponds to values of L_* for which the average concentration c^{bulk} falls into the interval $[c_b, c_{\sharp}^*]$. Note that $L_* \in [L_{\sharp}^*, L_b]$ is only a sufficient condition for the appearance of phase separation. The average concentration of counterions in the system is given by

$$c^{\text{bulk}} = \frac{2\Sigma_S}{ZeL_*}, \quad (6.34)$$

owing to the global electroneutrality condition. In Figure 6.9 we observe that, for the length

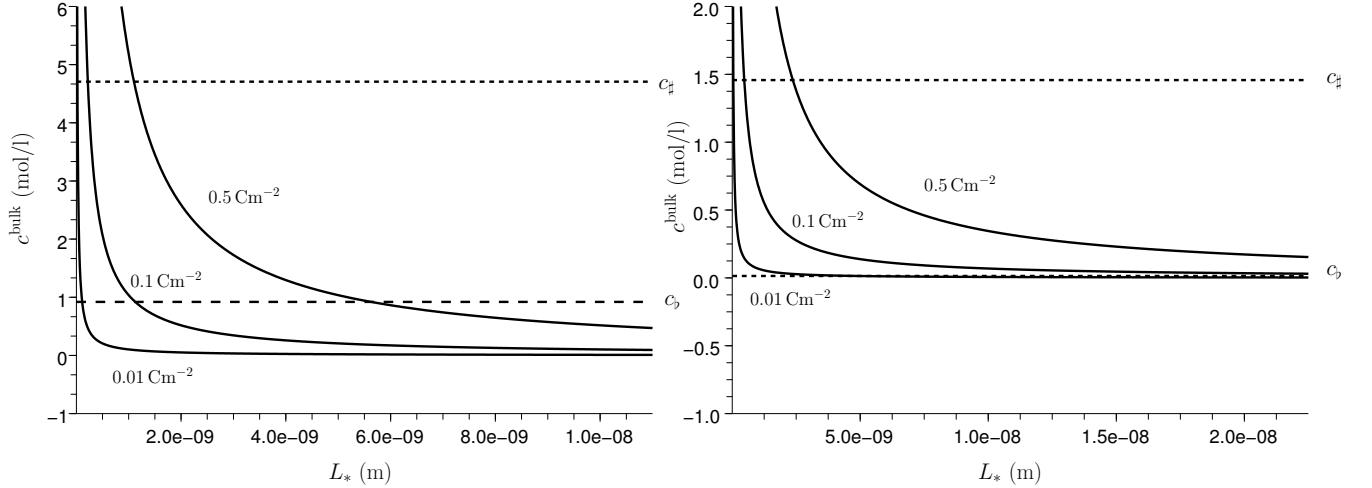


Fig. 6.9. Average concentration of counterions versus L_* . Left: divalent counterions with $\sigma = 2.2 \text{ \AA}$; Right: trivalent counterions with $\sigma = 4.5 \text{ \AA}$.

scales of interest, phase separation occurs for a wide range of surface charge densities for trivalent counterions. Since the surface charge density has a strong influence on the heterogeneity of the concentrations profiles, a finer analysis is needed to determine necessary conditions on L_* below which the discontinuity actually appears. For instance, we determine a critical length L_{\sharp}^{crit} for which the discontinuity does not occur by calculating several solutions for $L_* < L_{\sharp}^{\text{crit}}$ and using affine extrapolation in the concentration at the mid-plane $c(x_{\text{mid}})$ (with $x_{\text{mid}} = 0.5L_*$) to the value c_{\sharp}^* . Since the concentration takes its minimal value at the mid-plane, the determined value L_{\sharp}^{crit} corresponds to the first value of L_* where the concentration at mid-plane reaches the binodal value c_{\sharp}^* . Finally, as seen in Figure 6.9, the value of L_b typically exceeds 10^{-8} m. As we do not consider much larger scales, L_b^{crit} does not enter in this range of length scales except for small surface charge densities which we do not consider here. Values for L_{\sharp}^* and L_{\sharp}^{crit} are reported in Table 6.2 for various Σ_S and σ .

We now turn to the behaviour of concentrations and pressure. Since we consider the 1D geometry, the total pressure of the system can be reduced to determining the osmotic pressure p_{osm} since the divergence-free constraint for the Maxwell tensor is equivalent to

$$\Pi(x) = p_{\text{osm}}(c(x)) - \frac{\varepsilon}{2} (\psi'(x))^2 = \alpha, \quad \alpha \in \mathbb{R}. \quad (6.35)$$

The pressure function Π is defined up to an additive constant that we fix to 0, assuming that when the spacing L_* goes to infinity, the pressure in the system is 0. The constant α in (6.35) is

$Z = 2 - \sigma = 2.2 \text{ \AA}$			$Z = 3 - \sigma = 4.5 \text{ \AA}$		
Σ_S	$L_\#$	$L_\#^{\text{crit}}$	Σ_S	$L_\#$	$L_\#^{\text{crit}}$
0.5	1.1	0.236	0.3	1.42	0.457
1	2.2	0.305	0.5	2.37	0.573

Table 6.2. Computed values of $(L_\#, L_\#^{\text{crit}})$ (nm) for various Σ_S (Cm^{-2}) at $T = 300 \text{ K}$.

equal to the total pressure of the system. Since $\psi'(x) = 0$ at $x_{\text{mid}} = 0.5L_*$, we evaluate the total pressure at mid-plane as $p_{\text{osm}}(c(x_{\text{mid}}))$. Note that, in general, the finite element approximation of Π does not satisfy exactly equation (6.35). Figure 6.10 depicts the concentration at mid-plane as a function of L_* , and Figure 6.11 depicts the total pressure as a function of L_* . Both figures compare the behaviour of the non-ideal model and the standard Poisson–Boltzmann model (for which the solution is analytic for a 1D flat nanochannel, see Section 5.3). Even if phase separation occurs, the total pressure is still a positive decreasing function of the spacing between the charged plates, and the total pressure expectedly goes to 0 as $L_* \rightarrow +\infty$ (up to spatial discretization error). Indeed, even if the concentration at mid-plane is a discontinuous function of L_* , using the convex hull of the bulk free energy density prevents the appearance of negative pressure in the system. Furthermore, we observe that the Poisson–Boltzmann theory almost always predicts a larger pressure than the pressure obtained with the non-ideal model. The difference is more pronounced in the case where L_* is greater than the critical length $L_\#^{\text{crit}}$ since in this case the non-ideal model predicts a pressure close to 0.

An interesting feature of the non-ideal model is that it introduces naturally the concept of effective charge considered in the literature to correct the Poisson–Boltzmann theory since this theory is known to estimate poorly the concentration of counterions near a wall in highly charged systems (*i.e.* for concentrated solutions). We define the total charge in the condensed phase as

$$\Sigma_{\text{cond}} = \frac{Ze}{|\Omega|} \int_{\{c > c_\#^{\text{crit}}\}} c(x) dx. \quad (6.36)$$

An interesting consequence of our results is that nearly 99% of the charge is contained in the condensed phase. This behaviour does not seem to be affected by the spacing between the charged plates meaning that the negative charges at the surface are almost completely screened by the counterions. Figure 6.12 depicts the position x_{inter} of the interface in $[0, 0.5L_*]$ as a function of L_* . Quite interestingly, x_{inter} is essentially equal to the ion radius ($\sigma/2$) regardless of the value of L_* , indicating that one layer of counterions screens out the negative surface charge. Comparing the left and right plots of Figure 6.12, we observe that high valences reduce the influence of L_* on the results.

6.3.2 Periodic network of charged inclusions and wavy channel

In the 2D setting, the total pressure tensor is given as the sum of the osmotic pressure and the Maxwell tensor

$$\Pi(x) = p_{\text{osm}}(x)\text{Id} - \tau_{\text{m}},$$

with

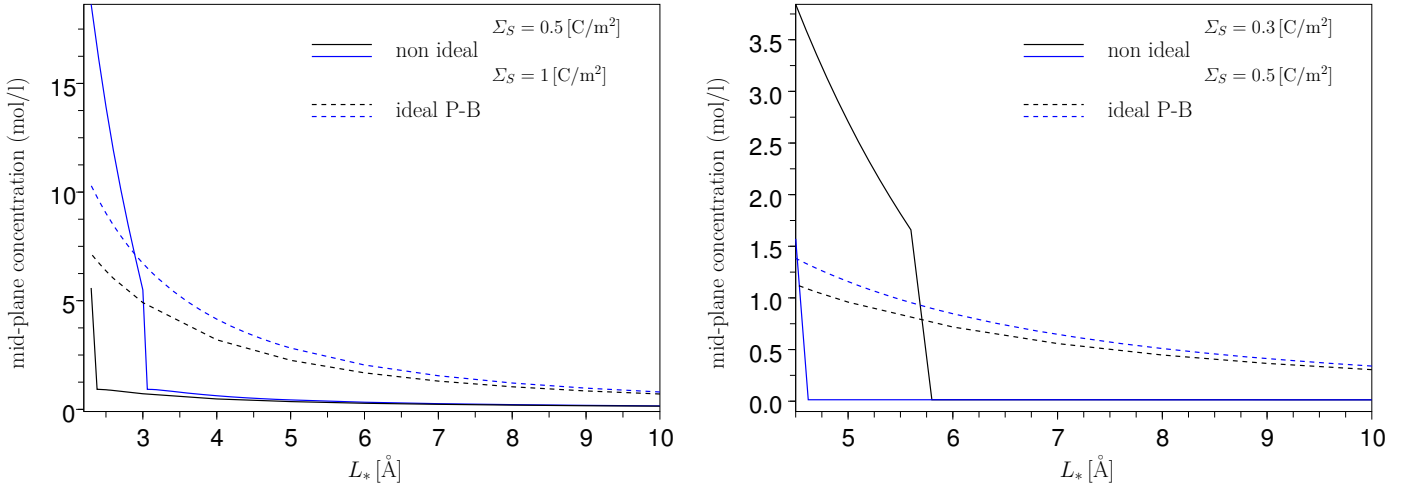


Fig. 6.10. Concentration at mid-plane as a function of L_* at temperature $T = 300$ K; Left: $Z = 2$, $\sigma = 2.2 \text{ \AA}$ and $\Sigma_S = 0.5, 1 \text{ Cm}^{-2}$; Right: $Z = 3$, $\sigma = 4.5 \text{ \AA}$, and $\Sigma_S = 0.3, 0.5 \text{ Cm}^{-2}$.

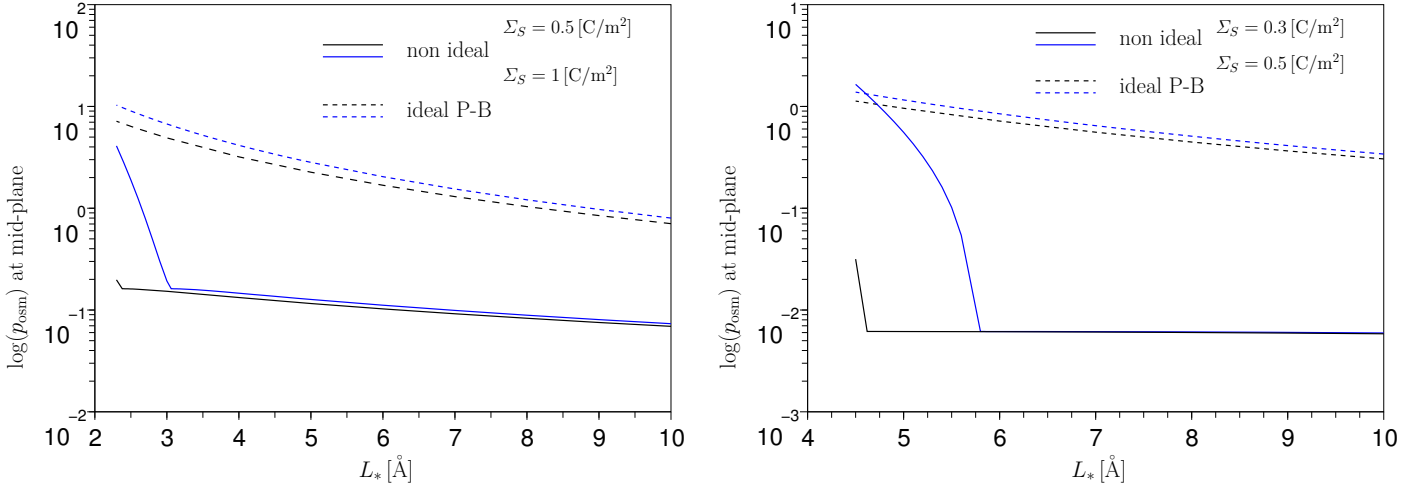


Fig. 6.11. Logarithm of the pressure at mid-plane as a function of L_* at temperature $T = 300$ K; Left: $Z = 2$, $\sigma = 2.2 \text{ \AA}$, and $\Sigma_S = 0.5, 1 \text{ Cm}^{-2}$; Right: $Z = 3$, $\sigma = 4.5 \text{ \AA}$ and $\Sigma_S = 0.3, 0.5 \text{ Cm}^{-2}$.

$$\tau_m = \frac{\varepsilon}{2} \left(2E \otimes E - |E|^2 \text{Id} \right),$$

(see Section 6.2.2). We evaluate the total pressure tensor at the upper right corner of the periodic cell since by symmetry, the electric field cancels at this point. Figure 6.13 depicts the concentration and the logarithm of the osmotic pressure at the cell corner. We observe the same kind of behaviour as for the case of a flat nanochannel regarding the monotonicity of the pressure as a function of L_* . In Figure 6.14, we present the shapes and positions of the interface for various values of L_* . We observe that the interface closely follows the shape of the charged object and that the thickness of the condensed phase depends weakly on the choice of the cell size L_* . Finally, we also present results for a periodic nanochannel with wavy walls. The waviness of the wall is described by a sinusoidal function of amplitude ζ . In this geometric setting, a high value for the waviness ($\zeta = 0.35L_*$) of the charged walls leads to the formation of a droplet of diluted phase, see Figure 6.15.

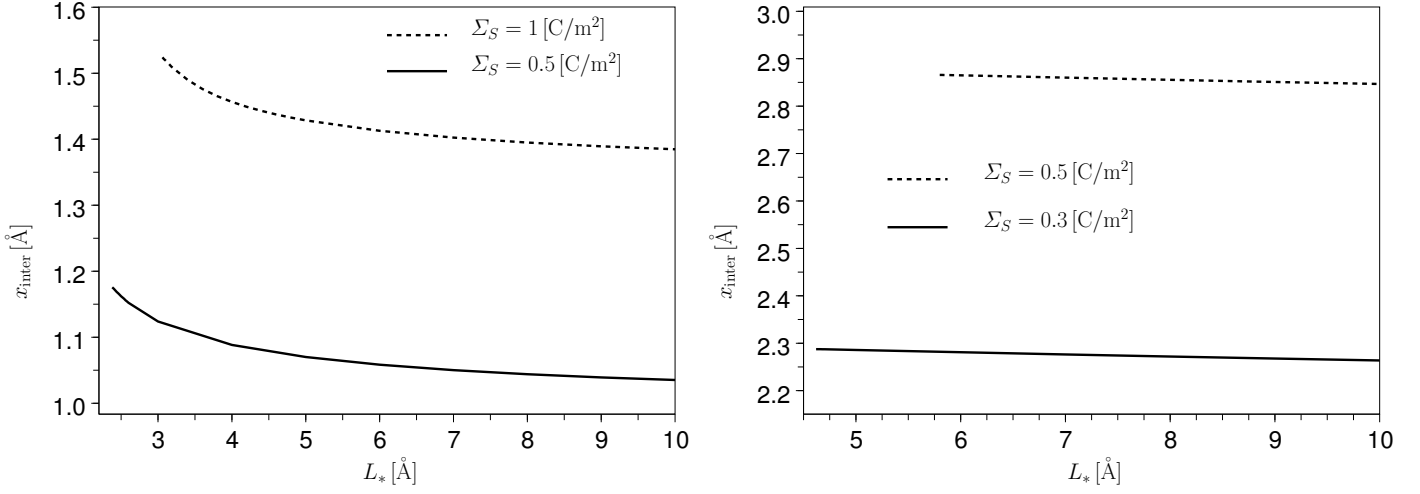


Fig. 6.12. Distance x_{inter} of the interface to the wall as a function of L_* at temperature $T = 300 \text{ K}$. Left: $Z = 2$, $\sigma = 2.2 \text{ Å}$, and $\Sigma_S = 0.5, 1 \text{ Cm}^{-2}$; Right: $Z = 3$, $\sigma = 4.5 \text{ Å}$, and $\Sigma_S = 0.3, 0.5 \text{ Cm}^{-2}$.

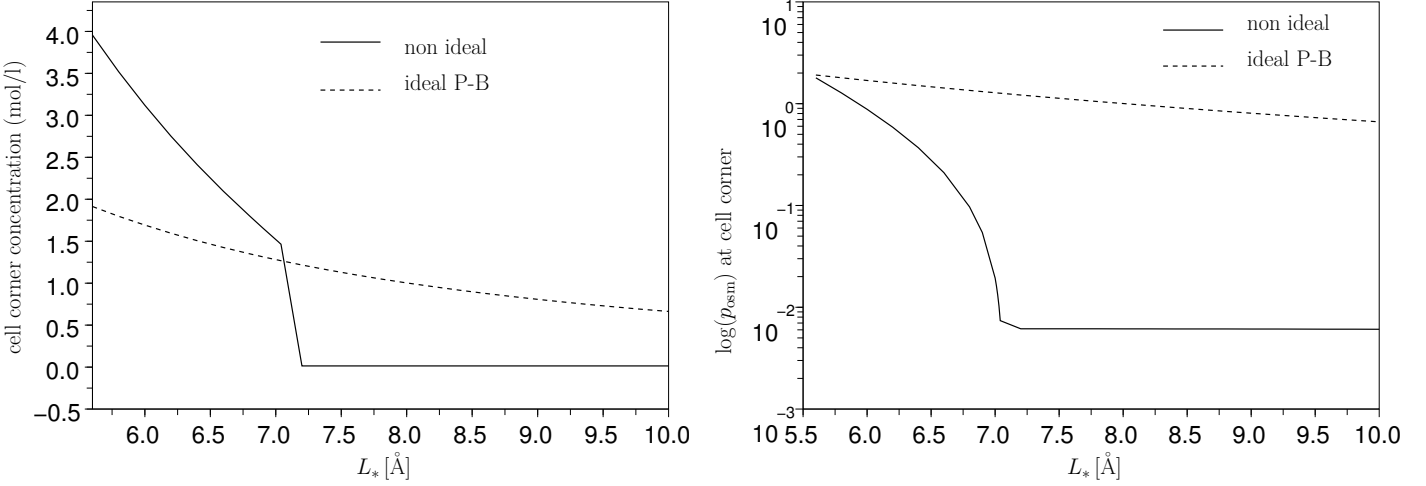


Fig. 6.13. Left: Concentration at the upper right cell corner as a function of L_* ; Right: Logarithm of pressure as a function of L_* at the upper right cell corner; $T = 300 \text{ K}$ for $Z = 3$, $\sigma = 4.5 \text{ Å}$, and $\Sigma_S = 0.5 \text{ Cm}^{-2}$.

6.4 An approach for symmetric salts

In the case where there is added salt to the counterions, the computation of the convex hull f^{**} is not straightforward since f becomes a bivariate function for which the Maxwell equal area rule cannot be applied. For symmetric salts (that is $Z_+ = -Z_-$ and equal diameters), we exploit the fact that the excess bulk free energy density is only a function of the total concentration

$$c_{\text{tot}} := c_+ + c_-, \quad (6.37)$$

since the ionic strength $I(c) = \frac{1}{2} \sum_{i=\pm} Z_i^2 c_i$ is proportional to c_{tot} . To emphasize this point, we rewrite the bulk excess free energy density as $f_{\text{corr}}(c_{\text{tot}})$ (with f_{corr} defined in Section 6.1). To handle the ideal term, we write the total bulk free energy density as

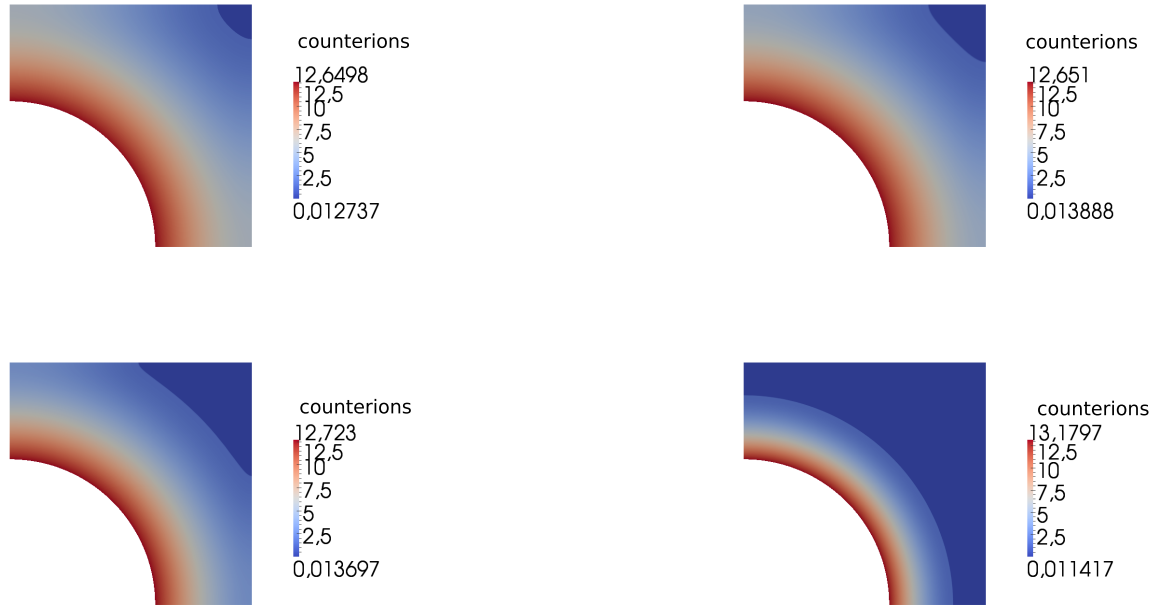


Fig. 6.14. Concentrations for $T = 300$ K, $Z = 3$, $\sigma = 4.5$ Å, $\Sigma_S = 0.5$ Cm $^{-2}$, and $L_* = \{7.6, 8.2, 10, 20\}$ Å (from left to right and top to bottom)

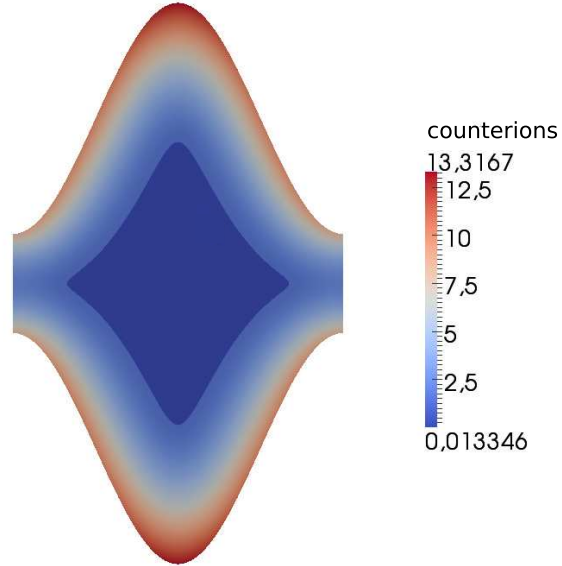


Fig. 6.15. Concentrations for $T = 300$ K, $Z = 3$, $\sigma = 4.5$ Å, $\Sigma_S = 0.1$ Cm $^{-2}$, $L_* = 10$ Å, and the channel waviness parameter $\zeta = 0.35$.

$$\begin{aligned}
 f(c) &= \beta^{-1} c_{\text{tot}} \left(\log \left(\sigma^3 c_{\text{tot}} \right) - 1 \right) + f_{\text{corr}}(c_{\text{tot}}) + \beta^{-1} \sum_{i=\pm} c_i \log \left(\frac{c_i}{c_{\text{tot}}} \right) \\
 &= \beta^{-1} \left(\sum_{i=\pm} c_i \left(\log \left(\sigma^3 c_i \right) - 1 \right) \right) + f_{\text{corr}}(c_{\text{tot}}).
 \end{aligned} \tag{6.38}$$

Then, we introduce the bivariate function f_{rel} and the univariate function f_{sum} such that

$$f_{\text{rel}}(c) = \beta^{-1} \sum_{i=\pm} c_i \log \left(\frac{c_i}{c_{\text{tot}}} \right), \quad (6.39)$$

and

$$f_{\text{sum}}(c_{\text{tot}}) := \beta^{-1} c_{\text{tot}} \left(\log \left(\sigma^3 c_{\text{tot}} \right) - 1 \right) + f_{\text{corr}}(c_{\text{tot}}). \quad (6.40)$$

This yields

$$f(c) = f_{\text{sum}}(c_{\text{tot}}) + f_{\text{rel}}(c). \quad (6.41)$$

The interesting feature is that the convex hull of f_{sum} is computable easily using the Maxwell equal area rule, while f_{rel} is a convex function of the concentrations $c = (c_+, c_-)$ (as easily verified). Computing the convex hull of the function f_{sum} , we are thus able to exhibit a convex function that provides a lower bound for f , but which is not necessarily f^{**} since we only have the inequality

$$f_{\text{sum}}^{**} + f_{\text{rel}} \leq f^{**}. \quad (6.42)$$

We refer to $f_{\text{sum}}^{**} + f_{\text{rel}}$ as the “pseudo” convex hull of f . We can perform computations accounting for added salt using this “pseudo” convex hull of f . To this purpose, we apply the same protocol as in the case of single counterions. The regularization is

$$\mathcal{F}_\kappa(c) := \frac{\kappa^2 L_*^3}{2\beta} \sum_{i=\pm} \int_\Omega |\nabla c_i|^2. \quad (6.43)$$

We observe in Figure 6.16 that phase separation occurs with only one interface. We also observe that, with the present approach, phase separation leads to avoiding concentrations in the region $\{c_+ + c_- \in (c_b, c_\#)\}$. This is shown in Figure 6.17 where $c_b, c_\#$ are now the binodal concentrations for the function f_{sum} . Interestingly, we also remark in Figure 6.16 that the coion concentration presents a bump in the condensed zone, creating an additional boundary layer within the condensed phase. This phenomenon is explained by the effective boundary condition satisfied by c_- (even in the limit $\kappa \rightarrow 0$) coming from the Neumann boundary condition on the electrostatic potential. It indicates that even if most of the coions lie in the condensed phase, they are repelled by the negative surface charge.

Remark 15 *A different problem is considered in the work of Carlen et al [17], where the authors consider a bulk fluid and observe phase separation and segregation into four states due to the presence of potentials presenting both attractive and repulsive features. In the present setting, we do not actually observe segregation between the two species.*

6.5 Some mathematical aspects

Returning to the one-species setting, we briefly discuss the existence, uniqueness, and properties of minimizers of the functionals \mathcal{F}^{**} and \mathcal{F}_κ^{**} . To simplify the discussion, we consider the case where the activity coefficient accounting for steric exclusion is $\gamma_{\text{HS}}(c) = \gamma_1^{\text{CS1}}(\xi(c))$ (defined by (6.9)), the extension to the general Carnahan–Starling expression requiring some additional work.

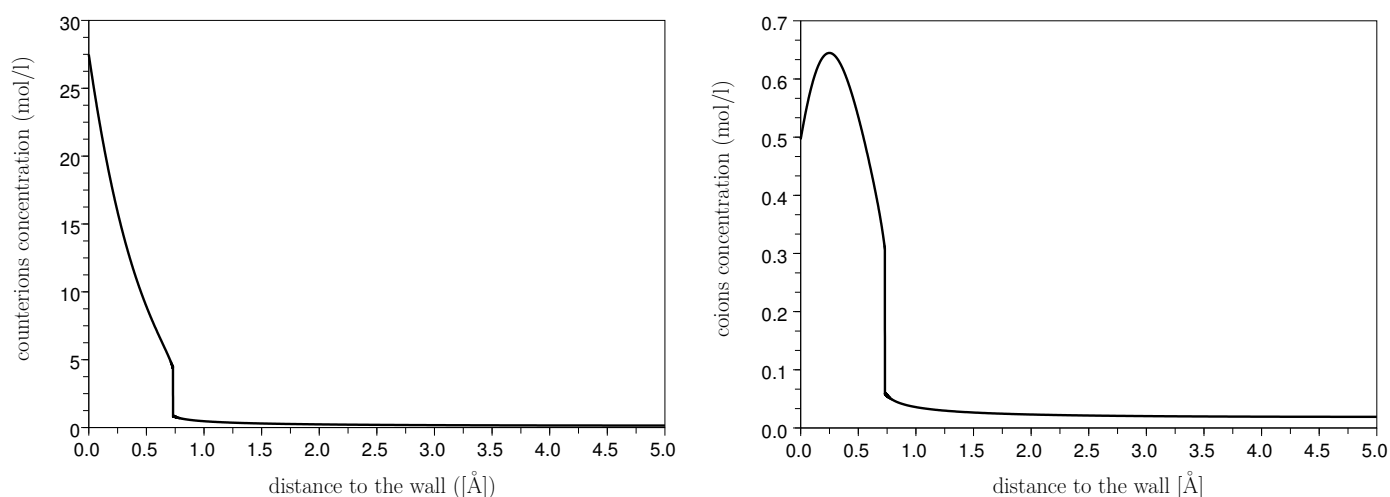


Fig. 6.16. Concentration of counterions (left) and coions (right) for a 2:2 mixture with 0.1 mol/l of added salt at $T = 300$ K, $\Sigma_S = 0.2$, $\sigma = 2.2$ Å, and $L_* = 10$ Å.

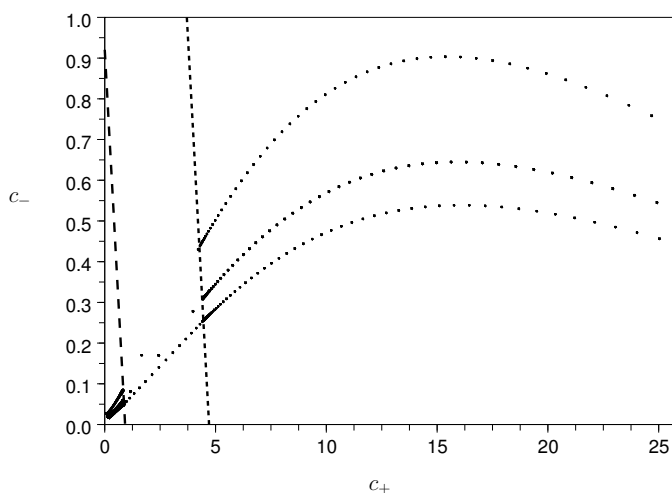


Fig. 6.17. Concentration of coions as a function of counterions for a 2:2 mixture with 0.1 mol/l of added salt at $T = 300$ K, $\Sigma_S = 0.2$, $\sigma = 2.2$ Å, and $L_* = \{8, 10, 16\}$ Å. The dashed lines delimit the binodal zone $c_b \leq c_+ + c_- \leq c_b$.

6.5.1 Minimizing properties of \mathcal{F}^{**}

We can apply almost all of the mathematical arguments developed in Chapter 5 to study existence and uniqueness of a critical point of \mathcal{F}^{**} . By a convexity argument, it is readily verified that the strictly convex functional \mathcal{F}^{**} , sum of the convex functional $\mathcal{F}_{\text{bulk}}^{**}$ and of the strictly convex functional \mathcal{F}_{mf} (see Section 4.2) possesses a unique minimizer $c \in L^2(\Omega)$ under the canonical constraint. To obtain a conclusion similar to the one of Theorem 7, the arguments of the proof of Lemmas 6 and 7 need to be adapted to the present setting since we used the particular form of the bulk free energy density, especially the structure of sum of the ideal term f_{id} and the non-ideal term f_{corr} . More precisely, the proof can be modified by defining the measurable set

$$A^n := \{x \in \Omega; c(x) > \max(2^n, c_\#)\},$$

and the measurable set

$$\Omega^n := \{x \in \Omega; 2^{-n} \leq c(x) \leq 2^n\}. \quad (6.44)$$

Then, we define $\tilde{\Omega}^n := \Omega^n \setminus \Omega_{b,\#}$ where the metastable/unstable zone $\Omega_{b,\#}$ is defined by

$$\Omega_{b,\#} := \{x \in \Omega; c(x) \in [c_b, c_\#]\}. \quad (6.45)$$

By perturbing the concentrations in the set $\tilde{\Omega}^n$, the evaluation of free energy differences can be performed by considering the bulk free energy density f . With these modifications, we can adapt the proof of Lemmas 6 and 7 (which are in fact simpler in the one-species setting) and obtain the conclusions of Theorem 7.

6.5.2 Minimizing properties of \mathcal{F}_κ^{**}

The existence theory concerning a minimizer of \mathcal{F}_κ^{**} under the canonical constraint can be obtained by adapting the arguments of Chapter 5 (in particular, thereby modifying the convex subset \mathfrak{H} , *i.e.* by searching a concentration $c \in H_{\text{per}}^1(\Omega)$). Nevertheless, the main conclusions of Theorem 7 (upper and lower bounds) are not straightforward and require some additional material. Indeed, the strategy of proof based on the perturbation of the concentration needs to be adapted since an additional constraint for the perturbed concentration appears, being that the perturbed concentration needs to be of class $H_{\text{per}}^1(\Omega)$ (which is not the case in the proof of Lemmas 6 and 7).

6.5.3 Existing Γ -convergence results

The natural question is whether the unique minimizer of the functional \mathcal{F}_κ^{**} converges (in a certain sense, say in the L^2 sense) towards the unique minimizer of the functional \mathcal{F}^{**} as $\kappa \rightarrow 0$. The numerical results of Section 6.2.5 encourage us to address mathematically this question, in order to motivate the numerical method employed. The problem of convergence of the minimizers of the penalized problem is often addressed within the theory of Γ -convergence (see the book of Braides [15]). The Γ -convergence is a notion of convergence of functionals defined on a metric space, thus a metric topology need to be specified when dealing with this notion.

Definition 1 *Let (X, d) be a metric space and let $F_\epsilon : X \mapsto \overline{\mathbb{R}}$. Then, F_ϵ Γ -converges toward F_0 as $\epsilon \rightarrow 0^+$ if the following two conditions are satisfied for all $x \in X$:*

- (i) *(lim inf inequality) for all $x_\epsilon \rightarrow x$, $\liminf_{\epsilon \rightarrow 0^+} F_\epsilon(x_\epsilon) \geq F_0(x)$.*
- (ii) *(existence of a recovery sequence) there exists $\bar{x}_\epsilon \rightarrow x$ such that $\lim_{\epsilon \rightarrow 0^+} F_\epsilon(\bar{x}_\epsilon) = F_0(x)$.*

The convergence of minimizers of F_ϵ to the minimizers of F_0 requires the equi-coerciveness of the function F_ϵ . We may impose the following additional sufficient compactness condition to the definition of Γ -convergence (which ensures the convergence of the minimizers):

Definition 2 *Let (X, d) be a metric space and let $F_\epsilon : X \mapsto \overline{\mathbb{R}}$. Then, F_ϵ Γ -converges toward F_0 as $\epsilon \rightarrow 0^+$ if the following three conditions are satisfied for all $x \in X$:*

- (i) (compactness) for all $x_\epsilon \in X$ such that $|F_\epsilon(x_\epsilon)| < C$ for some $C > 0$, there is a subsequence $x_{\epsilon'}$ such that $x_{\epsilon'} \rightarrow x \in X$.
- (ii) (lim inf inequality) for all $x_\epsilon \rightarrow x$, $\liminf_{\epsilon \rightarrow 0^+} F_\epsilon(x_\epsilon) \geq F_0(x)$.
- (iii) (existence of a recovery sequence) there exists $\bar{x}_\epsilon \rightarrow x$ such that $\lim_{\epsilon \rightarrow 0^+} F_\epsilon(\bar{x}_\epsilon) = F_0(x)$.

Condition (i) is in fact too demanding, and most of the time we only need to verify equicoerciveness of the functional F_ϵ [15].

Often, the Γ -convergence of functionals of the form

$$F_\epsilon(u) := \int_{\Omega} W(u) + \epsilon^2 |\nabla u|^2, \quad (6.46)$$

is considered in the literature, where the bulk free energy density W is commonly a double-well potential. The theoretical studies concern the different convergence regimes of the functional F_ϵ , $\epsilon^{-\alpha} (F_\epsilon(x_\epsilon) - m)$, for $\alpha > 0$ and $m = \min_{u \in X} F_0(u)$, (development by Γ -convergence). In equation (6.46), the bulk free energy density itself is considered (rather than its convex hull). Theoretical questions often concern the shape and width of the interface in the framework of geometric measure theory [5]. The arguments developed in [79, Section 3, Proposition 4] may be adapted to our setting, since the bulk free energy functional \mathcal{F}_κ^{**} that we consider is only perturbed with the functional \mathcal{F}_{mf} which has nice properties of convexity and continuity, for example for the metric of L^2 -weak convergence. We provide the following result from [15] when $\Omega := [0, L_*]$ (the extension to 2D or 3D requiring some care).

Theorem 6.1. *Assume that the bulk free energy density $W : \mathbb{R} \rightarrow \mathbb{R}_{\geq 0}$ is continuous and fulfills a 2-growth condition of the form*

$$C' u^2 - C'' \leq W(u) \leq C(1 + u^2), \quad \forall u \in \mathbb{R}, \quad (6.47)$$

and that W is a double-well potential with two minima $c_1 < c_2$ so that $W(c_1) = W(c_2) = 0$. Let the functional \mathcal{F}_κ be defined by

$$\mathcal{F}_\kappa(c) := \begin{cases} \int_{\Omega} \left\{ W(c) + \frac{\kappa^2 L_*^3}{2\beta} |\nabla c|^2 \right\}, & \langle c \rangle_{\Omega} = c^{\text{bulk}}, c \in H^1(\Omega), \\ +\infty, & \text{otherwise,} \end{cases} \quad (6.48)$$

while \mathcal{F}^{**} is defined by

$$\mathcal{F}^{**}(c) := \begin{cases} \int_{\Omega} W^{**}(c), & \langle c \rangle_{\Omega} = c^{\text{bulk}}, c \in L^2(\Omega), \\ +\infty, & \text{otherwise.} \end{cases} \quad (6.49)$$

Then, we have the following Γ -convergence result:

$$\mathcal{F}^{**}(c) = \Gamma - \lim_{\kappa \rightarrow 0^+} \mathcal{F}_\kappa(c), \quad (6.50)$$

with respect to the $L^2(\Omega)$ -weak metric. Moreover, let c_κ be a minimizer of (6.48) for every $\kappa > 0$. Then, up to extraction of a sub-sequence, as $\kappa \rightarrow 0$, c_κ converges weakly in $L^2(\Omega)$ towards c , minimizer of (6.49).

This result somehow motivates the numerical method described in Section 6.2. Let us give a few comments about the modifications that have to be performed to extend this type of result to the setting of equilibrium electrolytes. The first main modification is the addition of the mean-field free energy that couples the concentrations to the self-consistently computed electrostatic potential. The addition of such a term is in fact very simple in the framework of Γ -convergence owing to the stability of Γ -convergence with respect to continuous perturbation (with respect to the metric chosen). Owing to the compactness properties of Ψ_{Σ_S} as operator $L^2(\Omega) \mapsto H^2(\Omega) \hookrightarrow H^1(\Omega) \hookrightarrow L^2(\Omega)$ (the embeddings $H^2 \hookrightarrow H^1$ and $H^1 \hookrightarrow L^2$ being compact owing to the Rellich Theorem), we deduce that \mathcal{F}_{mf} defined by (6.21) is continuous with respect to the $L^2(\Omega)$ -weak metric (the convergence of the minimizers following from the fact that \mathcal{F}_{mf} is a positive functional and that $\mathcal{F}_\kappa(c)$ fulfills the compactness property owing to the 2-growth condition in the case of (CS1), the (CS) case requiring appropriate modifications).

The second modification concerns the properties of the bulk free energy density. A technical issue lies in the fact that for electrolytes, the bulk free energy density is defined on $\mathbb{R}_{\geq 0}$, since the concentrations are sought in a set of positive functions and the ideal free energy density

$$f_{\text{id}}(c) = \beta^{-1}c \left(\log(\sigma^3 c) - 1 \right), \quad c \geq 0, \quad (6.51)$$

(or the MSA term involving the square-root of c), forbids negative concentrations. Then, we need to verify that the Γ -convergence result of Theorem 6.1 is compatible with this constraint of positivity or maybe modifying the definition of f on $\mathbb{R}_{\leq 0}$. As we have seen in Section 6.1.5, for some physical parameters, we may prove that the bulk free energy density f has the double-well form of Theorem 6.1 in the case where f is evaluated with the ideal and non-ideal MSA and CS term. The existence of binodal concentrations $c_b, c_\#$ and μ^* allows us to build the convex hull of f , so that after affine shifting, the bulk free energy has the double-well form. Finally, the convergence of minimizers is in a weak L^2 sense which obviously is not entirely satisfactory.

Summary and perspective of future work (Part II)

In this second part of the thesis we considered a class of continuous models for electrolytes surrounded by a negatively charged solid object, based on the *Density Functional Theory* for ionic liquids.

In Chapter 4, we presented a formal derivation of the model. Several points still remain to be clarified both on the modelling and mathematical sides. An interesting question is to incorporate the steric exclusion effect between the ions and the negatively charged object. We believe that negative pressures observed in the work of Aguilar-Pineda, Jimenez-Angeles, Yu, and Lozada-Cassou [1] or in the works of Kjellander and Marceljà [58, 59] essentially lie in the presence of such an excluded volume effect. On the mathematical side, a clarification concerning the well-posedness of the Ornstein–Zernike equation and the various relations between the DFT and the Ornstein–Zernike equation is important in further understanding this class of models. Another question is to assess the accuracy of the approximations made in Section 4.4. These questions seem actually out of reach with the available mathematical tools.

In Chapter 5, we performed the mathematical analysis of the free energy for a two-species model when the bulk free energy density is a convex function of the concentrations (mild non-ideality). Extension of the obtained results to more general nonlinearities such as the Carnahan–Starling free energy density (6.12) would be appreciable. In fact, existence and uniqueness theory may be tackled in the same fashion by modifying appropriately the convex set where the ionic concentrations are sought. The main remaining difficulty is to prove the qualitative properties on the concentrations (uniform positive upper and lower bounds) in this singular case, leading to the Euler–Lagrange equations. We believe that the proof of Theorem 7 can be extended to this setting, perhaps by using suitable truncation or comparison principles.

In Chapter 6, we considered the case where the bulk free energy density is a non convex function of the concentration in a one-species setting, leading in general to phase separation (strong non-ideality). We derived an efficient numerical method that allowed us to perform numerical studies for a one-species setting and proposed an approach for the two-species setting. We observed that the model did not lead to negative pressures in contrast with the results obtained in [1, 58, 59]. On the mathematical side, the Γ -convergence result (Theorem 6.1) needs to be rigorously formalized in our setting. Nevertheless, such a result is only one step in the mathematical study of the minimizers of these regularized free energies. Indeed, the numerical simulations of the previous sections indicate that the minimizers of \mathcal{F}^{**} are discontinuous and

that the set $\Omega_{b,\sharp}$ defined by (6.45) has a zero Lebesgue measure. It would be interesting to prove rigorously this result. We have also seen in the numerical results (see Figure 6.7) that the concentration c_κ appears to converge towards $c_{\kappa \rightarrow 0}$ in L^1 -norm with the rate $\kappa^{\frac{2}{3}}$ in the non convex setting and κ^2 in the convex setting. These results may require to study higher order developments by Γ -convergence for the functional \mathcal{F}_κ . A rigorous proof of these rates of convergence would be a nice result in the present setting. Questions concerning the shape and behaviour of the interface in a charged system similar to the one we considered have been addressed by Goldman, Muratov and Serfaty in [32], with the difference that there is no charged inclusion in their domains, but even in this case the mathematical analysis is quite intricate. Let us point out that the extension to several species setting might require some care in the mathematical analysis. From the numerical viewpoint, we have discussed in Section 6.1.5 the possibility to resort to a numerical evaluation of the double Legendre transform of the bulk free energy density in order to treat asymmetric electrolytes, and assess numerically the use of the pseudo-convex hull introduced in Section 6.4. Promising results have been achieved in this direction by Contento [20].

Finally, a comparison of the numerical results obtained with this class of continuous models with molecular dynamics or Brownian dynamics simulation should foster a deeper understanding of the physical and chemical properties of these complex systems.

Part III

Annexes

Other work in fluid mechanics and thermal modelling

8.1 Numerical study of a thin liquid film flowing down an inclined wavy plane

This work has been performed during a Master internship at CERMICS, École des Ponts Paris-tech, with a funding of ANR METHODE [76]. We investigated the stability of a thin liquid film flowing down an inclined wavy plane using a direct numerical solver based on a finite element/arbitrary Lagrangian Eulerian approximation of the free-surface Navier–Stokes equations. We studied the dependence of the critical Reynolds number for the onset of surface wave instabilities on the inclination angle, the waviness parameter, and the wavelength parameter, focusing in particular on mild inclinations and relatively large waviness so that the bottom does not fall monotonously. In the present parameter range, shorter wavelengths and higher amplitude for the bottom undulation stabilize the flow. The dependence of the critical Reynolds number evaluated with the Nusselt flow rate on the inclination angle is more complex than the classical relation (5/6 times the cotangent of the inclination angle), but this dependence can be recovered if the actual flow rate at critical conditions is used instead. This work has been published in a journal article [A1].

8.2 A multiscale problem in thermal science

This work has been performed during the 2011 CEMRACS Summer School at CIRM, Luminy. We considered a multiscale heat problem in civil aviation: determine the temperature field in a plane in flying conditions, with air conditioning. Ventilated electronic components in the bay bring a heat source, introducing a second scale in the problem. We considered three levels of modelling for the physical phenomena, which were applied to the two sub-problems: the plane and the electronic component. Then, having reduced the complexity of the problem to a linear non-symmetric coercive PDE, we used the reduced basis method for the electronic component problem. This work has been accepted for publication in ESAIM proceedings [A2].

References

- [1] G. E. Aguilar-Pineda, F. Jiménez-Ángeles, J. Yu, and M. Lozada-Cassou. Van der Waals-like isotherms in a confined electrolyte by spherical and cylindrical nanopores. *J. Phys. Chem. B*, 111:2033–2044, 2007.
- [2] G. Allaire, R. Brizzi, J-F Duf r che, A. Mikelić, and A. Piatnitski. Role of non-ideality for the ion transport in porous media: derivation of the macroscopic equations using upscaling. *in preparation*, 2012.
- [3] G. Allaire, A. Mikelić, and A. Piatnitski. Homogenization of the linearized ionic transport equations in rigid periodic porous media. *J. Math. Phys.*, 51:123103, 2010.
- [4] M. P. Allen and D. J. Tildesley. *Computer Simulation of Liquids*. Oxford science publications. Oxford University Press, USA, 1989.
- [5] L. Ambrosio, N. Fusco, and D. Pallara. *Functions of Bounded Variation and Free Discontinuity Problems*. Oxford science publication, 2000.
- [6] G. S. Anderson, R. C. Miller, and A. R. H. Goodwin. Static dielectric constants for liquid water from 300 K to 350 K at pressures to 13 MPa using a new radio-frequency resonator. *J. Chem. Engrg. Data*, 45:549–554, 2000.
- [7] P. Attard, D. J. Mitchell, and B. W. Ninham. Beyond Poisson-Boltzmann: images and correlations in the electrical double-layer. I Counterions only. *J. Chem. Phys.*, 88:4987, 1988.
- [8] R. Balian. *From Microphysics to Macrophysics. Methods and Applications of Statistical Physics*, volume I - II. Springer, 2007.
- [9] M. Baus and J.-P. Hansen. Statistical mechanics of simple Coulomb systems. *Phys. Rep.*, 59:1, 1980.
- [10] L. Blum. Mean spherical model for asymmetric electrolytes. *Mol. Phys.*, 30:1529–1535, 1975.
- [11] L. Blum and J. S. H oye. Mean spherical model for asymmetric electrolytes. 2. Thermodynamic properties and the pair correlation function. *J. Phys. Chem.*, 81:1311–1316, 1977.

- [12] T. Bodineau and A. Guionnet. About the stationary states of vortex systems. *Ann. Inst. Poincaré*, 35:205–237, 1999.
- [13] I. Borukhov, D. Andelman, and H. Orland. Steric effects in electrolytes: A modified Poisson-Boltzmann equation. *Phys. Rev. Lett.*, 79:435–438, 1997.
- [14] A. Botan, B. Rotenberg, V. Marry, P. Turq, and B. Noetinger. Hydrodynamics in clay nanopores. *J. Phys. Chem. C*, 115:16109–16115, 2011.
- [15] Andrea Braides. *Γ -convergence for Beginners*. Oxford lecture series in mathematics, 2002.
- [16] E. Caglioti, P.-L. Lions, C. Marchioro, and M. Pulvirenti. A Special Class of Stationary Flows for Two-Dimensional Euler Equations: A Statistical Mechanics Description. *Commun. Math. Phys.*, 143:501–525, 1992.
- [17] E. A. Carlen, M. C. Carvalho, R. Esposito, J. L. Lebowitz, and R. Marra. Free energy minimizers for a two-species model with segregation and liquid-vapour transition. *Nonlinearity*, 16:1075, 2003.
- [18] R. Choksi and P. Sternberg. Periodic phase separation: the periodic isoperimetric and cahn-hilliard problems. *Interfaces and Free Boundaries*, 8:371–392, 2006.
- [19] F. Conrad and M. Grothaus. Construction, ergodicity and rate of convergence of N-particle Langevin dynamics with singular potentials. *J. Evol. Equat.*, 10:623–662, 2010.
- [20] L. Contento. The Discrete Legendre Transform and its application in phase separation of electrolytes, 2012. Master Thesis, University of Udine.
- [21] T. A. Davis. Algorithm 832: Umfpack, an unsymmetric-pattern multifrontal method. *ACM Transactions on Mathematical Software*, 30:196–199, 2004.
- [22] P. W. Debye and E. Hückel. The theory of electrolytes. I. lowering of freezing point and related phenomena. *Phys. Z.*, 24:185, 1923.
- [23] J.-F. Dufreche, O. Bernard, and P. Turq. Transport equations for concentrated electrolyte solutions: Reference frame, mutual diffusion. *J. Chem. Phys.*, 116:2085–2097, 2002.
- [24] J. F. Dufrière, V. Marry, N. Malíková, and P. Turq. Molecular hydrodynamics for electro-osmosis in clays: from Kubo to Smoluchowski. *J. Mol. Liq.*, 118:145–153, 2005.
- [25] J.-P. Eckmann and M. Hairer. Isotropic hypoellipticity and trend to equilibrium for the Fokker-Planck equation with a high-degree potential. *Arch. Ration. Mech. Anal.*, 171:151–218, 2004.
- [26] J.P. Eckmann, C.-A. Pillet, and L. Rey-Bellet. Non-equilibrium statistical mechanics of anharmonic chains coupled to two heat baths at different temperatures. *Commun. Math. Phys.*, 201:657–697, 1999.
- [27] I. Ekeland and R. Temam. *Analyse convexe et problèmes variationnels*. Dunod, 1974. Collection Études Mathématiques.
- [28] D. J. Evans and G. P. Morriss. *Statistical mechanics of nonequilibrium liquids*. Cambridge University Press, 2008.

- [29] R. Evans. The nature of the liquid-vapour interface and other topics in the statistical mechanics of non-uniform, classical fluids. *Adv. Phys.*, 28:143–200, 1979.
- [30] J. E. Flores-Mena, M. C. Barbosa, and Y. Levin. Criticality in confined ionic fluids. *Phys. Rev. E*, 63:066104, 2001.
- [31] D. Gillespie, W. Nonner, and R. S. Eisenberg. Density functional theory of charged, hard-sphere fluids. *Phys. Rev. E.*, 68:2003, 031503.
- [32] D. Goldman, C. Muratov, and S. Serfaty. The Gamma-limit of the two-dimensional Ohta-Kawasaki energy. I. Droplet density. *arXiv:1201.0222*, 2012.
- [33] E. M. Gosling, I. R. McDonald, and K. Singer. On the calculation by molecular dynamics of the shear viscosity of a simple fluid. *Mol. Phys.*, 26:1475–1484, 1973.
- [34] M. S. Green. Markoff random processes and the statistical mechanics of time-dependent phenomena. II. Irreversible processes in fluids. *J. Chem. Phys.*, 22:398–413, 1954.
- [35] B. Groh, R. Evans, and S. Dietrich. Liquid-vapor interface of an ionic fluid. *Phys. Rev. E.*, 57:6944–6954, 1998.
- [36] A. Yu. Grosberg, T. T. Nguyen, and B. I. Shklovskii. The physics of charge inversion in chemical and biological systems. *Rev. Mod. Phys.*, 74:329, 2002.
- [37] E. Hairer, C. Lubich, and G. Wanner. *Geometric Numerical Integration: Structure-Preserving Algorithms for Ordinary Differential Equations*, volume 31 of *Springer Series in Computational Mathematics*. Springer-Verlag, 2006.
- [38] M. Hairer and G. Pavliotis. Periodic homogenization for hypoelliptic diffusions. *J. Stat. Phys.*, 117(1/2):261–279, 2004.
- [39] M. Hairer and G. Pavliotis. From ballistic to diffusive behavior in periodic potentials. *J. Stat. Phys.*, 131:175–202, 2008.
- [40] J-P. Hansen and H. Lowen. Effective interactions between electric double-layers. *Annu. Rev. Phys. Chem.*, 51:209–242, 2000.
- [41] J. P. Hansen and I. R. Mac Donald. *Theory of simple liquids*. Academic Press, 2nd edition, 1976.
- [42] J. S. Hansen, Peter J. Daivis, Karl P. Travis, and B. D. Todd. Parameterization of the nonlocal viscosity kernel for an atomic fluid. *Phys. Rev. E*, 76:041121, 2007.
- [43] W. K. Hastings. Monte Carlo sampling methods using Markov chains and their applications. *Biometrika*, 57:97–109, 1970.
- [44] F. Hecht. *FreeFem++ documentation*, 2011. <http://www.freefem.org/ff++/>.
- [45] P. Helluy and H. Mathis. Pressure laws and Fast Legendre Transform. *Math. Models Methods Appl. Sci*, 21:745–775, 2011.
- [46] F. Hérau and F. Nier. Spectral properties of hypoelliptic operators. *Commun. Math. Phys.*, 235:233–253, 2003.

- [47] F. Hérau and F. Nier. Isotropic hypoellipticity and trend to equilibrium for the Fokker-Planck equation with a high-degree potential. *Arch. Ration. Mech. Anal.*, 171:151–218, 2004.
- [48] B. Hess. Determining the shear viscosity of model liquids from molecular dynamics simulations. *J. Chem. Phys.*, 116:209, 2002.
- [49] W. G. Hoover. Canonical dynamics - Equilibrium phase-space distributions. *Phys. Rev. A*, 31(3):1695–1697, 1985.
- [50] W. G. Hoover and W. T. Ashurst. Nonequilibrium molecular dynamics. *Adv. Theor. Chem.*, 1:1–51, 1975.
- [51] L. Hörmander. Hypoelliptic second order differential equations. *Acta Math.*, 119:147–171, 1967.
- [52] R. J. Hulse, R.L. Howley, and W.V. Wilding. Transient nonequilibrium molecular dynamic simulations of thermal conductivity. I. Simple fluids. *Int. J. Thermophys.*, 26(1):1–12, 2005.
- [53] J. H. Irving and J. G. Kirkwood. The Statistical Mechanical Theory of Transport Processes. IV. The Equations of Hydrodynamics. *J. Chem. Phys.*, 18:817–829, 1950.
- [54] M. Jardat, J.-F. Dufrêche, V. Marry, B. Rotenberg, and P. Turq. Salt exclusion in charged porous media: a coarse-graining strategy in the case of montmorillonite clays. *Phys. Chem. Chem. Phys.*, 11:2023, 2009.
- [55] M. Jardat, S. Durand-Vidal, P. Turq, and G. R. Kneller. Brownian dynamics simulations of electrolyte mixtures: computation of transport coefficients and comparison with an analytical transport theory. *J. Mol. Liq.*, 85:45–55, 2000.
- [56] C. Junghans, M. Praprotnik, and K. Kremer. Transport properties controlled by a thermostat: An extended dissipative particle dynamics thermostat. *Soft. Matt.*, 4:156–161, 2008.
- [57] O. Kavian. *Introduction à la théorie des points critiques*. Springer, 1993.
- [58] R Kjellander and S Marcelja. Interaction of charged surfaces in electrolyte solutions. *Chem. Phys. Lett.*, 127:402–407, 1986.
- [59] R Kjellander and S Marcelja. Surface interactions in simple electrolytes. *J. Phys.*, 49:1009–1015, 1988.
- [60] W. Kliemann. Recurrence and invariant measures for degenerate diffusions. *Ann. Probab.*, 15:690–707, 1987.
- [61] W. Kohn and L. J. Sham. Self-consistent equations including exchange and correlation effects. *Phys. Rev.*, 140:A1133–A1138, 1965.
- [62] R. Kubo. Statistical-mechanical theory of irreversible processes. I. General theory and simple applications to magnetic and conduction problems. *J. Phys. Soc. Jpn.*, 12:570–586, 1957.
- [63] J. L. Lebowitz and E. Waisman. Mean spherical model integral equations for charged hard spheres. I. Method of solution. *J. Chem. Phys.*, 56:3086–3093, 1972.

- [64] J. L. Lebowitz and E. Waisman. Mean spherical model integral equations for charged hard spheres. II. Results. *J. Chem. Phys.*, 56:3093–3099, 1972.
- [65] F. Legoll, M. Luskin, and R. Moeckel. Non-ergodicity of the Nosé-Hoover thermostatted harmonic oscillator. *Arch. Ration. Mech. Anal.*, 184:449–463, 2007.
- [66] F. Legoll, M. Luskin, and R. Moeckel. Non-ergodicity of Nosé-Hoover dynamics. *Nonlinearity*, 22:1673–1694, 2009.
- [67] T. Lelièvre, M. Rousset, and G. Stoltz. *Free energy computations: A mathematical perspective*. Imperial College Press, 2010.
- [68] T. Lelièvre, M. Rousset, and G. Stoltz. Langevin dynamics with constraints and computation of free energy differences. *Math. Comput.*, 81:2071–2125, 2011.
- [69] Y. Levin and M. Fisher. Criticality in the hard-sphere ionic fluid. *Physica A*, 225:164, 1996.
- [70] B. Li. Continuum electrostatics for ionic solutions with non-uniform ionic sizes. *Nonlinearity*, 22:811–833, 2009.
- [71] B. Li. Minimization of electrostatic free energy and the Poisson-Boltzmann equation for molecular solvation with implicit solvent. *SIAM J. Math. Anal.*, 40:2536–2566, 2009.
- [72] J. R. Looker. Semilinear elliptic Neumann problems with rapid growth in the nonlinearity. *Bull. Austral. Math. Soc.*, 74:161–175, 2006.
- [73] Hartmut Löwen, Jean-Pierre Hansen, and Paul A. Madden. Nonlinear counterion screening in colloidal suspensions. *J. Chem. Phys.*, 98:3275–3289, 1993.
- [74] G.A Mansoori, N.F Carnahan, K.E Starling, and T.W. Leland. Equilibrium thermodynamic properties of the mixture of hard spheres. *J. Chem. Phys.*, 54:1523, 1971.
- [75] D.A. McQuarrie. *Statistical Mechanics*. Harper and Row, 1976.
- [76] METHODE. Modélisation de l’écoulement sur une topographie avec des hétérogénéités orientées et différences d’échelles. <http://methode.netcipia.net>.
- [77] N. Metropolis, Rosenbluth A. W., M. N. Rosenbluth, A. H. Teller, and E. Teller. Equations of state calculations by fast computing machines. *J. Chem. Phys.*, 26:1087–1091, 1953.
- [78] L. Mier-y Teran, S. H. Suh, H .S White, and H. T. Davis. A nonlocal free energy density functional approximation for the electrical double layer. *J. Chem. Phys.*, 92:5087, 1990.
- [79] L. Modica. The gradient theory of phase transitions and the minimal interface criterion. *Arch. Ration. Mech. Anal*, 98:123–142, 1987.
- [80] A. G. Moreira and R. R. Netz. Binding of similarly charged plates with counterions only. *Phys. Rev. Lett.*, 87:078301, 2001.
- [81] C.B. Muratov. Droplet phases in non-local Ginzburg-Landau models with Coulomb repulsion in two dimensions. *Comm. Math. Phys.*, 299:45–87, 2010.
- [82] Agence nationale pour la gestion des déchets radioactifs. web site. <http://www.andra.fr/inventaire2012/#/localisation/>.

- [83] R. R. Netz. Electrostatics of counter-ions at and between planar charged walls: From Poisson-Boltzmann to the strong-coupling theory. *Eur. Phys. J. E*, 5:557, 2001.
- [84] R. R. Netz and H. Orland. Field theory for charged fluids and colloids. *Europhys. Lett.*, 45:726, 1999.
- [85] S. Nosé. A unified formulation of the constant temperature molecular-dynamics methods. *J. Chem. Phys.*, 81:511–519, 1984.
- [86] H.C. Öttinger. *Beyond equilibrium thermodynamics*. Wiley, 2005.
- [87] M. Ottobre and G. Pavliotis. Asymptotic analysis for the generalized Langevin equation. *Nonlinearity*, 24:1629–1653, 2010.
- [88] G. Pavliotis and A.M Stuart. Periodic homogenization for inertial particles. *Physica D*, 204:161–187, 2005.
- [89] O. Pizio, A. Patrykiewicz, and S. Sokolowski. Phase behavior of ionic fluids in slitlike pores: a density functional approach for the restricted primitive model. *J. Chem. Phys.*, 121:11957, 2004.
- [90] O. Pizio and S. Sokolowski. Phase behavior of the restricted primitive model of ionic fluids with association in slitlike pores. density-functional approach. *J. Chem. Phys.*, 122:144707, 2005.
- [91] A. Prohl and M. Schmuck. Convergent finite element discretizations of the Navier-Stokes-Nernst-Planck-Poisson system. *Math. Model. Numer. Anal.*, 44:531–571, 2010.
- [92] M. Requardt and H.-J. Wagner. Modifications of the Ornstein-Zernike Relation and the LMBW Equations in the Canonical Ensemble via Hilbert-Space Methods. *J. Phys.: Condens. Matter*, 16:5679, 2004.
- [93] L. Rey-Bellet. Ergodic properties of markov processes. In Stéphane Attal, Alain Joye, and Claude-Alain Pillet, editors, *Open Quantum Systems II*, volume 1881 of *Lecture Notes in Mathematics*, pages 1–39. Springer Berlin / Heidelberg, 2006.
- [94] D. Ruelle. *Statistical Mechanics: : Rigorous Results*. Imperial College Press, 1999.
- [95] L. Samaj and E. Trizac. Counterions at highly charged interfaces: From one plate to like-charge attraction. *Phys. Rev. Lett.*, 106, 2011.
- [96] M. Schmuck. Analysis of the Navier-Stokes-Nernst-Planck-Poisson system. *Math. Models Methods Appl. Sci.*, 19:993–1015, 2009.
- [97] M. Segad, Bo Jonsson, T. Akesson, and B. Cabane. Ca/na Montmorillonite: Structure, forces and swelling properties. *Langmuir*, 26(8):5782–5790, 2010.
- [98] T. Shardlow and Y. B. Yan. Geometric ergodicity for dissipative particle dynamics. *Stoch. Dynam.*, 6:123–154, 2006.
- [99] T. Soddemann, B. Dunweg, and K. Kremer. Dissipative particle dynamics: A useful thermostat for equilibrium and nonequilibrium molecular dynamics simulations. *Phys. Rev. E*, 68, 2003.

- [100] G. Stoltz. *Some mathematical methods for molecular and multiscale simulation*. PhD thesis, École des Ponts, 2007.
- [101] G. Stoltz. *Molecular simulation: Nonequilibrium and dynamical problems*, 2012. Habilitation à diriger les recherches.
- [102] A.-S. Sznitman. *Topics in propagation of chaos.*, 1989.
- [103] D. Talay. Stochastic Hamiltonian dissipative systems: exponential convergence to the invariant measure, and discretization by the implicit Euler scheme. *Markov Proc. Rel. Fields*, 8:163–198, 2002.
- [104] B. D. Todd and P. J. Daivis. Homogeneous non-equilibrium molecular dynamics simulations of viscous flow: Techniques and applications. *Mol. Sim.*, 33:189–229, 2007.
- [105] B. D. Todd, Denis J. Evans, and Peter J. Daivis. Pressure tensor for inhomogeneous fluids. *Phys. Rev. E*, 52:1627–1638, 1995.
- [106] C. Trozzi and G. Ciccotti. Stationary nonequilibrium states by molecular dynamics. II. Newton’s law. *Phys. Rev. A*, 29:916–925, 1984.
- [107] M. Tuckerman. *Statistical Mechanics Theory and Molecular Simulation*. Oxford University Press, 2010.
- [108] L. Verlet. Computer “experiments” on classical fluids. I. Thermodynamical properties of Lennard-Jones molecules. *Phys. Rev.*, 159:98–103, 1967.
- [109] C. Villani. Hypocoercivity. *Mem. Amer. Math. Soc.*, 202, 2009.
- [110] J. A. White and S. Velasco. The Ornstein-Zernike equation in the canonical ensemble. *Europhys. Lett.*, 54:475, 2001.